Parametric Studies Based Mechanical and Thermal Modelling of Spot Welded Joints

Andrew Alan William Norbury

A thesis submitted in partial fulfilment of the requirements of

Liverpool John Moores University

for the degree of Doctor of Philosophy

August 2016

ACKNOWLEDGEMENTS

I would like to express my sincere gratitude and special thanks to my supervisors, Prof. James Ren and Dr. Glynn Rothwell, who have provided guidance, advice and encouragement during this research study.

Many other academic, secretarial and technical members of staff have facilitated the realisation of this thesis and I express them all my gratitude. I would like to thank Mr. Clive Eyre and Dr. Gareth Bradley for their invaluable technical support with material testing and the sample manufacturing process.

I am indebted to many of my work colleagues from both nuclear power & process and pharmaceutical manufacturing industries. The experience I have gained during this time has been invaluable to aid and determine potential applications for my research.

I would like to take this opportunity to thank my group mates, Dr. Jensen Aw, Dr. Nyoman Budiarsa, Dr. Jarema Krywonos and Prof. Yaodong Gu for their friendship and sharing their experience. I am also grateful for the help from my friends, who gave me help in many ways and shared a great time in my studies and life at Liverpool John Moores University.

Finally, my sincere thanks go to my family for sustained encouragement, continuous and unselfish love and support during my Ph.D. study.

Abstract

This work has focused on developing advanced modelling programs for simulating spot welded joints and using the programs to investigate the effects of the key dimensional or material parameters on the mechanical or thermal response of spot welded joints of steels and different thermocouple joints relevant to their applications. An Abaqus plug-in of spot welded joints is developed using Python scripting and is used to investigate the effect of nugget size and sheet thickness on the stress and deformation of spot welded joints of steel. The interfaces included; geometry, material and shear (plastic) properties, sectioning of HAZ layers, boundary, loading conditions and crack partition path. The program is able to incorporate the plastic material parameters (yield stress and work hardening coefficient) as well as fracture models. The plug-in is used in numerical modelling the elastic-plastic-fracture of spot welded joints under tensile-shear test conditions. The validated numerical models are further used to investigate the effects of nugget size and thickness of the metal sheets on the strength of welded joints. The analysis on stress (Von Mises) distribution within the nugget and the HAZ zone next to the nugget and the ratio of the Mises stress at the inner and outer side along the loading axis suggests that the HAZ is more likely to act as the crack initiation and propagation path, which is in agreement with experimental observation.

Detailed FE models of different types of thermocouples have been developed including bare-wire thermocouple, ungrounded sheathed thermocouple and grounded thermocouple. The predicted time-temperature data showed a reasonable agreement with experimental data. Plug-in interfaces are developed for different types of thermocouple consisting geometry, material and contact condition modules. The plug-in for thermocouples not only includes the conventional parameters such as, geometry and material, it also includes application specific features such as, contact condition (full tip contact and partial contact). The plug-in for sheathed TC successfully incorporated the function of automatic verification of the tip position, which is effective for studying the effect of key design factors on the response of sheathed thermocouple. The results show that the temperature of the tip of the sheathed thermocouple is more uniformly heated but the response time is slow due to the effect of the sheath and the insulation layers. It also shows that the position of the nugget could have a significant influence on the measurement response. It has laid a framework for future development in more complex TC systems (including dual or multiple tip systems) and manufacturing process optimisation.

The main development work and results associated with the temperature and structure of electrical resistance spot welding included; development of a testing method to remotely measure temperature in spot welding, development of an FE thermal model of the spot welding process, evaluation of the use of artificial neural network (ANN) based inverse modelling with remote thermocouples and discussion. The experimental work consists of measuring the temperature during the electrical spot welding process using remote thermocouples, characterisation of the welded zones for different material (mild steel, stainless steel and dual phase steels); the structure of the spot welded joint with different material systems. The effects of some key testing conditions (including using different types of thermocouples (bare-wire or sheathed) and location) were established. The results show that the temperature can be reliably measured using remote thermocouples. The welded bare-wire thermocouple shows more rapid response to the temperature change than sheathed thermocouples. The temperature measured by the remote thermocouple showed a clear difference between different materials in the same material welding (MS-MS, SS-SS) and dissimilar material systems (MS-SS). The mild steel shows a relatively unchanged temperature under repeated welding, while the temperature for repeated tests on stainless increases when the welding is repeated in the same position. Metallurgy observation has been conducted on several material systems and reveals that the welding zone for stainless-mild steel is different from the same material weld. Stainless steel forms a larger volume in the nugget and grows into the mild steel forming a taper shape nugget. In numerical work, an electrical-mechanical-thermal model for spot welding is developed and temperature zone is compared with the structure observation. The FE model also provided data for developing an Artificial Neural Network (ANN) method to predict the temperature and cooling curve of HAZ from remote thermocouple measurements. The network was set up and the optimum level of training was determined. Three approaches of representing the cooling curves (i.e. point based, polynomial trend-line and linear trend-line methods), were successfully evaluated to determine prediction accuracy in the neural network; each of the methods has shown to be able to predict the temperature at the HAZ position based on the temperature history of remote thermocouples. The slope (linear) method showed a better robustness, which requires less training data. These works are important to establish an integrated approach to study the electrical, mechanical and thermal process of the spot welding process. Some key issues regarding remote temperatures, including choice of thermocouples are discussed towards the end.

Contents

List of Figures and Tables

Chapter 3

Chapter 4

Chapter 5

Nomenclature

Symbols

F	Force
kN	kilonewtons
Q	quantity of thermal energy (Ws)
Ws	Watt seconds
I	current (Amps)
r	resistance across weld (Ω)
Ω	Ohms (resistance)
t	Welding time (60 Cycles per second)
μ	Micro
n	stain hardening exponent
σy	Initial yield stress
εy	yield strain
q	Porous Metal Plasticity
f_0	Initial void volume fraction
f_n	volume fraction of void nucleating
D	Density
E	Youngs Modulus
V	Poissons Ratio
b	ANN scalar bias
w	ANN weight
f	ANN transfer function
p	ANN input
a	ANN output

Acronyms/Abbreviations

ANN	Artificial Neural Network
ASTM	American Society for Testing and Materials
BM	Base Material
CAE	Computer Aided Engineering
CGHAZ	Course-Grained Heat Affected Zone

DAS	Data Acquisition System
DP	Dual Phase steel
EMF	Electro-Motive Force (Voltage)
ESPI	Electronic Speckle Pattern Interferometry
FAD	Failure Assessment Diagram
FE	Finite Element
FGHAZ	Fine-Grained Heat Affected Zone
GAMP	Good Automated Manufacturing Practices
GMAW	Gas Metal Arc Welding
GIMP	Graphical Image Manipulation Program
GTK	Graphical Tool Kit
GTN	Gurson-Tvergaard-Needleman model
GUI	Graphical User Interface
HAZ	Heat Affected Zone
HTM	Harmonization Technical Memorandum
ICHAZ	Intercritical Heat Affected Zone
IEC	International Electrotechnical Commission
ISPE	International Society of Pharmaceutical Engineering
LBW	Laser Beam Welding
mdb	Model Database
MI	Mineral Insulated (thermocouple)
MS	Mild Steel
Nugget	Weld fusion zone
odb	Open document database
OO	Object Oriented
Plug-in	Parametric interface used to generate FE simulation models
Python	Computer programming scripting language
RMSeW	Resistance Mash Seam Welding
rpy	replay file
RSW	Resistance Spot Welding
SCHAZ	Subcritical Heat Affected Zone
SS	Stainless Steel
TC	Thermocouple, temperature measurement device
TIG/GTAW	Tungsten Inert Gas/ Gas Tungsten Arc Welding

CHAPTER 1

INTRODUCTION

1.1 Introduction

Welded joints are extensively used in many different structures and systems, either as part of a structure or individual parts with a specific function (Lippold, 2015). Electrical resistance welding is a typical case widely used for joining thin metal sheets, in which two metal parts are jointed together through the heat generated when high current is passed through the interface of the metal sheets. This is the main method used in the assembly of automobile bodies. Each car may have thousands of spot welded joints. Another important case of spot welded joints is temperature measurement thermocouples, in which two thin wires are joined together through capacitor welding or TIG welding, the change of the electrical response to temperature of the welded tip serves as an indicator for temperatures. During a welding process, the material will go through a complex mechanical and thermal process, which results in a complicated structure within a small volume of materials. This made the modelling process of these structures difficult, either as part of a larger system or as an individual functional part, this made it difficult or time consuming for consistently meshing, suitable material properties and boundary conditions. On the other hand, given that welded joints have repeatable overall structures, this offers an opportunity to use advanced modelling techniques, such as user interfaces which have been successfully used in some parts with reproducible shapes or functions. For example, ABAQUS plug-ins are used in gear systems (Winker et al, 2005), as gears have relatively repeatable shapes and positions. Abaqus plug-ins are also used in key engineering systems, such as the nuclear core systems for holding the fuel rod system, which has a reproducible shape and features (Xia, 2012). A system, such as a plug-in, once validated and developed, could offer a quick and easy way to model a complex system, in the meantime offering engineers other functions, such as, data safety and optimum processing time, and will be part of the overall drive in digital engineering. Spot welded joints could potentially be modelled through generating such a technique to develop a plug-in program consisting of reproducible features with specialised structures or function focus. One key issue is to develop a plug-in to suit different structures, materials or functions for serving both academic research and industrial use. This is particular critical for electrical resistance spot welding of steels and temperature measurement thermocouples, which are the two main focuses of this thesis.

Resistance spot welding (RSW) is widely used in the fabrication of sheet metal assemblies in automotive and aerospace industries of material such as steel, aluminium, titanium and

copper alloys (Aslanlar, 2006). The main advantages of spot welding are the high speeds and adaptability for automation in high-volume production. The welding process is a complex thermal mechanical process and the finished assembly consists of regions with significantly different microstructure and properties (e.g. the nugget and the heat affected zone (HAZ)). For steel, the weld nugget formed in the fusion zone, consists of a martensitic structure due to the high cooling rate while the HAZ is a mixture of tempered structure (Easterling, 1993). A user interface program has to properly parameterise the structure to reflect these complex structures or materials for either mechanical or thermal simulation in order to investigate the effect of key dimensional or material factors. Such a program will also make it more effective to combine FE modelling with programs, such as inverse modelling methods like Neural Networks (Zaw, 2009), to investigate or predict key design or process parameters. For example, the temperature history of the HAZ is very important, however, the consistent measurement of the HAZ temperature is difficult, a potential approach is using a remote thermocouple, i.e. measuring the temperature at a position from a remote location then predicting the temperature at the point of interest through combining experimental and FE modelling. This has been used in applications such as cutting (Ren et al, 2004), etc. An established investigation and program will offer a potential route to estimate temperature with complex heating sources.

Thermocouple design, manufacturing and application is another case where parametric programming such as, Plug-ins user interface with application specific functions could significantly improve the modelling efficiency. A thermocouple is assembled by spot welding two dissimilar wires together. There are three main types of thermocouples: bare wire, insulated and grounded insulated. Bare wire thermocouples are in a simple form with the wire directly jointed together and used in temperature measurement. In an insulated thermocouple, the welded tip and wires are embedded with an insulation (normally MgO) covered by a sheath of protective material. Modelling the thermocouple is important for improving the design and manufacturing of thermocouples. As a temperature sensor, a parametric program could offer an effective tool for research and development of thermocouples. With the demand on fast response of thermocouple in process control, it is increasingly important to use such a tool in guiding the design, improving the manufacturing and application of different types of thermocouple. Thermocouples vary in size but the basic design is the same/reproducible, this is a unique case for using a program such as plug-in. However, detailed research is required since such a program not only needs to consider the conventional

features such as materials, dimensions, it also needs to consider the contact conditions, heating areas, etc, as unique issues for thermocouples in temperature measurements.

The main philosophy of the works is to formulate a novel experimental/numerical framework for the investigation of spot weld properties and performance. The flow diagram in Figure 1.1 shows the philosophy used to generate a logical approach to outline the research structure.
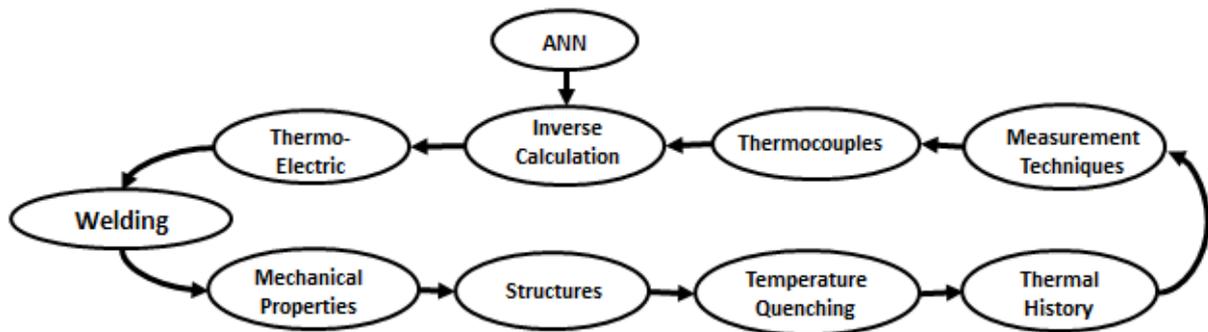
Figure 1.1 Thesis structure diagram

Identified from the thesis structure diagram are the key areas of interest and the philosophy for the works. The following chapters cover the features of the structure diagram. A background of all the aspects of the framework were researched and reviewed in chapter 2. The mechanical properties and structures were investigated in chapter 3. Thermal History, measurement techniques and measurement devices such as, thermocouples tested and evaluated in chapter 4. Experimental work and inverse measurement techniques used for calculating thermal history of electro-thermal welds was performed in chapter 5.

1.2 Aim & Objectives

This work aims to develop advanced modelling programs for simulating spot welded joints and use the programs to investigate the effects of key dimensional or material parameter on the mechanical or thermal response of spot welded joints of steels and different thermocouple joints relevant to their applications.

Main objectives are:

• To develop a user interface in the form of Abaqus Plug-in of spot welded joint and investigate the effect of key parameters (sheet thickness and nugget size) on the mechanical strength and stress distribution of spot welded joints of steel.

• Expand the application of the user interface Plugin-in approach in Abaqus for different types of thermocouples (bare wire, sheathed and grounded thermocouples) and investigate the effect of material, design, boundary and loading conditions on the response of different types of thermocouples.

• To inversely measure the temperature in an electrical spot welding process when welding different material systems and welding parameters using remote thermocouples

• To develop an inverse prediction program using Neural Network and FE modelling to estimate the temperature in spot welding and explore the use of the remote thermocouple method to estimate the temperature at HAZ during welding.

1.3 Outline of the thesis

In chapter 2, there is background information and current research on spot welding, mechanical testing, thermal process of welding and the use of optimisation parametric techniques such as, inverse modelling and computational scripting. It covers several different types of mechanical testing techniques and recent development of instrumentation used to measure temperature in challenging process environments. A review of methods used to inversely predict results from experimental testing relating to Artificial Neural Networks are given. Different approaches of programming languages were evaluated to determine an approach for optimizing FE modelling techniques in the form of computational scripting and graphical user interfaces.

Chapter 3 is concentrated on the development of an Abaqus plug-in program for spot welded joints of steel sheet with detailed geometry representing the welding zones and properties. The model is used to simulate tensile shear testing of spot welded joints and investigate the effect of sheet thickness and nugget size. A systematic/automatic FE modelling program of spot welded joints has been designed using Python scripting to develop Abaqus plug-in interfaces. Several interfaces were generated to create parametric models, the approach used different features of the weld that impact the mechanical properties. The interfaces included;

geometry, material and shear (plastic) properties, sectioning of HAZ layers, boundary, loading conditions and crack partition path. The plastic material parameters (yield stress and work hardening coefficient) and fracture model are incorporated in the plug-in and used in numerical modelling of tensile-shear deformation of spot welded joints. The validated numerical models are further used to investigate effects of nugget size and thickness of the metal sheets on the strength of welded joints. The stress within the nugget and HAZ is analysed in details and used to predict the potential crack initiation and propagation within the HAZ and compared to experimental observation.

Chapter 4 presents the development of a new approach for modelling different thermocouple types. The application of a plug-in interface method aims to provide a simpler and more practical approach to model types (regarding material), thermal loads, contact areas and varying geometries of thermocouples. The method is validated against standard laboratory tests of thermocouples` time response. A comparison of diverse thermocouples (bare wire, Sheathed Ungrounded and Sheath grounded) and types (J, K and R) are presented. Functions of the plug-in are shown characterising the impacts slight changes to the models have on the resulting output data. Variations of numerical models investigating the effects of thermal contact surfaces, material properties, sheath thickness and nugget location and size are detailed in this section

Chapter 5 investigates the thermal analysis of spot welded joints. In the first part, experimental work using remote thermocouple methods were conducted to measure the temperature when spot welding different material systems under different conditions. The material included a mild steel, stainless steel and dual phase steel. The welding zones were characterised through metallurgical studies. An FE model has been developed to simulate the nugget growth and thermal history of spot welding considering the electrical, thermal and mechanical process. An inverse program based on Artificial Neural Networks is developed to predict the temperature of key locations from the remote thermocouples. Three methods have been developed to represent the temperature data, i.e. point based approach, polynomial approach and slope based approach. Each method is used to produce a large amount of data and the accuracy and feasibility of the ANN is assessed. Finally, the key factors that affect the remote thermocouple method, material influence on temperature and potential use for the program in future development is discussed.

In Chapter 6, overall conclusions are given and future works are highlighted.

CHAPTER 2

LITERATURE REVIEW

The literature review was performed using the framework defined in Figure 1.1. The flow diagram identifies key areas of interest for research. This chapter contains, a review into the current research and background related to the main research structure (Figure 1.1) and techniques. The review comprises of different types of welding, thermal process of welding and the use of optimisation parametric techniques such as, inverse modelling and computational scripting in process monitoring and design. The review includes, several different types of mechanical testing techniques and recent development of instrumentation used to measure temperature in challenging process environments. Methods relating to Artificial Neural Networks used to inversely predict results from experimental testing are given. To determine an approach for optimizing FE modelling techniques in the form of computational scripting and graphical user interfaces a review of different approaches of programming languages were evaluated.

2.1 Spot welding process and applications

Resistance spot welding (RSW) is a complicated materials joining process, including interactions of electrical, thermal, mechanical and metallurgical phenomena. As shown in Figure 2.1, during a spot welding process, two or three overlapped or stacked components are welded together as a result of the heat created by the electrical resistance (Figure 2.1 (a)). Two electrodes clamp the two sheets of metal together with a considerable force, while passing a high current through the metal. Thermal energy is produced as the current passes the electrical contact resistance between the two sheets, as given by: $Q = I^2 \bullet r \bullet t$ (*Weman*, 2012); where Q = quantity of thermal energy (Ws); I = current (A); r = the resistance across the weld (Ω); t = welding time duration (s). The secondary circuit of a resistance welding machine and the work-piece being welded constitute a series of resistances (Li et al, 2002) including the resistance of electrode, work pieces and the work-piece interface. The total resistance between the electrodes is made up of $2r_1 + 2r_2 + r_3$ (Figure 2.1(c)); Where r_1 = contact resistance between each electrode and the work-piece; r_2 = the resistance through the metal of each of the pieces to be joined; r_3 = the contact resistance between the two work-pieces of metal (this consists of constriction resistance (base material surface roughness) and film resistance (Oxides, oil and water vapour)). The overall resistance also varies with material and the sheet thickness, but the resistance at the work-piece interface is much higher

than the other resistance. *Song et al* (2005) highlighted the electrical contact resistance in resistance welding of mild steel, stainless steel and aluminium using normal pressures and temperature. Contact resistance between aluminium was 20-180μΩ, mild steel was 50-300μΩ, and stainless steel 500-2500μΩ. The work concluded that the resistance decreases when the pressure increases, however, the influence of temperature has on resistance is more complex than its effect on the electrical and mechanical properties of the base material. The welding force applied to the electrodes is an important parameter of resistance spot welding, because the force functions to ensure electrical contact and to retain weld nuggets from expulsion. As illustrated in Figure 2.1 (b), current (I) and force (F) changes during the different welding stages: squeeze, welding, hold and off. The force increases in the squeeze stage, is then maintained at a constant level during the welding and hold stages, before being released in the off stage.
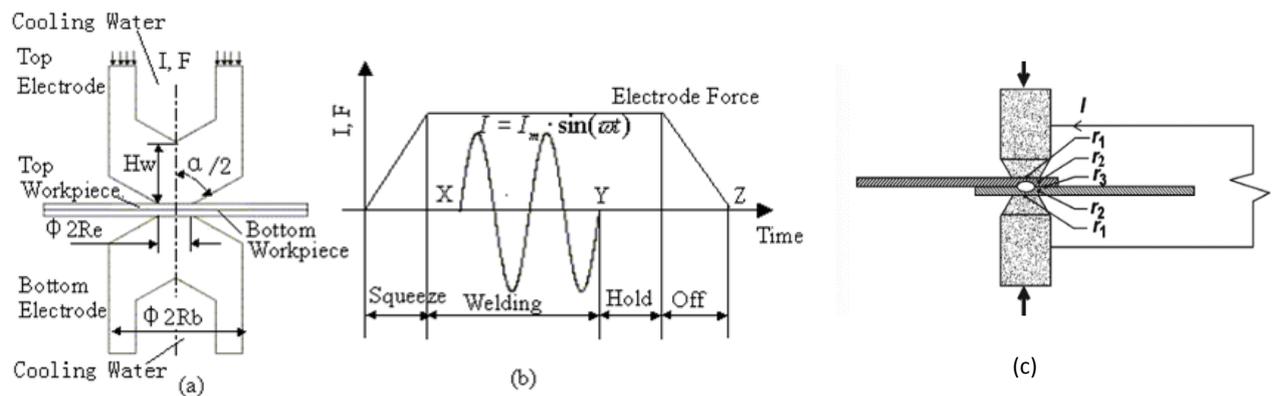
Figure 2.1 The setup of a spot welding system and the resistances occurring in the welding (*Li et al,* 2002 (a,b) &*Weman*, 2012 (c)).

The sequence of operation must first develop sufficient heat to raise a confined volume of metal to the melting point, then the material from both work-pieces mixed together, the molten metal is then allowed to cool while under pressure until it has adequate strength to hold the parts together. The current density and pressure must be such that a full nugget is formed, but not so high as to cause molten metal to be expelled from the weld zone, which causes severe quality problems. In addition, the duration of weld current must be sufficiently short to prevent excessive heating of the electrode faces.

The force and current applied varied between different materials and dimensions (*Aslanlar,* 2006). Figure 2.2, shows the typical welding time cycles of 5, 10, 15, 20 & 25 on galvanised

chromided micro-alloyed steel. A complete frequency wave of electrical current is one cycle, at a 60-cycle per second, weld time is usually measured in cycles. This has become a convenient measuring standard for duration of weld heat. In this case, a force of 6kN is applied. When welding other materials, the current level and force may be significantly different. For example, the welding current for aluminium is higher and the welding time is shorter (*Ambroziak et al*, 2010).
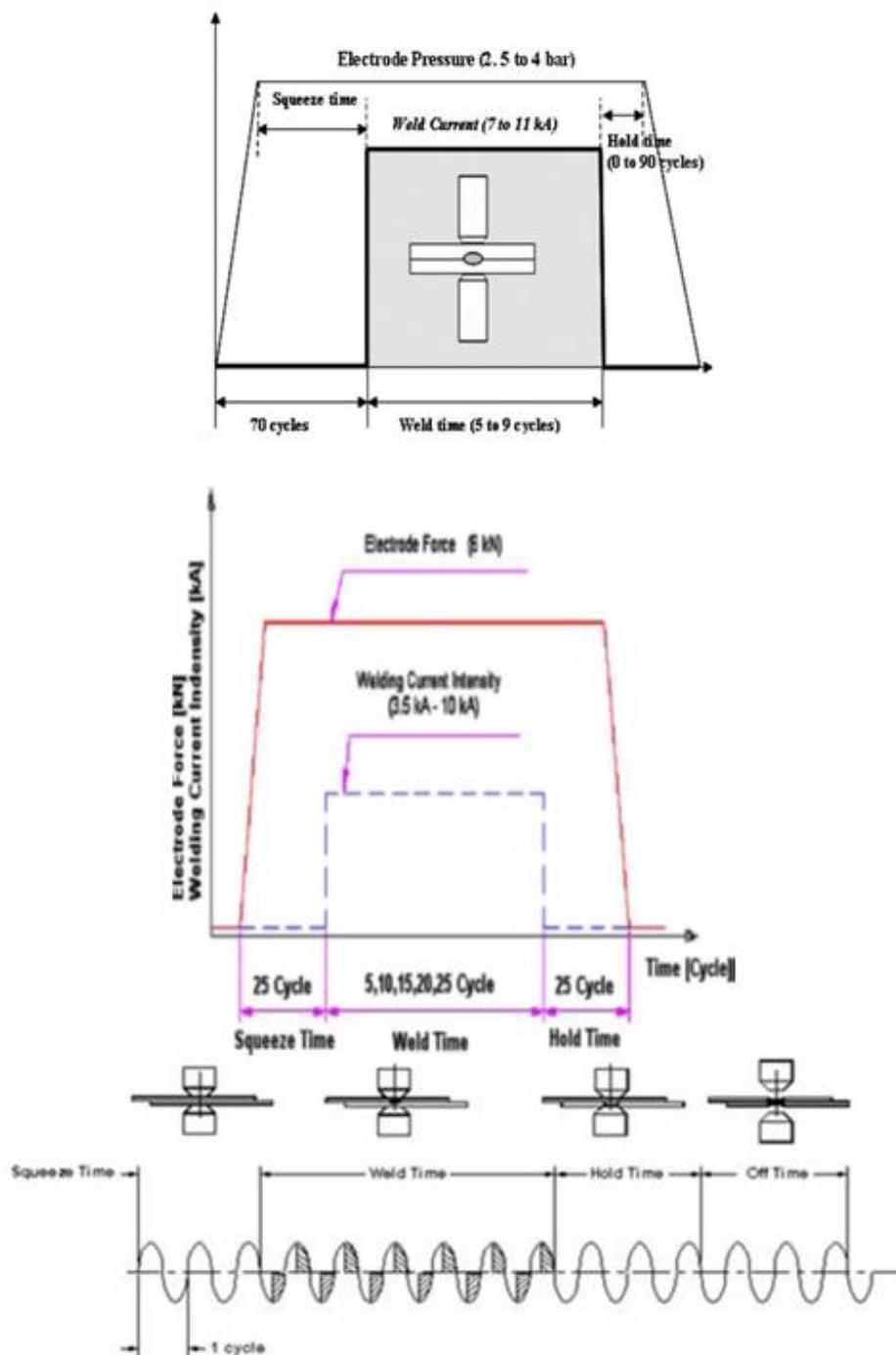
Figure 2.2 Basic welding cycle(s) for spot welding (*Aslanlar*. 2006 & Pouranvari 2007).

The welding process is a complex thermal mechanical process and the finished assembly consists of regions with different microstructures and properties, including the base metal, heat affected zone (HAZ) and weld nugget (Fan et al,2007), all these directly influence the structural integrity and the service performances of the weldment. Figure 2.3 shows the main parameters in resistance welding influence the weld quality (Zhang, 2003). As shown in the Figure, the main factors include electrode, interface, machine and process and the work-piece.

Electrodes can be liquid cooled via a medium such as water pumped through the hollow internal area of the electrode. The size of the electrode tip can vary dependent on the required application. The greater the surface area contact between the tip and the work-piece the larger nugget is. Repeated use of Electrodes without redressing the tips affects the repeatability of the weld, including the mechanical properties, nugget size and surface finish. Energy delivered from the electrodes to the work piece is dictated by the Welding machine. This includes variations of electrical and mechanical characteristics. Process parameters such as welding current and squeeze/hold force can be adjusted and controlled on the welding machine. The work-pieces have an impact on the resistance of the weld, regarding the material properties, geometry (specifically thickness) and the surface finish. Greater resistance is created if the work-piece is dull or coated.
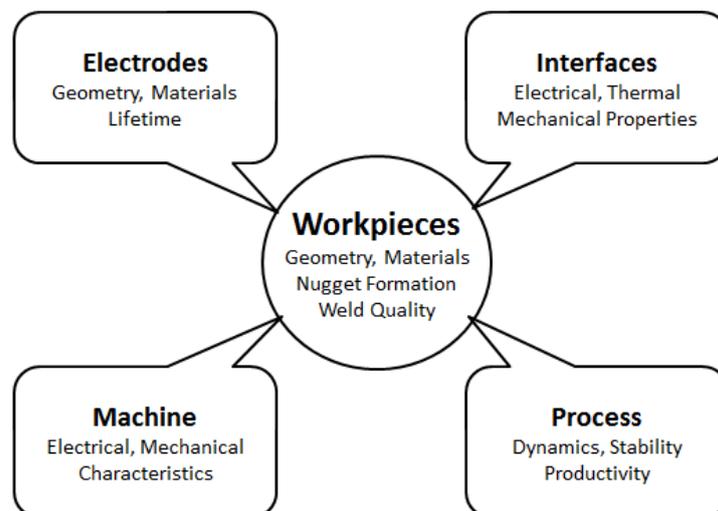
Figure.2.3 A system of parameters in resistance spot welding (Zhang, 2003,).

The selection of these three parameters is normally determined by generating a weld lobe as shown in Figure 2.4. The weld lobe curve is a graphical representation of the range of welding variables over which acceptable spot welds are formed on a specific material welded

with a pre-selected electrode force (Williams and Parker, 2004). It is determined by making spot welds using different combinations of welding time and current. Only welds made with currents and duration lying within the lobe area are acceptable. Welds made with currents and times exceeding the upper curve experience expulsion; while welds made with currents and times below the lower curve are of insufficient size, or no weld is formed. In both cases, the weld is not acceptable (Aslanlar, *et al,* 2008).
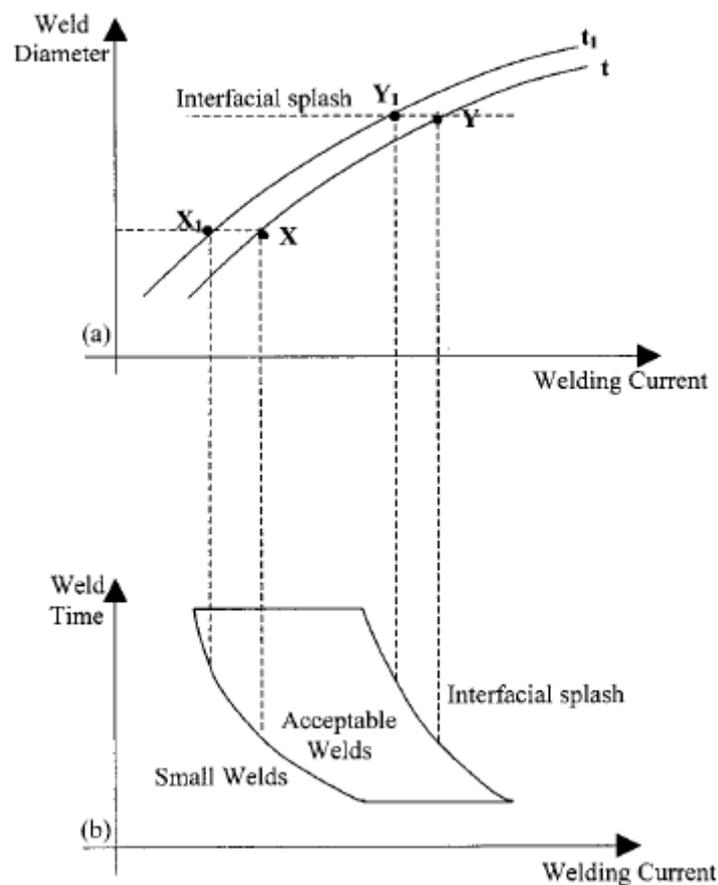
Figure.2.4 Typical spot welding lobe curve (Williams and Parker, 2004).

The spot welding process requires relatively simple equipment; therefore, it can be easily converted into an automated operation over a wide range of industrial sectors. Once the welding parameters are established, it should be possible to produce repeatable welds. Resistance spot welding is the most widely used joining process for sheet materials. The process is used in preference to mechanical fasteners, such as rivets or screws, when disassembly for maintenance is not required (Cho and Rhee, 2003). The process is used extensively for joining low carbon steel components for the bodies and chassis of automobiles, trucks, trailers, buses, mobile homes, motor homes and recreational vehicles and

rail road passenger cars, as well as cabinets, office furniture, and white-goods manufacturing industries (Hasanbasoglu *et al*, 2007). Many metallic materials such as mild steel, high strength steel, galvanized interstitial free steel, stainless steel, austenitic stainless steel, nickel, aluminium, titanium alloy and brass can be welded by resistance spot welding (Jou, 2003; Vural *et al*, 2006; Kahraman, 2007). Small scale resistance spot welding (SSRSW) or micro welding is also one of the main micro-joining processes being employed in the fabrication of medical packaging (lead/pad interconnections and hermetic sealing) electronic components and devices (e.g. cell phone batteries) to joint thin sheet metals of thickness less than 0.2-0.5 mm (Chang *et al*, 2003).

2.2 Microstructure and properties of spot welded joints

As described in the section above, spot welding involves thermal, metallurgical and mechanical processes, which result in a structure of mixed phases and properties. Figure 2.5 shows a typical microstructure of a cross-section of a spot welded joint of a low carbon steel (Bayraktar, 2004). There are three main different regions – the base material, the nugget and the heat-affected-zone (HAZ). The block in the centre is the nugget that consists of martensite and bainitic phases (Ni *et al,* 2004). The region around the nugget, the so-called heat-affected zone (HAZ), has a mixed microstructure consisting of martensite, bainite, ferrite and pearlite (Khan, et al, 2008). The nugget is much harder than the base material due to the quenching effect, while the HAZ has a gradient mechanical property and a mixed microstructure with the strength decreasing from the nugget to the base. In many cases, failures of spot welded joints tend to occur around this region, specifically around the heat-affected zone (HAZ) (*Mukhopadhyay*, 2009; *Vural and Akkus*, 2004, *Pouranvari, et al*, 2007).

Much research has been conducted to improve the understanding on spot welded joint as the interactions between electrical, thermal, metallurgical and mechanical phenomena. (Hou *et al*, 2006, *Esme*, 2009). One active area of research is on the prediction of the dimension of spot welded joints by simulating the welding process with the finite element modelling (Seeger, 2008; Rahman et *al*, 2008). The dimension of the nugget is important for the quality of the weldment and the energy required to melt the material. The size of the heat affected zone is also very important, but it is much more difficult to predict. The study of

microstructure development is also very important (Sun et *al*, 2007; *Bakavos et al*, 2010, *Pouranvari, et al*, 2007). The microstructure models have to consider the thermo-physical properties of the materials in order to describe the phase transformations during heating and cooling stages (*Jou*, 2003, *Tan et al*, 2007; *Ma*, 2010). These works have resulted in several models to describe the simultaneous formation that has made it possible to predict the microstructure development and transformations during the spot welding process, and also to investigate the characteristics and behaviour of materials, relating with the applied load conditions on the spot weld joint (Nodeh, 2007). All this work has laid a foundation that makes it possible to directly link welding parameters to structural integrity prediction, which in turn makes integrating process simulation and the structure analysis possible.

Base	Nugget	Heat affected zone (HAZ)

Grain growth zone	Recrysatllised zone	Partial transformed zone	Tempered zone
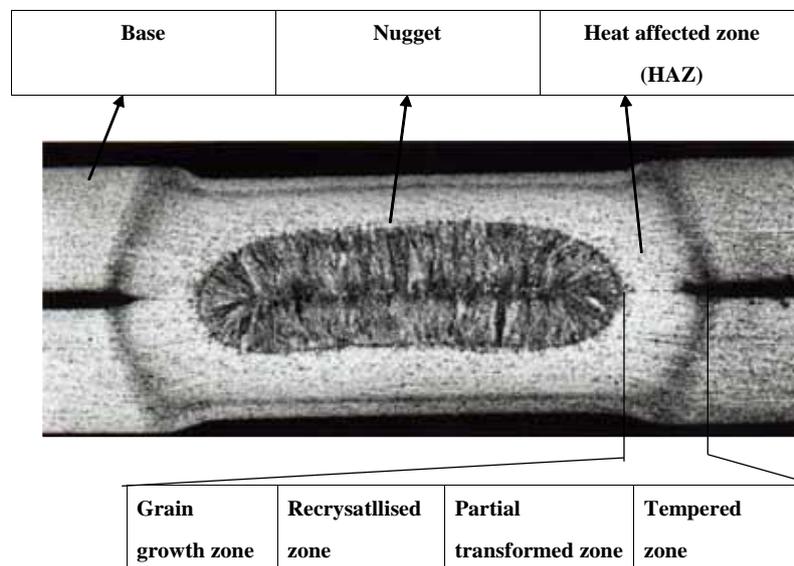
a) Different structure zones of steel weldment (Bayraktar et al, 2004)
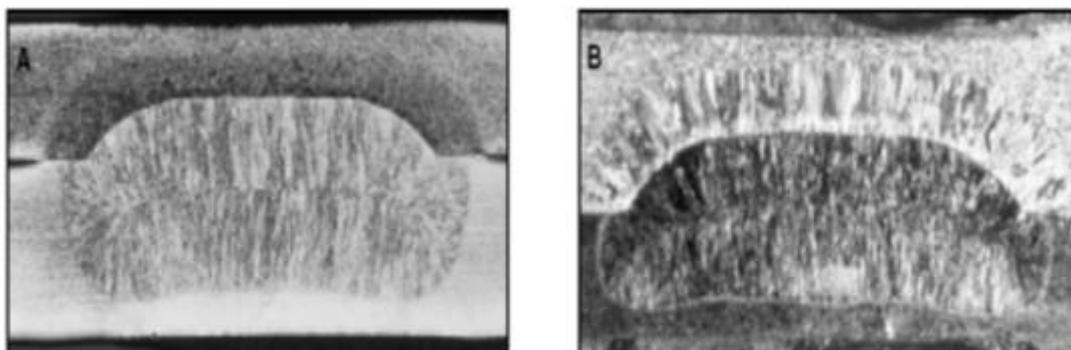
b) Typical structure of welded joint of dissimilar materials, A- Asymmetric penetration in the dissimilar metal joint of EN 1.4318 2B and ZStE260BH steels; B - dissimilar metal joint of EN 1.4318 2H and DX54DZ steels (Alenius et al, 2006)

Figure. 2.5 Different structure zones of spot welded joints.

2.3 Structural integrity of welded joints

The shape and dimension of the final welded joint is strongly dependent on the welding parameters and the materials being welded. Accurate prediction of these processes will rely on fundamental laws of physical processes that determine the operational characteristics and weldment properties. In the case of arc welding, the physical processes include arc-plasma interactions, gas-metal reactions, slag-metal reactions, solidification and solid-state phase transformation (Fukumoto *et al*, 2008). Over the past three decades, significant progress has been made in the fundamental understanding of individual physical process, such as, droplet formation, heat transfer and cooling. Many theoretical and computational models have been developed to describe individual process as well as some of the complex interaction (Mackerle, 1996; Lu *et al*, 2006, Capriccioli, 2009). These have greatly advanced the engineering technical capacity to predict and control the final weldments quality for different welding techniques such as spot welding, electrode welding, resistance spot welding, capacitor welding and TIG welding (Bonifaz, 2000; Chiozzi*et al*, 2008; Fukumoto *et al*, 2008; Eisazadeh*et al*, 2010).

Micro-structural evolution in the different regions of the weld zone is closely linked with the local thermomechanical cycle experienced during the joining process. Important parameters of the thermomechanical cycle that control micro-structural evolution are the total strain, the strain rate, and the temperature. The thermomechanical cycle experienced by the material in the welded joint essentially involves hot working. The welding zone is subjected to the greatest strain and strain rates, as well as the highest temperatures. This combination of parameters apparently results in dissolution of strengthening precipitates as well as continuous dynamic recrystallization (Lienert, 2003).

Associated with the complex welding process, are many issues that affect the structure integrity. Typical defects of spot welding includes: Weld expulsion caused by excessive Electrode indentation (Pouranvari et al, 2008), shrinkage voids (related to interfacial fractures) caused by richer materials, coatings and the hold time phase of the spot weld cycle (Marya & Gayden 2005, Joaquin et al, 2007), voids deeply embedded within the fusion zone caused by impurities and rapid cooling (Tong et al, 2005). Additionally, the hardness is unevenly distributed within the welded joints. Figure 2.6 is a schematic illustration of the different regions of the HAZ of a friction stir weld on mild steel and their relation to effective

temperatures in the P91 steel system. The diagram shows the zones of the weld (fusion zone [FZ], course-grained zone [CGHAZ], fine-grained zone [FGHAZ], intercritical zone [ICHAZ], subcritical zone [SCHAZ] and base material [BM]) under different thermal cycles depending on the zones distance from the source of heat (Marzocca *et al*, 2013). (b) Shows Micro-hardness traverse for friction stir welded 1018 mild steel. Hardness readings are spatially correlated to the different regions of the weld, (Lienert, 2004) the different region corresponds to different structure and resulted in different hardness profiles.
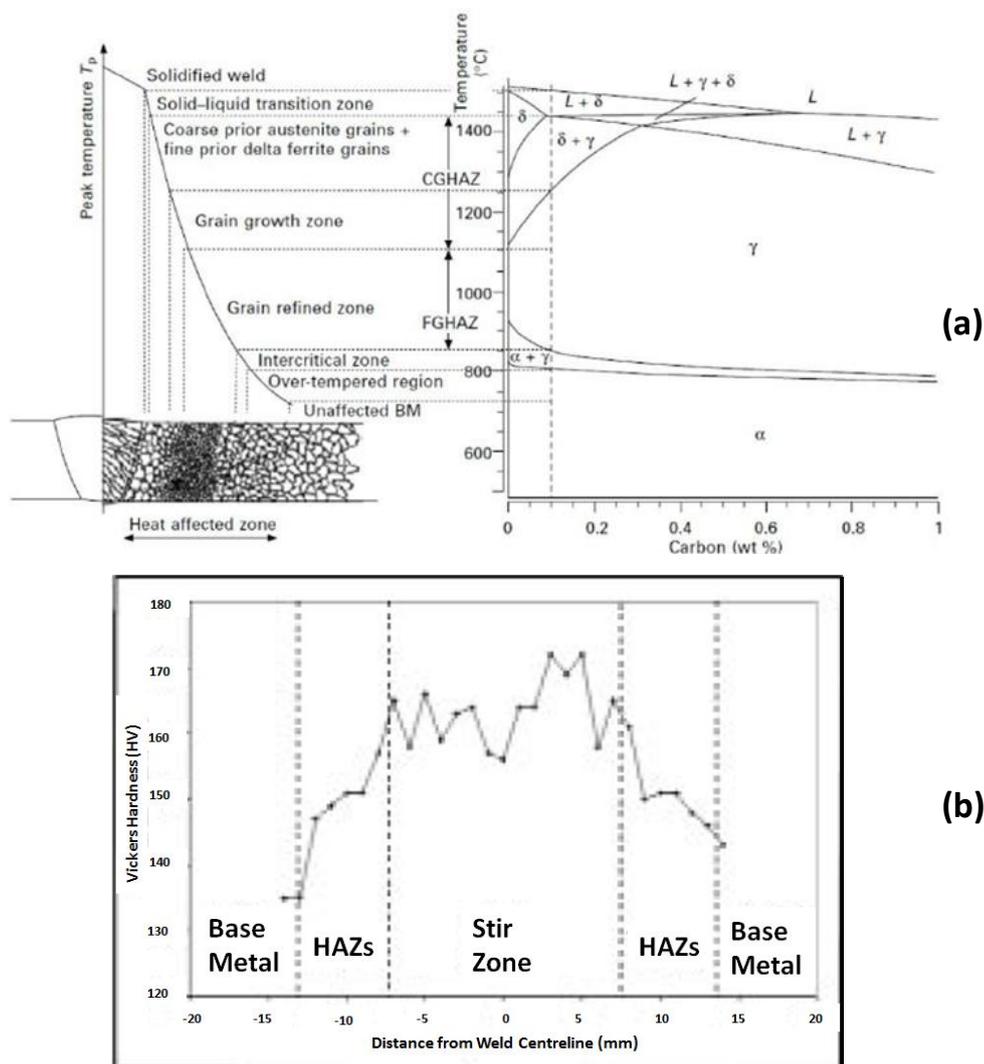
Figure 2.6 (a) Schematic illustration of the sub-zones of the HAZ corresponding to the calculated equilibrium phase diagram (Marzocca *et al*, 2013) **(b)** Is a micro-hardness traverse for friction stir welded 1018 mild steel (Lienert, 2004).

Rapid thermal cycles and tempering of a resistance weld has a direct effect on the microstructure of the weld. Tempered martensite microstructure occurs at the sub-critical

HAZ at a temperature below the lower critical temperature. The severity of tempering is highly dependent on the maximum temperature and the time at peak temperature during isothermal heat treatments (*Henandez et al*, 2009). The final microstructure depends on the tempering (cooling) of the weld from the peak temperature. Associated with complex temperature and phase changes, residual stresses are generated within the weldment during the thermal cycle (expansion and shrinkage of material) of the weld. The geometry (plate thickness and width) also affects the residual stress concentration around the nugget. Residual stresses within the welded joints may influence the mechanical stress (e.g tensile, hardness, etc.) and time dependent behaviours, such as fatigue. Residual stress should be considered when calculating Fatigue strength since it affects crack initiation.

2.4 Mechanical testing methods of spot welded joints

Spot welded joints are widely used in many load bearing situations and their mechanical strength has a strong influence on the integrity of the whole structure. A large amount of research has been conducted to study the deformation of spot welded joints, experimentally or numerically, under different loading, such as tensile, bending, impact etc. (Darwish, 2003; Cavalli*et al,* 2003; Yang *et al*, 2005). As shown in Figure 2.7, typical mechanical testing methods of spot welded joint includes lap shear test, cross-tension tests (a), peel test (b), Impact test (c), corrosion fatigue test, and stress corrosion cracking tests (d) (Alenius, 2006). Each test has its own purposes and the selection of a test should be dependent on the service conditon of the structure being concerned. It is important to accurately predict the deformation behaviour (elastic, plastic, fracture, fatigue) of a welded joint over a range of different loading conditions to avoid overloading or excessive time-dependent deformation. Coach-Peel test method (Figure 2.7 (b)) is intended to establish the relative peel resistance between the welded materials. A Peel test specimen is clamped into a tension test machine, then a tensile load is applied at a consistent speed perpendicularly at 90° above the nugget. The same directional load is applied for the Cross-tension test (Figure 2.7 (a)), however, the machine secures the work piece with fixtures (bolts) through the plates in the Lap shear test (Figure 2.7 (a)) a specimen is loaded into the tension machine grips, and a tensile load is applied laterally along the length of the work piece. The Charpy impact test (Figure 2.7 (c)) is used to establish a specimen's toughness. A pendulum of a known mass and length is released from a known height into a notched specimen. The surface of the impacted material

can be used to establish percentage ductile / brittle fracture. Corrosion Fatigue phenomena (Figure 2.7 (d)) is an important and complex failure mode, testing involves accumulated cyclic loads in aggressive environments.
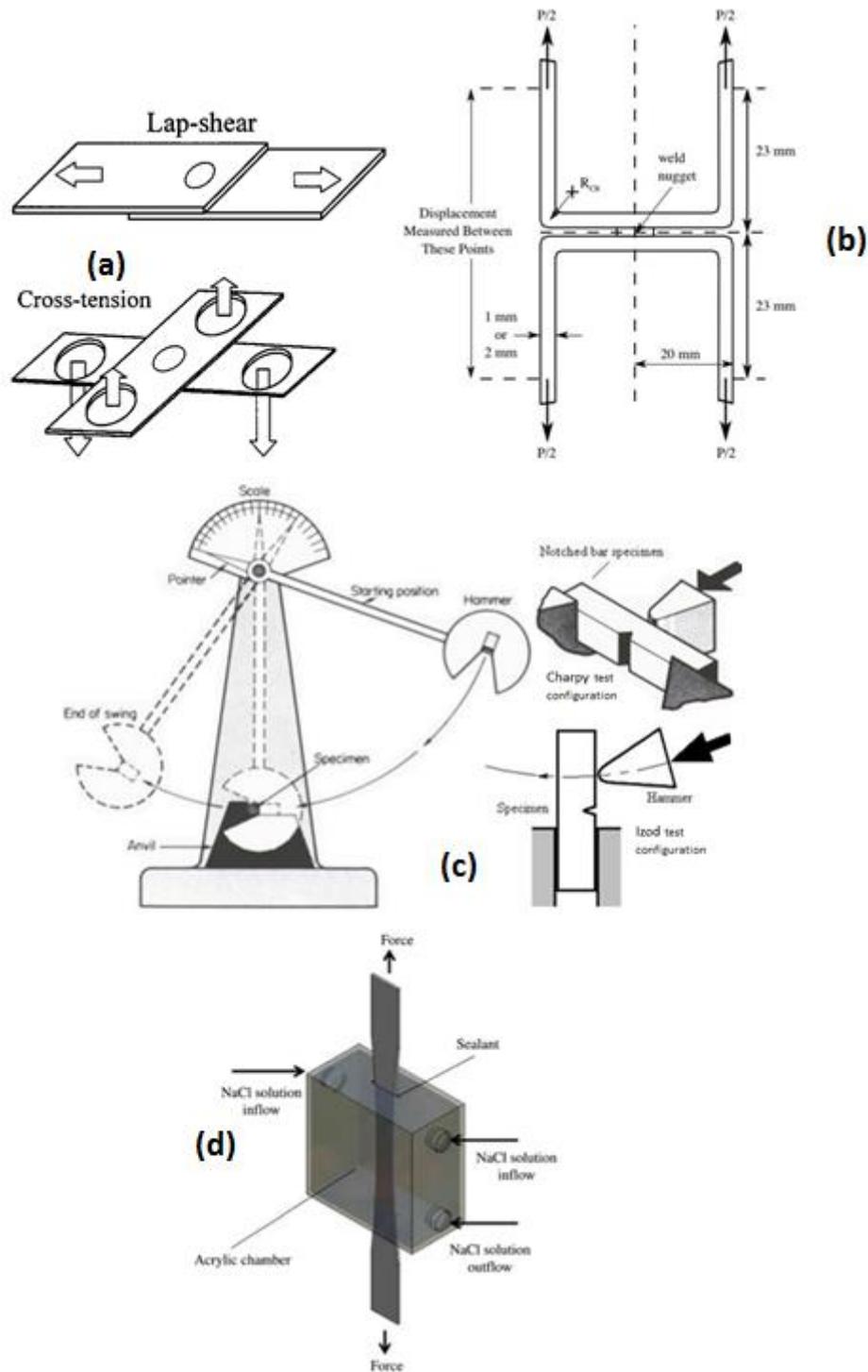
Figure 2.7 Different testing modes to determine the ultimate strength and failure mechanisms of resistance spot welded joints. **(a)** Tensile/ shear load testing (Chao, 2003), **(b)** Coach-peel testing (Cavalli et al, 2003), **(c)** Pendulum Impact Test (ASTM D-256, Charpy ASTM D-4812), **(d)** Corrosion Fatigue testing (Gamboni et al, 2013).

2.5 Thermal process of welding and temperature measurement techniques

Monitoring a welding process is very important for process control and quality assurance, such as welding penetration, temperature etc. Welding penetration (depth of fusion) is the distance that fusion extends into the base metal. A shallow depth of penetration may contribute to failure of a welded structure (*Mostafa et al*, 2006). The measurement of weld penetration plays a crucial role in the closed-loop control of weld quality. There are a number of concepts used to monitor the weld penetration including weld pool oscillation, ultrasonic sensing, infrared sensing, bead width sensing, radiographic sensing, back-side bead width sensing and back-side infrared sensing (Childs et al, 2000). Pool oscillation can be used to distinguish the complete penetration case from the incomplete one. However, to extract the accurate pool size, more information may have to be used. In the case of ultrasonic sensing, contact transducers have been used which are inconvenient in practical welding (Beardsley 1999). Given the temperature changes when the volume or position of the welding pool changes, temperature measurement can in some cases be used as a reference for the weld penetration. Many studies have been performed to determine the weld penetration by monitoring the heat transfer of welding processes, for example, Venkatraman et al (2006), applied online non-destructive technique to ascertain weld quality. Thermal imaging infrared sensors were used to detect defects and estimate the depth of penetration of fusion during the welding process.

Measuring the thermal history of a welded joint can also be used to establish the weld's microstructure and mechanical performance, energy consumption, etc. Due to the setup of a welding process, it is a challenging task to accurately measure the temperature in welding. Different techniques have been developed. An example of a technique used to measure the cooling rate of a welded joint is the infrared thermography sensing system as shown in Figure 2.8 (a). Invisible infrared radiation emitted from the top surface of the work-piece is converted into equivalent voltage signals, which represent the temperature field (Beardsley, 1993). Newly-developed measurement method, electronic speckle pattern interferometry (ESPI), has been applied widely into many scopes of measurement including stress and strain measurement during welding (Toubal et al, 2004). Since ESPI is a non-contact, full-field method with high precision, strong parasitic light resistance, it is used to carry out the measurement of the real displacement field during welding. In Figure 2.8 (b) an ESPI

measurement system has been used to measure the thermal history of a tungsten inert gas (TIG) welding process (Dongqing, 2003).
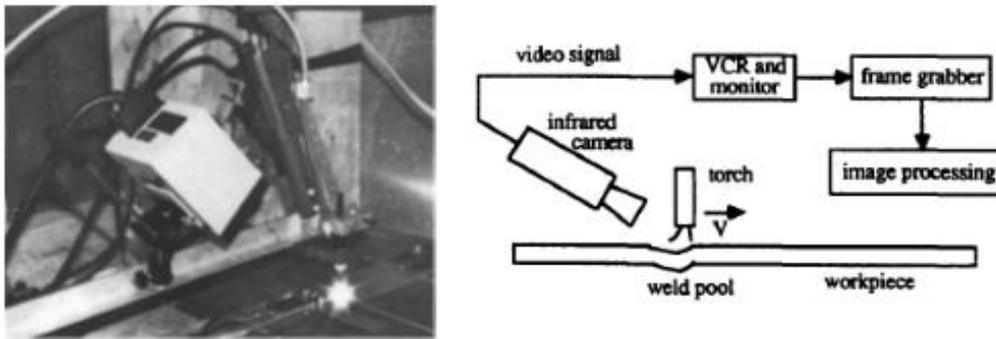
a) Experimental set-up for infrared sensing of GTA welding and Thermography sensing system (Beardsley 1993). The work is to illustrate the possible depression associated with the GTA weld pool, the work piece is shown by a cross section.
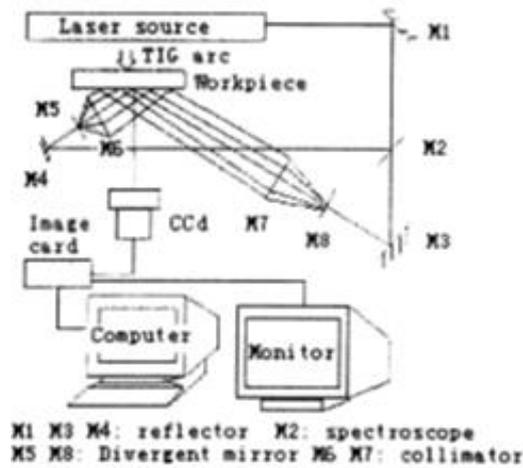
b) The diagram shows a method of thermally monitoring a TIG arc welding process, using Electronic Speckle Pattern Interferometry (ESPI) (Dongqing, 2003).
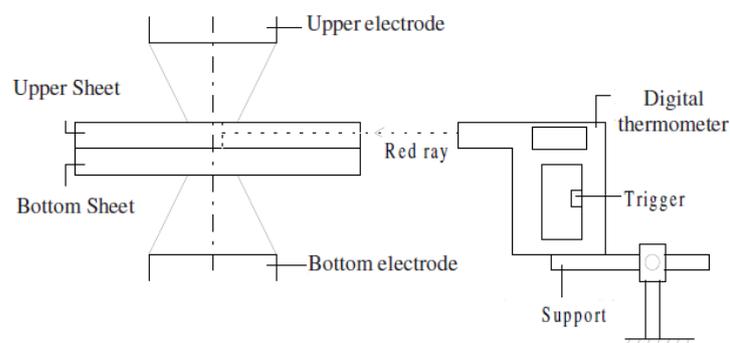
c) A schematic view of a digital thermometer that determined temperatures in the welding zone, it can measure three values per second & record results (Akkus 2008).

Figure 2.8 Temperature measurement/ monitoring techniques.

Due to advances in measuring devices and technology, various dynamic parameter-monitoring systems have been developed. In recent studies, new controller-based dynamic resistance monitoring systems have been introduced for in-process system environments such as automobile manufacturing lines. A method using a digital high-speed camera monitoring system was implemented. When a spot weld was created the relation between the mechanism of nugget formation and the corresponding process parameter was observed along with illumination heat transfer information (Cho, 2003). In resistance spot welding (RSW), work pieces are joined to each other by using pressure and heat. Heat is generated by the resistance to passage of current according to Joule's Law.

Temperature is the highest at contact surface between the work-pieces. The fusion is mainly happening within a confined volume connected to the work-piece of larger area exposed to ambient temperature, the cooling speed in RSW is very high. Fig 2.8 (c) shows the use of a digital thermometer in measuring the temperature of the welded joint between the electrodes (Akkus, 2008).

Thermocouples are the most widely used temperature sensors, which function by quantifying the change of the electrical resistance at the weld joint of two disimiliar metals with tempertaure changes (Childs, 2001; Drebushchak, 2009). In many cases, special mineral insulated (MI) thermocouples have to be used to avoid the electrical noise from contacts with the work-pieces (Zell *et al*, 2009). The manufacturing process of an insulated thermocouple involves tungsten inert gas (TIG) and capacitor discharge welding processes. The sensitivity and reliability of the product are directly associated with size, structure and integrity of the welded thermocouple joint (Venkatraman *et al*, 2007). However, quantitative understandings of the relationship between key welding parameters and dimensional attributes are very limited, mainly due to lack of research in this special area. This has limited the ability of the industry to develop new products of different size and shapes to meet the market demand. In addition, modern high volume production and remote wireless sensing technology also require the development of new approaches to monitor temperature, at locations where measurement probes cannot be directly placed, by using remote thermocouples combined with numerical modelling (e.g. finite element method) to predict the temperature at locations of interest.

The position of the thermocouple is critical for the accuracy and consistence of the measurement results. Thermocouples placed to intersect the stir zone region often are crushed

or displaced by the deforming material of the welding zone before reaching peak temperatures, thereby introducing uncertainties in measurement. In addition, thermocouples attached to the top surface of the work-piece close to the edge of the weld zone are often severed by extrusion of the flashing from under the electrode shoulder before reaching peak temperatures. To circumvent this problem, a feasible approach is to attach thermocouples to the work-piece in shallow grooves at several locations on the top and bottom surfaces as used in the study by Lienert (2003). This method allowed the flashing to slide over the top of the groove without disturbing the thermocouples. Tool and work-piece temperatures were further monitored using an Infrared System.

When studying the electro-thermal response of the weld and the nugget diameter change, it is very difficult to analyse the heat distribution of the faying interface since the welding is electrically and thermos-mechanically coupled. Research efforts have been made to predict cooling rates for a range of steel gauges welded with a number of automotive welding processes. These processes include Resistance Spot Welding (RSW), Resistance Mash Seam Welding (RMSeW), Laser Beam Welding (LBW), and Gas Metal Arc Welding (GMAW). Cooling rates are calculated using a range of analytical and numerical simulation methods. These results are then compared to critical cooling rates (for a martensite formation) (Gould, 2006). Thermocouples are conventionally used to measure temperature by placing the probe in direct contact with the component or materials. However, in many cases (as shown in Figure 2.9), this operation is not possible (Gonçalves *et al*, 2002; Ren *et al*, 2004; Gonçalves *et al*, 2005;). Typical examples include the cutting tool tip in a machining operation; the heat affected zones in a welding process; the cooling mould used in an injection moulding process. These challenging conditions have greatly limited the application of the thermocouple method. Recent development of inverse modelling has opened up the possibility of combining experimental and numerical modelling to predict the parameters, which previously could not be measured (Lawrence and Li, 1999; Al-Samhan and Darwish, 2003; Lindgren, 2004, Ren *et al*, 2004). As shown in Figure 2.9(a), Ren *et al* (2004) successfully applied the approach to predict the cutting tip temperature in machining welded hard facings. In the work, the thermocouple was placed between the cutting insert and the shim, and then the temperature of the tip was predicted by matching the numerical and experimental results. Moreira *et al* (2007) also used thermocouples to produce a temperature trace of gas metal arc welding. These could be potentially transferred to study the heat-affected zone (HAZ) of a spot welded joint to predict the temperature history using thin

thermocouples. As shown in Figure 2.9, Gonçalves *et al* (2005) uses ten thermocouples (type K) located (remotely) underneath a test plate, at the opposite face to the weld bead (heat source). The thermocouples were connected to a data acquisition system (DAS) to gain a greater understanding of the thermal history of the material. Based on the measurement from remote thermocouples, it is possible to predict the thermal history of the HAZ region. Direct temperature measurement is possible through inverse FE modelling in which FE modelling and inverse program is jointly used. Details of FE models and inverse programs are briefly presented in the next two sections.
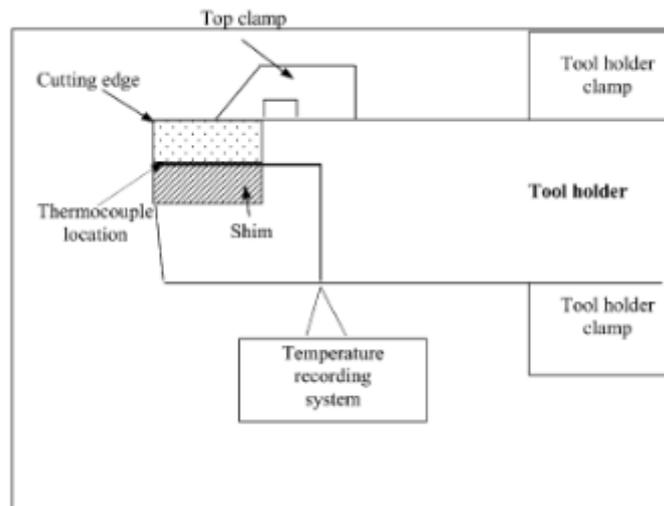
a) A schematic to show the set-up of the temperature measurement system to determine the thermal history of a machining tool. A remote thermocouple was placed at the interface between the tool insert and supporting shim. The results were coupled with FE modelling to provide the best solution (Ren et al, 2004).
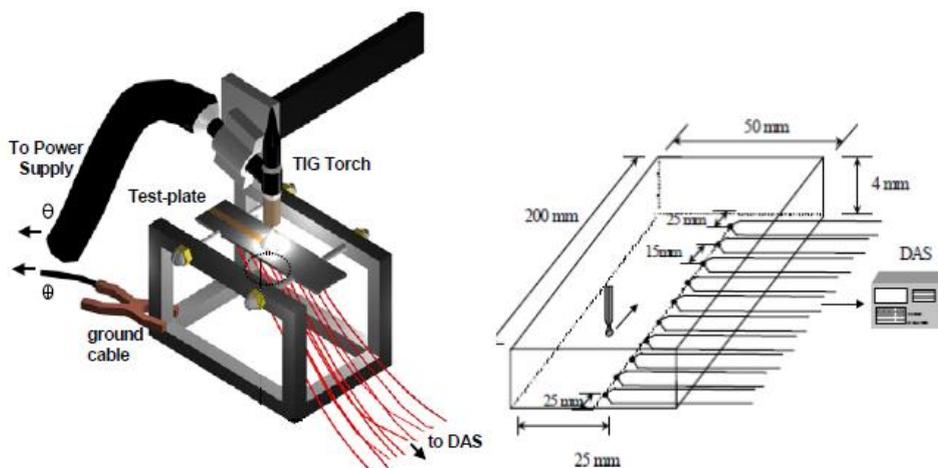
b) Experimental rig to monitor the temperature gas tungsten arc welding (GTAW).
   (Gonçalves 2002)

Figure 2.9 Remote temperature sensing and process control.

2.6 Inverse FE modelling method and application

As reviewed in the previous sections, many of the issues for spot welding can't be directly analysed or determined directly due to the complex nature and associated uncertainties. This situation may be improved by combining direct finite element analysis and inversed prediction programs. Finite Element methods are now widely used to solve structural, fluid, and multi-physics problems numerically (Fagan, 1992). Figure 2.10 is a breakdown of the finite element method.
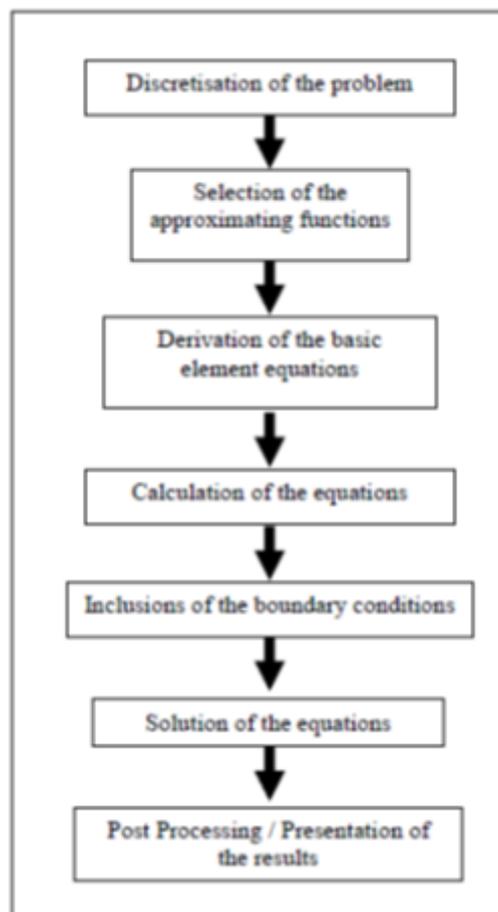
Figure 2.10 The main steps in a Finite modelling process.

The methods are used extensively by engineers and scientists who can mathematically model and numerically solve very complex problems. The analyses in engineering are mainly performed to assess designs. The analyses in the various scientific fields are carried out largely to obtain insight into (and ideally) predicting natural phenomena. The Finite Element approach involves dividing the continuum into Finite Elements which are small enough for the stress or displacement fields (or other physical parameters) to be approximated with displacements that are continuous and are in equilibrium, thus satisfying the problem's

boundary conditions. The approximation comes about when transforming the differential equation approach to an algebraic problem, wherein the building blocks or Finite Elements have all the complex equations solved for a simple shape. Once this is completed the problem is transformed to a linear algebraic relation and not a differential equation and can easily be solved with computers.

There are many different commercial packages available such as the ABAQUS, ANSYS etc. Modern computing allows large datasets to be analysed. With the aid of FE modelling, parameter estimation can be treated as one form of inverse problem of optimisation that deals with the determination of the system (mechanical, thermal, etc.) with unknown parameters such as material properties, geometry sources or boundary conditions, from the knowledge of response to given loading on its boundary (Neaupane and Sugimoto, 2003). With the improvement of FE packages in parameterising variables and flexibility in programming (details to be presented in section 2.8), the parameters can be in boundary, materials or dimensional parameters, or processing parameters (as shown in Figure 2.10). A successful program for predicting unknown parameters has to be accurate, efficient and robust and this depends on testing method/data used, inverse program, optimisation method etc.

Figure 2.11 shows a typical inverse modelling approach based on an interactive method (Meuwissen et al, 1998). This process involves interactively changing the measurable parameters in the FE models until the immeasurable predicted results match the experimental results. A user defined objective function is normally used to measure the optimality of the parameters until an acceptable fit between the simulated data and the experimental is reached. This approach has been used for different situations. (Kauer 2001; Bolzon et al, 2004; Gerard et al, 2005; Ren et al, 2006; Hendriks et al, 2009). In a material testing research, Ren et al (2006) used a parametric approach to determine the results from in vivo surface testing as shown in Figure 2.12. This work involved a two-staged approach using a rough range data first and then refines the parameter searching area. This method could effectively reduce the amount of computational works required but it has to be based on a good pre-knowledge of the material(s). As shown in the Figure, in a parametric based approach, the FE modelling is repeated with changing material parameters until an optimum combination of material properties is found. This approach required re-running the FE models during the optimisation process, which may take a large amount of time to reach the optimal solution without increasing the computational cost.
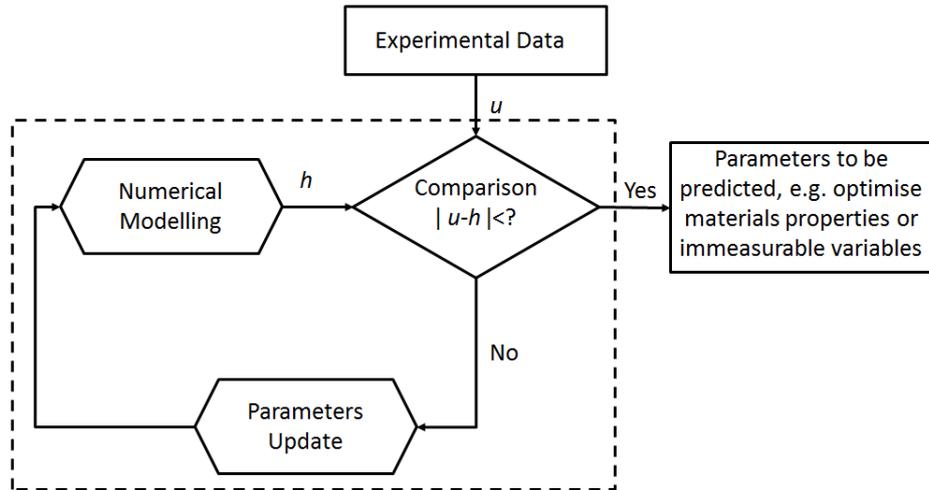
Figure 2.11 Block diagram to show the structure of a mixed numerical-experimental method (*u* denotes the observation of experiments, *h* is the output of the numerical/finite-element modelling) (Meuwissen et al, 1998).
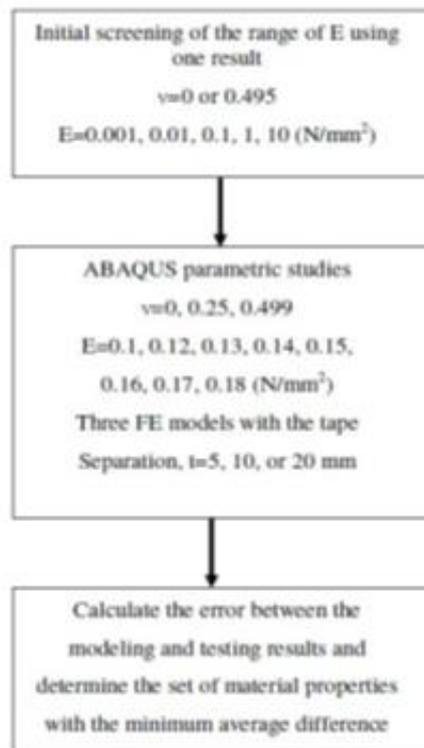
Figure 2.12 A typical parametric modelling approach to extract the material properties based on surface tension tests (Ren et al, 2006).

Another potential method being explored for materials characterisation is the Artificial Neural Networks (ANN) method (Zaw et al, 2009; Esfahani et al, 2009). ANN method is

known to be able to deal with complex problems, with multiple parameters, which is normally the case for material processing parameters characterisation. Zaw et al (2009) has used a rapid inverse analysis ANN approach to identify the ''unknown'' elastic modulus (Young's modulus) of the interfacial tissue between a dental implant and the surrounding bones. In 2009, Esfahani et al presented an Artificial Neural Network to model the influences of chemical composition and process features on the yield strength of hot strip steels, in which the ANN prediction showed good agreements with experimental data. Neural networks find their origin in biological science. However, the basis of that has been extended to artificial neural networks, which is the general terminology used to describe the mathematical models. A number of studies have shown the benefits of this approach for studying welding processes (Lightfoot, 2005). The ANN method can be particularly useful for spot welding in order to characterise the HAZ thermal history of a spot welded joint if the temperature of zone close to the welding zone can be reliably measured, despite the uncertainties of the heating source. Details of each approach is presented in the next section.

2.7 Artificial Neural Network (ANN) and its applications

Artificial Neural Network (ANN) is a non-linear mapping structure based on the function of the brain (Lek and Guegan, 1999) as shown in Figure 2.13 (a). The parallelism of the biological neural system provides an extremely high speed of execution of different tasks and processes. The scalar input 'p' is transmitted through a connection that multiplies its strength by the scalar weight 'w' to form the product 'wp', again a scalar. Here the weighted input 'wp' is the only argument of the transfer function 'f', which produces the scalar output 'a'. The neuron has a scalar bias, 'b'. The bias is simply being added to the product 'wp' as shown by the summing junction or as shifting the function 'f' to the left by an amount 'b'. The bias is much like a weight, except that it has a constant input of 1.

One important factor for an effective ANN is the transfer/activation function. A hard limit transfer function is restricted to Boolean operations and, as such, the output (denote by 'a') activation can only be zero or one. Linear transfer functions cannot perform non-linear computations, but often find use in the output layer of networks designed to solve non-linear problems, since the activation value is unlimited. Sigmoid functions are commonly used in neural networks which requires solving non-linear problems and addressing the limitations of

both the hard limit and linear activation functions and typically passing output value between 0 and +1 or -1 and +1.

One type of ANN is unsupervised learning, which is often used to perform clustering as the unsupervised classification of objects without providing information about the actual classes. Figure 2.13 (a) shows a typical unsupervised learning network: Kohonen SOMs (self organising mapping) commonly used for ecological modelling (Lek and Guegan, 1999). In this process, the desired response is not known; thus, explicit error information cannot be used to improve network behaviour. Since no information is available as to correctness or incorrectness of responses, learning must somehow be accomplished based on observations of responses to inputs containing limited knowledge. For example, unsupervised learning can easily result in finding the boundary between classes of input patterns distributed. Apparent, this approach will not be suitable for materials parameters indentation based on the indentation test as the problem to be studied in this work.

Another type of ANN is supervised network. Figure 2.13 (b) schematically shows a typical supervised learning network based on a multilayer feed-forward neural network (Pal et al, 2008). The structure of a feed-forward neural network is often considered in terms of its layers. As shown on the left-hand side of the diagram, there are a number of inputs that are considered to be fully connected, i.e. every node in the previous layer is connected to each node in the next layer. The "output" is that which takes its inputs from a preceding hidden layer of neurons and outputs its result to the environment. The notion of information propagating through layers from the inputs through to the outputs (strictly in this direction only) gives this structure the name "feed-forward network". The number of hidden layers is not limited to one and it is possible to have multiple hidden layers of neurons. However, it has been proven that, if the input to the function to which one is trying to approximate definitive bounds, a network with a single hidden-layer can successfully learn it (Rummelhart et al,1986; Lippman, 1987). One advantage of single layered system is the lower computing time than a multiple hidden layered system.

Some research studies have been made in which ANN have been applied to predict desirable outputs in welding processes. Using the MATLAB Artificial Neural Network program Martin (2006) was able to classify resistance spot welds in several quality levels through their respective ultrasonic oscillograms. In thermocouples there is a nonlinear relationship between the thermal voltage of the output and the temperature, the output signal must be rectified with

nonlinear rectification circuit in hardware. An artificial neural network was successfully implemented to predict the relationship with thermal voltage and temperature (Zhe-Ying, 2003).
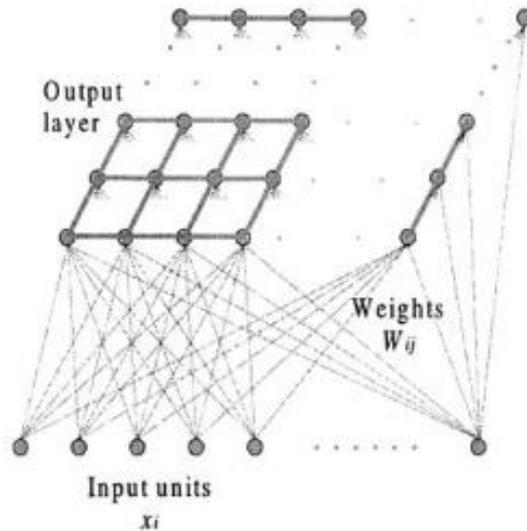
(a) A typical unsupervised learning network: Kohonen SOMs (Self-Organizing Maps) for ecological modelling (Leket al, 1999)
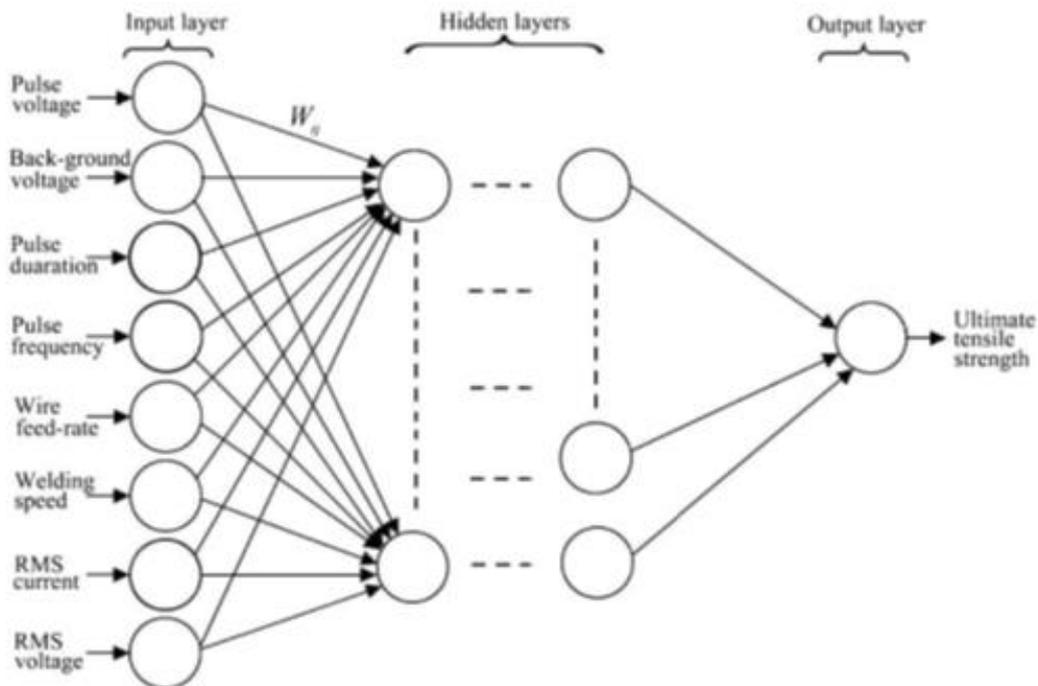
(b) A typical supervised learning networks of a multilayer feed-forward neural network for weld joint strength prediction (Pal et al, 2008).

Figure 2.13 Artificial Neural Network (ANN) non-linear mapping structures based on the function of the brain (Lek and Guegan, 1999)

The simplest idea of optimization based on numerical models is using randomly generated design variables. It is a simple way but requires a large number of analyses and is effective only when the dimension of solution space is small. It is advantageous to use tools, which can infer based on a finite number of analyses results and propose a candidate solution instead of randomly. Such a tool should find relation between optimized parameters and objective function value. In cases of more time-consuming analyses, an option with the use of neural network as an estimation tool is available (Szajek, et al, 2008).

2.8 Python script application and development

2.8.1 Programming Language Comparison

Many disciplines (if not most) of science now routinely use and develop software as part of the research. Software development systems have been designed to aid the software engineering process, of which writing the original code is an integral part. All software starts with some source code written in a file or storage system (Koranne, 2011).

Computational modelling can be time consuming when investigating variations of a model and its conditions. To optimise this process, programming language scripts are used to generate models and analyse data. There are numerous programming languages available to use to create scripts, such as, Perl, Python, Rexx, Tcl, C, C++, Java and Fortran. Each programming language can perform differently regarding, run time, memory consumption, source text length, comment density, program structure, reliability, and the amount of effort required for writing them. A specific programming language is selected based on the model, analysis task requirements and the most critical programming properties of the language (Prechelt, 2000). Figure 2.14 shows charts comparing different languages depicting examples of typical times taken to write scripts, the length of codes and the memory required.

Dwarampudi, et al (2010) discussed a comparison of numerous languages, including; Java, Scala, C++, Haskell, VB.NET, AspectJ, Perl, Ruby, PHP and Scheme, in an effort to realise the edge of one language over another one. The paper concluded that specific languages should be selected relevant to the required application, as all of the languages are useful and have their own qualities as expressed in tables in Figure 2.14.
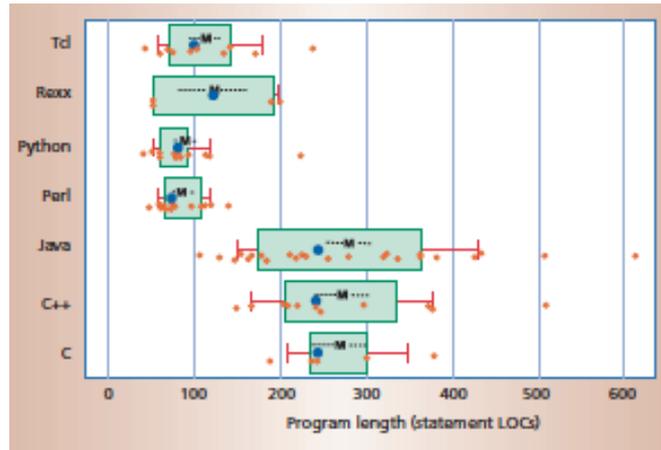
Figure 2.14 (a) Program length, measured in Lines of Code (LOC)
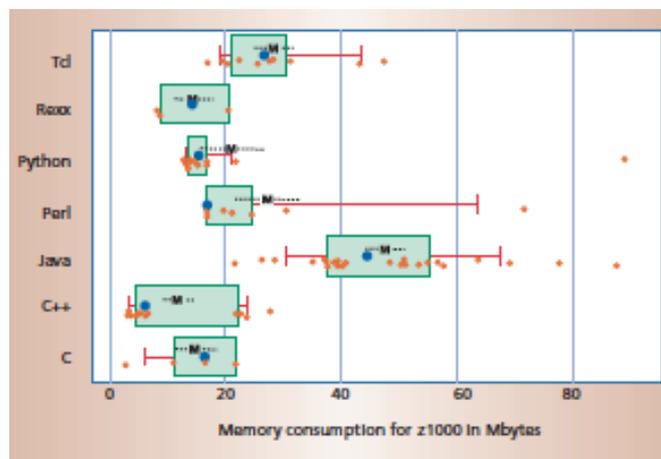
Figure 2.14 (b) Amount of memory the program required.
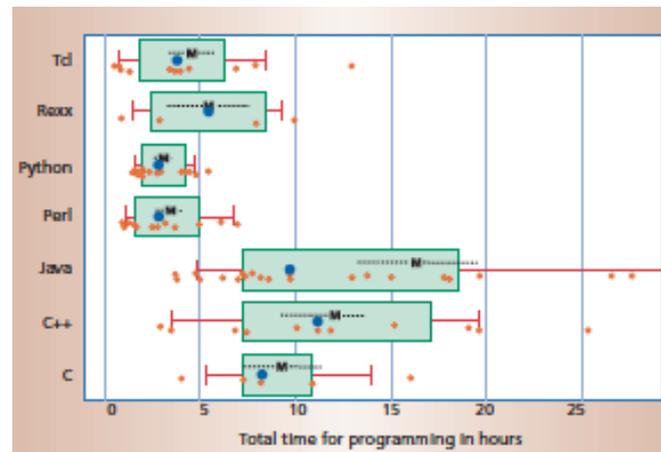
Figure 2.14 (c) Time taken to generate script (Prechelt, 2000)

Python excels in the areas of rapid prototyping, gluing, graphical user interfaces and networking among others. By combining Python with other languages, one can obtain fast development and fast execution as shown in Figure 2.15 (Seberino, 2000).

There is a strong tradition among computational scientists to use compiled languages, in particular Fortran 77 and C, for numerical simulation. Demand for increased software flexibility during the last decade has also popularised the more advanced compiled languages C++ and Fortran 95. However, in recent years many computational scientists and engineers have moved away from compiled languages to interpreted problem solving environments, such as Matlab, Maple, Octave, and R (or S-Plus). The programming language Python is now emerging as a potentially competitive alternative to Matlab, Octave, and other similar environments (Cai, 2005)

	FORTRAN	C	C++	JAVA	PERL	PYTHON
COMPACTNESS	√	√				√
HIGH LEVEL DATA STRUCTURES		√	√	√		√
AUTOMATIC PORTABILITY			√	√	√	
TYPE & RUN DEVELOPMENT				√	√	
GARBAGE COLLECTION			√	√	√	
RUN TIME ERROR CHECKING			√	√	√	
DYNAMIC TYPING				√	√	
EXTENSIBILITY		√	√	√	√	√

Figure 2.15 (a) Chart shows features applicable to specific languages (Fortan, C, C++, Java, Perl and Python) (Seberino, 2000)

Criteria/PL	Java	Scala	C++	Haskell	VB .NET
Default more secure programming practices	Good secure programming features with GC, no pointers, packages and threads.	Good Default Security with features like GC, Exception handling & works on JVM so uses its Security Manager	not a secure programming language, buffer overflow is not detected.	Good secure programming features with a GC, no pointers and good type system	Built-in secure features provided by .net and programming itself can implement secure features
Web Applications	Quite popular for web applications. Abundant libraries and servlets serve this cause.	Can develop flexible, highly scalable, secure applications with help of web development frameworks	Used for standalone applications, difficult to create by default.	Can develop we applications with rich set libraries.	Vb.net supports web applications
Web Services Design and Composition	Good for web services because of portability and large number of APIs for XML available.	RESTful services provided with help of frameworks. Provision of other services still under construction. XML processing simple	Supports REST,XML, WSO2 frame work	Provides services like SOAP and REST but is still immature in terms of WSDL and UDDI.	Vb.net can implement web services such as HTTP,SOAP, XML. , WSDL. , UDDI and .Net remoting service can implement it self
Object-Oriented based Abstraction	Primarily an object oriented language with powerful features.	Supports 2 types of abstraction .Alternative to functional abstraction. Mainly used for modeling families that vary covariantly	Supports Object Oriented principles but not as a default.	Object-Oriented Concepts are not supported by Haskell. It requires an extension called OOHaskell.	Vb.net is an object oriented language .It supports OO abstraction.
Reflection	Powerful reflection mechanism. Supplies a rich set of operations for using metadata and avoids complications.	Its a subsystem, Reflection API .Limited scope.Modular, hence reduce foot-print & be efficient	Limited reflection capabilities.	Haskell do have libraries for dynamics, but they still do not support complete reflection.	Vb.net supports reflection using built-in called "system.reflection"
Aspect-Oriented Programming	AspectJ, an extension to Java treats AOP concepts as first-class elements of the language.	Provides 2 different types.Mainly, Mixin composition stacks	With static type of language it is difficult , AspectC++ supports it	Does not directly support. Has an extension called AOP Haskell.	Aop Engine in .NET to implement AOP programming but it supports only at run time
Functional Programming	No functions.Instead, using interfaces & inner classes it is fairly easy to mimic some features of FP.	Powerful Support and well suited. Light-weight syntax. Supports High-order, nested functions, and currying	Doesn't support to fuller extent but can be done using FC++	This is a functional programming language.	Vb.net is not a pure functional programming but it supports Lambda calculus
Declarative Programming	Libraries like JSetL and JSolver offer a number of facilities to support DP.	Uses a Prolog interpreter called ScalaLogic. Emphasises on Simplicity and not performance	By default not possible but merging prolog is an alternative.	Haskell, one can use Monards to implement Declarative/ Logic programming.	Doesn't implement declarative programming by itself
Batch Scripting	Easy, involves the use of two Java classes, the Runtime class and the Process class.	Supports Batch/Bash/Perl scripting. Used as real scripting language	Including libraries allows to do so. But decreases performance.	Shell Scripting is possible with Haskell using HSH.	Vb.net supports batch scripting and macros
UI prototype design	Rich set of libraries for UI applications but the code is verbose and can be mysterious for stakeholders.	Supports UI with basis on Java swing framework but hides much of its complexity	Difficult to implement by default but supports some libraries.	Has rich set of libraries for GUI applications.	vb.net supports rich UI interfaces and IDE give good support to programmer.

Figure 2.15 (b), Detailed chart showing the depth of the features applicable to Java, Scala, C++, Haskell and VB.Net languages (Seberino, 2000)

Criteria/PL	AspectJ	PHP	Ruby	Perl	Scheme
Default more secure programming practices	It capture the returned values of methods in both the execution and method invocation. It implements execution handling itself.	Insecure, weakly typed language. No input validation, etc Security provided with help of few frameworks, currently.	secure, dynamic and has GC. No pointers, Exception handling.	Has no proper GC mechanism, has no pointers but references and no type system hence, one cannot safely code.	Less pros and more cons. Problems with types, records, threads, etc.
Web Applications	It supports web applications by proving secure features during transactions	Excellent features. Dynamic easy less code required. Can be embedded into HTML	Using Rails, supports for fast and secure applications	Has excellent features for web application development.	Powerful features for web development but fewer libraries than mainstream.
Web Services Design and Composition	AspectJ supports web services such as AXIS but doesn't support all features by itself.	Good choice for web services Provides SOAP support inbuilt in PHP5.Supports REST,WS-*	Supports many frame works as it is a flexible language.	Is indeed a good choice for this as it has almost all the features.	PLT Scheme has good web services support.
Object-Oriented based Abstraction	It supports OO Abstraction	Not ideal for OO-based abstraction, but has a clear and simple implementation	By default it is object oriented language and supports abstraction.	Has a straight forward implementation.	Closures can be used to capture object state. But the code is verbose with obvious redundancy.
Reflection	It can implement Reflection using " "org.aspectj.lang.reflect.*"	Implemented using standard included Reflection API	Supports reflection programming.	has good reflection mechanisms.	Homoiconic language; can meta program during runtime.
Aspect-Oriented Programming	AspectJ itself is an AOP programming. It can support at static and dynamic time.	Supported using Libraries. Aspects are statically weaved. Dynamics weaving is possible using extensions	Supports AOP and can be done with Aspect Ruby	Has a straight implementation with a built in package called Aspect.	Continuation marks and language-defining macros help in implementing AOP in Scheme.
Functional Programming	AspectJ implement a profiler that records statistics concerning the number of calls to each method.	Supports but its functional calls are verbose. Few FP primitives introduced to improve	Supports but doesn't force to do it.	Some support with the help of References and Closures.	Primarily a functional programming language.
Declarative Programming	It supports declarative programming using Annotations	Do not support by default. Uses lesser known technique of Annotations and has considerable limitations	By default not possible merging prolog is an alternative	Perl has many limitations when it comes to Declarative / Logic programming.	Capable of doing declarative programming. Schelog and Kanren serve this cause.
Batch Scripting	It doesn't support itself	Supports but with limited advantage. Must be compiled as a CGI binary	Supports scripting.	It is a scripting language and is well suited for this.	Some Schemes allow to define Unix-style scripts containing Scheme code
UI prototype design	It increases UI performance such as fast response of UI	Basic version does not support. Implemented using supporting frameworks	Very easy to implement.	Has rich set of libraries for GUI applications.	Good for UI applications. Syntax is consistent and easy for stakeholders.

Figure 2.15 (c) Detailed chart showing the depth of the features applicable to AspectJ, PHP, Ruby, Perl and Scheme languages (Seberino, 2000)

2.8.2 Application of Python program in engineering modelling

Python was created in the early 1990s by Guido van Rossum at Stichting Mathematisch Centrum (CWI) in the Netherlands as a successor of a language called ABC (Rossum, 2003). Python is a general purpose programming language; some features of Python are especially suited for high-performance scientific computing and solving engineering problems (Koranne, 2011).

In computer science, the versatility of Python language has a strong and steadily increasing position as a general-purpose programming tool for diverse areas such as system administration, dynamic Websites, distributed systems, software engineering, graphical user interfaces, computational steering, search engines (Google in particular), network communication, education, and even large-scale business applications. Cai, et al (2005) researched the computational efficiency of the Python programming language. The results obtained suggested that future scientific computing applications should be created using Python, with its clean and simple syntax, its high-level statements, its numerous library modules, its vectorization capabilities, and its bindings to MPI, can be used in large portions

of an application where performance is not first priority or when vectorised expressions are sufficient. This will lead to shorter and more flexible code, which is easier to read, maintain, and extend.

A particular advantage of Python is that the language is very rich and powerful, especially in comparison with Matlab, Fortran, and C. In particular, Python is an interpreted object-oriented language that supports operator overloading and offers a cross-platform interface to operator system functionality. Another advantage of Python is that interfacing legacy software written in Fortran, C, and C++ is much simpler than in most other environments. This is because Python was designed to be extendible with compiled code for efficiency, and several tools are available to ease the integration of Python and compiled code. (Cai, 2005).

Python is a modern, interpreted, object-oriented, open-source language used in all kinds of software engineering. Though it has been around for two decades, it exploded into use in the atmospheric sciences just a few years ago after the development community converged upon the standard scientific packages (e.g., array handling) needed for atmospheric sciences work. Python is now a robust integration platform for all kinds of atmospheric sciences work, from data analysis to distributed computing, and graphical user interfaces to geographical information systems. Among its salient features, Python has a concise but natural syntax for both arrays and non-arrays, making programs exceedingly clear and easy to read; as the saying goes, "Python is executable pseudocode." Also, because the language is interpreted, development is much easier; you do not have to spend extra time manipulating a compiler and linker. In addition, the modern data structures and object-oriented nature of the language makes Python code more robust and less brittle. Finally, Python's open-source pedigree, aided by a large user and developer base in industry as well as the sciences, means that your programs can take advantage of the tens of thousands of Python packages that exist. These include visualization, numerical libraries, interconnection with compiled and other languages, memory caching, Web services, mobile and desktop graphical user interface programming, and others.

Python has real disadvantages, including the fact that pure Python code runs much slower than compiled code, there are fewer scientific libraries compared to Fortran, and documentation and support for new science users is relatively sparse. There are tools to overcome the speed penalty, the collection of scientific libraries is growing, and science support resources are becoming more robust. For most Earth science applications, the

strengths of Python outweigh the weaknesses.

The Earth sciences community has begun to recognize the unique benefits of Python, and as a result its population of users is growing. Adoption of Python by Earth sciences users is no longer confined to "early adopters." Institutional support includes groups at Lawrence Livermore National Laboratory's Program for Climate Model Diagnosis and Intercomparison, NCAR's Computer Information Systems Laboratory, and the British Atmospheric Data Centre (Lin, 2012)

2.8.3 Graphical User Interface (GUI) technologies

2.8.3.1 Command Prompt Kernel Scripts

Generating models manually is primitive and time consuming method, from drawing points, lines, polygons, and adding detailed sections, to abstraction for user input (including keyboard and mouse). Script based language can be used to generate models without graphical representation, making processing more efficient, and placing little demands on the computer (CPU and memory).

The interactive operation between ABAQUS\CAE and Python script: The interactive operation likes following: From top down, PDE interpreter compile and run the Python Script from GUI, commander line or the starting interface, and then build ".rpy" file and "Input" file by transferring the kernel of ABAQUS. At last, ABAQUS will run the "Input" file and build the output database.

The way to access module: When doing an analysis using ABAQUS, the ".rpy" file will record each step in Python, and the different objects will be used to record different modules. For example the "odb…" represents Output database module. When visiting one module, you should abide the hierarchy strictly. For example, you should import "odb.steps.historyRegions.point[i]" if you want to know the history output database on one point (Lou et al, 2011).

The Parametric Parameters can be obtained from the ".rpy" file after you have done the modelling and analysis process. The whole process is without the restart of ABAQUS, this point can save a lot of computational resource. At the beginning of the analysis, users should input the basic parameters (initial crossover probability and so on) through an interface, then click "OK" to start the analysis. The output will be shown on the main interface of ABAQUS.

Szajek, et al (2008) implemented an optimisation procedure with the use of Python scripting language and artificial Neural Networks. The FE model, numerical analysis and post-processing of results were performed with the use of the Abaqus Unified FEA product suite from SIMULIA. The integration of NN libraries with FE tools was done by using the Abaqus Scripting Interface (ASI). The procedure of FE model building during the optimisation process is shown in Figure 2.16.
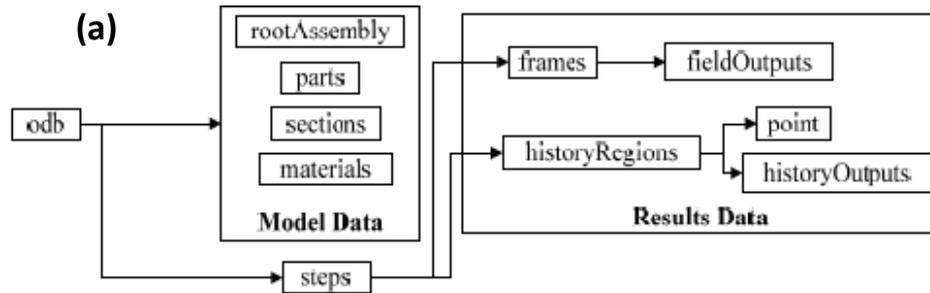
Figure 2.16 a) The intact visiting ways in Output database module (Lou, et al 2011)
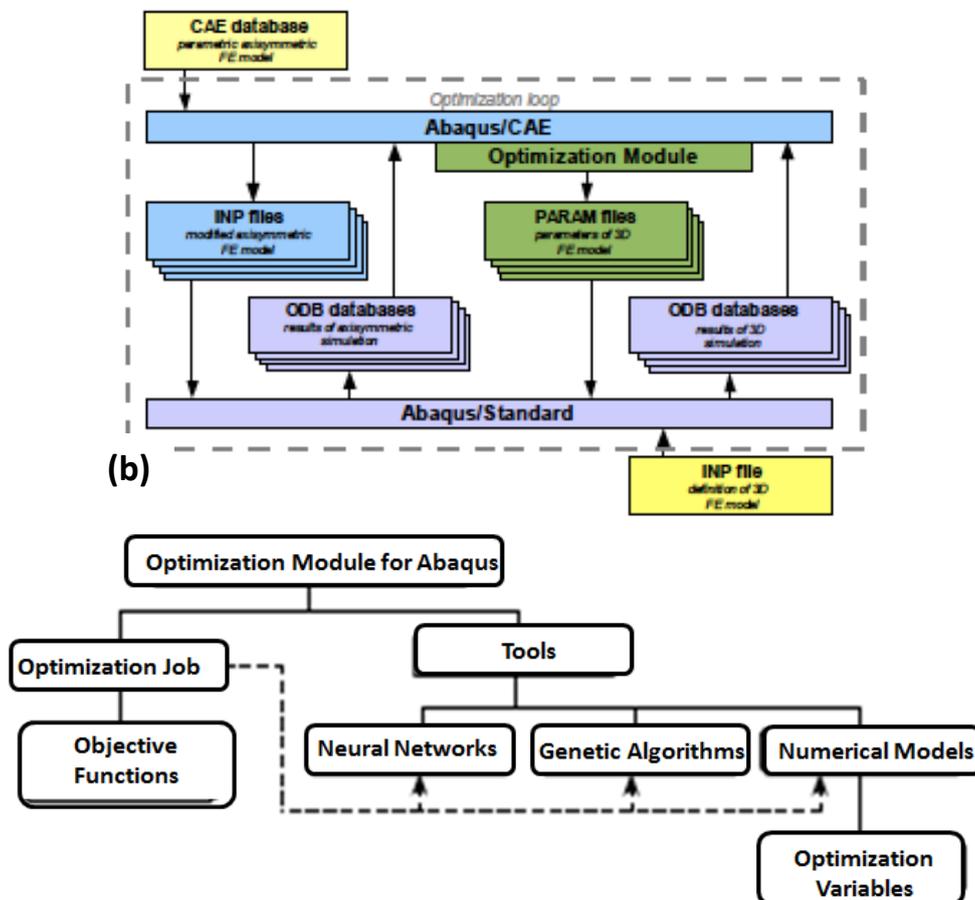
Figure 2.16 b) The procedure of FE model building during optimization (Szajek, et al 2008)

2.8.3.2 Modelling tool plug-in

Information visualization is an important part of any software system, since an image can transmit and convey a large amount of information. In some domains (such as robotics), and computational geometry, visualization can lead to insights into problems, which otherwise would be difficult.

While it is true that most high-performance computing environments have excellent batch processing capabilities, more and more users are demanding a graphical user interface (GUI) front-end (at least to ease in the transition to new features or tools).

Koranne, *et al* (2011) discuss the use of Graphical User Interfaces (GUI). Designing user interfaces by compositing widgets by hand gets tedious and time consuming, thus most widget systems have developed GUI tools to design GUIs. Two examples of GUI's are, GNU Image Manipulation Program (GIMP) Toolkit (GTK), Figure 2.17 (a) and Nokia/Trolltech's Qt application, Figure 2.17 (b). The GUIs provides cross-platform widget toolkits for designing and implementing graphical user interfaces (GUI), meaning that the same source code can be compiled on UNIX, GNU/Linux, Microsoft Windows, Apple Mac OS X, even embedded Linux. GTK and Qt are object oriented (OO) widget toolkits written in the C programming language but program bindings exist for many other programming languages, including but not limited to, C++, Python, and Java. The OO is implemented using the GLib object system (GObject). Parametric studies can benefit from widget toolkits, where multiple simulations are required, exploring variations of conditions in order to accumulate a range of results that provide sufficient data.

By creating a Graphical User Interface (GUI) via a plug-in it will allow the user to input all analysis information in an intuitive way within the familiar simulation software environment. This plug-in will take the information from the user and use it to automatically configure both the subroutines and the model itself so that an analysis can be performed. This automation removes many of the sources of error possible in previous incarnations of the method, whilst at the same time providing a more convenient and faster way. Using a single procedure, allowing much of the required data to be input using a simple text file rather than changes to the code itself.

Finite Element package ABAQUS/CAE has an application called GUI Toolkit. This widget toolkit has been widely used in parametric research studies. Winkler et al (2005) created plug-ins to generate spur and worm gear models. Figure 2.18 show the plug-in created and

the variable input data used to generate parametric gear models. Ure et al (2012) used the GUI Toolkit to develop a plug-in for EDF Energy in the Nuclear industry. The plug-in was able to generate multiple models based on data accumulated from a Linear Matching Method (LMM) developed as a tool to assess the structural integrity of components subjected to cyclic loading conditions.
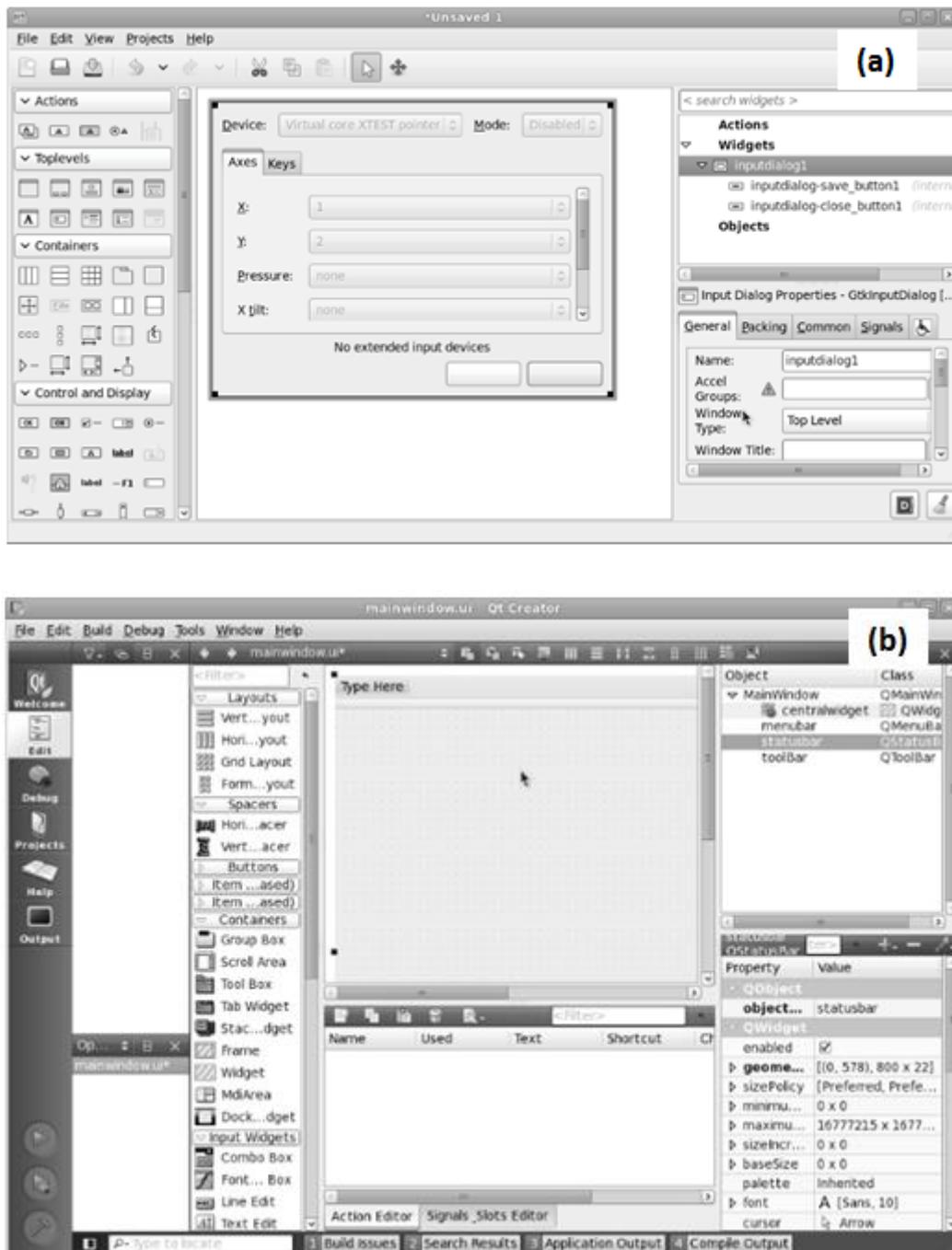
Figure 2.17: User interface designer for GTK **(a)** and Qt **(b)**
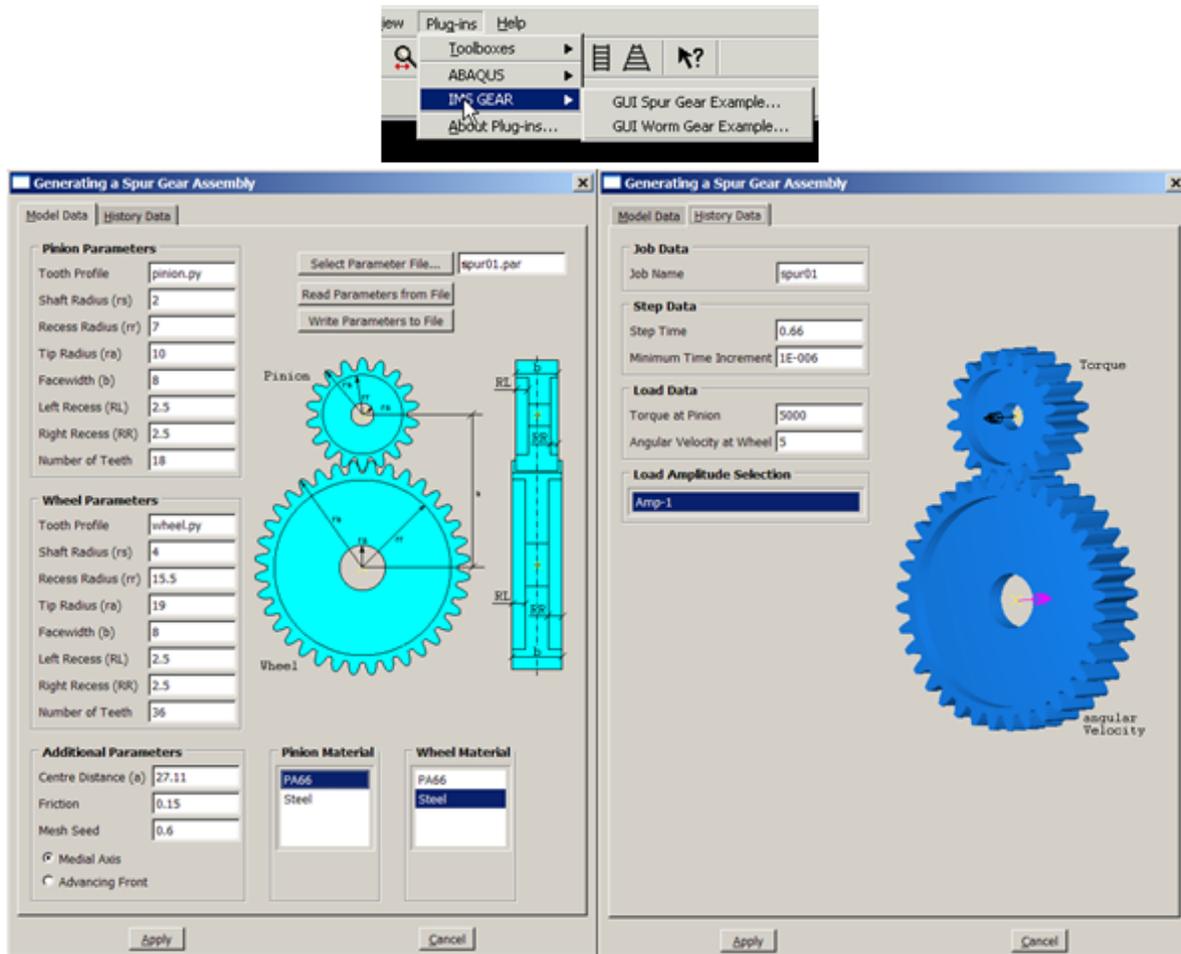
Figure 2.18: ABAQUS CAE Plug-in toolkit, used by Winker, et al (2005) to generate gear models

2.9 Challenges in modelling and analysis of resistance spot welded joints

As reviewed in this chapter, spot welded joints are formed by a complex thermal and mechanical process, resulting in complex material structures and properties. This made the prediction and modelling of the thermal and mechanical behaviour of spot welded joints very difficult. With the increasing use of spot welded joints, an automatic interface tool could effectively standardise the modelling process incorporating complex material properties and structures balancing the effectiveness and efficiency of the program. In addition, for industries, a formal user friendly interface program is also an important contribution in digital manufacturing.

One key feature which needs to be considered is the fusion zones and the HAZ zones, both made the building of an FE model and the subsequent meshing process a complex process. A parametric program would make the modelling process much easier for research or product

development. Another factor which needs to be considered is to develop a module based on the detailed model of the spot-welded joints for different testing modes. For example, for electrical resistance spot-welded joints, a series of tests need to be conducted. A program to automatically simulate the mechanical behaviour of spot welded joints will make the process much more efficient. This can be a challenge. For example, different fracture models need to be incorporated for different fracture modes. For example, for tensile-shear test, the process is normally controlled by void formation based fracture model; while for nugget pull-out modelling, cohesive model could be used. In addition, the model also could consider fatigue or creep modelling as a research and material development tool. For other forms of sport welded joints, such as thermocouples formed by welding of dissimiliar metals, a detailed parametric model is also required for simulating the thermal response in both heating and cooling processes.

The thermal history of resistance spot welding is one of most important characteristics of the process, as it has a direct effect on the resultant microstructure and properties. Among the different zones of the spot welded joint, the HAZ zone is the most crucial part for the structural integrity and loading bearing capacity. Direct measurement of the temperature at the HAZ zone is not feasible due to setup of the welding process. One potential approach is to use the remote thermocouple method to measure the temperature at locations with fixed distance from the welding zones, then inversely predict the temperature at the HAZ. The most critical temperature change is the cooling process as the phase change is mainly dependant on the critical cooling temperature. Given the complex multi parameters nature, ANN represents a more feasible approach than other inverse modelling approaches. However, there are many factors that needed to be investigated. One is the robustness of the measurement and the inverse prediction process as in some case, the measure has to be able to provide sensitive data which allows the prediction of the temperature. FE modelling of the spot welded joint is a challenging process, requiring dimensional, mechanical, thermal and electrical properties. A proper program incorporating all the parameters will help us to understand the nugget formation, electrode penetration, distortion and residual stresses required. A fully validated model will be able to be used to predict the HAZ temperature change and it will allow the use of dummy samples for making large scale samples for material testing and characterisation. It will also be able to provide a guideline for process optimisation and monitoring.

This review has identified the gaps that have formed the basis of this research, as outlined in the thesis structure diagram (Figure 1.1)

CHAPTER 3

Development of Plug-in Interface Program for Mechanical Modelling of Electrical Resistance Spot Welded Joints

3.1 Introduction

As listed in the research structures (Figure 1.11), mechanical behaviour is an important part. This chapter presents the key findings on the development of optimised approach for modelling mechanical testing of spot welded joints. Using the flow diagram this chapter focuses on the mechanical properties and structure of the welds. To develop parametric programs in the form user interfaces, using Python scripts and Abaqus plug-ins. Then apply the methodology to mechanical modelling of electrical resistance spot welded joints.

In this chapter, a systematic/automatic FE modelling program of spot welded joints has been designed and developed in the form of ABAQUS Plug-in developed in Python. The program created consists of the key welding and material zones including the nugget, heat affect zones and the base. The program consists of geometry modules, materials modules, loading and boundary conditions and post processing. In the geometry module, a sequential cut and merging approach has been developed in order to model the nugget and HAZ with different zones suitable for different situations. In the material module, detailed material property has been developed including elastic-plastic behaviour and fracture models. The post processing module not only able to extract the typical outcome such as, force-displacement data, it is also able to extract the stress and strain relative to fracture, and fatigue analysis. The modelling results have been compared to experimental and show a good agreement. The plug-in program is then used to study the effect of the key dimensional and material properties of different welding zones on the elastic-plastic and fracture behaviour of the spot welded joints.

As shown in Figure 3.1, this chapter consists of three main parts. In the first section, the detailed design concept and the procedure in developing and evaluating the Abaqus Plug-in program is presented. Initially a plug-in was created for a single spot welded plate model with detailed HAZ and nugget. The second part highlights key features, the structure of the python and key functional blocks. The results are focused on the tensile shear tests but are transferable to other forms of testing or conditions. Tensile shear testing is where two joined plates are pulled apart until mechanical failure, to determine the tensile strength property of joint. One plate placed into a fixed position clamp (free from all degrees of movement), the other plate is then secured into a clamp that moves in the same plane, laterally along the length of the work-piece. A linear load is applied to pull the work piece apart. The results are given in force-displacement data. This type of testing is synonymous with mechanical testing

of welds in construction, automotive, aerospace, nuclear, oil and gas industries. The reason for performing this type of testing is to ensure equipment and structures installed are fit for purpose and intended use. A safety factor (for safe working load) would be given depending on the results of the tensile test. The comparison between FE modelling and experimental work is presented, then the model is used to study the effect of key dimensional fracture such as, thickness and nugget size on force-displacement data, fracture, and stress-stain in the key zones such as, the nugget, and HAZ zones. Finally the future of the plug-in in different conditions is discussed in detail.

```
┌─────────────────────────────────────┐
│           Plug-in Design            │
└─────────────────────────────────────┘
                  ⇩
┌─────────────────────────────────────┐
│ Plug-in for a single plate spot welded model with detailed │
│              HAZ and nugget          │
└─────────────────────────────────────┘
                  ⇩
┌─────────────────────────────────────┐
│ Program for assembly of two plates for tensile-shear │
│                 testing              │
└─────────────────────────────────────┘
                  ⇩
┌─────────────────────────────────────┐
│      Comparison of FE results with   │
│              experiment              │
└─────────────────────────────────────┘
                  ⇩
┌─────────────────────────────────────┐
│ Systematic investigation of the effects of sheet │
│          thickness and nugget size   │
└─────────────────────────────────────┘
                  ⇩
┌─────────────────────────────────────┐
│      Link between stress and fracture │
└─────────────────────────────────────┘
```
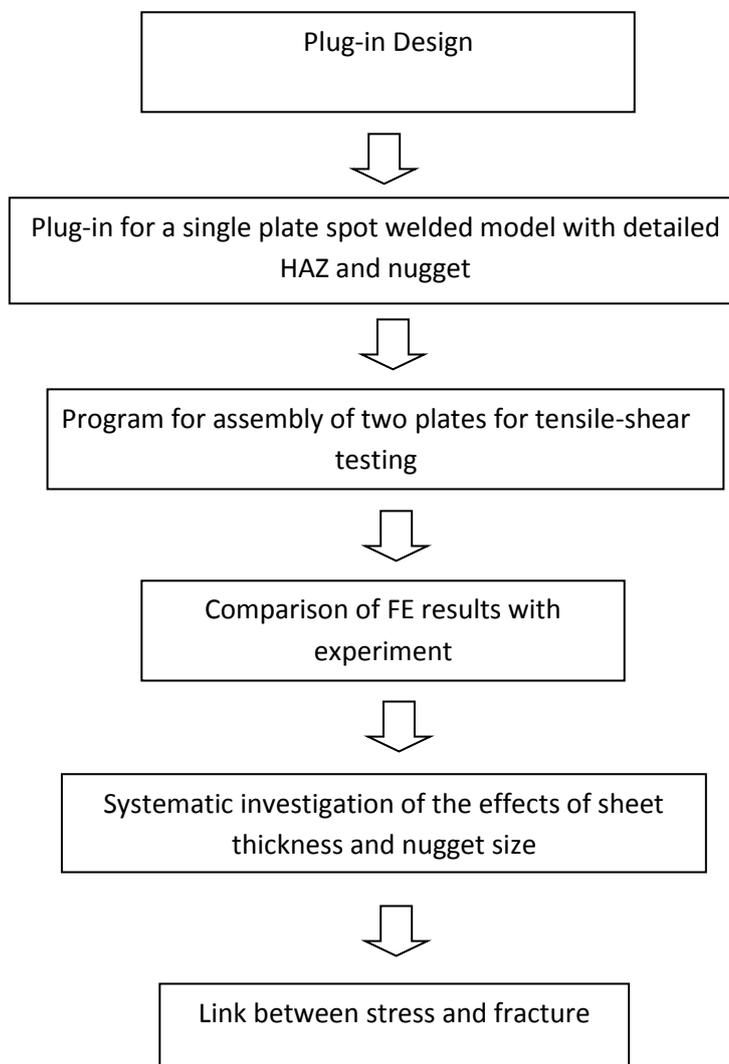
Figure 3.1 Flow Chart Showing the Main Work

3.2 Key components/ focus of the plug-in program for modelling spot welded joints.

3.2.1 Main factors and design concepts of Abaqus plug-in.

Figure 3.2 details the key components of a plug-in interface specifically for mechanical modelling of welded plates. It is also able to be used in thermal analysis and heat transfer process, the results are to be presented in chapter 6. There are many items to consider when designing a plug-in for mechanical modelling. Listed in the concept are issues that need to be considered in the process of developing an interface that can produce variations of a mechanically tested spot welded model.
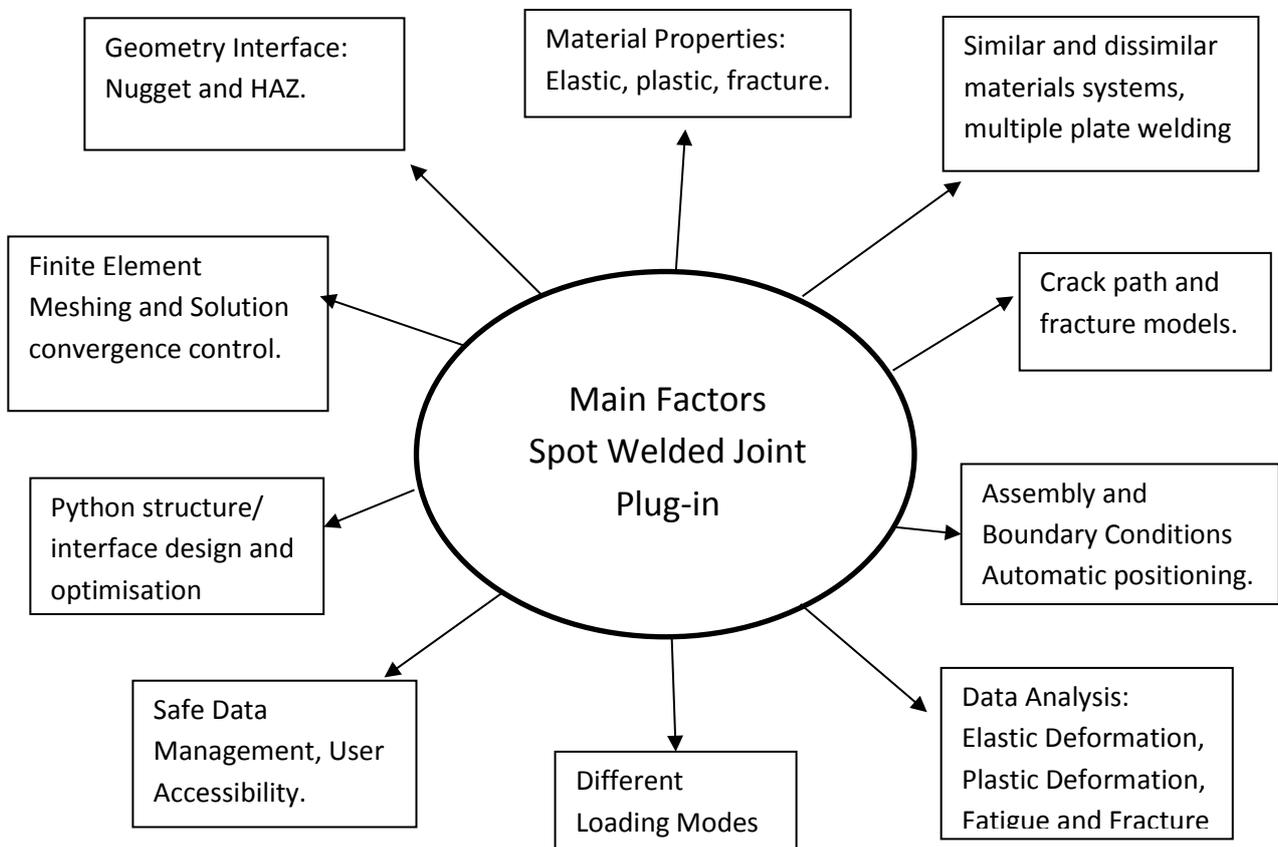
Figure 3.2 Key components/focus of the plug-in program for modelling spot welded joints.

The geometry is particularly important as spot welding involves combined thermal, mechanical and physical process resulting in complex microstructure zones with different mechanical properties. For steel the elastic properties are relatively unchanged, but the key plastic properties such as, the yield strength, work hardening and fracture may vary between different zones. A plug-in program with a function that automatically changes the dimensions accordingly will help to make the modelling process effective and efficient. Other key factors such as, size of the nugget and thickness are also all relevant to the manufacture process. The spot welding process is very versatile, which can be applied to many material systems either with the same materials or different materials, a framework of the plug-in could effectively cope with different material systems. The material properties is a key issue which needs to considered: elastic, plastic, fracture etc. depending on the particular testing mode and applications.

The boundary conditions for testing of spot welds is relatively better defined pending on the tests form, this made it particularly feasible and relevant for developing a plug-in program, which can be transferred to many different forms. The data required from FE simulation varies between different applications pending on user requirements. The plug-in should be able to give the user the freedom in extracting data as well obtaining data directly relevant to some more complex analysis such as, fatigue, creep etc. An application within plug-in, based in digital manufacturing, the interface such as, a program within a frame of a digital system is also important. Data safety and confidentiality is increasingly important for industrial users. The plug-in concept also considered the data management interface used for controlling confidential information and security of material properties and results data; tamper proof output files so that results cannot be manipulated to achieve the desired values; network and cloud upload locations for user defined access to files and results data. Use of a plug-in a longer term could provide end user with a powerful tool through proper data management system.

3.2.2 Procedure of building plug-in in python

To develop a fully functional plug-in interface a Python script must be structured, to prevent model generation errors. Initially an FE simulation model of mechanically tested spot welded plate was created on ABAQUS software. When a model is generated in ABAQUS a number of output files are produced, one of which is the RPY file. For every action made to generate

the model in ABAQUS a command was written in the RPY file. The RPY file generated from the original model was used as a platform to build the parametric Python script.

The structure of the python program was developed to build FE models for spot welded joints using ABAQUS. Python scripts were created to make the model parametric so that the model could be modified without having to start from the beginning of the process. To generate a functioning simulation model, different phases of work must be completed. The phases consist of generating the geometry, defining boundary conditions, material properties, Finite Element processing steps, identifying sets (areas of interest) for data history outputs as part of post processing. Python files were generated for each of the work phases and these scripts were collated by a Python master file.

For the plug-in for spot welded joints, the geometry Interface applies specific attention to parametric adjustable dimensions (length, width and thickness etc), size of nugget and specifically the number of HAZ layers. The plug-in is also capable of altering the geometry aspect including the shape of the nugget; in the case of welding dissimilar metals together the nugget is not a symmetrical shape (less cylindrical more conical/tapered). Material Properties Interface allows the user to apply different properties to defined sections of the model. The concept included applying properties for the joining of similar and dissimilar metals. The scope for mechanical material properties in this plug-in was elastic, plastic, fracture properties. Boundary conditions interface was to automatically identify, position and define the sections for the fixed end and loaded areas. In this phase a parametric value for the load was given as an adjustable value, this included the direction of the load applied in order to give the user an option of different mechanical load cases (tensile shear, peel, bending, torsion etc). Fracture modelling interface considers the tensile shear fracture FE modelling. The frame is able to be modified to include defects within the fracture FE models. As the failure mode and crack initiation of spot welded joints is relatively better defined in some type of failure mode, then the crack path can also be defined based in the geometrical features to generate a model for fatigue analysis. With a plug-in, the user would define the location of a potential crack (i.e. the HAZ) and give a crack length. The model would automatically generate a seam and apply a crack path.

Post processing Interface was to be used to automatically produce output data files for odb files. The user would identify areas of interest from data sets for the nugget and heat affected zones (these sets were generated within the model script assembly). The python program

made it possible to produce output data files in different formats and it was considered that the post process script could be used to compile output data for other simulation models (not just welded models) odb files.

3.3 Python Script

Python scripts can be used to generate parametric simulation models. To create functional Python scripts the parametric values must be identified, an example of a parametric value for geometry is length. To make length parametric, the numerical units have to be replaced with a 'keyword', such as, 'L' (for Length). The use of 'keywords' makes the model parametrically variable, by changing the value of the keyword instead of replacing each numerical occurrence of the parameter within the script. Ordinarily the parametric keywords are listed at the beginning of scripts. The user would open the scripts then edit the values for model variation. The scripts can then be run in the simulation software.

Three types of Python scripts are required to generate Plug-in user interface. The first script utilises the parametric Python script [1] used to generate models, another script is used to design the interface dialog windows [2] and the final master script [3] is used to load both scripts and the kernel functions. An example of the Python commands used to generate the geometry interface are listed; ***defweldmodelFunction(L, W, H …)*** command details the kernel Functions. All of the "keywords" (variable parameters/values replaced with keywords) used in the script are listed in Kernel Function brackets.

An example of the keywords has been used in the section of Script [1]; ***S.Line(point1=(-L, -W), Point2=(-L, W))*** this command sketches a line of interface defined values for L(length) and W(width). ***p.BaseSolidExtrude (sketch=s, depth=H)*** this command extrudes the sketch of the plate to a thickness (H) value defined on the interface.

```
from abaqus import *
from abaqusConstants import *
from caeModules import *
def createVariableLoadSpotweldedPlatesFunction(partName, L, W, H, R, D1, E1, V1, D2, E2, V2, D:
#PLATE
    s = mdb.models['Model-1'].ConstrainedSketch(name='__profile__', sheetSize=200.0)
    g, v, d, c = s.geometry, s.vertices, s.dimensions, s.constraints
    s.setPrimaryObject(option=STANDALONE)
    s.Line(point1=(-L, -W), point2=(-L, W))
    s.Line(point1=(-L, W), point2=(L, W))
    s.Line(point1=(L, W), point2=(L, -W))
    s.Line(point1=(L, -W), point2=(-L, -W))
    p = mdb.models['Model-1'].Part(name='Plate', dimensionality=THREE_D, type=DEFORMABLE_BODY)
    p = mdb.models['Model-1'].parts['Plate']
    p.BaseSolidExtrude(sketch=s, depth=H)
    s.unsetPrimaryObject()
    p = mdb.models['Model-1'].parts['Plate']
    session.viewports['Viewport: 1'].setValues(displayedObject=p)
    del mdb.models['Model-1'].sketches['__profile__']
```

Section of Script [1] of Plug-in (parametric python script to generate model)

DialogBox command identifies the name of the plug-in, the kernel module (master script used to generate the model), the kernel function used to identify all of the keyword commands (these should match against the master script [1] and the interface design script [2]

TabItem_1 refers to location of the variable or note appears on the interface

RsgIcon command is used to assign an image to the interface (the image file must be in the same folder address)

fieldType='String'command is used to return the user input as text to the script (i.e. the partname)

fieldType='Float'command is used to return the user input as a number to the script (i.e. a dimension size)

*ncols=12*command is used to define the size (in number of units) of the user input box on the interface.

RsgTextField(p=TabItem_1', fieldType='Float', ncols=12, labelText='Length (L)', keyword='L', default='0.05') is an example of the code required to generate a user input box on interface (in this instance it is for the Length of the Plate and it give a default value of 0.05m).

RsgLabel is the command to apply a text note to the interface, in this case it was defining the script rule applied for the radiuses of the HAZs.

```
from rsg.rsgGui import *
from abaqusConstants import INTEGER, FLOAT
dialogBox = RsgDialog(title='Spot Welded Plates (Variable Load)', kernelModule='VariableLoad_spotwelded_plates', kernelFur
RsgTextField(p='DialogBox', fieldType='String', ncols=12, labelText='Model Name', keyword='partName', default='weldassembl
RsgTabBook(name='TabBook_1', p='DialogBox', layout='0')
RsgTabItem(name='TabItem_1', p='TabBook_1', text='Geometry')
RsgGroupBox(name='GroupBox_3', p='TabItem_1', text='Diagram', layout='0')
RsgIcon(p='GroupBox_3', fileName='SpotWeldedPlate.png')
RsgTextField(p='TabItem_1', fieldType='Float', ncols=12, labelText='Length (L)', keyword='L', default='0.05')
RsgTextField(p='TabItem_1', fieldType='Float', ncols=12, labelText='Width (W)', keyword='W', default='0.0125')
RsgTextField(p='TabItem_1', fieldType='Float', ncols=12, labelText='Height (H)', keyword='H', default='0.0015')
RsgTextField(p='TabItem_1', fieldType='Float', ncols=12, labelText='Radius (R)', keyword='R', default='0.0025')
RsgLabel(p='TabItem 1', text='Note: HAZ is (R*1.5), HAZ2 is (R*2), HAZ3 is (R*2.5)', useBoldFont=False)
```

Section of Script [2] of Plug-in Data Base (Interface design script)

toolset.registerGUIMenuButton (buttonText='SpotWeldedPlates(VariableLoad)', is the code required to generate a named button (in this case 'spotweldedPlates (VariableLoad)') within the Abaqus tool bar. If this button is selected it will launch the Interface.

Object=Activator(os.path.join(thisDir, 'VariableLoadspotWeldedPlatesDB.py')), provides the command to use the data base script [2] which launches the design of the Interface.

kernelInitString='Import VariableLoad_SpotWelded_plates', this command initialises the parametric plug-in script [1] to generate the model.

```
thisPath = os.path.abspath(__file__)
thisDir = os.path.dirname(thisPath)

toolset = getAFXApp().getAFXMainWindow().getPluginToolset()
toolset.registerGuiMenuButton(
    buttonText='SpotWeldedPlates(VariableLoad)',
    object=Activator(os.path.join(thisDir, 'VariableLoadspotWeldedPlatesDB.py')),
    kernelInitString='import VariableLoad_spotwelded_plates',
    messageId=AFXMode.ID_ACTIVATE,
    icon=None,
    applicableModules=ALL,
    version='N/A',
    author='N/A',
    description='N/A',
    helpUrl='N/A'
```

Section of Script [3] of Plug-in (Master Script)

3.4 key functional modules of the Abaqus plug-in of the spot welded joints.

3.4.1 Structure of Geometry Interface program and Key functions

Figure 3.3 is a plug-in interface for defining the model name and dimensions of the spot welded model. There was scope for geometry interfaces as multiple and varied models are required to validate work throughout industry. This requirement was also important as it reduces user input time. The Geometry interface generates a three dimensional resistance spot

welded model. An advantage of this interface is that it can rapidly produce multiple models of varying dimensions for different cases. The interface is user friendly and requires minimal input in order to generate a model. The plug-in also reduces man hours required to assemble a model manually.

The assembly is made by generating individual solid parts for the nugget, Heat Affected Zones and Plates.

(a) Interface of a typical single plate with default values.	(b) Key procedural and functional block of the plug-in
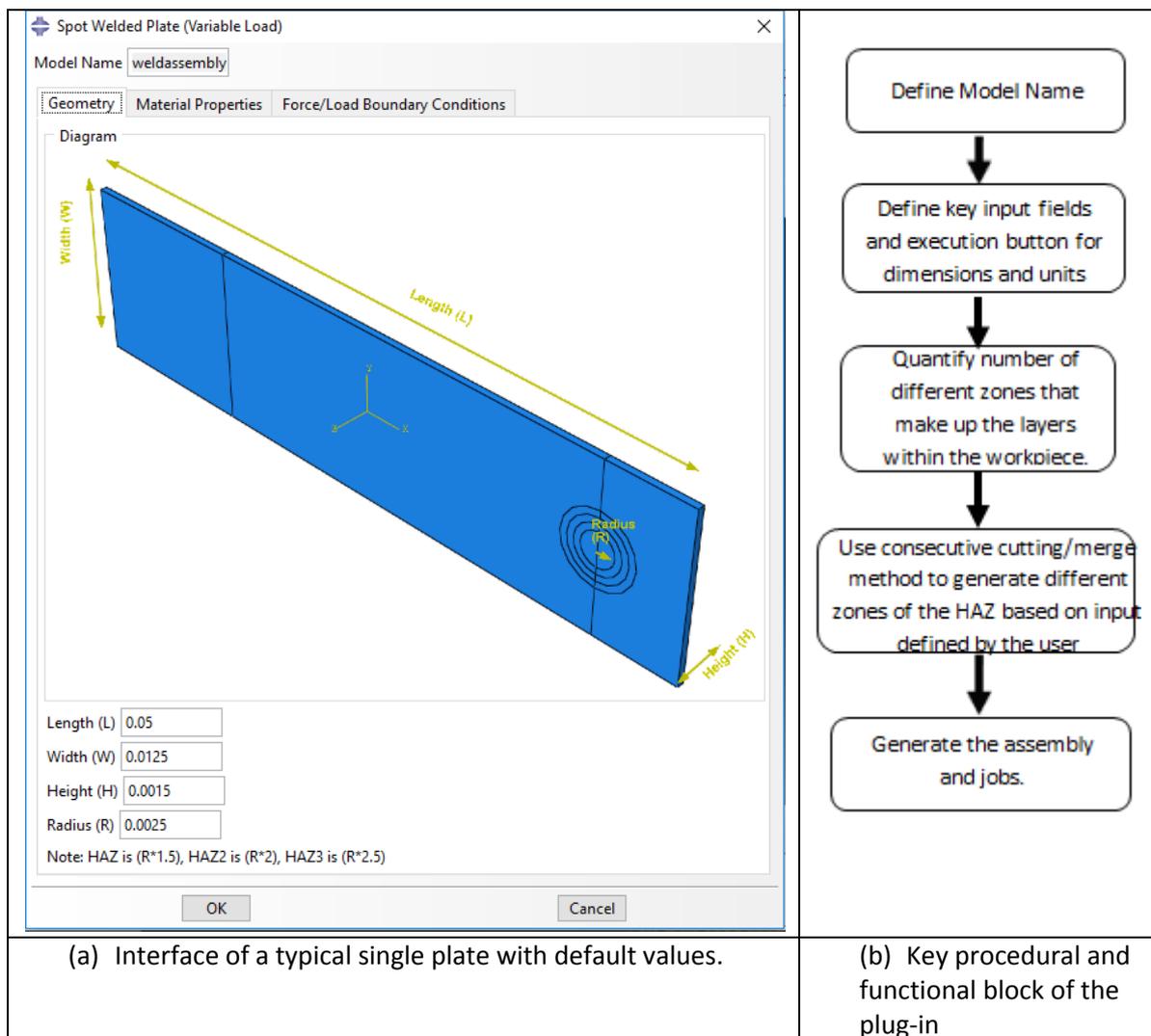
Figure 3.3 Structure of geometry Interface program for a single plate **(a)** and key procedural and **(b)** functional block of the plug-in.

The geometry Interface displayed in Figure 3.3 (a) shows a sectioned image of the single plate spot welded model. It is labelled to identify the location the dimension that can be adjusted. It also has user defined fields to provide a model name and the adjustable

dimensions; length (L) is the length of a single plate, width (w) is the width of the plate, Height (H) is the thickness of the plate and Radius (R) is the radius of the nugget. There is also a note on the interface, it is regarding how the Python script has been written to symmetrically predefine the radiuses of the HAZ's. Nominal Default values automatically appear on the interface and these can be changed as per the user requirements.

As shown in the Figure, the key technical challenge is the representation of the nugget and heat-affected-zones (HAZ). A consecutive cutting method was used to generate different layers of the HAZ; for example, if the HAZ is divided into three zones, the Plate is cut by the HAZ-3, HAZ-2 is cut by HAZ-2, HAZ-2 is cut by HAZ-1 and HAZ-1 is cut by Nugget. All of the cut parts are then merged together to generate a single spot welded plate assembly (retaining instances so that each section of the model can have its own material properties and be defined as a set). The part is then automatically sectioned to define tension machine grip sections, and section through weld to assist defining of data sets, aligning of nugget surfaces to tie and mesh generation. The single spot welded plate assembly is then automatically copied to generate the second plate and automatically assembled based on the updated positions from the input values.

Figure 3.3 (b) details the step phase user commands (inputs) required to operate the interface and produce the geometry. Define a unique model name (with no spaces or characters). Numerically input geometry values for the length, width and thickness of the base plate and define the nugget size (radius). A model will then be generated to the user specified dimensions. The way the program is generated makes it flexible in developing models with different numbers of HAZ layers and radius of HAZ's is to be defined in interface. Works during the development showed that it can be used to partition the nugget and the HAZ zones both laterally and vertically. Another geometry aspect included the shape of the nugget, in the case of welding dissimilar metals together the nugget is not a symmetrical shape (less cylindrical more conical/tapered). In addition, the spot welded plate assembly can also be sectioned to halve the model as this would reduce processing time.

3.4.2 Structure of Material Properties Interface program and key functions

Figures 3.4 and 3.5 show the key material property interfaces. Figure 3.4 is for general properties, while Figure 3.5 is for fracture model and parameters, which is particularly relevant to spot welded joints. Material property parameters is a very important interface, as there are arrays of material properties are used in different applications and properties change dependant on the weld. This requirement was also important as it reduces user input time. Generating material properties using FE simulation software can be a time consuming task, as material properties have to be selected, created, then sections created and assigned to a specific part of a model (as long as it has been sectioned).

| (a) Plug-in Interface showing a two plate assembly with the HAZ partitioned into three zones. | (b) Key procedures and functions for the material module |
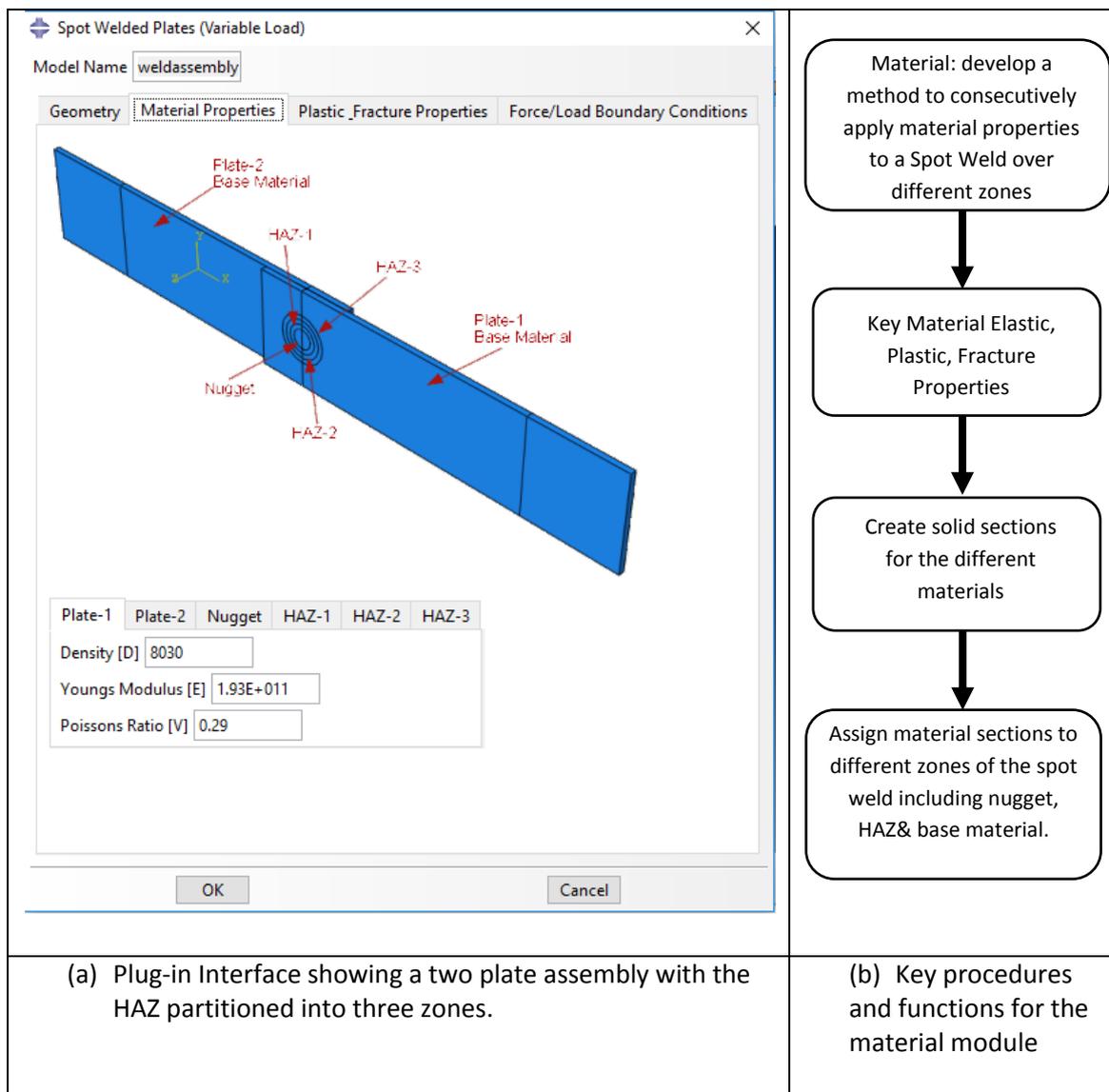
Figure 3.4 Structure of material properties Interface program **(a)** and key procedural and functional block **(b)**

As shown in Figure 3.4, the material Properties Interface allows the user to apply different properties to defined sections of the model. This could include applying properties for the joining of similar and dissimilar metals. The scope for mechanical material properties in this plug-in was Density (D), Youngs Modulus (E) and Poissons Ratio (V) properties. The weld assembly has been sectioned for the different zones that make up the layers within the work-piece.

The material properties Interface displayed in Figure 3.4 (a) shows an image of the complete two plate spot welded model. It is labelled to identify the different sections material properties will be applied to. It contains six material property tabs (Plate-1, Plate-2, Nugget, HAZ-1, HAZ-2, HAZ-3). To input material properties for a specific part of the model the user must click on the relevant tab. Within each of the tabs it has user defined fields to provide the adjustable properties; Density (D) the volumetric mass density, Youngs Modulus (E) mechanical elastic property, Poissons Ratio (V) Coefficient of expansion of the material. Nominal Default values automatically appear on the interface and these can be changed as per the user requirements. The flow chart in Figure 3.4(b) details the step phase user commands (inputs) required to operate the interface and apply the material properties. Numerically input material property values for all sections (each tab) of the work-piece. Click 'Ok' once all input boxes contain a value. The interface then consecutively applies the material properties to all of the defined sections of the spot welded assembly.

Figure 3.5 is a plug-in interface for defining the plastic and fracture material properties of the spot welded model. Plastic fracture material property parameters were selected as a useful interface, as there are arrays of shear material properties required to provide an accurate representation of a weld under plastic deformation. It is directly relevant to the prediction of yielding, and top load of the spot welded joints.
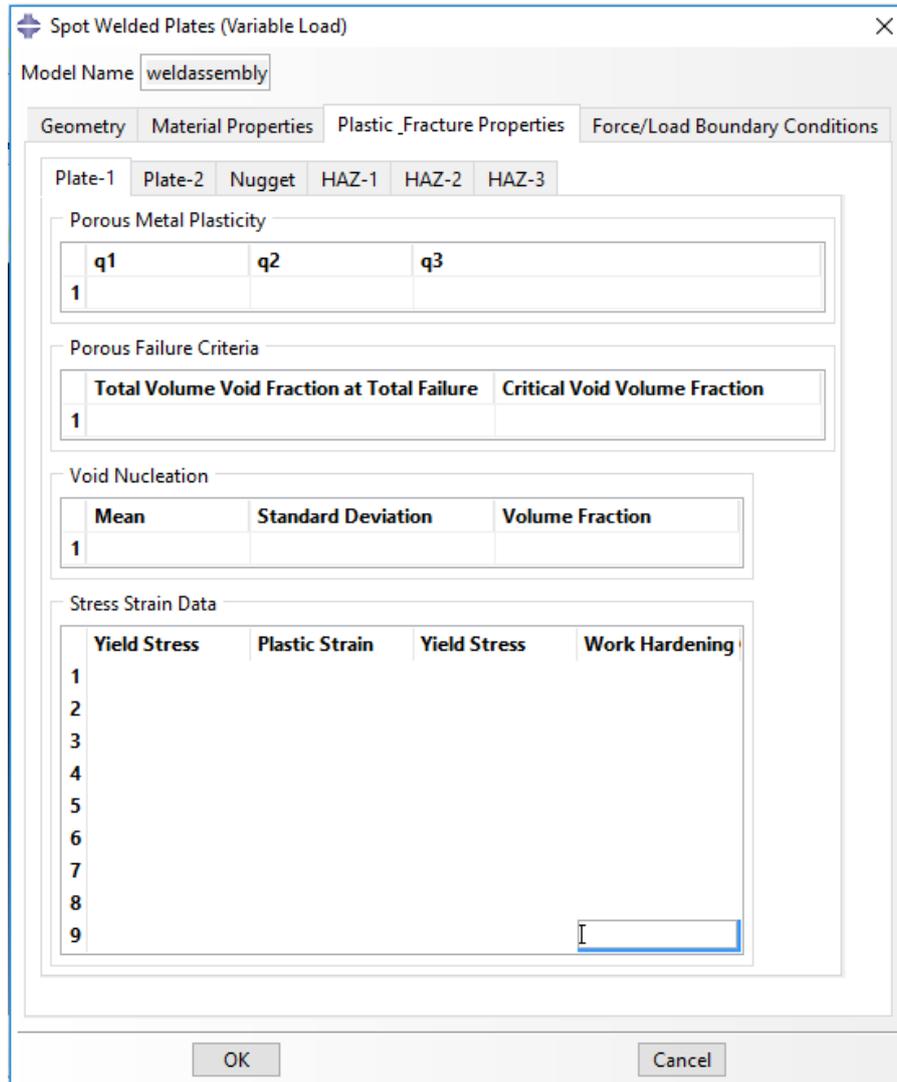
Figure 3.5 Main properties used for elastic-plastic fracture analysis and user input field

In the models, the material was treated as an elasto-plastic material with a true stress–strain behaviour following the constitutive law (Eq. 3.1).

$$\sigma = \begin{cases} E\varepsilon, \, for\, \sigma \leq \sigma_y \\ R\varepsilon^n, \, for\, \sigma \geq \sigma_y \end{cases} \tag{3.1}$$

Where 'E' is the Young's modulus, 'R' is a strength coefficient, 'n' is the strain hardening exponent, 'σ_y' is the initial yield stress and 'ε_y' is the corresponding yield strain, such that

$$\sigma = E\varepsilon_y = R\varepsilon_y{}^n \tag{3.2}$$

Here the yield stress (σ_y) is defined at zero offset strain. So the true stress–true strain behaviour is rewritten to be (Swaddiwudhipong *et al*, 2005 b):

$$\sigma = \begin{cases} E\varepsilon, \\ \sigma_y \left(\dfrac{E}{\sigma_y} \right)^n \varepsilon \end{cases} \tag{3.3}$$

In these tensile-shear FE models, the Young's modulus 'E' of the work piece materials was set to 200 GPa and Poisson's ratio was set to 0.3, which were commonly used values for steels (Chen*et al*, 2007).

Manually inputting plastic data such as, Yield stress and plastic stress can be a time intensive process. Using the Python command;

popupFlags='AFXTable.POPUP_COPY|AFXTable.POPUP_PASTE|AFXTable.POPUP_READ_FROM_FILE' The interface has an option to either copy and paste data into the table or read data into the table to form a file. The shear material properties interface applies individual material properties to all sections of the resistance spot welded model.

The plastic fracture material properties Interface displayed in Figure 3.5 contains six material property tabs (Plate-1, Plate-2, Nugget, HAZ-1, HAZ-2, HAZ-3). To input material properties for a specific part of the model the user must click on the relevant tab. Within each of the tabs it has user defined fields to provide the adjustable properties; The parameters for the fracture behaviour was assumed to be the following Gurson-Tvergaard-Needleman (GTN) model (Xue, 2007). Details can be found in ABAQUS (6.14). The micromechanical parameters introduced in the GTN model were subdivided into the following groups: Parameters of the matrix material, i.e. Young's modulus, E, Poisson's ratio, ν, and the initial true stress-strain curves, initial parameters of the rigid inclusion, i.e. the initial void volume fraction f_0 and the volume fraction of void nucleating particles f_n. Parameters affecting the nucleation, growth and coalescence of voids during the loading process includes $q_1, q_2, q_3, \varepsilon_N$, s_N, f_c, f_F. In Abaqus, Porous Metal Plasticity (q1,q2,q3), Porous Failure Criteria (Total Volume Void Fraction at Total Failure, Critical Void Volume Fraction) Void Nucleation

(Mean, Standard Deviation, Volume Fraction) and Plastic Data (Yield Stress, Plastic Strain). Nominal Default values automatically appear on the interface and these can be changed as per the user requirements.

The plastic fracture phase user commands (inputs) required to operate the interface and apply the material properties. Numerically input material property values for all sections (each tab) of the work-piece. Click 'Ok' once all input boxes contain a value. The interface then consecutively applies the shear material properties to all of the defined sections of the spot welded assembly.

3.4.3 Structure of Boundary Conditions - loading interface program

Figure 3.6 is a plug-in interface for defining the Boundary conditions and load mode of the spot welded model. Boundary conditions and load mode parameters were selected to create a useful interface, as there are ranges of Boundary conditions and loads that influence the use and applications of a weld joint. This requirement was also important as it reduces user input time. Applying various boundary conditions and load cases using FE simulation software can be a time consuming task, as sections have to be created, selected and then conditions assigned. The boundary conditions interface applies displacement and rotation constraints (encastre) on a fixed end then a directional load of a defined force on the other plate sections of the resistance spot welded model. An advantage of this interface is that it can automatically position and apply boundary conditions and forces to the end sections of the spot weld assembly model. This interface can be used to produce multiple load cases. The interface is user friendly and requires minimal input in order to generate a model. The plug-in also reduces man hours required to manually generate and apply boundary conditions to specific sections of the model. Boundary conditions interface was to automatically identify, position and define the sections for the fixed end and loaded areas. In this phase a parametric value for the load was given as an adjustable value, this included the direction of the load applied in order to give the user an option of different mechanical load cases (tensile shear, peel, bending, torsion etc.). The key developments in the case of tensile shear tests, are to automatically produce clamped area loading positioning and apply boundary conditions to the whole model. To input boundary conditions user defined fields have been provided to create loads modes. The adjustable parameters are; Tensile/ Compressive (F1), Shear (F2) moments, Bending (F3) moments/ Peel loads. Nominal Default values automatically appear on the

interface and these can be changed as per the user requirements. Mesh sensitivity studies were performed on the spot weld FE model. The model has been sectioned to define regions of HAZ, to apply a fine mesh to areas of interest and a more course mesh to the base material to make more effective use of computational resources. The user interface has the functionality to apply a general mesh seed size.
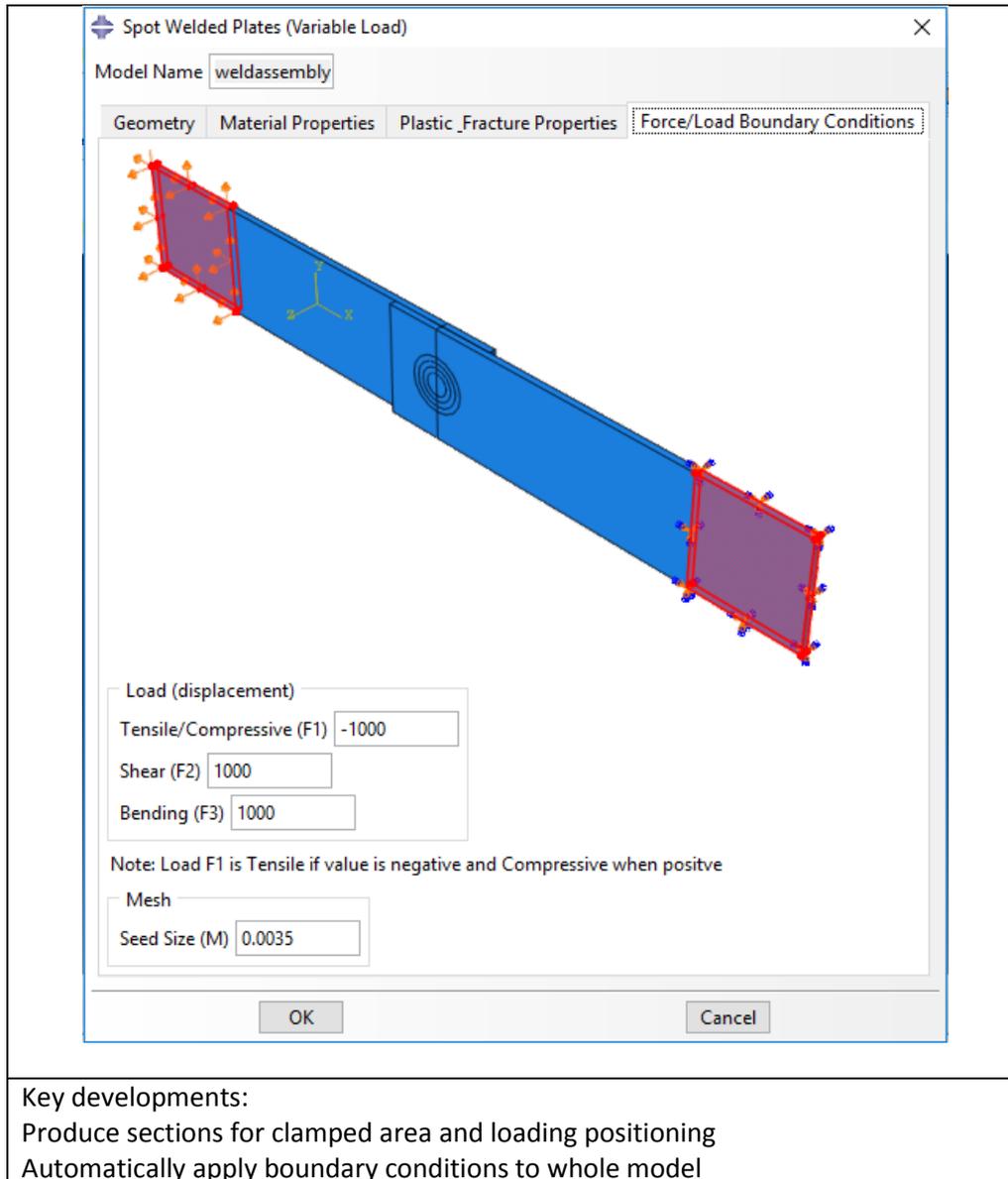
Figure 3.6 Structure of boundary conditions and loading interface program

The force/load boundary conditions phase user commands (inputs) required to operate the tensile-shear interface and apply the boundary conditions. Numerically input boundary conditions for each end of the work-piece. Including the magnitude of load applied in each

direction. Click 'Ok' once all input boxes contain a value. The interface then consecutively applies the displacement and rotation constraints and load conditions to all of the defined sections of the spot welded assembly.

In a situation where fatigue or fracture with a pre-defined crack is required, the plug-in could provide a useful tool. The crack path for spot welded joints is relatively better defined, so the user can apply predefined crack paths for different situations. Fatigue defect modelling interface is used to generate a model for fracture and failure analysis. The user would define the location of a potential crack (i.e. the HAZ) and give a crack length. Figure 3.7 illustrates a case, where the model would automatically generate a seam and apply a crack path.

This model is used to determine the design life of a welded joint that contains defects of varying crack sizes. In the case shown, the complete two plate spot welded model contains a crack defect within HAZ-1.

To input a seam and crack defect of a set length, user defined fields have been provided. The adjustable parameters are; Crack/Defect location (Nugget, HAZ-1, HAZ-2, HAZ-3), Crack length (L). Nominal Default values automatically appear on the interface and these can be changed as per the user requirements. The pre-defined crack defect phase user commands (inputs) are required to operate the interface and automatically apply the location and size of the crack length. Numerically input defect location and crack length in the work-piece. Click 'Ok' once all input boxes contain a value. The interface then consecutively applies the Seam and defect to the defined section of the spot welded assembly. The use of the plug-in work would also allow the user to include factors such as, residual stresses as residual stress varies within different welding zones. With a suitable load for fatigue and output data, the process can also be linked to other model such as, Failure Assessment Diagrams FAD (BS7910) and R6, which is the Assessment of the Integrity of Structures Containing Defects. These are important for standardising and communicating procedures for assessing the safety of flawed structures.
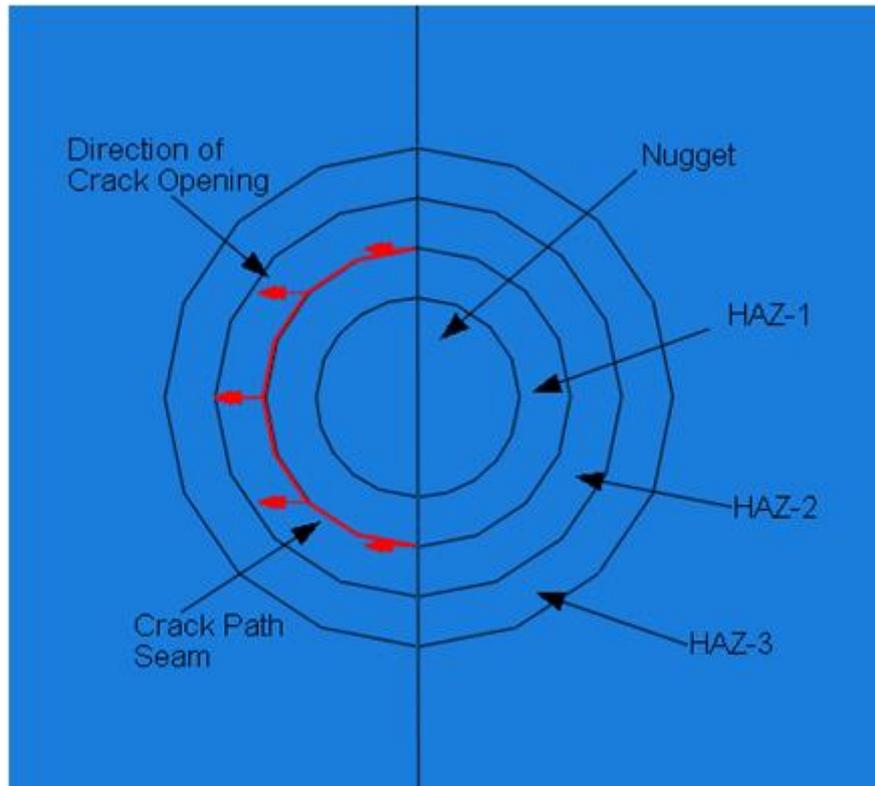
Figure 3.7 An image illustrating a procedure to define seam and crack paths using the parametrical model of spot welded joint

3.4.4 Post Processing interface program

Figure 3.8 is a flow chart detailing the main consideration factors for the design of a post process plug-in interface, for post processing data from executed simulations of the spot welded models. Validation of work usually requires a number of load cases executed, which necessitates post processing of data from the FE models. Therefore, it was beneficial to produce an interface that automatically post processed the data from an executed FE simulation. An advantage of this interface is that it can automatically post process executed FE model output data to an excel spreadsheet or database. It allows the analysis of the previous result sets in a formal way. This interface can be used to produce multiple load cases in a user friendly system and requiring minimal resources to generate the output files. The interface only requires odb files to generate the output data files, this technique can be applied to remotely sensitive data. If a company uses confidential material properties boundary conditions or load cases within the model, the use of this interface provides a level of security as the CAE file that would contain this information is not required. The FE

processing interface has identified sets for key areas of interest such as, the HAZ's and nugget.
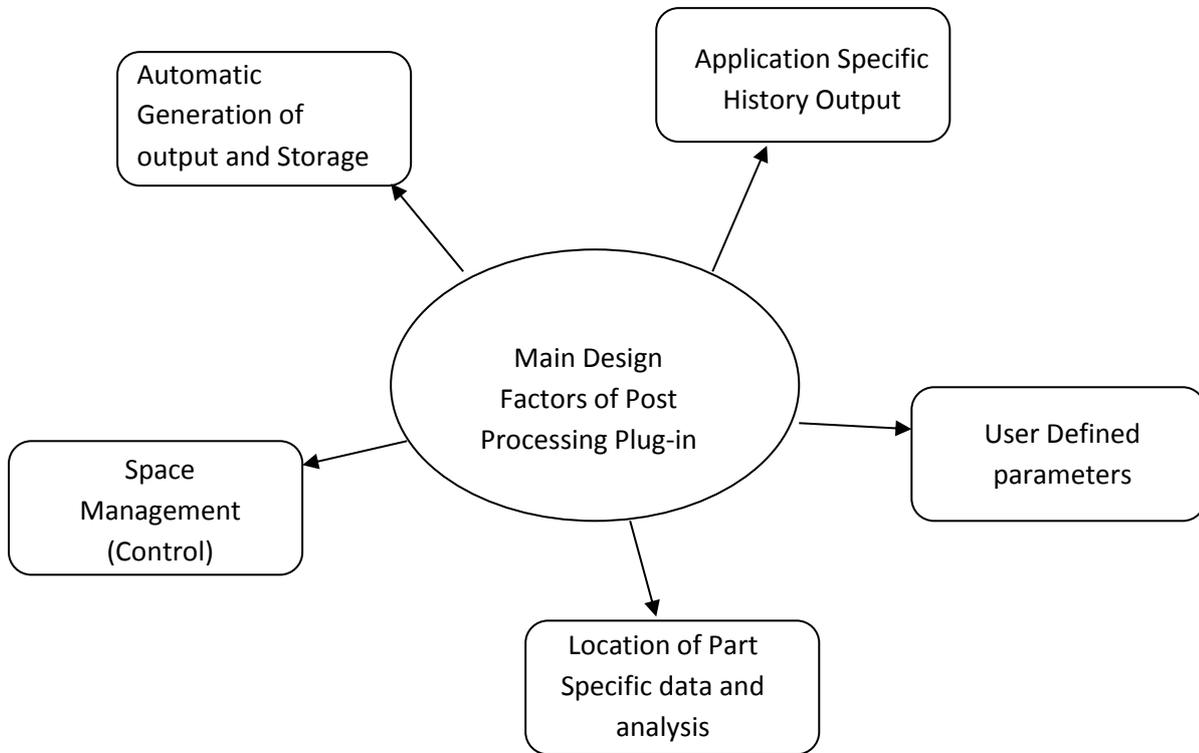
Figure 3.8 Main consideration factors for design of a post processing plug-in

The Post Processing Interface should have an application to request history output data from specific locations (parts) of the assembly. The plug-in should allow the user to identify the sections of the model that contain data sets. A user defined field should be used that requests an input of a file name and path. A folder directory button can be used to input the file location. The Python script command that generates the directory button is *default='',* *patterns='All files (*)'*. The next field requires the user to select the node set from the scroll bar menu. The scroll bar menu contains a list of the following data sets (previously defined during the assembly of the model); Nugget, HAZ-1, HAZ-2, HAZ-3. The final two interface fields require file names for the excel spreadsheet and contour image plot. Nominal Default values automatically appear on the interface and these can be changed as per the user requirements.

Phase user commands (inputs) would be required to operate the interface. Input the odb file name and file address, select the data set to extract data from, define the file names for the excel output data spreadsheet and deformed model image. Click 'Ok' once all fields contain input. The interface then automatically generates History outputs data (such as, Von Mises, forces and displacement, etc.) for the defined set (Nugget, HAZ-1, HAZ-2, HAZ-3).. A contour image of the deformed model can also be created.

It was considered that the post process script could be used to compile output data for other simulation models (not just welded models) odb files. In a longer term, the frame of the plug-in concept also considered the data management interface used for controlling confidential information and security of material properties and results data; tamper proof output files so that results cannot be manipulated to achieve the desired values; network and cloud upload locations for user defined access to files and results data.

3.5 Modelling tensile-shear test and effect of nugget size and sheet thickness

Figure 3.9 shows a typical FE modelling result in comparison with experimental tests. The force displacement data of a spot welded joint covers the elastic, plastic and fracture stage. It involves elastic tension and bending of the specimen in the early stage and, then yielding and eventually fracture within the HAZ. Figure 3.9(b) shows that the numerically predicted deformation pattern resembles the experimental observation at the fracture stages of the test. Both the force-displacement data and the fractured shape showed a good agreement between the experimental data and numerical modelling results. The modelling approach is then used to investigate the effect of the nugget size and thickness on the deformation of spot welded joints and the stress and strain within different zones which is relevant to the optimisation of the spot welded joint.
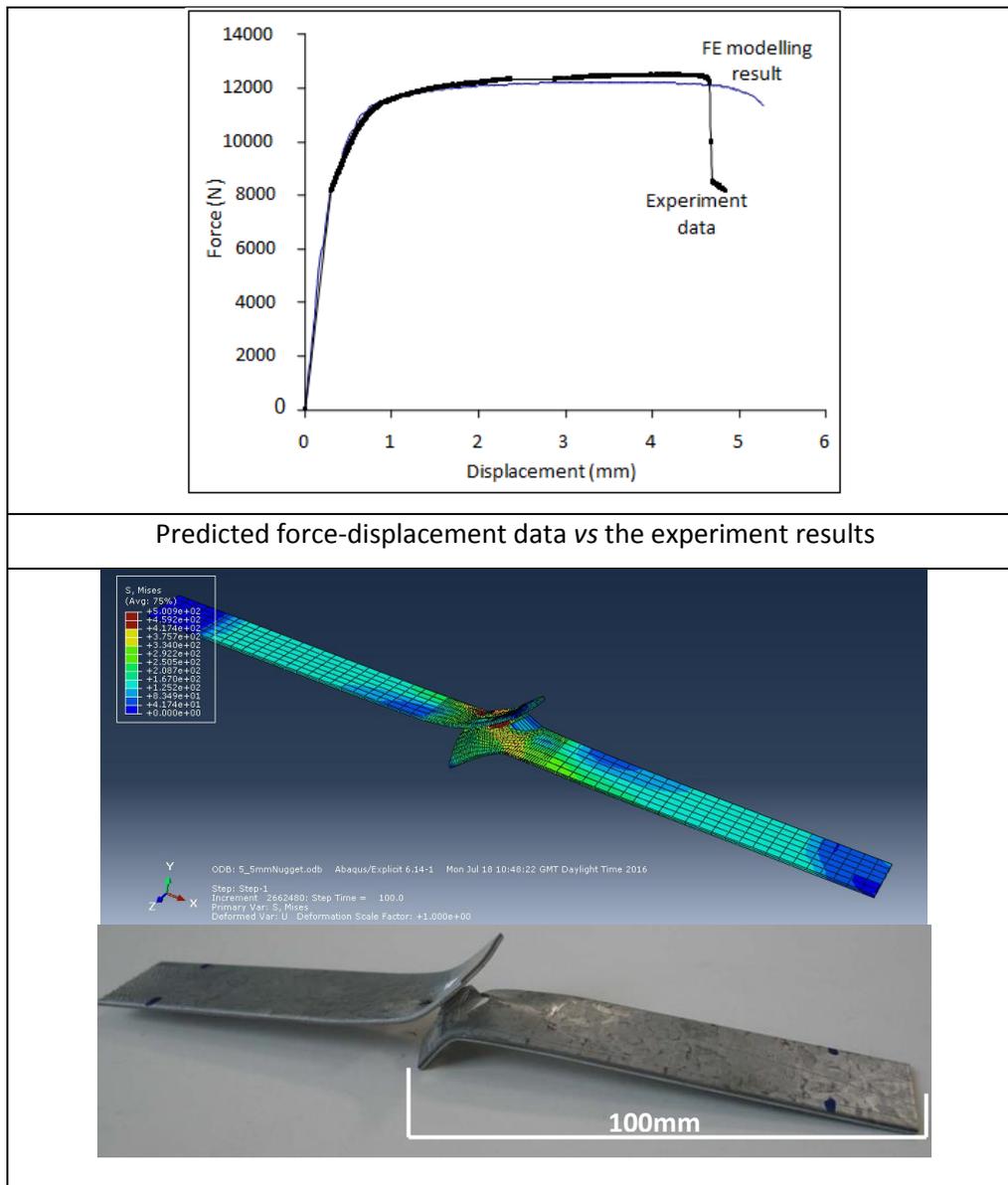
Predicted force-displacement data *vs* the experiment results

Figure 3.9 Comparison between numerical and experimental results of tensile shear tests.

In the work in investigating the effect of sheet thickness, the thickness of the metal sheet is varied and the full elastic-plastic-fracture is performed. A typical result of three conditions of varying thicknesses are shown in Figure 3.10**.** The spot welded models had identical material properties and boundary conditions applied. As shown in the figure, the thickness has a significant effect on the strength, including the yielding point, the ultimate strength and the fracture strength. But, it showed very limited effect on the stiffness of the structure.
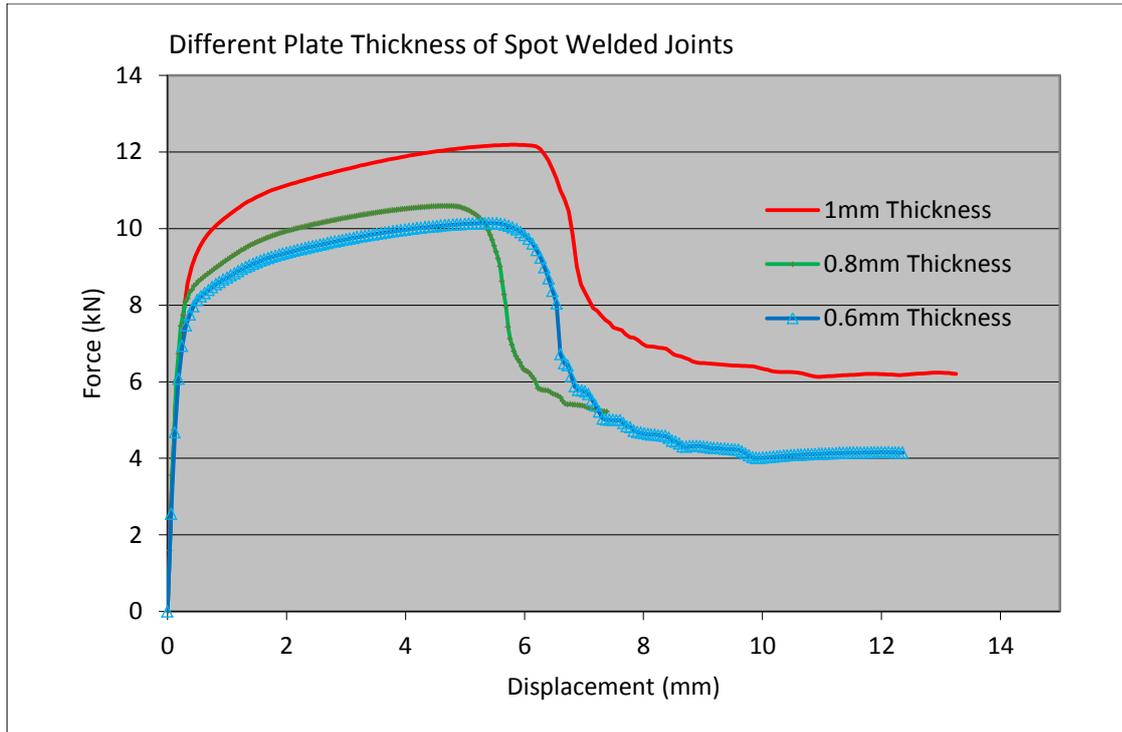
Figure 3.10 Force-displacement data of spot welded joint different sheet thickness.

Figure 3.11 shows the stress within the nugget and HAZ1's with different sheet thicknesses. As shown in Figure 3.11 (a-c), the overall stress distribution pattern is similar between the thickness of 0.8 and 1mm, there is some difference in the nugget of the case of thickness 0.6mm. This is reflected more significantly in the bending/rotation when the sample is thinner. Figure 3.11 (d-f) shows the Von Mises stress distribution within the HAZ1, which is the zone directly connected to the nugget. This is the zone where fracture is understood to occur during fatigue analysis (Khan, 2008). Its stress distribution is directly relevant to the fracture initiation and propagation. As shown in the figures, the overall pattern is similar among the cases for three thicknesses. The stress at the point of the interface between the HAZ and the nugget is slight lower than the point within the nugget.

| a) Von Mises Stress for nugget (0.6mm Thickness) | b)Von Mises Stress for nugget (0.8mm Thickness) | c)Von Mises Stress for nugget (1.0mm Thickness) |

| d)Von Mises Stress for HAZ-1 (0.6mm Thickness) | e)Von Mises Stress for HAZ-1 (0.8mm Thickness) | f)Von Mises Stress for HAZ-1 (1.0mm Thickness) |
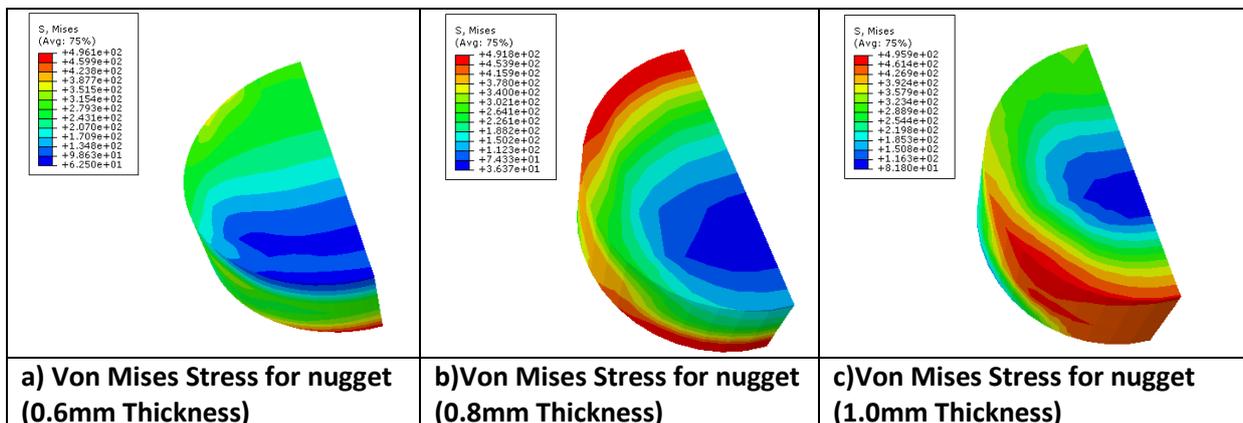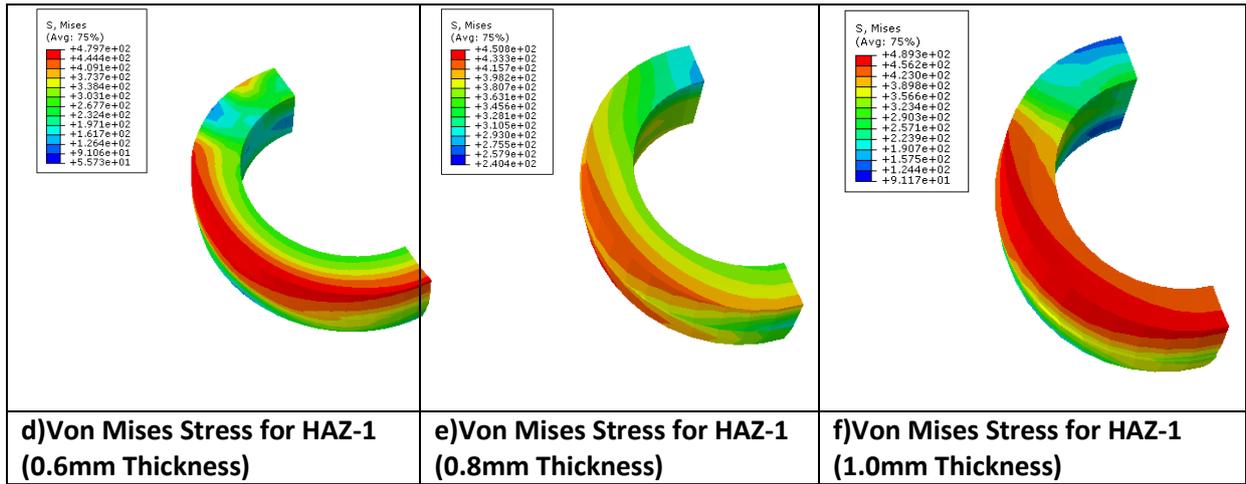
Figure 3.11 Typical stress (Von Mises) distribution within the nugget and the HAZ zone1 for different sheet thicknesses.

To further evaluate this, the stress ratio between two points at the interface between the HAZ-Nugget and HAZ1-HAZ2 is explored, which could reflect the likely crack initiation points. Some typical data is shown in Figure 3.12. In all the cases, the stress ratio is very similar, the stress between HAZ1-2 is higher than the HAZ-Nugget interface. The stress for a thinner plate is higher. This suggests that the region between HAZ1-2 is more likely to be the site of crack initiation.
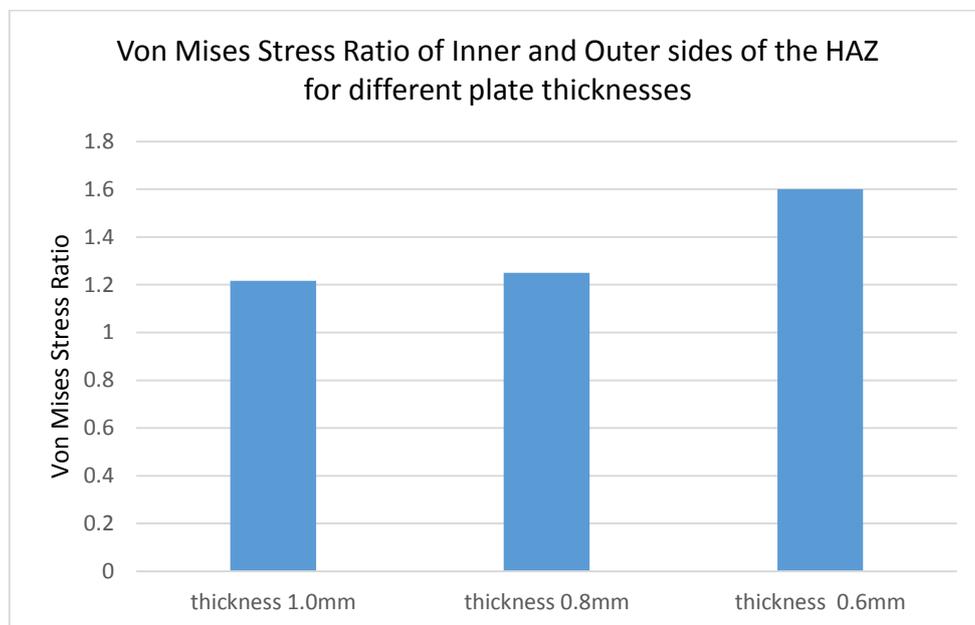
Figure 3.12 The ratio of the Von Mises stress within the HAZ1 at the inner and outer side along the loading axis which is more likely to be the crack initiation point.

Figure 3.13 shows three FE simulation spot welded models of varying nugget diameters. In the model, the thickness and other dimensions (HAZ zones) is fixed while the nugget size varied. Comparing the different force-displacement data from these models clearly shows that the nugget size has a significant effect on the strength, including the yielding point, the ultimate strength and the fracture strength.
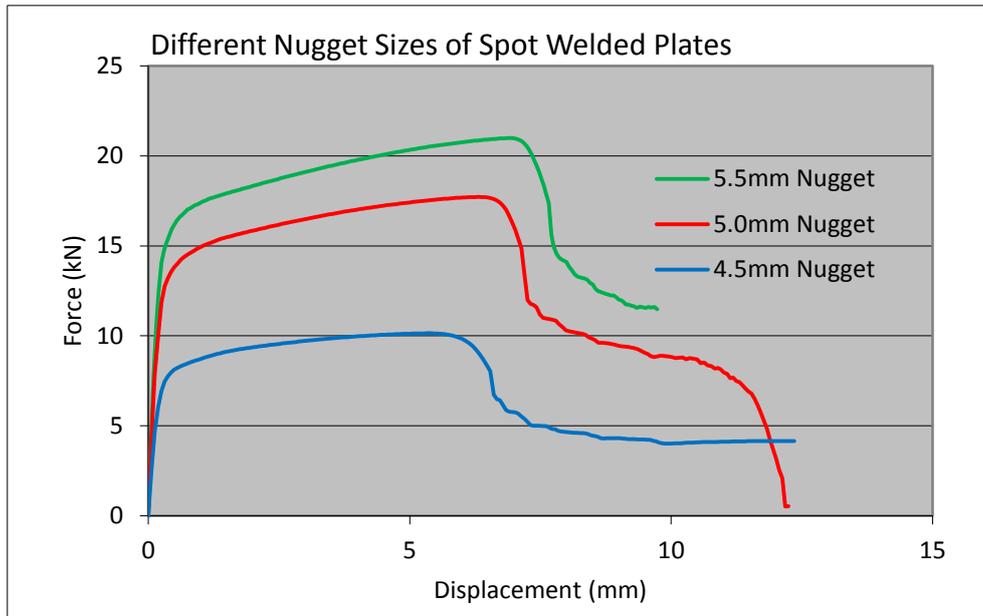
Figure 3.13 Force-displacement data of spot welded joint different nugget size.

Figure 3.14 shows the stress within the nuggets and HAZ1's using different Nugget diameters. Figure 3.14 (a-c), shows the Von Mises stress distribution within the HAZ1, which is the zone directly connected to the nugget. This is the zone where the onset of fracture occurs during fatigue testing. The overall stress distribution pattern is similar between the diameter of 5.0mm (b) and 5.5mm (c), there is some difference in the HAZ1 in the case of nugget diameter 4.0mm (a). This is caused by the deformation (thinning) of the nugget. That reflects more significant bending/rotation when the sample nugget diameter is larger. Figure 3.14 (d-f) shows the Von Mises stress distribution within the different nugget sizes (4.0mm, 5.0mm & 5.5mm). The stress distribution is directly relevant to the fracture initiation and propagation. As shown in the figures, the overall pattern contours are similar among the cases for the three nugget diameters. The stress at the point of the interface between the HAZ and the nugget is slight lower than the point within the nugget.

| | (a) Von Mises Stress HAZ-1 (Nugget 4.5mm) | (b) Von Mises Stress HAZ-1 (Nugget 5.0mm) | (c) Von Mises Stress HAZ-1 (Nugget 5.5 mm) |
| (d) Von Mises Stress Nugget (Nugget 4.5mm) | (e) Von Mises Stress Nugget (Nugget 5.0mm) | (f) Von Mises Stress Nugget (Nugget 5.5 mm) |
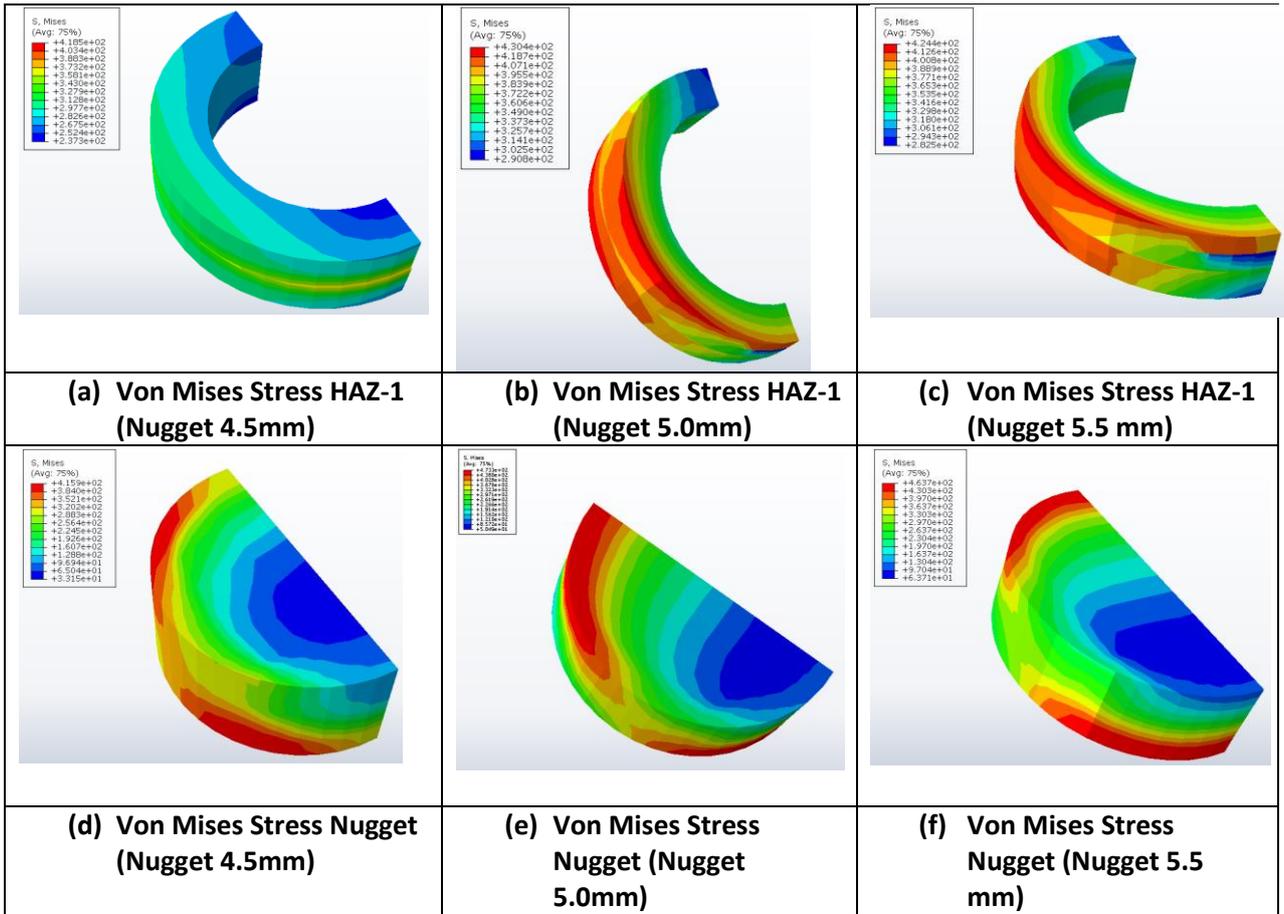
Figure 3.14 Stress distribution of the HAZ-1 and nugget with different nugget size.

To further evaluate this, the stress ratio between two points of the interface between the HAZ-Nugget and HAZ1-HAZ2 is explored, which could reflect the likely crack initiation points. Some typical data is shown in Figure 3.15. In all the cases, the stress ratio is very similar, the stress between HAZ1-2 is higher than the HAZ-Nugget interface. The stress for all nugget diameters is similar, therefore, nugget diameter is not likely to impact the region for crack initiation. Figure 3.16 is a photo showing experimental tensile-shear test work-pieces. The location of the crack is located in the HAZ comparable to the location of the peak stresses shown in the contour plots shown in figures 3.11 & 3.14 (d, e, f).
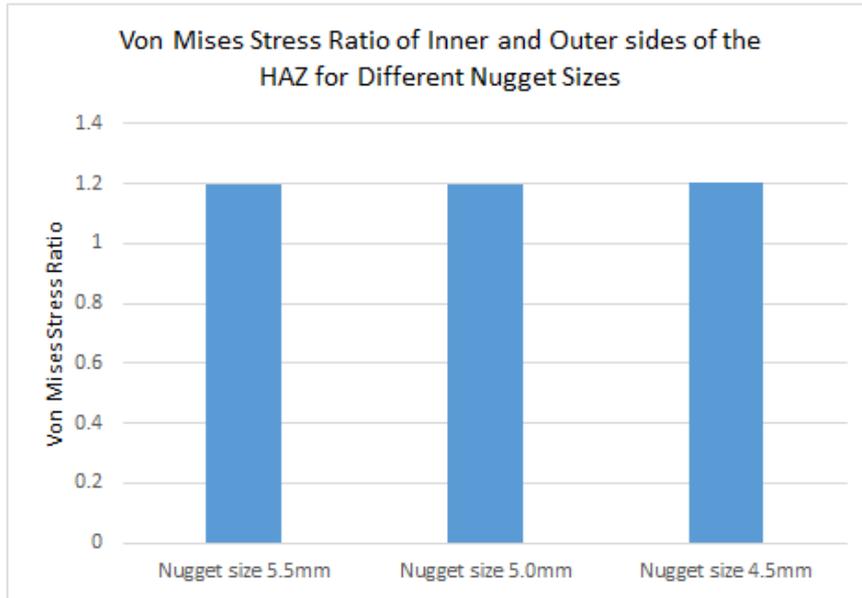
Figure 3.15 The ratio of the stress of the HAZ-1 at the inner and outer side within the loading axis which is more likely to be the initial crack propagation point.
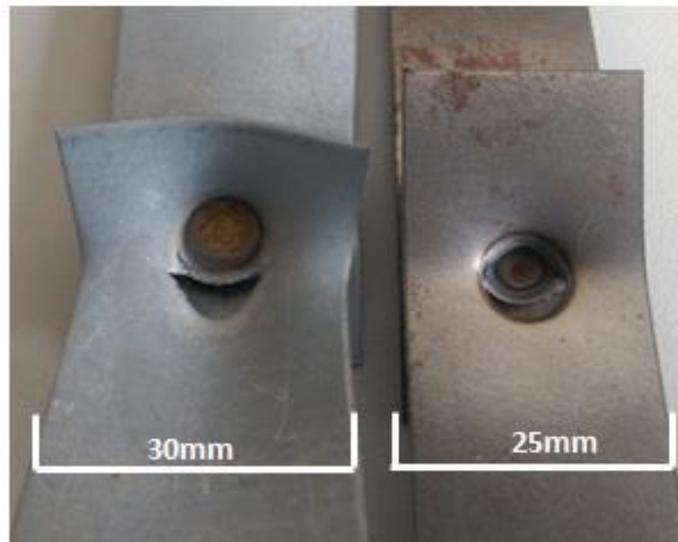
Figure 3.16 Photograph to show the crack path within the HAZ

3.6 Summary

In this chapter, an FE model and an Abaqus plug-in of spot welded joints is developed and used to investigate the effect of nugget size and sheet thickness on the stress and deformation of spot welded joints of steel. A systematic/automatic modelling approach of spot welded

joints was designed and coded using Python scripting. Several interfaces were generated to create parametric models, the approach used different features of the weld that impact the mechanical behaviours. The interfaces included; geometry, material and shear (plastic) properties, sectioning of HAZ layers, boundary, loading conditions and crack partition path. The program is able to incorporate the plastic material parameters (yield stress and work hardening coefficient) as well as fracture models. The plug-in is used for numerical modelling of the elastic-plastic-fracture of spot welded joints under tensile-shear. The validated numerical models are further used to investigate effects of nugget size and thickness of the metal sheets on the strength of welded joints. The analysis on stress (Von Mises) distribution within the nugget and the HAZ zone next to the nugget and the ratio of the Von Mises stress at the inner and outer side along the loading axis suggests that the HAZ is more likely to act as the crack initiation and propagation path, which is in agreement with experimental observation.

CHAPTER 4

FE Modelling of response of spot welded Thermocouples tips under different conditions

4.1 Introduction

Identified in framework Figure 1.1 is the thermal history and quenching of welded joints. These key areas of interest directly impact the microstructure of the weld and mechanical properties. Therefore, it was important to investigate temperature measurement techniques, sensitivity and time response. This chapter focuses on extending the user interface Abaqus plug-in approach to thermal models. Then apply the methodology to modelling of different types of thermocouples. This chapter reports experimental and numerical work performed to characterise the thermal response, and factors that affect the performance of temperature measurement thermocouples. Figure 4.1 illustrates the structure and materials of three types of thermocouples studied in this work. The key measurement is through a welded tip between metal wires. The bare-wire thermocouple wires are butt welded, and the wires are insulated to provide a seal against liquid or gas penetration. This junction style provides the fastest possible response time but leaves the thermocouple wires at the junction unprotected against corrosive or mechanical damage.
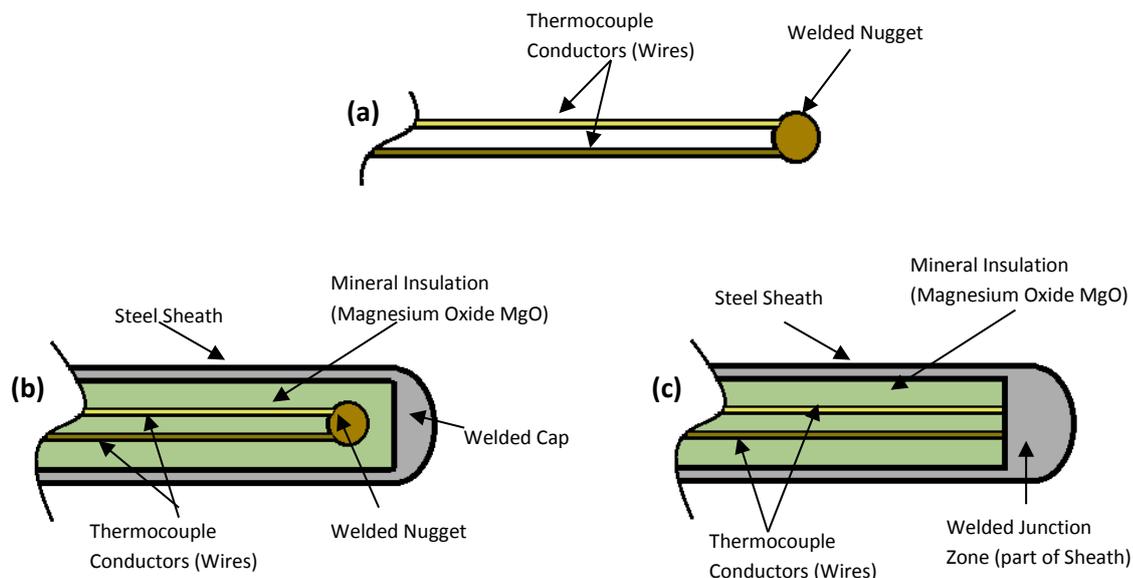
Figure 4.1 Sketches showing different thermocouple Junction Types **(a)** Bare-Wire (Exposed) **(b)** Sheathed Ungrounded Tip **(c)** Sheathed Grounded Tip.

The grounded thermocouple has the lead wire shielded and attached to the sheath. The sheath and conductors are welded together, forming a completely sealed integral junction. This thermocouple is specifically used in the presence of liquids, moisture, gas or high pressure. The wire is protected from corrosive or erosive conditions. Response time with this style approaches that of the exposed (bare-wire) junction.

The ungrounded junction thermocouple avoids ground loops between instruments, power supplies and the sensor.On this type the thermocouple junction is fully insulated from the welded sheath end. The ungrounded junction is excellent for applications where stray EMFs would affect the reading and for frequent or rapid temperature cycling. Response time is longer than for the grounded junction.

Thermocouples/resistance probes are used to obtain a direct measurement of temperature in order to regulate it. The working principle of thermocouples is essentially based on the SEEBECK effect (standardization CEI.584 DIN43720). It consists of creating an electromotive contact force, which varies according to the temperature, at the point of contact between two metals. A thermoelectric couple is formed by two metal wires or different alloys soldered together at one point. If the joint between the wires is heated (point of measurement), a tension is created at both free extremities (joint point). The free extremities are prolonged by compensation cables up to an area of known temperature (compensation point). The thermocouples measure the difference in temperature between the measurement point and the compensation point. The temperature at the compensation point must be known and constant. If this temperature isn't constant or is unknown, it must be measured using a second sensor.

There are a number of Thermocouple types suitable for a range of applications. The dissimilar metals that for the junctions of the thermocouple define the Thermocouple type are signified by a letter and colour. Standard ASTM E 230 color coding (United States) and IEC 584-3 (International) is used on all insulated thermocouple wire and extension wire when type of insulation permits. Accuracy of different Types of Thermocouples is based on characteristics of thermocouple materials, including the EMF vs. temperature relationship. This may change with time in use and consequently, test results and performance obtained at time of manufacture may not necessarily apply throughout an extended period of use.

Tolerances given in Table 4.1 apply only to new wire and do not allow for changes in characteristics with use. The magnitude of such changes will depend on such factors as wire thickness, temperature, time of exposure and environment. It should be noted that due to possible changes in homogeneity of the material the temperature range tolerance may change over time.

Table 4.1 Thermocouple element material types, temperature range and tolerances

Type	Thermo-element Alloy	Temperature Range ^{o}C	Tolerance ^{o}C
B	Pt 30% Rh (B + Positive)	870 to 1700	+/- 0.5%
	Pt 6% Rh (B - Negative)		
E	Chromel (E + Positive)	0 to 870	+/- 1.7^{o}C or +/- 0.5%
	Constantan (E - Negative)	-200 to 0	+/- 1.7^{o}C or +/- 0.1%
J	Iron (J + Positive)	0 to 760	+/- 2.2^{o}C or +/- 0.75%
	Constantan (J - Negative)		
K	Chromel (K + Positive)	0 to 1260	+/- 2.2^{o}C or +/- 0.75%
	Alumel (K - Negative)	-200 to 0	+/- 2.2^{o}C or +/- 2%
N	Nicrosil (N + Positive)	0 to 1260	+/- 2.2^{o}C or +/- 0.75%
	Nisil (N - Negative)		
R	Pt 13% Rh (R + Positive)	0 to 1480	+/- 1.5^{o}C or +/- 0.25%
	Pure Pt (R - Negative)		
S	Pt 10% Rh (S + Positive)	0 to 1480	+/- 1.5^{o}C or +/- 0.25%
	Pure Pt (S - Negative)		
T	Copper (T + Positive)	0 to 370	+/- 1.0^{o}C or +/- 0.75%
	Constantan (T - Negative)	-200 to 0	+/- 1.0^{o}C or +/- 1.5%

Industry specifications have established the accuracy limits of thermocouple sensors. These limits define initial sensor performance at time of manufacture. Time, temperature and environment operating conditions may cause sensors to change during use. The overall system/process accuracy will depend on the instrument and other installation parameters. Temperature accuracy is not as precise in the negative temperature range. The diameter of the sensor wires also determines the uppermost operating temperature (so the temperature ranges in the table will vary dependent on the wire thickness). The larger the diameter, the higher the temperature rating. Research work is required to understand these factors. Thermocouples are made of thin wire to minimise thermal shunting and increase response times. The smaller diameter the wires are, the higher the resistance, this can cause errors due to the input impedance of the measuring instrument. Thicker wires can withstand more mechanical stress at higher temperatures. Over wide temperature ranges you can have changes in crystal structure, phase changes in alloys, grain growth, and probably other effects. Some of those

might affect the output of a thermocouple, especially at high temperatures and small diameters. Mechanical expansion and the strength of the material might result in sagging or breaking. The manufacturing process - drawing into wire - may result in imperfections (due to inclusions, grain boundaries, and so on) which create unacceptable errors at high temperatures. Oxidation and reactions with the isolation material will change the Seebeck coefficient sensitivity of the TC. It is a function of temperature and the ratio of surface to material i.e. smaller diameter faster change in sensitivity. Elevated temperatures which cause migration of the metals across the junction if held at high temperatures or repeatedly cycled to high temperatures in an oxidizing environment. This causes a Seebeck shift which effects the accuracy, larger diameter wire slows down that process.

The length of a thermocouple has no major effect on its measurement accuracy or its ability to transfer the signal to the instrument. In other words, thermocouples do not experience "voltage drops" or power loss along their length as a high current power line might possess. The reason for this is due to the very low current and voltages associated with temperature measurements and that the thermocouple wire becomes the voltage source. In reality the sensor can be inches or thousands of feet long and the accuracy will not be affected. In practical applications where the thermocouple is a substantial distance from the instrument, electrical noise can be induced and the sensor selected should be shielded and grounded at one end. In severe environments, or when the distance is in excess of 150 feet, a 4-20mA signal conditioner is suggested. Thermocouple wires create low voltage signal and should be kept away from any electromagnetic fields. To minimize noise pickup, they should not be used near power wires, motors, etc. However, the length regarding the location of the nugget junction or the size of the junction impacts the measurement response time. The further the nugget is away from the temperature source the slower the response. The larger the junction the slower the response. All these issues require researching through an integrated investigation.

The response time of thermocouples are very important, which is a function of the mass of the sensor and its efficiency in transferring heat from its outer surfaces to the wire sensing element. A rapid time response is essential for accuracy in a system with sharp temperature changes. Time response varies with the probe's physical size and design. It will take about five time constants to obtain steady state readings. Several factors come into play: the most

commonly noted is "time constant" (thermal response time). Time constant, or thermal response time, is an expression of how quickly a sensor responds to temperature changes.
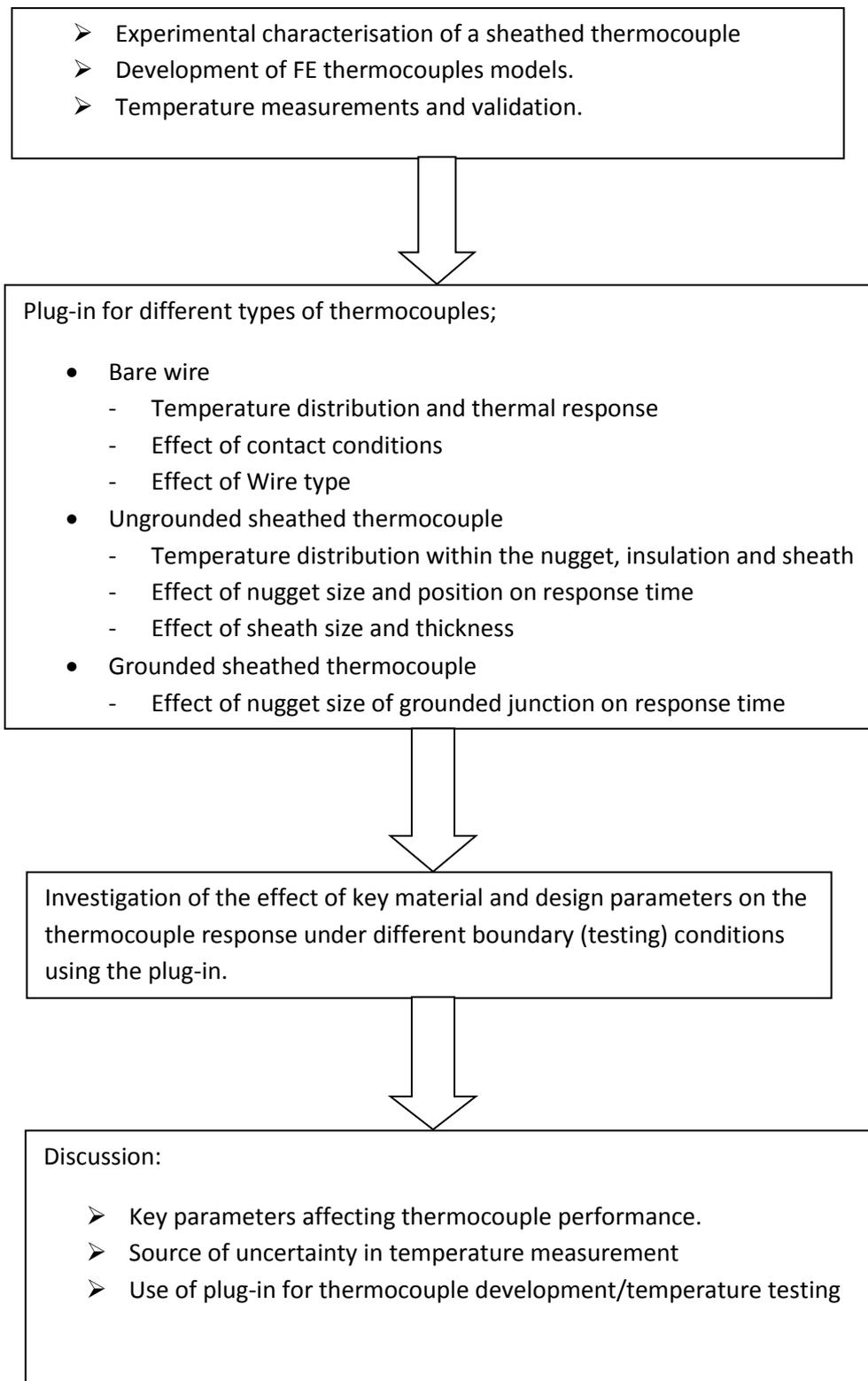
Figure 4.2 Flow chart showing the main research works.

As shown in Figure 4.2, the work in this chapter consists of three interlinked parts. The first section includes work on developing FE models for simulating the thermal response of the thermocouple using a thin sheathed thermocouple as a case. In Figure 4.2, the work included characterisation of the sheathed thermocouple by sectioning it to obtain the key dimensions' parameters. The parameters are used in building a finite element model of a sheathed thermocouple. The FE modelling results are compared to experimental tests.

In the second section, the work on developing Abaqus plug-in for three types of thermocouples has been presented. In each section, the main features designed for different types of thermocouple are detailed, the plug-in is designed such that it can be used to investigate some special cases for thermocouples such as, contact or heating conditions. For example, in certain applications the thermocouple may be in partial or full contact with the medium being measured. Some typical results using the plug-in to investigate the effect of heating conditions on the response of thermocouple are presented. For the bare-wire thermocouple, the main focus is on the heating area and the response time: the ungrounded sheathed thermocouple has a range of issues that are investigated including, the size of the welded tip junction and the position of the welded tip (distance from the end of the thermocouple), and the sheath width. For the grounded sheathed thermocouple, the size of the welded grounded junction is studied (a large junction maybe used for improved mechanical properties). Different thermo-element alloy wire materials are investigated at a range of temperatures using the plug-in. The three types of thermocouples are compared against temperature response time.

Some key issues regarding the thermal modelling of thermocouples are disused, such as, Key parameters affecting thermocouple performance, Source of Uncertainty in temperature measurement, Use of plug-in for thermocouple development/temperature, and Development of Abaqus plug-in for thermocouple wells and complex temperature measurement assembly. A program for designing and modelling a multipoint thermocouple system is also developed and illustrated by some type cases.

4.2 Characterisation of sheathed thermocouple, FE model development and validation

Figure 4.3 is a microscope image of a sheathed thermocouple cross section. The thermocouple sample had been used in the experimental work. It had been cut to determine the position of the wires and the tip/nugget (hot junction) within the sheath and insulation. The tip end of the thermocouple is firstly cut, then mounted in a plastic epoxy thermosetting phenolic material (Bakelite) before being ground and polished. The sample is a section from the tip-section of the thermocouple, detailed measurements were then made to determine the nugget size and its position. The diameter of the wires, insulation thickness and the sheath can also be determined. These will provide data for building a detailed FE model. The longitudinal section shows the location and size of the tip/nugget. The size of the nugget is limited by the geometry of the sheath and wires; it is important that a solid joint forms the junction between the wires. The location of the nugget may have an effect on the time response of the thermocouple to reach the measured temperature. This is also dependant on the point of contact the thermocouple has with a heat source.

| Longitudinal cross-section of the sheathed thermocouple | Thermocouple sample used in the experimental work. |
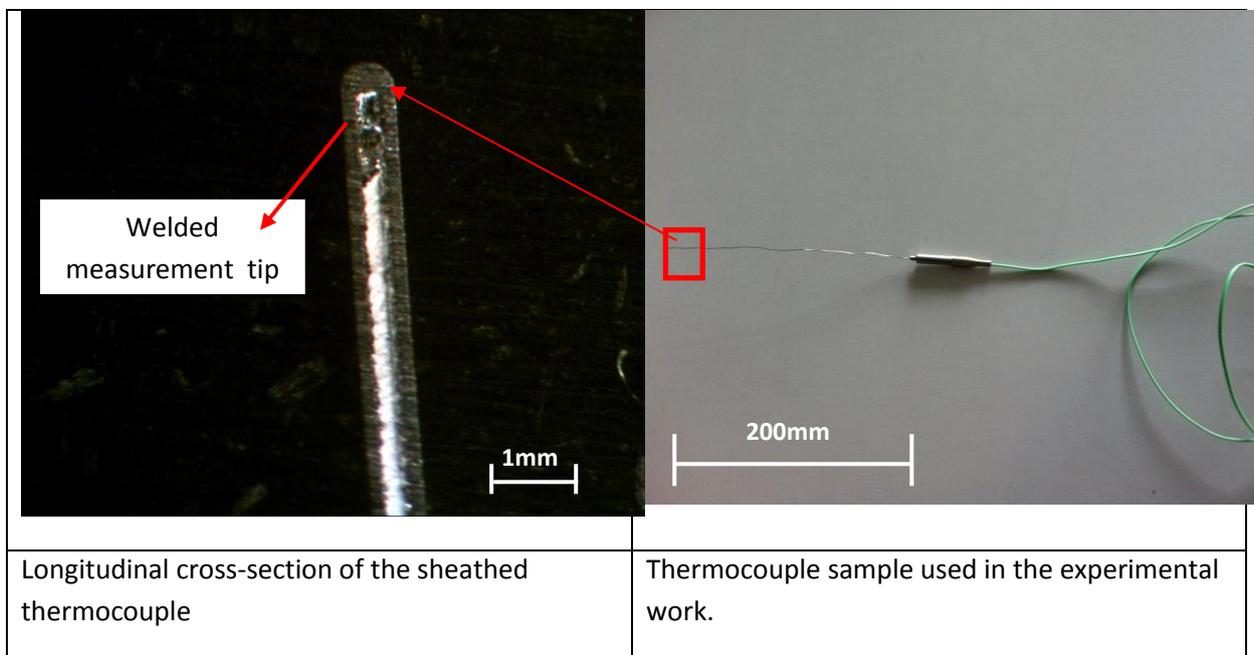
Figure 4.3 Experimental sample of thermocouple.
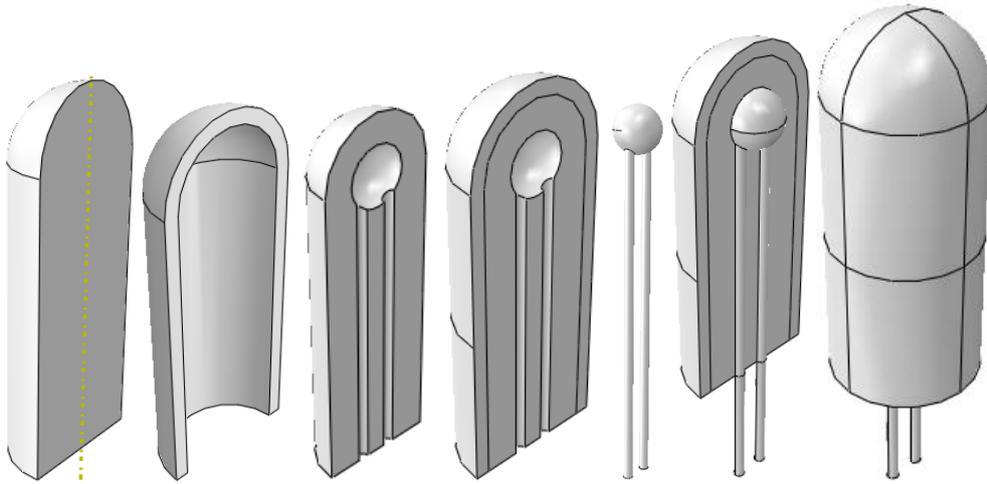
Figure 4.4 (a) Sequential cutting and merging method used in building the assembly of sheathed thermocouple.

Figure 4.4 (a) shows the method used to generate the FE model of the sheathed thermocouple. The FE model of the sheathed thermocouple consists of the welded tip, wires, insulation and the sheath. All these parts have different shapes and properties. One key issue is to produce a proper assembly. Many different approaches have been evaluated and the most effective method is through sequential cutting and merging. In the process, rather than produce the part based on it dimensions, the interface between the wire and insulation is produced in an operation using the tip and wire to cut the insulation, then using the assembly to cut a sheath block.
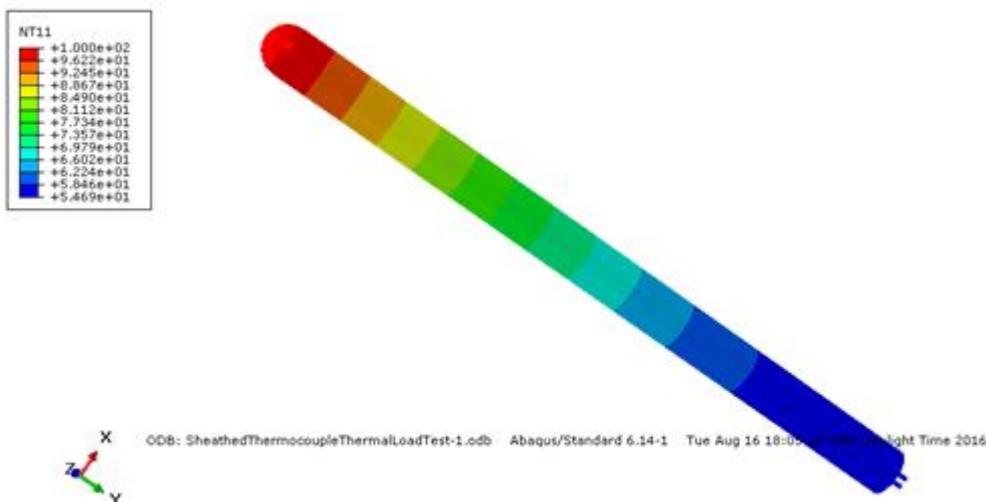
Figure 4.4 (b) FE model of sheathed thermocouple based on the dimension of a real thermocouple (Figure 4.3).

Figure 4.4 (b) shows a contour plot of the complete FE model of the sheathed thermocouple under typical thermal load test conditions. Meshing the assembly posed a challenging task, given the complex nature, in particular the insulation with the embedded joint of wire. Detailed partition is required to be able to mesh the system properly. The final 3D dimension assembly consists of 4922 elements. The element types are DC3D4, DC3D6 and DC3D8. Mesh sensitivity tests have been conducted.

Due to the complexity of the sectioning required to achieve a fully converged mesh, a 2D model was also generated. This was to compare the sensitivity of the 2D model against the 3D model. The benefit of using a 2D model would be to reduce processing time so that multiple tests for varying load cases can be executed. Changes to the 2D model would have very little impact on the re-meshing convergence. The results (in Figure 4.6) of the test showed that the 2D and 3D models were similarly accurate.
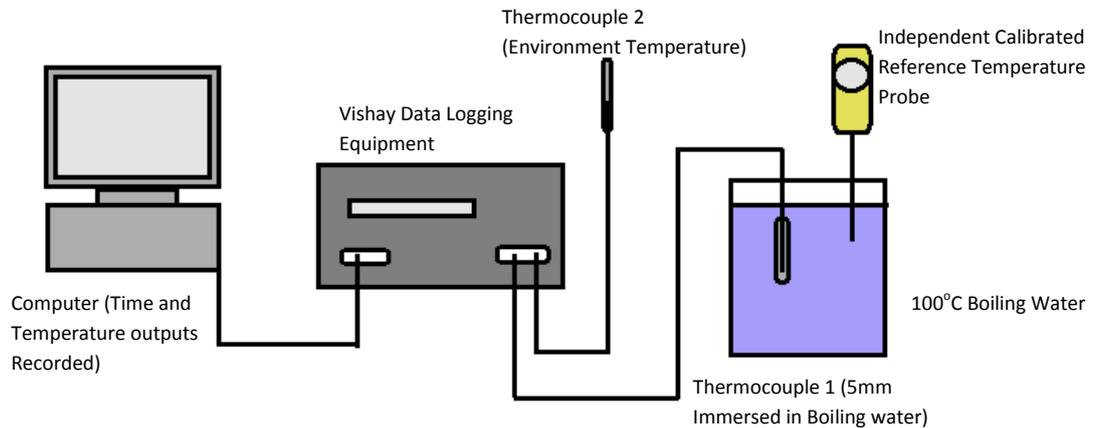
Figure 4.5 Schematics of Set-up of the boiling water tests for characterising the performance of the sheathed thermocouple.

Experimental work has been conducted in order to validate the FE models. Figure 4.5 shows a typical set for testing measurement devices against a known reference temperature. In the test set up boiling water was used, as water boils at 100°C. It was used to determine the response time a thermocouple takes to reach 100^{0}C from ambient temperature. These results would validate FE Simulation models. As the boiling water is still in liquid form the thermocouple is submerged and full contact occurs with the heat source. Another test performed (not shown) is a furnace test, the temperature in the chamber is independently monitored by a calibrated temperature sensor. This test is performed to determine the response time a thermocouple takes to reach 100°C from ambient temperature. The thermocouple is placed in the chamber to measure the air temperature, the response may vary

due to the environment (hot air rises) therefore, the position of the thermocouple in the chamber may have an impact on the result. These two test methods are similar to the standard devices used to calibrate thermocouples against reference temperatures in industries such as, petro-chemical, oil, gas, nuclear, aerospace and pharmaceutical manufacturing. Stirred Liquid Baths and Dry Block Baths for instrumentation engineers to calibrate thermocouples (ASTM E220-13& BS EN 60584-1:2013).
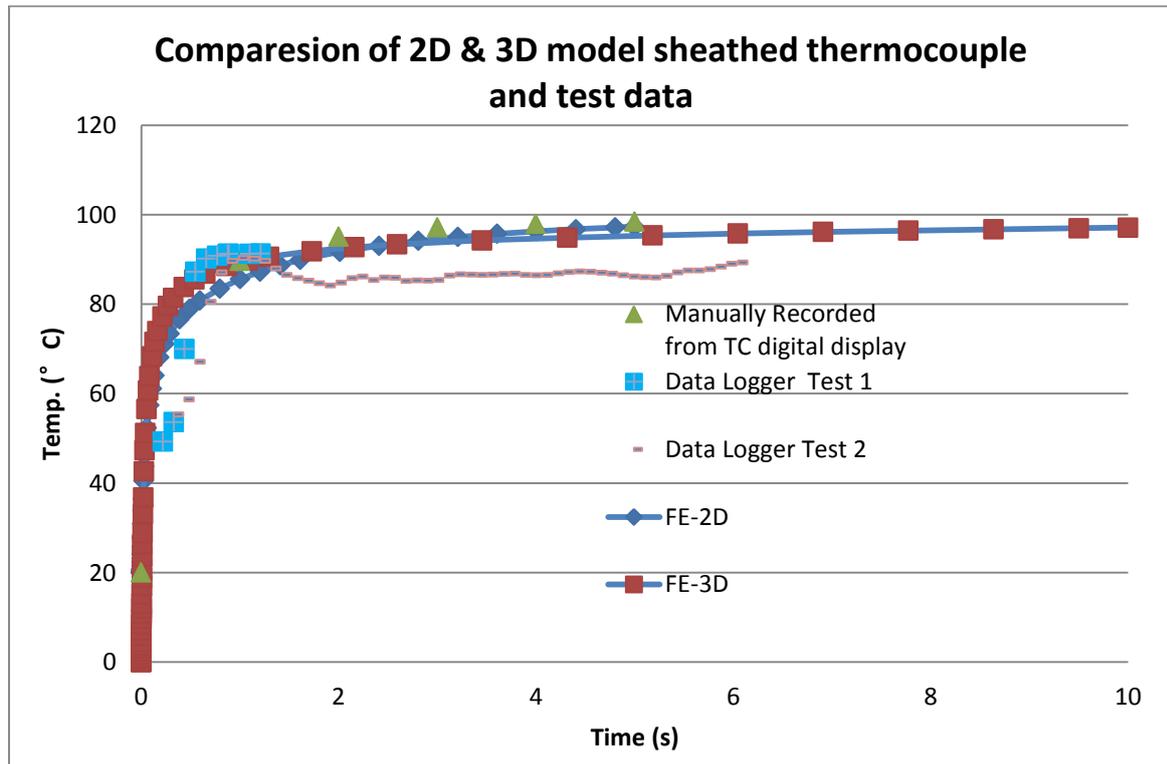
Figure 4.6 Comparison between the modelling results based on the FE models in comparison with the experimental test data.

Figure 4.6 shows a comparison between the modelling results based on the 2D and 3D models in comparison with the experimental tests data from using the instrumental method. In all the cases, the FE data showed a reasonable agreement with the testing data. All temperature measurements achieved over 80% of the reference temperature in less than one second. After the first second the experimental test sample thermocouple responded similarly to both the 3D and 2D FE model heat up trends. The thermocouple FE models and experimental samples had a near identical temperature-time response for the remainder of the test, until the reference temperature was achieved. The experimental data validated the

simulation models. There was minimal difference between the 2D and 3D model trends, both had similar curves and temperature profiles. The percentage error was between the FE models and experimental data was approximately 15% (during the first second) and less than 2% for the remainder of the test. A potential cause for the difference in temperature-time response during the first second, could be that the number of measurements the data recorder logs per second was too low. As the temperature increased rapidly in during the first second, too few temperature changes have been recorded. When the rate of temperature increase is slower the data logger results completely converge with the FE model data.

4.3 Key factors and design concepts of the plug-in for different thermocouples

Table 4.2 Main plug-in parameters and loading conditions of different types of thermocouples

Thermocouple type	Main parameters in the Plug-in	Loading condition
Bare-wire	Tip size, tip shape, wire diameters. Wire types, effectives heating length	Fully contact, partial tip contact, radiation
Sheathed thermocouple	• Tip size, tip shape, wire diameters. Wire types, effectives heating length. • Sheath thickness, sheath material. • Insulation material	•Fully contact, partial tip contact, radiation
Grounded sheathed thermocouples	• Tip size, tip shape, wire diameters. Wire types, effectives heating length. • Sheath thickness, sheath material. • Insulation material • Tip-sheath contact conditions	•Fully contact, partial tip contact, radiation. •Mechanical deformation of the sheath under compression and indentation.
Multi point thermal well	Size of the tube, thermocouple coupled number, thermocouple position,	Response time in open/closed heating(apply surface temperature)

Table 4.2 Lists the key factors and design concepts of the plug-in for different thermocouples. The three thermocouples vary in geometry and design, therefore, the procedure to assemble the models was slightly different in each case. Each model was sketched using the x,y,z co-ordinates 0,0,0 as a reference. This was done so that if there was a requirement to make the model parametric, it would be easier to make adjustments.

The bare-wire model consisted of the three parts (two wires and a tip/nugget). Although in a practical environment the tip of a thermocouple isn't perfectly circular, it was decided that this model would be created with the assumption that it is circular.

The assembly is made by generating individual solid parts for the tip/nugget and wires. A consecutive cutting method was used; Wire-1 and Wire-2 were cut by tip/nugget. All of the cut parts are then merged together to generate a bare-wire thermocouple assembly (retaining instances so that each section of the model can have its own material properties and be defined as a set).

In industry, temperature instrumentation that is in situation normally gives an accurate representation of process temperature measurement as the device is completely exposed to the environment. However, this is not always the case, as some processes do not allow intrusive devices within closed systems. Therefore, sometimes surface contact is only feasible (such as, clip-on thermocouples, use of thermal heat sinks etc.). The response of the bare-wire thermocouple is reasonable, when there is only partial contact with the load the remaining surface area of the junction is still exposed to the ambient temperature.

Placement of the sensor in relationship to the work load and heat source can compensate for various types of energy demands from the work load. Sensor placement can limit the effects of thermal lags in the heat transfer process. The controller can only respond to the temperature changes it "sees" through feedback from the sensor location. Sensor placement will influence the ability of the controller to regulate the temperature about a desired set point. Inside most thermal systems, temperature will vary from point-to-point.

4.4 Structure of the Plug-in for bare-wire thermocouple and effect of contact conditions.

Figure 4.7 is a plug-in interface for defining the thermocouple type and relevant material properties, thermal load, and dimensions. The program consists of geometry module, material properties and boundary and loading modules, there was scope for generating this interface as multiple and varied models are required to validate work throughout industry. This requirement was also important as it reduces user input time. The Geometry interface generates a three dimensional bare-wire thermocouple model. An advantage of this interface is that it can rapidly produce multiple models of varying dimensions for different cases. The interface is user friendly and requires minimal input in order to generate a model. The plug-in also reduces man hours required to assemble a model manually.

The geometry interface displayed in Figure 4.7 (a) shows a sectioned image of the bare-wire thermocouple model. It is labelled to identify the location of the dimension that can be adjusted. It also has user defined fields to provide a model name and the adjustable dimensions; length (L) is the length of the wires, width (w) is the width of the wires and Radius (R) is the radius of the Tip/nugget. Nominal Default values automatically appear on the interface and these can be changed as per the user requirements. The step phase user commands (inputs) are required to operate the interface and produce the geometry. Define a unique model name (with no spaces or characters). Numerically input geometry values for the length, width of the wires and define the tip/nugget size (radius). Click 'Ok' once all input boxes contain a value. A model will then be generated to the user specified dimensions. Given the complex nature of different testing conditions, the user can modify the heating length or positon easily. As shown in Figure 4.7 (b), the material module provides an interface to input the material properties for the wires and welded junction. The key material properties for thermal can be temperature dependent. The boundary condition for thermocouples is also very critical. The boundary can be applied as a surface temperature or through using a heat sink as shown in Figure 4.8. The model can also allow the application of boundary conditions such as, convection or radiation coefficient through specifying the film properties. One important factor for thermocouples is the contact condition. In different measurement conditions, for example solid to solid contact condition, the thermocouple will only be in partial contact with the surface to be measured. To investigate the potential effect

82

of partial contact, in the FE model, the tip for the thermocouple is partitioned into different sections to be able to systematically simulate.
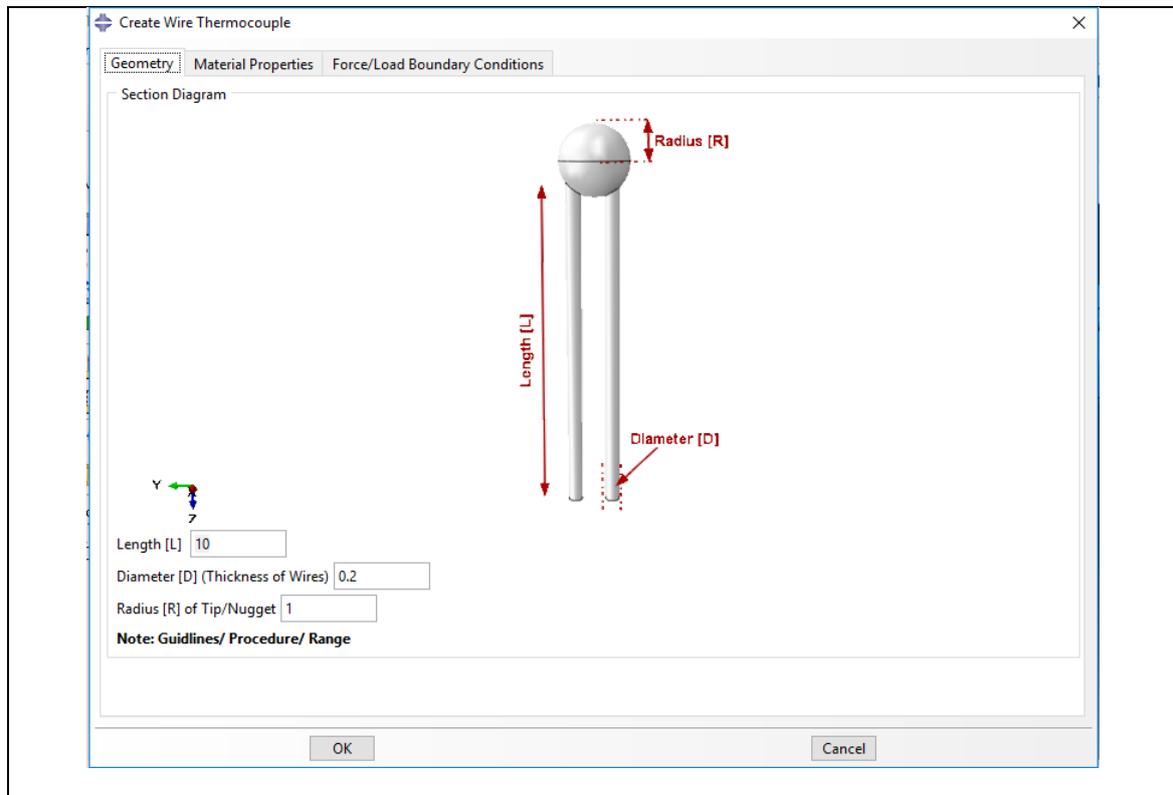
a) Structure of the Geometry Interface for the Plug-in
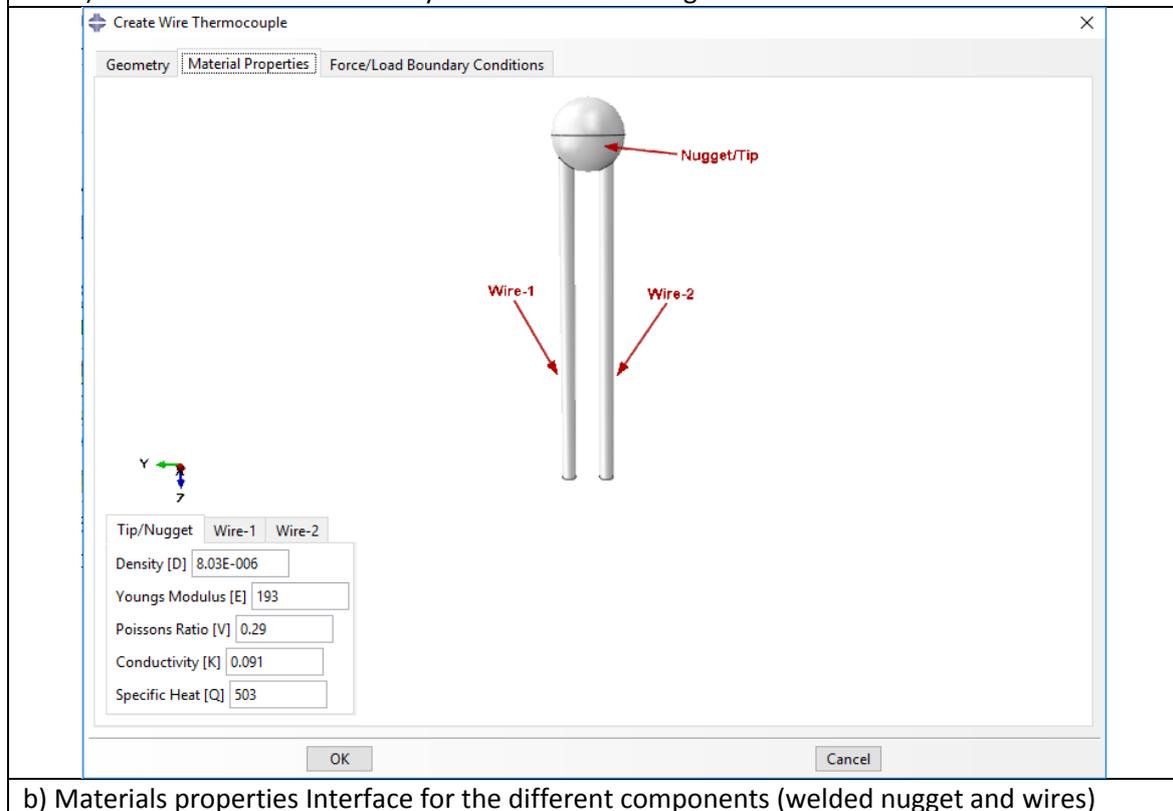
b) Materials properties Interface for the different components (welded nugget and wires)

Figure 4.7 Design of the plug-in for bare wire thermocouple: key components

Figure 4.8 illustrates the typical boundary conditions (point contact and full contact conditions to be investigated. As shown in the figure, the nugget of the thermocouple has been partitioned into sections to define surface contact area. Certain applications may only allow limited surface contact and exposure to the environment that is thermally being measured. Therefore, the model has been divided into sections to apply loads on either a quarter, half or the whole nugget surface. Selecting different contact conditions is essential for accurately measuring temperature response. The plug-in interface provides an option that allows the user select a contact condition, the plug-in then systematically applies these conditions, effectively and efficiently producing a model reflective of a practical application.
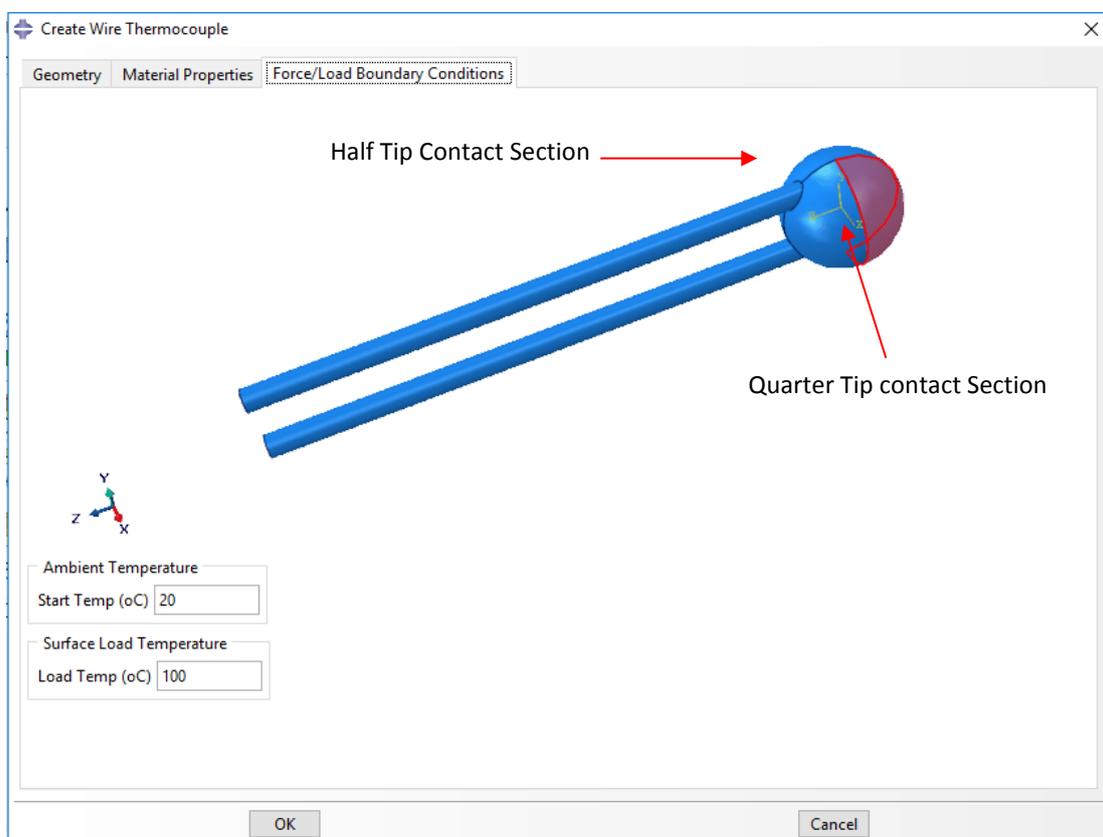
Figure 4.8 Design of Plug-in Typical boundary conditions (point contact, full contact and nugget and wire contact).

Figure 4.9 shows the time taken for a bare-wire thermocouple to measure the load temperature (set at 100°C) when the nugget of the thermocouple is in full contact with the heat source. The results of the test show that the final temperature is measured within one second. The nugget reached 90% of the temperature within about 0.2 second. The nugget reached a temperature close to the measuring temperature while the wire is still in a transient

heating stage. The effect of the contact area (loaded area) is studied using the plug-in by assigning the temperature in controlled areas. The average temperature response for all nodes within the thermocouple tip (nugget) was taken to plot the results. To ensure the test data was comparable between the results, the only variable between models executed was the area of contact used. Three surfaces were selected for each load case, quarter, half and full surface contact of the thermocouple tip. The same dimensions for the nugget and wires, the same material properties and the same temperature of $100^{o}C$ was used as the surface load temperature.

(a) Typical temperature distribution within the nugget and the wire after exposure to a load temperature of 100°C.

(b) Temperature-time curve of the nugget
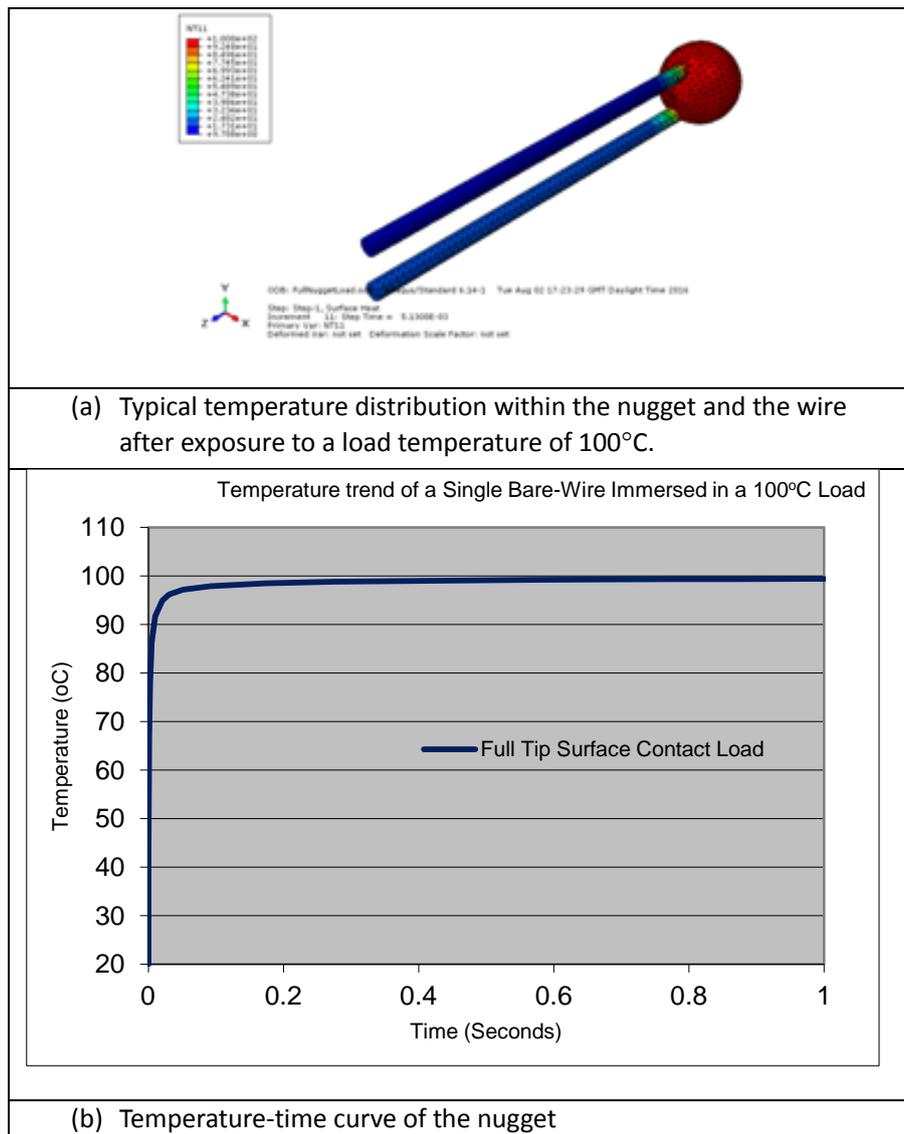
Figure 4.9 Typical Temperature response time of a bare-wire thermocouple.

The resulting temperature contour is shown in Figure 4.10 (a) and the temperature response curve is shown in Figure 4.10 (b). As shown in Figure a, at the initial stage (0.05 second), the heating pattern is clearly different with different loading areas. The average temperature of the tip also shows a different response. The data shows that each load case achieves the load temperature of 100°C in less than a second. The data confirms that a greater surface contact zone on the nugget causes a more rapid response.

a)   Typical temperature distribution in the heating up stage under different contact conditions

b)   Temperature-time response
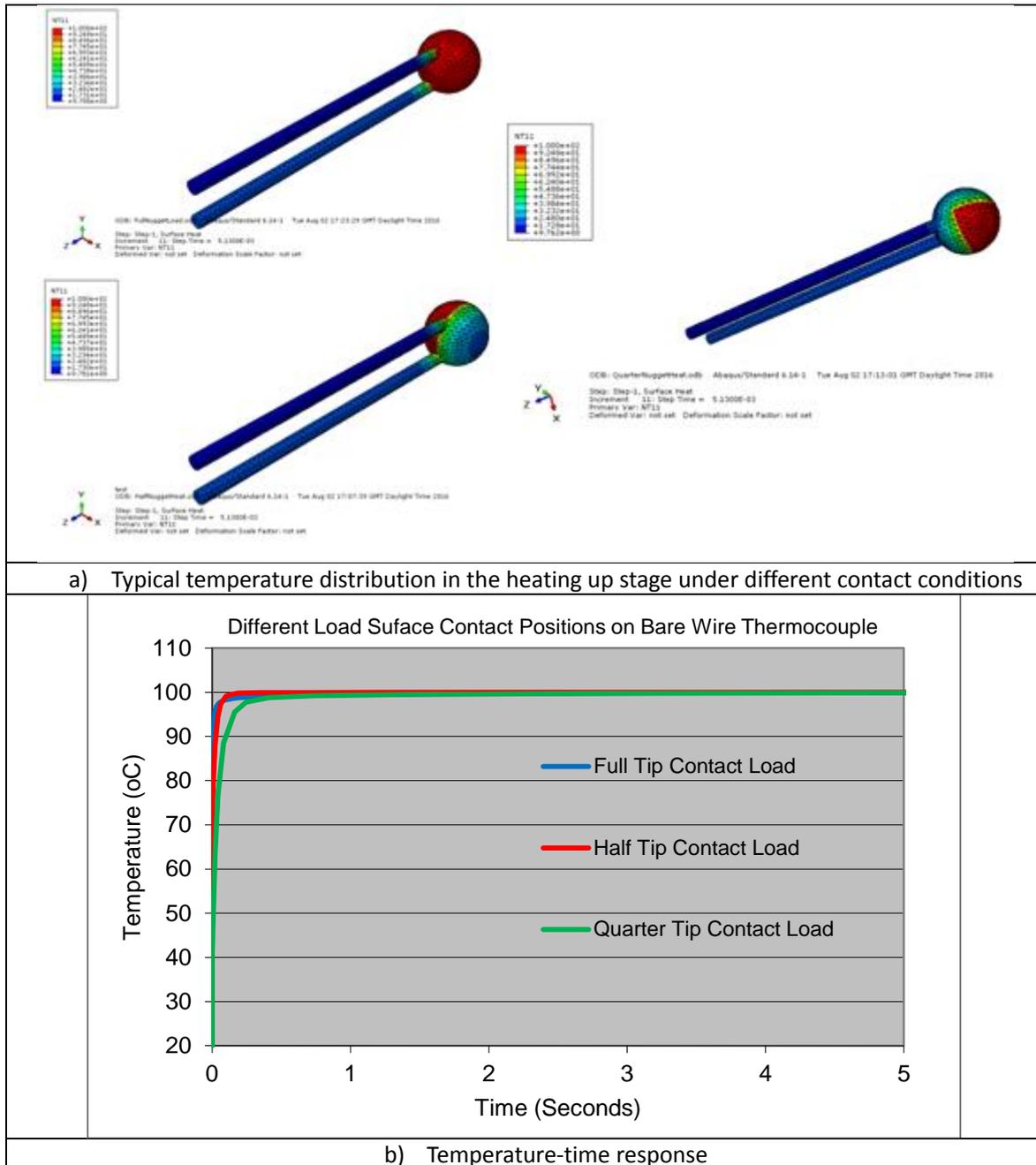
Figure 4.10 Temperature distribution showing the effects of different surface contact positions for a bare-wire thermocouple.

4.5 Structure of the Plug-in for sheathed thermocouple and effect of nugget position and contact conditions. (this includes both ungrounded and grounded)

Figure 4.11 is a plug-in interface for defining the ungrounded sheathed thermocouple. As shown in Figure 4.11 (a), (b) and (c), ungrounded sheathed thermocouples have a much more complex structure with multiple components. All the components including, the welded nugget tip, wires, insulation and the sheath have different properties. The property for the wire and the welded nugget tip varies among different thermocouple types, the insulation material is a ceramic, magnesium oxide power. MgO has high electrical resistance. The sheath is normally stainless steel with better corrosion resistance.

a) Structure of the Geometry module of the Plug-in
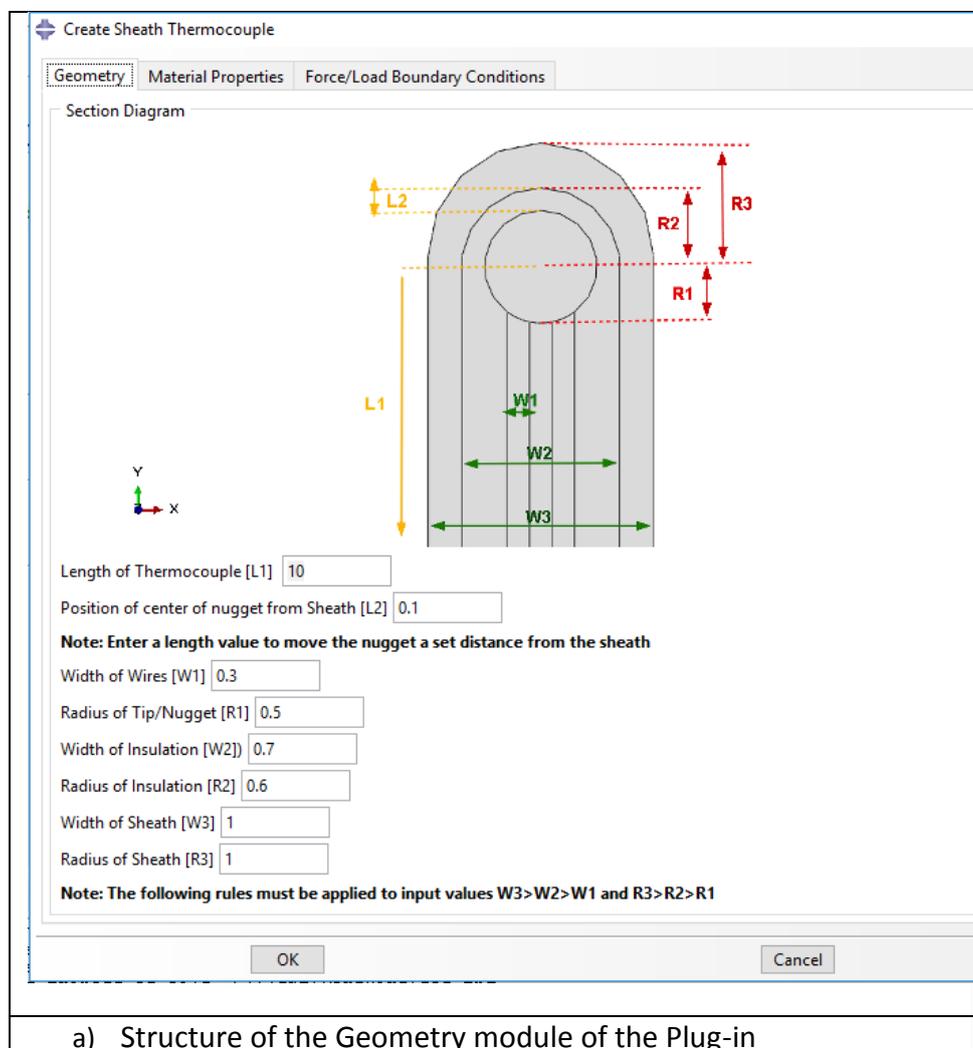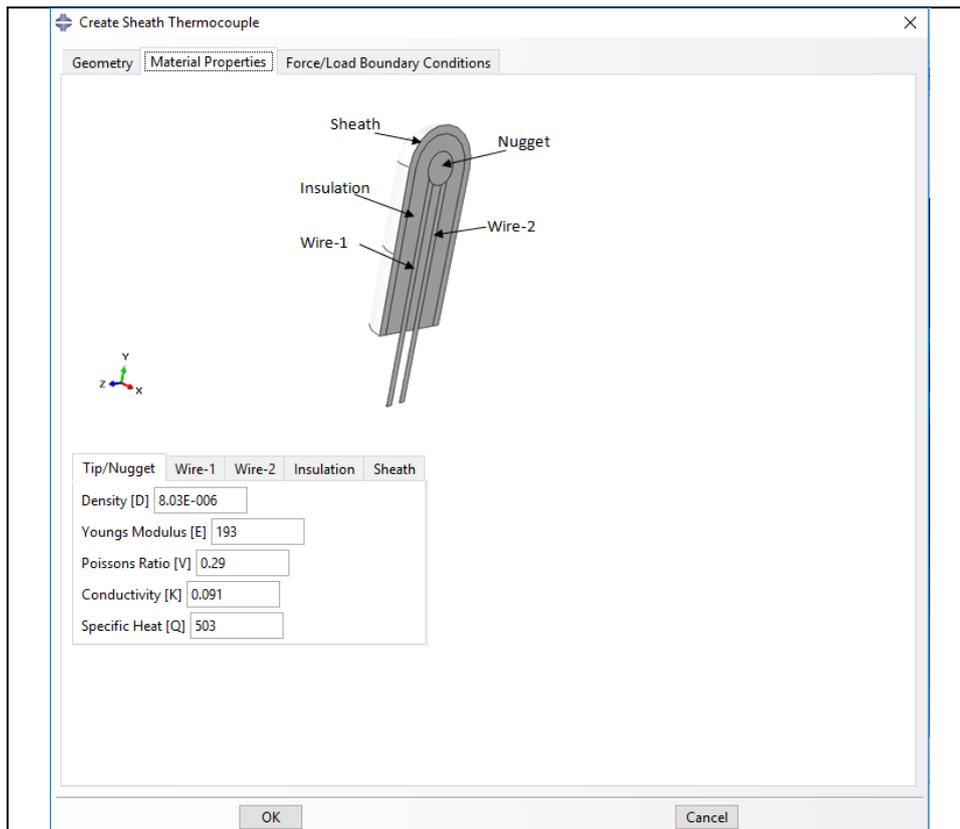
b) Materials Properties module for the different components
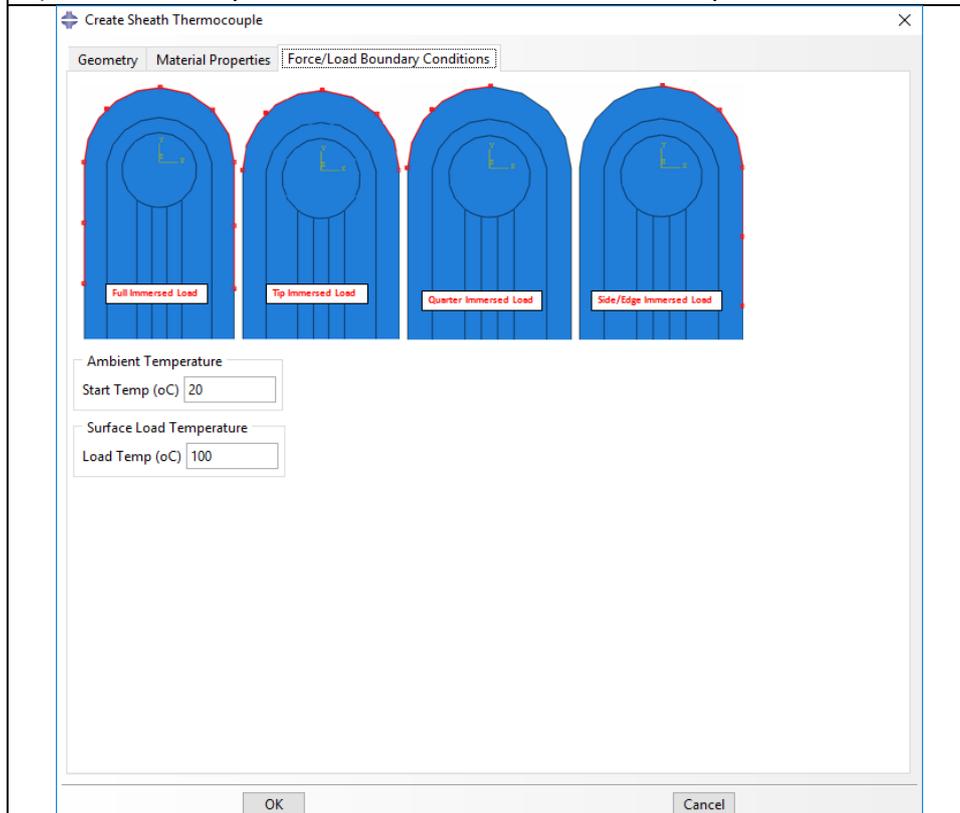
(c) Initial and Boundary conditions including design of tip for studying the effect of load contact area

Figure 4.11 Design of the plug-in for sheathed Ungrounded Tip Thermocouple: key components, dimension, material and boundary condition.

The geometry module (a) for a sheathed thermocouple is much more complicated than the module for bare-wire thermocouple. It consists of normal dimensions such as, the size of the wire and tip, the dimension of the insulation and sheath controlled by the radius of the tip and the width. One key new feature is the introduction of the parameters representing the position of the welded tip junction. This allows the study of the welded tip position on the response/performance of the thermocouple. The material properties module (b) covers all relevant material properties such as, densities, thermal conductivity, specific heat, etc. The Boundary loading conditions module (c) shows the tip of the thermocouple partitioned in order to apply temperature or heat to localised areas for the study of the influence of heating areas.

The geometry interface is the main executive interface with a sectioned image of the bare-wire thermocouple model. It is labelled to identify the location the dimension that can be adjusted. It also has user defined fields to provide a model name and the adjustable dimensions; length (L) is the length of the wires, width (w) is the width of the wires and Radius (R) is the radius of the Tip/nugget. Nominal Default values automatically appear on the interface and these can be changed as per the user requirements. The step phase user commands (inputs) are required to operate the interface and produce the geometry. Define a unique model name (with no spaces or characters). Numerically input geometry values for the length, width of the wires and define the tip/nugget size (radius). Click 'Ok' once all input boxes contain a value. A model will then be generated to the user specified dimensions.

Figure 4.12 shows the temperature-time curve of the individual components that generate a sheath thermocouple assembly when a temperature of 100°C is applied to the full tip of the thermocouple through the sheath surface.The temperature response for all components that generate a sheath thermocouple was taken to plot the results. A 100°C load was applied to the surface of the sheath tip. Temperature measurements were taken at the nugget, wires, sheath and insulation parts of the sheath thermocouple. Each part achieves the load temperature of 100°C in less than a second. The data confirms that sheath part has the greatest response and achieves the load temperature in the shortest time.
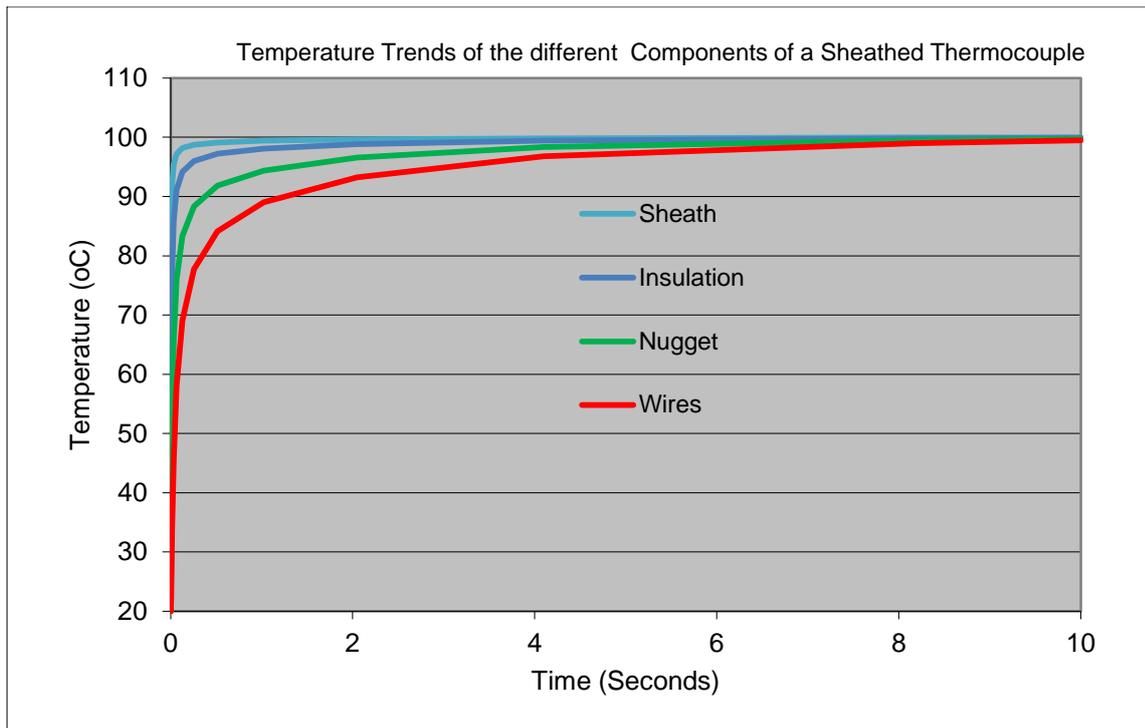
Figure 4.12 Temperature-time curve of the individual components (nugget, wires, sheath and insulation)

Figure 4.13 shows how the tip of the thermocouple is partitioned in order to model the effect of contact boundary conditions (point contact, full contact and nugget and wire contact) on the response of a sheathed thermocouple. As shown in the figure,the sheathed thermocouple has been partitioned into sections to define surface contact area. This study is essential as certain applications may only allow limited surface contact and exposure to the environment that is thermally being measured. Therefore, the model has been divided into section to apply loads on either a quarter, half or the whole sheath surface. Selecting different contact conditions is essential for accurately measuring temperature response. The plug-in interface provides an option that allows the user to select a contact condition, the plug-in then systematically applies these conditions, effectively and efficiently producing a model reflective of a practical application.
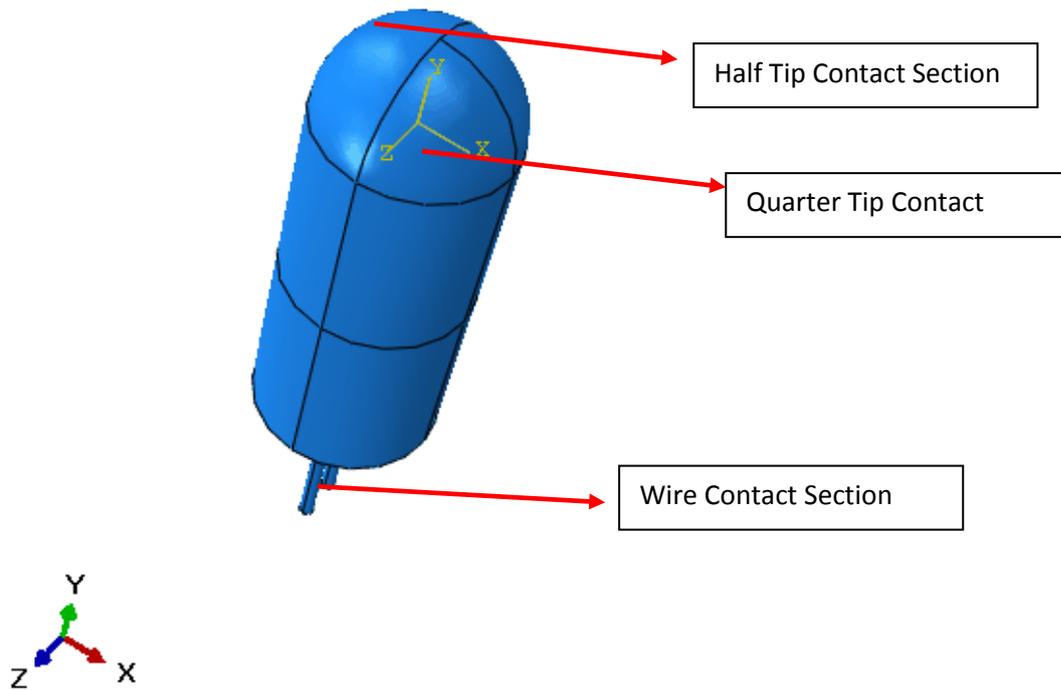
Figure 4.13 Diagram to show the contact boundary conditions (point contact, full contact and nugget and wire contact).

A typical set of data for K type thermocouple under different heating conditions (i.e. loaded area) is plotted in Figure 4.14. The average temperature response for all nodes within the thermocouple nugget was taken to plot the results. To ensure the test data was comparable between the results, the only variable between models executed was the area of contact used. Four surfaces were selected for each load case: fully immersed, tip contact, quarter contact and side/edge contactsurface contact of the sheath thermocouple tip. Identical dimensions for the nugget and wires, the same material properties and the same temperature of 100^oC was used as the surface load temperature.

Figure 4.14 (a) shows the temperature contour plots for each contact condition (Fully immersed, tip contact, quarter contact and side/edge contact) 0.05 seconds after contacting the heat source. The chart in figure 4.14 (b) shows temperature trends for the three contact load cases. Each load case achieves the load temperature of 100^oC in less than a second. The data confirms that a greater surface contact zone on the nugget causes a more rapid response.

Full Immersed Surface Load	Quarter Tip Surface load
Tip Surface Load	Side/Edge Surface Load

Different heat/load surface contact locations temperature-time response

Figure 4.14 Temperature distribution and temperature-time response showing the effects of different surface contact positions.

Figure 4.15 is a plug-in interface for defining the grounded sheathed thermocouple. In a grounded thermocouple, the wire is directly linked to the end of the sheath. As shown in

Figure 4.15 (a), (b) and (c), grounded sheathed thermocouples have a much more complex structure with multiple components, with regards to model development. All the welded grounded junction, wire, insulation and the sheath have different properties. The property for the wires and the welded nugget onto the sheath varies among different thermocouple types, the insulation material is a ceramic, magnesium oxide power. MgO has high electrical resistance. The sheath is normally stainless steel with better corrosion resistance.
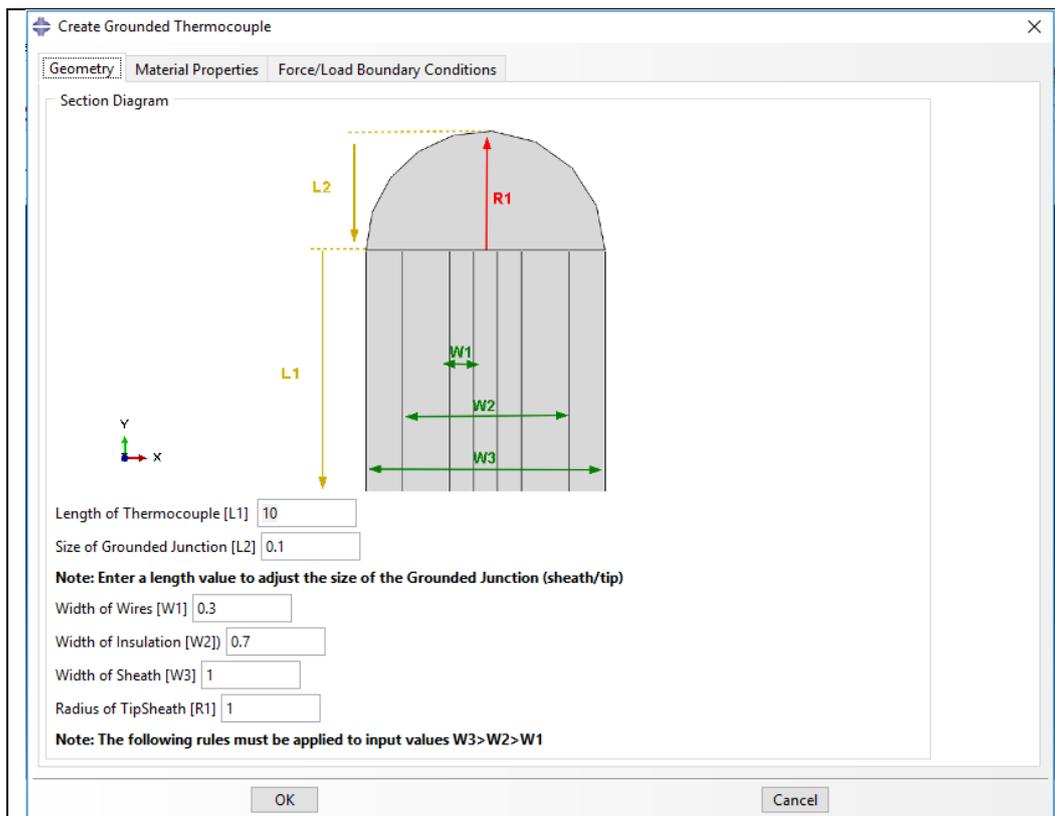
a) Key dimensions of thermocouple in which the wire is welded onto the sheath for the grounded thermocouple Plug-in
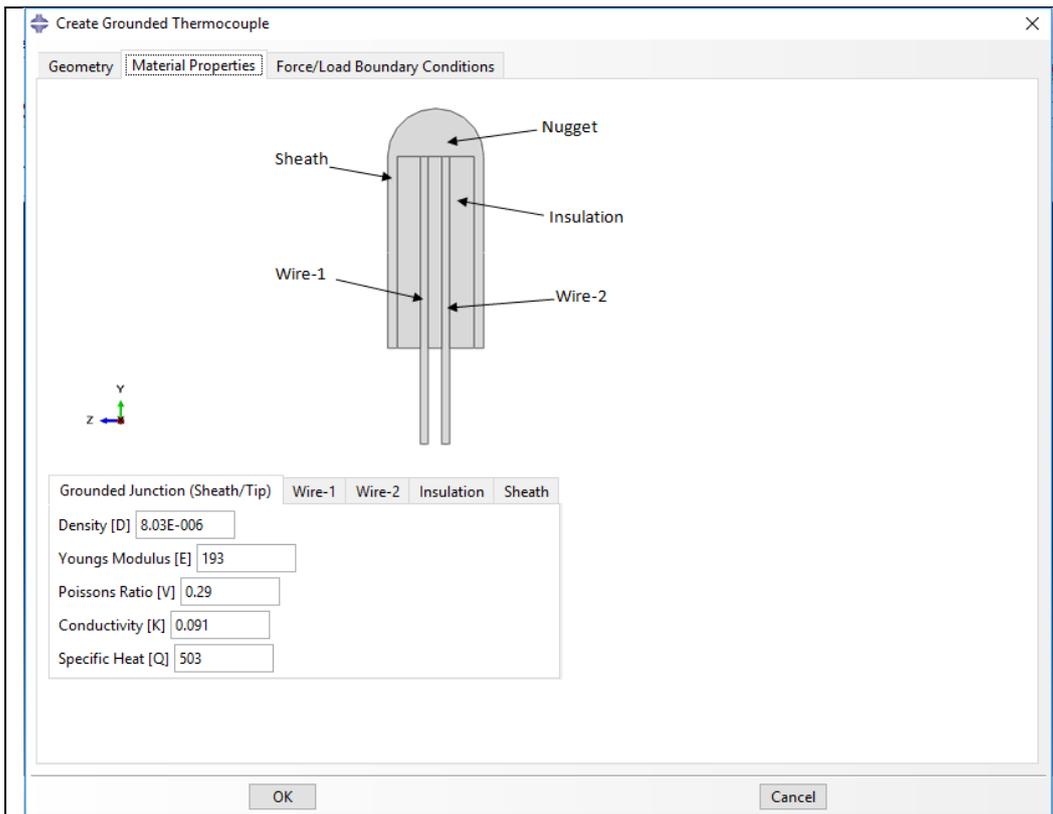
b) Materials Properties Input for the different parts
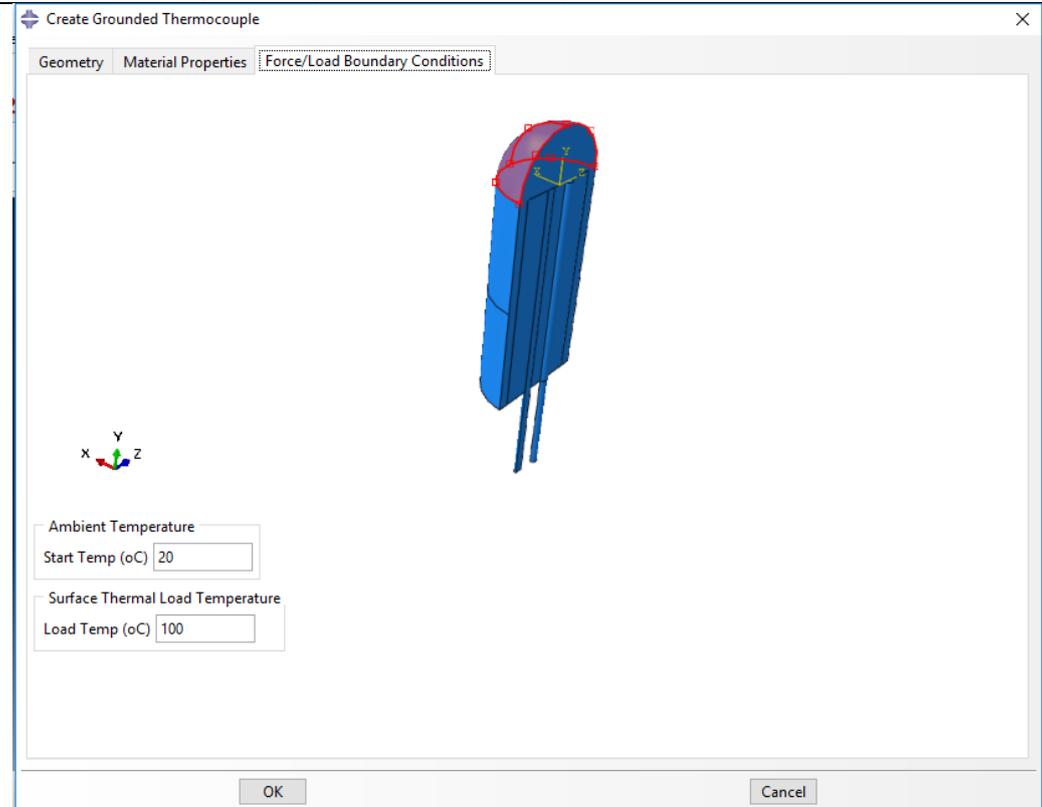
(c) Boundary conditions and testing

Figure 4.15 Design of the plug-in for sheathed Grounded Tip Thermocouple

94

The material of the sheath is dependent on the environment for intended use. In mild corrosive environments and general purpose applications, 304 SS and 316 SS are usually the best choice when considering cost versus performance. Alloy Inconel 600 and 310 SS when temperatures exceed 899°C (1650°F). Alloy 600 has high resistance to oxidization and corrosion at high temperatures. Pyrosil D has superior oxidation resistance to other sheath material properties, and high temperature strength that is compatible with the thermal co-efficient of expansion to nickel based type K and type N thermo-element wires. Magnesium Oxide (MgO) is a compact mineral powder used for electrical insulation in sheathed thermocouples. In these applications, the properties unique to this type of insulation are, its thermal stability, incombustibility, tolerance of high levels of irradiation, which cannot be matched by organic polymers, and high electrical resistivity at temperatures of the order of 1000°C are exploited.

The geometry module (a) for a grounded sheathed thermocouple is much more complicated than the module for bare-wire thermocouple. The welded grounded nugget junction differs from the conventional ungrounded sheath and bare-wire thermocouples. The grounded thermocouple consists of normal dimensions such as, the size of the wire, the dimension of the insulation and sheath thickness controlled by the width of the thermocouple. One advantage of this plug-in interface is the introduction of the parameters representing the size of the grounded welded junction. This allows the study of the size of grounded welded junction on the response/performance of the thermocouple. The material properties module (b) covers all relevant material properties such as, densities, thermal conductivity, specific heat, etc. The Boundary loading conditions module (c) shows the tip of the thermocouple partitioned in order to apply temperature or heat to localised areas for the study of the influence of heating areas.

Figure 4.16 shows the temperature-time response for the system under different surface contact loading conditions (Fully immersed, tip contact, quarter contact and side/edge contact). In all the cases, the temperature reaches 90% of the testing temperature within 0.2second. But the data showed a clear difference in response among different surface contact conditions. Each load case achieves the load temperature of 100°C in less than a second. The data confirms that a greater surface contact zone on the nugget causes a more rapid response.
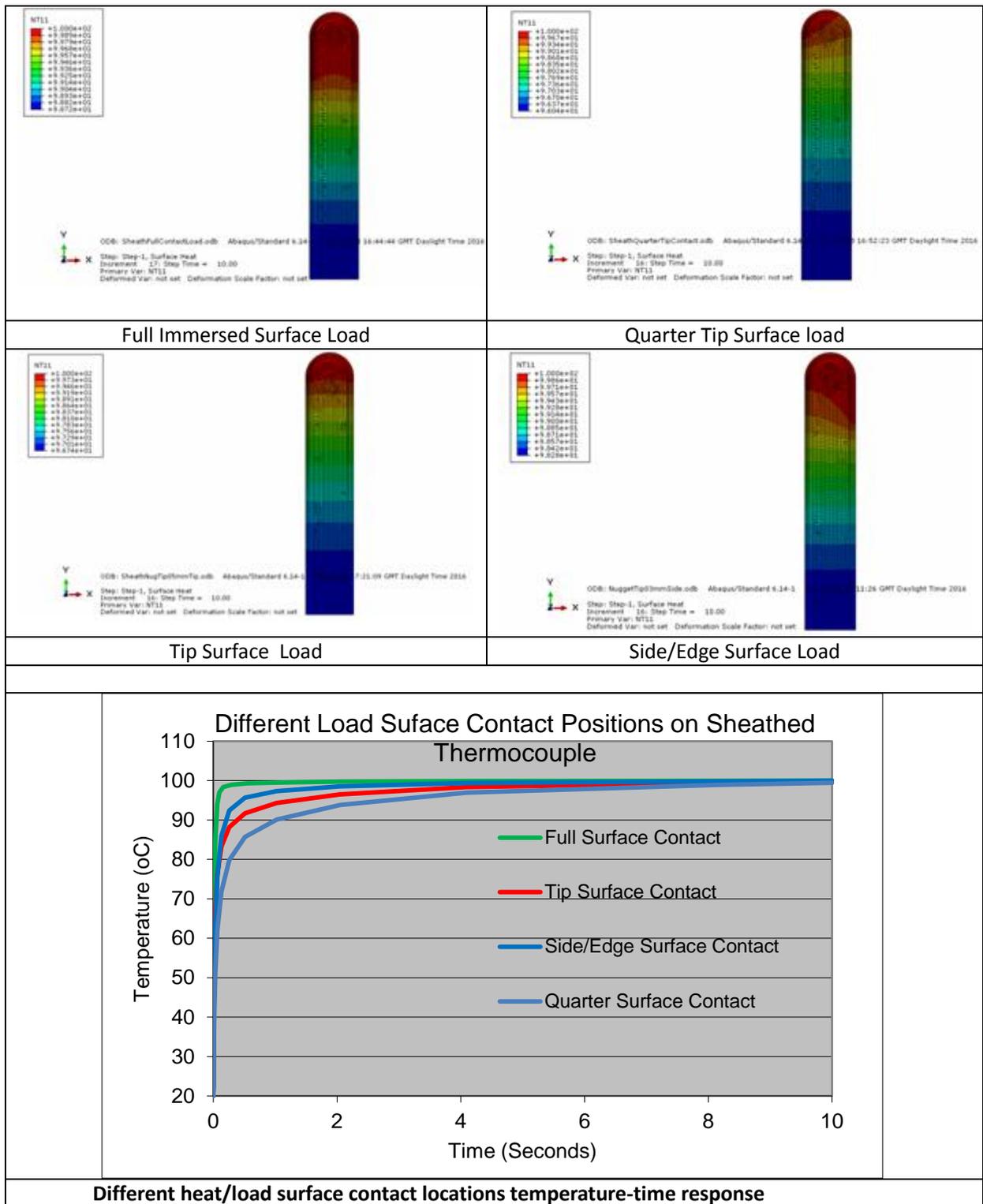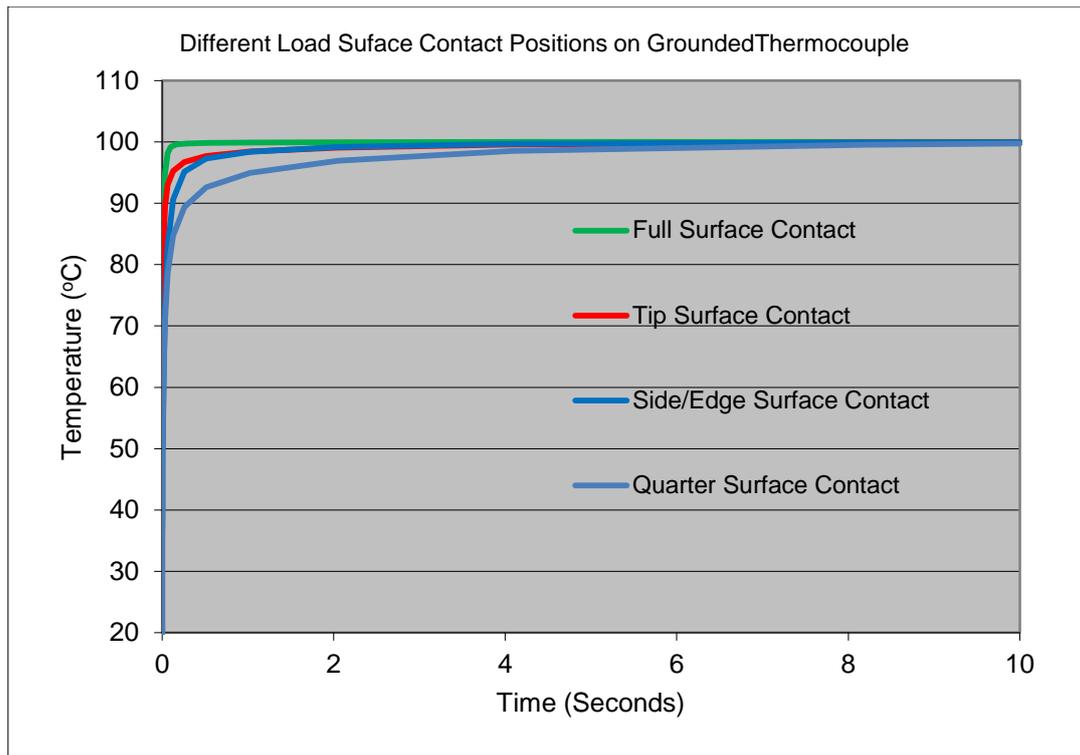
Figure 4.16 The effect of the contact condition on the thermocouple response (tip, tip+side, half tip and side)

4.6 Effect of welded nugget junction size position and contact conditions

As shown in the previous section, the thermocouple plug-in could provide a useful tool for modelling thermocouple responses to different conditions. Discussed in this section are the effects of wire type, nugget position, junction size and sheath thickness size.

Figure 4.17 shows temperature distribution comparing different time responses of bare-wire, sheathed and grounded thermocouples. To ensure the test data was comparable between the different thermocouple types, the same area of contact was used in the models (the tip), the same dimensions for the nugget and wires, the same material properties and the same temperature of $100^{\circ}C$ was used as the surface load temperature. The bare-wire thermocouple had the quickest response. It achieved 99.3% of the reference temperature in less than a second. The grounded and ungrounded sheathed thermocouples had a similar response measuring 99.3% of the reference temperature in less than four seconds.
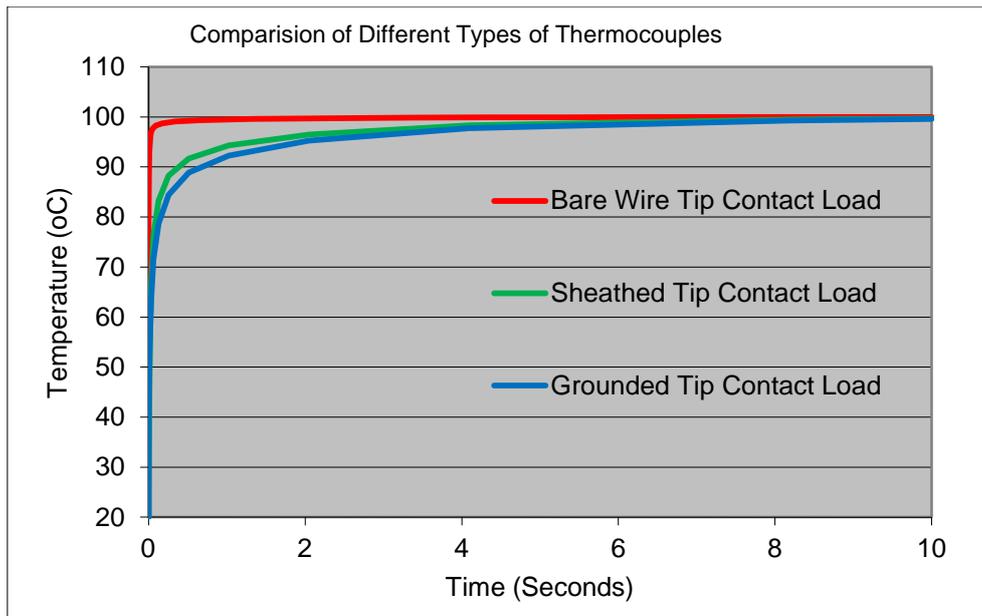
Figure 4.17 Response time of different types of thermocouples

Figure 4.18 (a), (b) & (c) show three examples of the changes made to the geometry of the ungrounded sheath thermocouple. Using five models the effects of varying distances between the welded nugget and sheath tip has been investigated. The user field for the function 'L2' was utilised within the plug-in. Distances of 0.4mm, 0.6mm, 0.8mm, 1.3mm and 1.8mm were defined in the ungrounded sheathed thermocouple plug-in. The output trend from the FE simulations is detailed in Figure 4.18 (d). The temperature-time results demonstrate that the position of the welded nugget, has a direct impact on the response of the thermocouple. The further away the welded nugget is from the sheath tip, the slower the temperature-time response.

| (a) 0.4mm between nugget and sheath tip. | (b) 0.8mm between nugget and sheath tip. | (c) 1.8mm between nugget and sheath tip. |

(d) Different Nugget Position temperature-time response
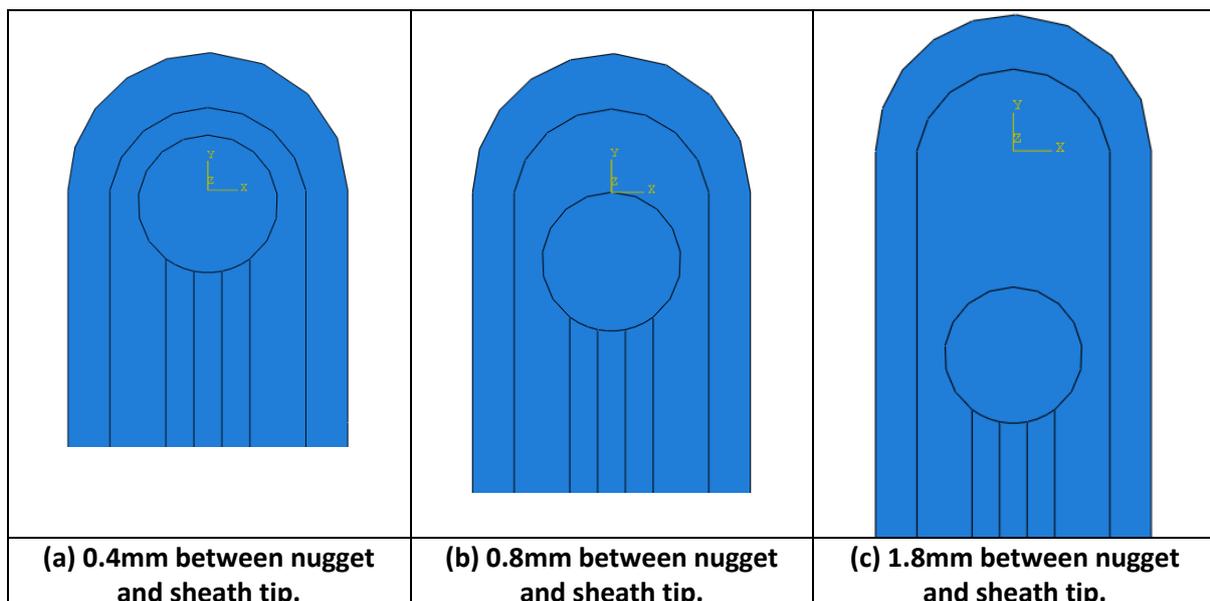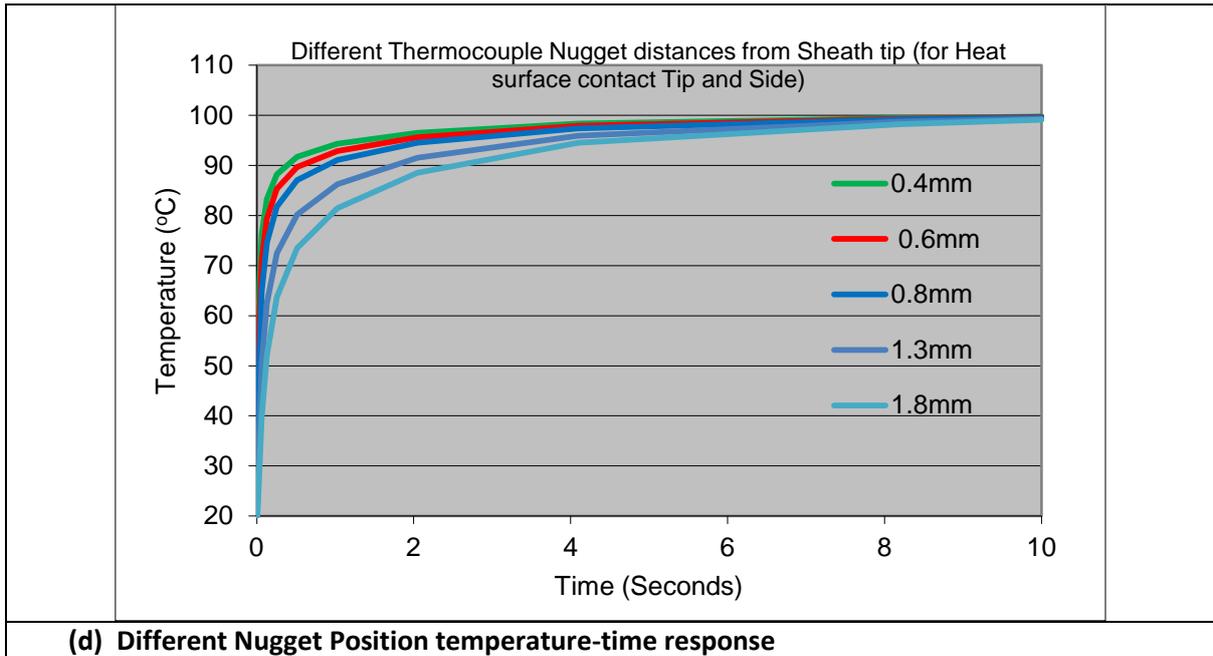
Figure 4.18 Response curve demonstrating the effects of variations in junction geometry, for Sheath Ungrounded thermocouple

The grounded junction thermocouple offers the best compromise of performance and reliability. It is the best choice for general purpose measurements. Figure 4.19 (a), (b) & (c) show three examples of the changes made to the geometry of the grounded sheath thermocouple. Using five models the effects of varying sizes of welded grounded junctions has been investigated. The user field for the function 'L2' was utilised within the grounded thermocouple plug-in. The output trend from the FE simulations is detailed in Figure 4.19 (d). The temperature-time results demonstrate that the size of the welded junction, has a direct impact on the response of the thermocouple. The larger the size of the welded junction, the slower the temperature-time response. A larger grounded tip is used to improve the mechanical properties of the thermocouple to make it more durable and robust, to withstand impacts and repeated use.

(a) 0.4mm Length of grounded nugget	(b) 0.8mm Length of grounded nugget	(c) 1.8mm Length of grounded nugget

(d) Temperature response with different sheath tip dimension
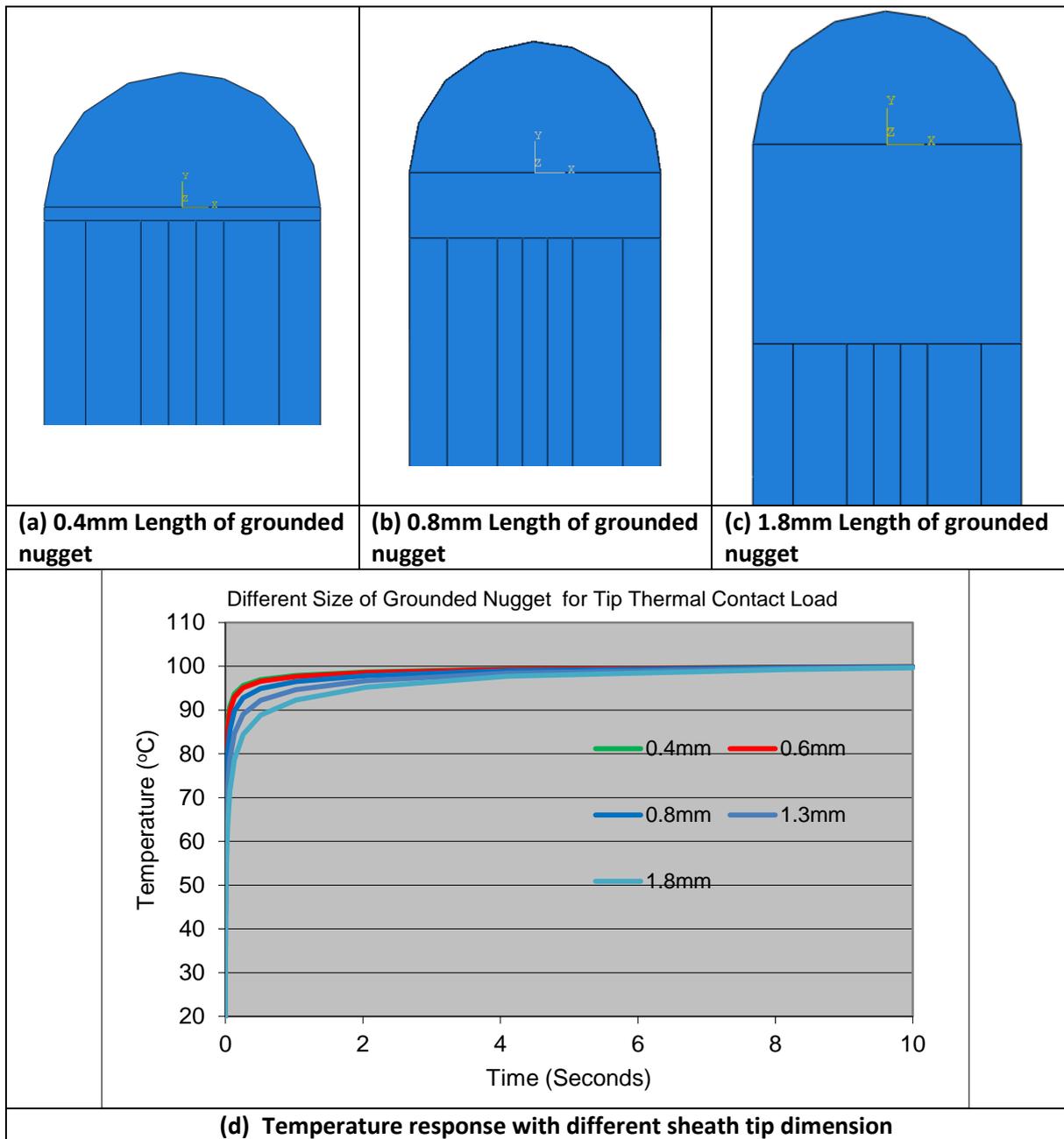
Figure 4.19 Temperature response curve demonstrating the effects of variations in junction geometry for a grounded sheathed thermocouple

Table 4.3 compares the response between the ungrounded and grounded sheathed thermocouples for the different load cases executed using the plug-in function 'L2' user input field. The table was populated using the raw output data from the FE simulations. The results are based on the thermocouples achieving 63.2 percent of the final reading, or to the first time constant. The thermal response time constant, is an expression of how quickly a sensor responds to temperature changes (approximately 5 time constants to achieve steady state temperature measurements). Expressed here, is time response is defined as how long it takes a sensor to reach 63.2 percent of a step temperature change. The table shows that the

geometry change (size of welded junction) made to the grounded thermocouple has an improved response time by approximately 50 percent compared to the position changes to ungrounded nugget thermocouple.

Table 4.3 Time response comparison of different ungrounded and grounded sheathed thermocouples models generated using plugin to adjust nugget geometry

Response Time of thermocouples to achieve the reference temperature of 100°C			
Length (L2) of Junction Element from Surface Thermal Load	Type of Thermocouple	Response Time (Seconds) to measure percentage of Reference Temperature	
		63.2%	99.3%
0.4mm	Sheath Ungrounded Nugget	0.028	7.818
	Sheath Grounded	0.005	4.093
0.6mm	Sheath Ungrounded Nugget	0.042	8.019
	Sheath Grounded	0.006	4.097
0.8mm	Sheath Ungrounded Nugget	0.063	9.225
	Sheath Grounded	0.009	7.985
1.3mm	Sheath Ungrounded Nugget	0.146	9.910
	Sheath Grounded	0.017	8.124
1.8mm	Sheath Ungrounded Nugget	0.248	>10.0
	Sheath Grounded	0.033	8.2

Figure 4.20 Temperature-time response for different wire types (J, K, R) at varying reference temperatures (100°C, 300°C & 500°C). Type R has the quickest response, especially at higher temperatures. Type J has a very similar response to Type k at 100°C and 300°C, but responds faster at 500°C. The difference between the thermocouple types response is only a fraction of a second. Type R thermocouples consist of platinum based wires. It is a more expensive option compared to Type J and K thermocouples. It is used for higher accuracy monitoring and control of critical processes.
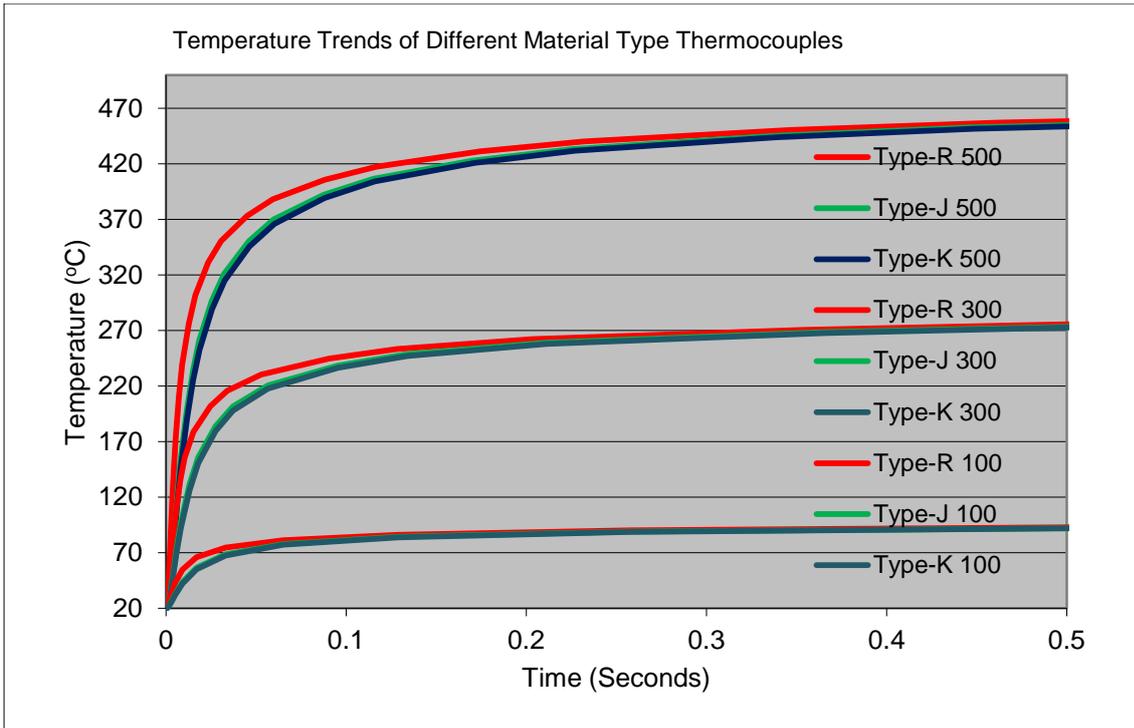
Figure 4.20 Temperature time response for different wire Types (J,K,R) at 100°C, 300°C and 500°C

Figure 4.21 Temperature-time response for different sheath thicknesses (0.50mm, 0.75mm & 1.00mm) using a reference temperature of 100°C. When measuring the temperature of the surrounding medium, accuracy depends on the ability of the sensor to conduct heat from its outer sheath to the element wire. The trend in Figure 4.21 shows a sheath thickness of 0.50mm has the most rapid response and a sheath thickness of 1.00mm is the slowest. The smaller the diameter, the faster the thermocouple will respond. However, a thinner sheath makes the thermocouple less robust and more prone to mechanical failure.
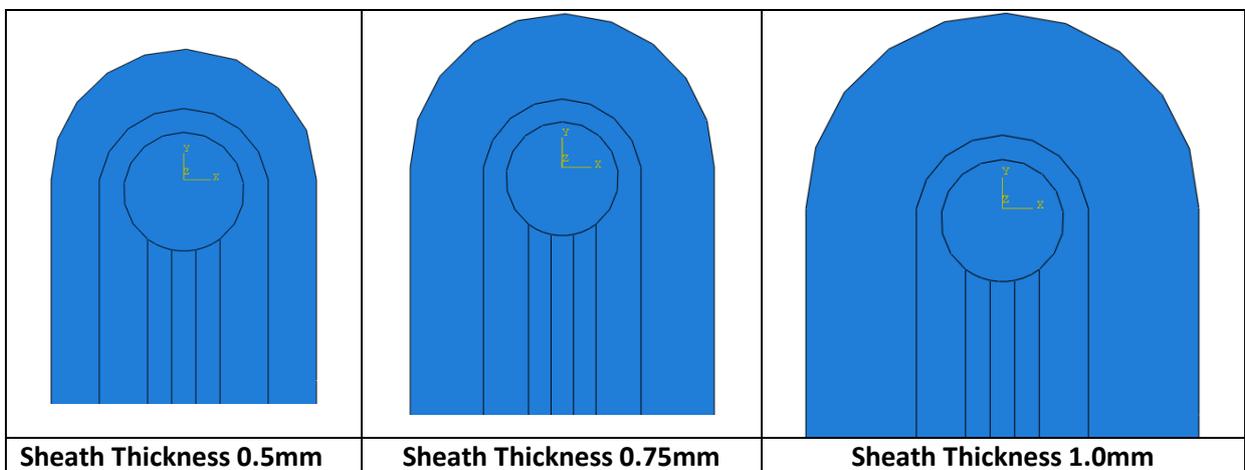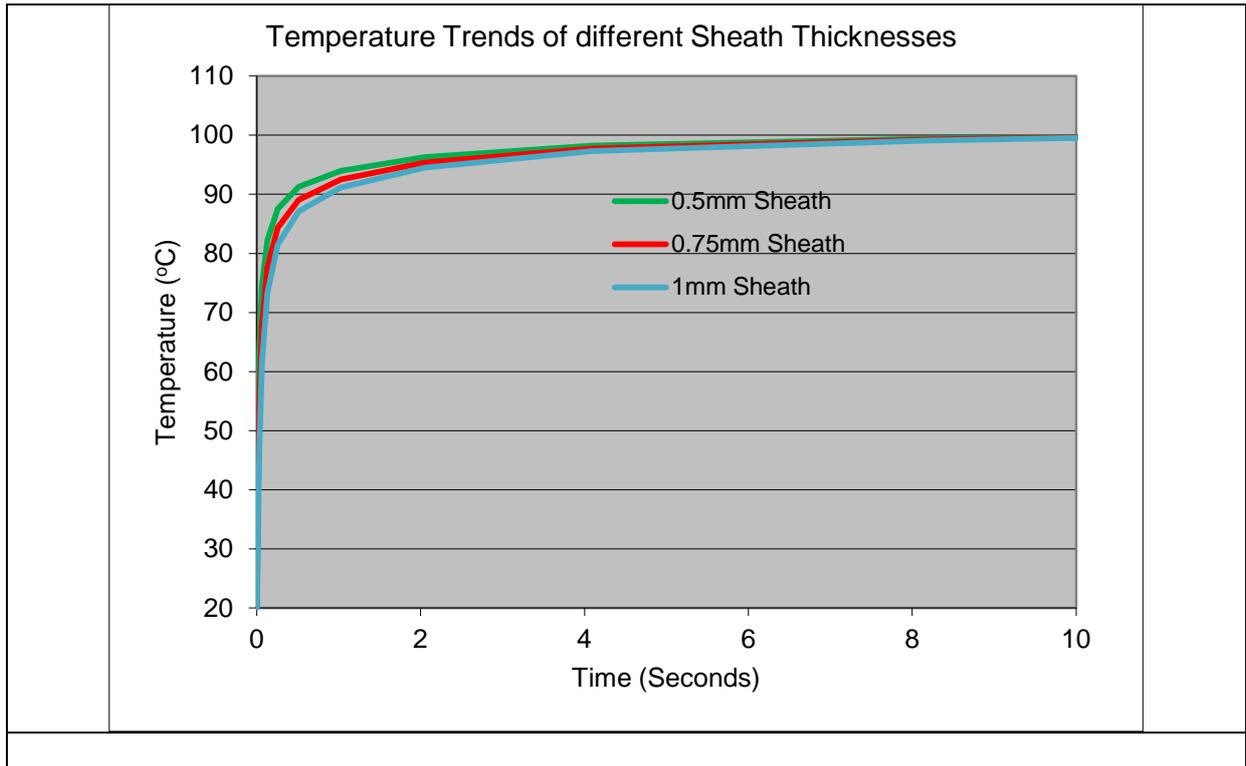
Figure 4.21 Effect of different sheath thickness (0.5, 0.75, 1mm) temperature-time response.

4.7 Discussion

4.7.1 Evaluation of the response time of thermocouples

Compared to other methods, thermocouples are in direct contact with the measuring target and are flexible in size and volume. This made them very versatile for different applications and a wide range of products of different types and sizes are available. In some cases, companies have their own onsite thermocouple welder for bare-wire thermocouples. The FE model developed could be useful for simulating the validation of thermocouples, applications or design. When validating equipment, thermocouples are calibrated prior to use, during the calibration the thermocouple is tested for response and offsets maybe applied if out of tolerance to the measured reference temperature. Once validation testing is complete the calibration is checked to ensure there has been no temperature measurement drift out of tolerance (BS EN 60584-1:2013). Stirred Liquid Baths and Dry Block Baths are two commonly used methods for instrumentation engineers to calibrate thermocouples in industry. Stirred liquid baths are similar to the boiling water approach in, that their calibration

accuracy can be considerably greater than that which can be achieved in any dry block bath. They also have a larger calibration area, that allows more probes to be calibrated and a greater immersion depth which provides a superior thermal environment for probe immersion since air gaps exist between the probe and the medium. Thermal coupling is therefore much better than the alternatives described and as a result of stirring, heat distribution is very even throughout the liquid. Water is used for temperature from 0° to 80°C and oil for temperature up to 300°C, various molten salts and sand baths are used for temperatures in excess of 300°C. Negative temperature bath or ice bath is mainly used for RTD calibration which provides negative temperature for low temperature calibration application. In this device a compressor & CFC gas is used for cooling purposes. Methanol is used as a medium for temperatures below 0°C. Another validating method, Dry block baths, provides the most convenient, portable facilities for checking temperature sensors and they usually achieve reasonably rapid heating and cooling. The units consist of a specially designed heated block within which is located an insert having a well for the probe. The block temperature is controlled electronically to the desired temperature (BS EN 60584-1:2013). The whole assembly is housed in a freestanding case. As with any comparison technique, a certified sensor and indicator should be used to measure the block temperature and used as a reference for the test probe. The FE model could be used as an additional way to simulate these validating methods with predefined contact condition by modifying the Abaqus plug-in.

The dynamic response of a sensor is often an important consideration in designing a measurement system. When the thermocouple (TC) is subjected to a rapid temperature change, it will take some time to respond. If the response time is slow in comparison with the rate of change of the temperature that you are measuring, then the TC will not be able to faithfully represent the dynamic response to the temperature fluctuations. The requirement for the response time varies between applications. For some general applications, it is required that the thermocouple reach the target temperature with 30 or 60 seconds (BS EN 12830), but increasingly some critical applications require much higher response rate, qualification of this response process is very important for the latter. The requirement of quicker response may be for quicker response for the control system or for reducing the expose time between the thermocouple and the environment thus reducing corrosion or contamination. For example, the response of a thermocouple is critical for safety in the nuclear industry, TC's are associated with heating elements to measure gamma heating, Temperature measurement of fuel outlet radial distribution of the core temperature offer protection against nucleate boiling

on fuel (Joung et al, 2013). TC's are also used in the pharmaceutical industry. Pharmaceutical companies use thermocouples to validate equipment and processes, the time required for the thermocouple to reach the target temperature is 30 seconds (BS EN 285 & HTM2010). Thermocouple is also used to monitor and control production of vaccines, products which are temperature critical in the case of live (cell culture) vaccines. The sterility of production and equipment has to be confirmed and thermocouples are used as a reliable instrument to validate (International Society for Pharmaceutical Engineering, ISPE, good automated manufacturing practice, GAMP). In some situations, thermocouples are used for controlling the size of drug crystallisation, a very fast response time is required on the thermocouples. A design and modelling for characterising the response time will be beneficial for these application. The plug-in based on validated simulation could provide a useful tool for such purposes. The work presented in this chapter not only developed a thermocouple process, it also offered a tool to consider the specific/unique factors important for thermocouple validation, characterisation, application and design. The study of the effect of many design factors (such as, nugget size, position), material factor (wire types) and boundary conditions (such as, contact) has provided a frame adaptive to different situations.

4.7.2 Factors that affect the thermocouple response and FE modelling

As shown in the main results, the response of a thermocouple is influenced by many factors. One is the thermocouple types between bare-wire, sheathed and grounded sheathed. As shown in section 4.6 (Figure 4.17), bare-wire thermocouple is easy to make and cheaper, the response time is quicker than sheathed thermocouples. The assembly of bare-wire to the part to be measured can also be versatile, it can be welded, cemented or mechanical assembled. However, the temperature distribution of the nugget could be less uniform as the noncontact side of a bare-wire maybe expose to a different temperature (in other words, when the heating to the tip is less uniform than sheathed). In addition, bare-wire thermocouples also cause interference when in contact with metal (Santos Jr, 2013). The heating time of the sheathed thermocouple is much more complicated and expensive. As shown in section 4.5 (Figure 4.12), the heating up process needs to go through the sheath, insulation and the tip and wire, so the response time is lower. But the sheath system offers protection to the measuring tip both mechanically and electronically. As shown in Table 4.3, a grounded thermocouple has a different response time from ungrounded thermocouples. The manufacture of grounded is relatively simpler than ungrounded. Ungrounded thermocouple have to go through

capacitator welding for the wire tip, then tig welding of the tube of the sheath, while the grounded thermocouples can be made by direct welding. But grounded thermocouples can be less flexible and lacks continuous insulation.

As shown in the results, the response of thermocouple is influenced by the contact condition. When the tip is in different contact (as represented by full contact, half and quarter utilising the function for the plug-in), there is a clear difference in the response time. For the bare-wire TC, there could be a direct difference between the contacting and the non-contacting side (as shown in Figure 4.10). For the sheathed thermocouple, the main components sheath, insulation and TC tip increase in temperature at different rates (Figure 4.12), the tip temperature is relatively uniform as the heating is transferred from the sheath to the whole tip through the insulation (Figure 4.14). At 1 second point, the temperature difference could be as much as 10-degree C when the contacting condition is different. Even though the contact may not be as simple as the case studied, the results highlight the importance of contact conditions as a potential source of error.

One potential use of FE modelling is for design optimisation. As shown in this work, the plug-in can alter the dimensions and systematically study the effect of some key dimensions. This is an advantage of the plug-in. For bare-wire thermocouples, the key part is the tip and the wire diameter. For sheathed TC, the situation is more complicated. As identified for both the ungrounded and the grounded thermocouple, the position of the nugget from the tip exhibits significant influence on the response of the thermocouple (Figure 4.18). The size of the nugget also shows significant effect. This is an important factor for controlling the welding process. The welding of the tip within the sheath could be difficult to control, the work highlighted that it is important to control the size and shape of the nugget, this is subject to a more material focused project at LJMU. The design and development of the thermocouple plug-in will add the development work. The plug-in developed will also be extended to more complex thermocouple systems such as, dual tip thermocouples.

4.8 Summary

In this section, detailed FE models of different types of thermocouples have been developed including bare-wire thermocouple, ungrounded sheathed thermocouple and grounded thermocouple. The predicted time-temperature data showed a reasonable agreement with experimental data.

A plug-in interface is developed for different types of thermocouple consisting of geometry, material and contact condition modules. For the bare-wire thermocouples, the plug-in consists of functions to study influence of materials, dimension (nugget tip and wire dimeter) as well as tip condition (full tip contact and partial contact). The FE model is able to predict the time period during which the measurement is prone to variation due to partial tip contact. The plug-in for ungrounded sheathed TC successfully incorporated the function of automatic verification of the tip position, which is effective for studying the effect of key design factors on the response of sheathed thermocouple. The results show that the temperature at the of tip of sheathed thermocouple is more uniform but the response time is slow due to the effect of the sheath and the insulation layers. It also shows that position of the nugget could have significant influence on the measurement response. The plug-in for the grounded TC incorporated the key dimensions of the end of the sheath. The modelling showed that the thickness of the sheath tip could cause temperature measurement variations. The plug-ins are successfully used to systematically study the effect of nugget size, nugget position, sheath size and the tip dimensions. It has laid a framework for future development in more complex TC systems (including dual or multiple tip systems) and manufacturing process optimisation.

CHAPTER 5

Thermal Modelling of Spot Welding Process

5.1 Introduction

As detailed in the flow diagram in Figure 1.1, a requirement to measure the temperature of the welding process, and inverse temperature measurement approach has been identified. The previous section showed that the thermocouple measurement approach could be applied to welding. In this chapter, works have been presented detailing the development of an experimental method and FEA model. To apply the approach of inversely measuring temperature to determine the thermal history of an electro-thermal analysis of resistance spot welded joints. The ANN technique has also been tested and the results of predict thermal history of welds has been evaluated.

Resistance spot welding (RSW) is a complicated process, including interactions of electrical, thermal, mechanical and metallurgical phenomena. The thermal history of the spot welding process is one of most important characteristics of the process, as it has a direct influence on the resultant microstructure and properties. The weld quality depends on process and material variables that affect the heat generation or the electrode pressure, among which, the current, force and time are the three main parameters which determine the structure and strength of the welded joint of a material (Zhang, 2003). During the weld process a region around the nugget is formed called heat-affected zone (HAZ). It has a mixed microstructure consisting of martensite, bainite, ferrite and pearlite. The nugget is much harder than the base material due to the quenching effect, while the HAZ has a gradient mechanical property and a mixed microstructure with the strength decreasing from the nugget to the base. In many cases, failures of spot welded joints tend to occur around this region, specifically around the heat-affected zone (HAZ) (Mukhopadhyay, 2009; Vural and Akkus, 2004). From the work presented in chapter 4, the dimensional parameters (such as, thickness, nugget size) are having a direct effect on the mechanical strength of the spot welded joints, while factors such as, nugget size is directly associated with the thermal process in spot welded joints. As shown in the experimental observation and FE stress analysis, the fracture initiates in the HAZ zones, so it is important to obtain the thermal history of the HAZ, but is difficulty to measure the HAZ thermal history directly. In this work, we explored the use for remote temperature measurement with remote thermocouples.

When studying the electro-thermal response of the weld and the nugget diameter change, it is very difficult to analyse the heat distribution of the faying interface since the welding is electrically and thermo-mechanically coupled. Research efforts have been made to predict

cooling rates for a range of steel gauges welded with a number of automotive welding processes. These processes include RSW, RMSEW, LBW, and GMAW. Cooling rates are calculated using a range of analytical and numerical simulation methods. These results are then compared to critical cooling rates (for a martensite formation) (Gould, 2006). Direct measurement of the temperature at the HAZ zone is not feasible due to the setup of the welding process. One potential approach is to use the remote thermocouple method to measure the temperature at locations with fixed distance from the welding zones, then inversely predict the temperature at the HAZ. This approach (i.e. remote thermocouple method and inverse FE modelling) has been successfully used in the temperature prediction in different material systems and situations (Ren et al, 2004), which can be transferred to electrical spot welding.

Development of testing method to remotely measure temperature of the welded joint.
Setup of the measurement system and evaluation (repeatability, reliability, etc.)
Measurement of the temperature at different positions on the work piece and the electrode
Investigation of the effect on material systems, thickness, on the welding process and strength

---

Development of an FE thermal model of the spot welding process.
Procedure of coupling of mechanical-electrical, thermal process
Heat input based approach
Comparison between welding nugget and experimental work

Evaluation of Artificial Neural Network (ANN) based inverse modelling program with remote thermocouples
Development of the NN network and training of the ANN using finite element data.
Method of evaluating prediction accuracy.
i) Use of Point based approach to represent the cooling
ii) Use of Polynomial (Non-Linear) Trend-line approach to represent the cooling
iii) Use of Linear Trend-line approach to represent the cooling

---

Discussion:
Potential use of remote thermocouples
Different approach of processing the data
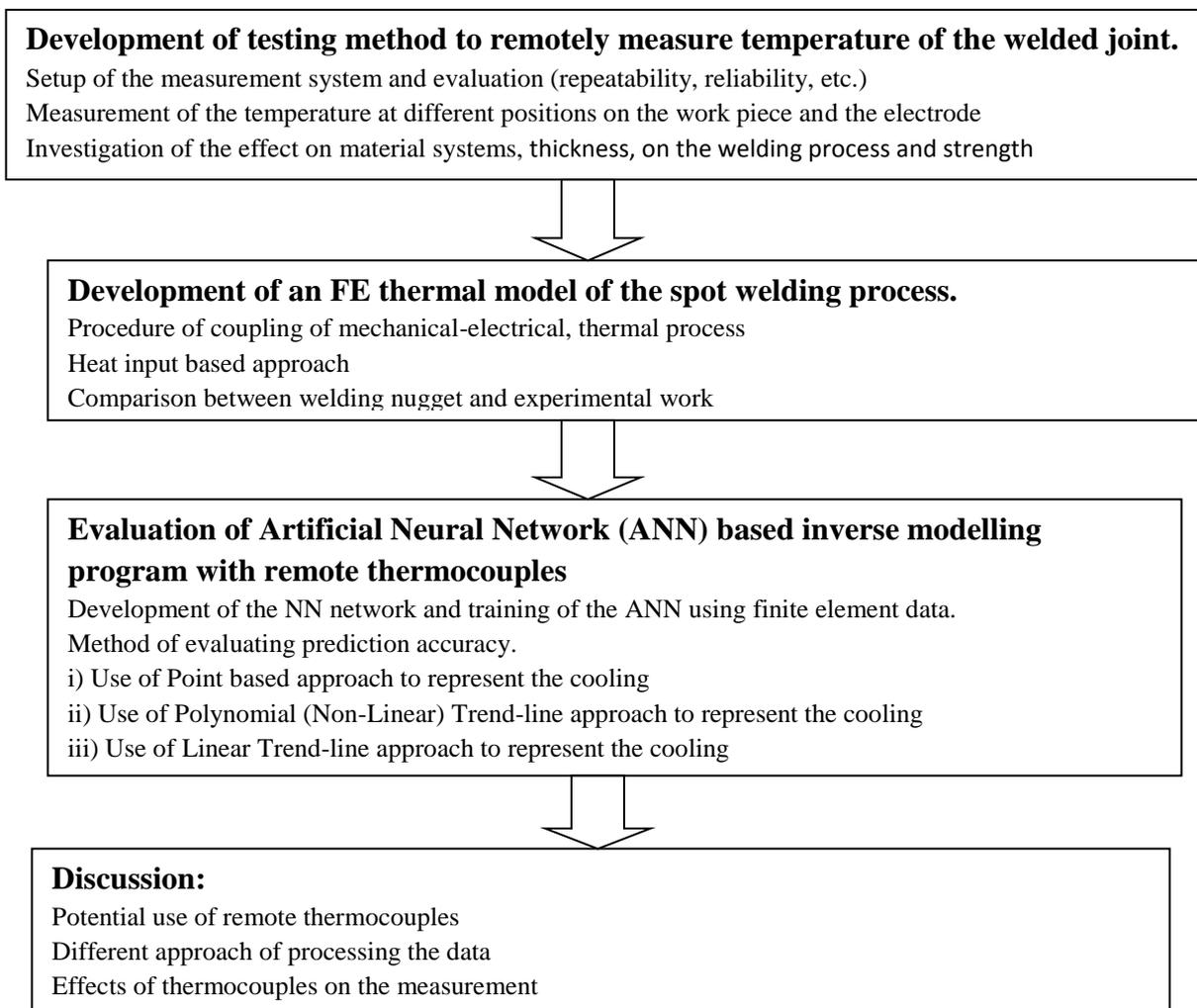Effects of thermocouples on the measurement

---

Figure 5.1 Flow chart showing the main works conducted and key developments of the research work

As shown in Figure 5.1, this chapter consists of four main parts, including development of a testing method to remotely measure temperature in spot welding, development of FE thermal

model of the spot welding process, evaluation of use of artificial neural network (ANN) based inverse modelling with remote thermocouples and discussion. The experimental work includes measurement of temperature during electrical spot welding process, characterisation of the welded zones for different material (mild steel, stainless steel and dual phase steels); the structure of the spot welded joint with different material systems was experimentally studied. The effect of some key testing conditions (including using different types of thermocouples (bare-wire or sheathed) and location) were assessed such as repeatability and reliability of the measurement system and evaluation setup. In the preliminary work, measurement of temperature at different locations on the work piece and the electrode were verified.

In numerical work, an electrical-mechanical-thermal model for spot welding is developed and temperature zone is compared with the structure observation. The FE model also provided data for developing an Artificial Neural Network (ANN) method to predict the temperature and cooling curve of HAZ from remote thermocouple measurements. Furthermore, investigations on the effects of material systems, thickness of specimens and parameters were tested and evaluated. Using the established simulation based inverse modelling program developed. The network was set up and a level of training was determined. Three approaches of representing the cooling curves (i.e. point based, polynomial trend-line and linear trend-line methods), were evaluated to determine prediction accuracy in the neural network. The results of different methods were analysed and the most effective approach in predicting the temperature and cooling rate was established. These works are important to establish an integrated approach to study the thermal, electrical and thermal process of spot welding. Some key issues regarding remote temperatures, including choice of thermocouples are discussed towards the end.

5.2 Typical experimental work-setup

Figure 5.2 shows the set of the welding test and temperature measurement. The welding tests were performed on a Sciaky S4C25 (model Rapid 25) resistance welding machine equipped with a coil and a time control SciakyU.J.S.4.H.C. A SciakyWCM/1 resistive current meter was used to monitor the welding current. The test specimens used were industrial grade Mild Steel, Stainless Steel and dual phase steel. The base plate specimens in this experimental study had set dimensions; width 25mm, length 100mm, thickness 1mm. It is difficult to

accurately measure the temperature of the nugget and HAZ during the spot welding process. This is due to contact between the electrodes (welding tips) and the work piece. Two remote thermocouples were placed at set distances away from the contact zone of the spot welding process. This approach was performed for two purposes. One is to gain sufficient and reliable test results with recorded temperatures on a range of common materials used in spot welding. The other is to establish the effect of a variation of welding parameters and materials on the temperature. Each thermocouple was positioned on the base plate specimen at a set distance from the centre of the nugget. TXA was placed 10mm away from the centre of the nugget and TXB was placed 20mm from the centre of the nugget.
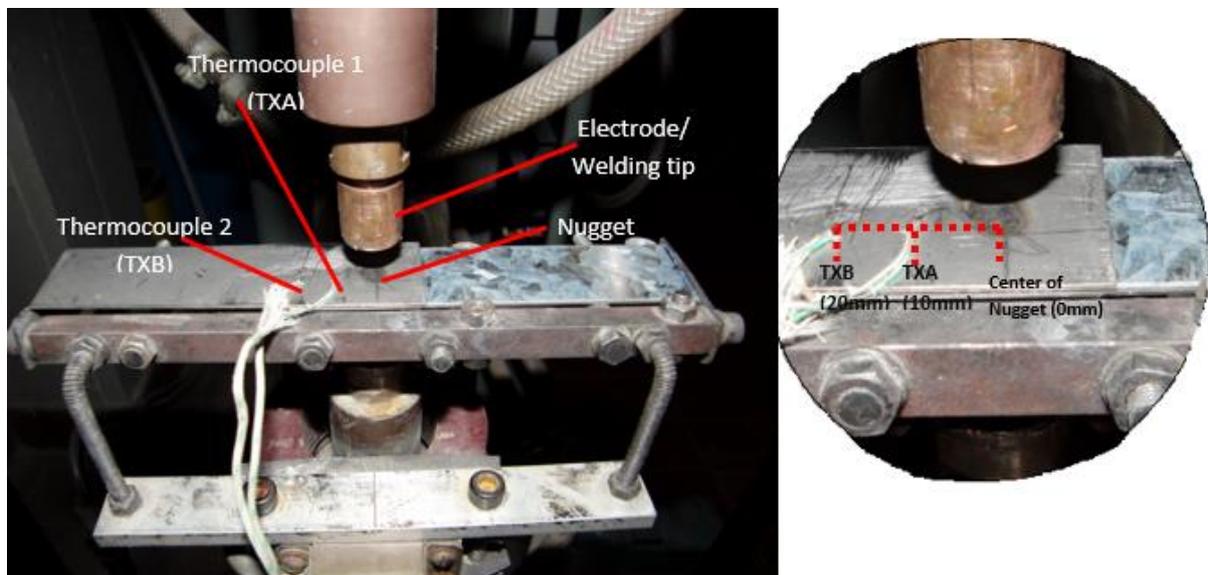
Figure 5.2 Typical experimental work set up, detailing the remote thermocouple positions in relation to the spot welded nugget.

Figure 5.3 shows the typical equipment used to record the data required to create the curve charts depicting the thermal history of the welded materials. The type-K thermocouple was selected as the most suitable temperature measurement device, as it is the most commonly used thermocouple type in industry due to its ability to measure a wide range of temperature (-250°C to 1350°C) with a sensitivity of approximately 41 µV/°C and its capacity to communicate with the data recording equipment. The type-K thermocouple dissimilar metal wires consist of Nickel- 10% Chromium and Nickel- 5% Aluminium Silicon. There are two main forms of type-K thermocouples; sheathed and bare-wire 'bead'. The sheathed thermocouple consists of the type-K thermocouple wires contained in a stainless steel sheath insulated by fine Magnesium-Oxide powder. Whereas, the bare-wire 'bead' thermocouple

consists of the type-K thermocouple wires with a welded joints. The bare-wire thermocouple can be directly used or in some cases they are insulated in part by Fibreglass (Childs et al, 2000, and Zhao et al, 2014).
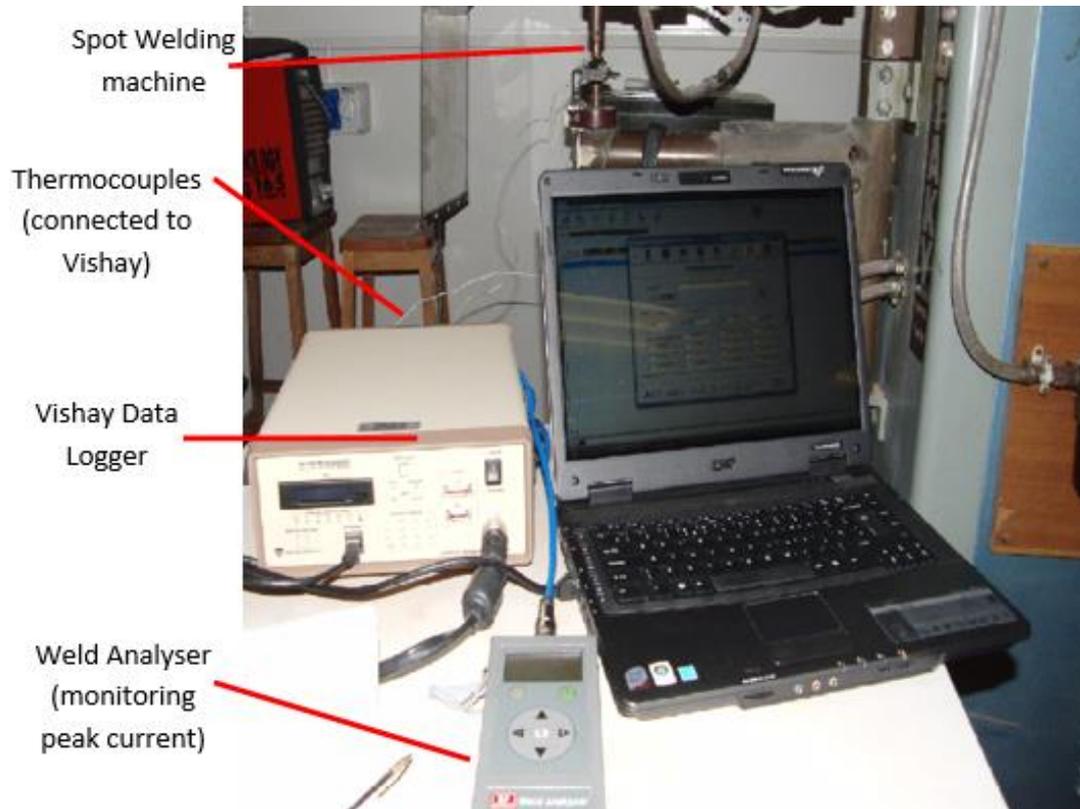
Figure 5.3 Typical experimental work set up and instrumentation

The welding parameters were determined before the preliminary tests. Initially a performance characterisation of welded joints fabricated with different welding parameters was executed. Pairs of Mild Steel plates were spot welded together over a range of machine parameters. This initial work was conducted to investigate the effects of welding parameters (voltage, dwell time) and wire thickness on the shape and size of the weld joint. 'Design of Experiments' (DoE) techniques were used to study the sensitivities of all these parameters to the quality of the weld. The joints were visually inspected for quality; the amount of splash, reduction in width of the welded zone, size of nugget and HAZ. Mechanical testing was also performed to assess the mechanical integrity of the welded joints using tensile tests. The nugget zone, heat affected zone were characterised (shape, dimension and microstructure).

Tests were performed on same material welding and two material systems. Two different materials were used in the experimental works; stainless steel and mild steel. Some work has also been performed in a dual phase steel. The dimensions of the specimen were 25mm x 100mm x 1mm. These two materials were selected for testing because they are two of the most commonly used materials in manufacturing/automobile industries. It was also ideal to use a range of materials with varying thermal properties, as the test method would be proven with more than one material. Table 5.1 details the thermal properties of the materials used in the experimental work.

Table 5.1 Material thermal properties

Material	Density (kg/m^3)	Specific Heat Capacity (J/kgK)	Thermal conductivity (W.m^{-1}.k^{-1})
Stainless Steel	8030	503	16.27
Mild Steel	7850	620	46
DP steel	7600	846	27.6

5.3 Typical temperature measurement results with remote thermocouples

5.3.1 Response of different types of thermal couples (welded bare-wire vs. sheathed thermocouple) in measuring the temperature in spot welded joints

The selection of the thermocouples represents an important factor for the efficiency and effectiveness of the system. The preliminary tests were performed to establish the most effective method of recording temperature during the welding process. Both forms of Type-K thermocouples were tested on identical layout and specimen materials. The bare-wire thermocouples were fixed (welded) to the top plate in the set positions for TXA and TXB. The sheathed thermocouples were laid flat on the base material and attached using magnets

and thermal cement. The thermocouples were positioned at the same location (30mm from the centre of the nugget).

Figure 5.4 shows the temperature change at the thermocouple positions for two different material systems: mild steel to mild steel (a) and stainless steel (b). In both cases, the response of the bare-wire welded thermocouple is quicker than the sheathed method. This is due to the fact that the welded thermocouple has a greater surface area contact with the specimen material causing it to record a higher peak temperature at a shorter time.

The different response of the types of thermocouple is a good example why studying the response of thermocouples is important (as detailed in the previous chapter). The dynamic response of a sensor is often an important consideration in designing a measurement system. When the thermocouple (TC) is subjected to a rapid temperature change, it will take some time to respond. If the response time is slow in comparison with the rate of change of the temperature that you are measuring, then the TC will not be able to faithfully represent the dynamic response to the temperature fluctuations. The different response time between bare-wire and sheathed thermocouples agree with the general trend of the results presented in the previous chapter.
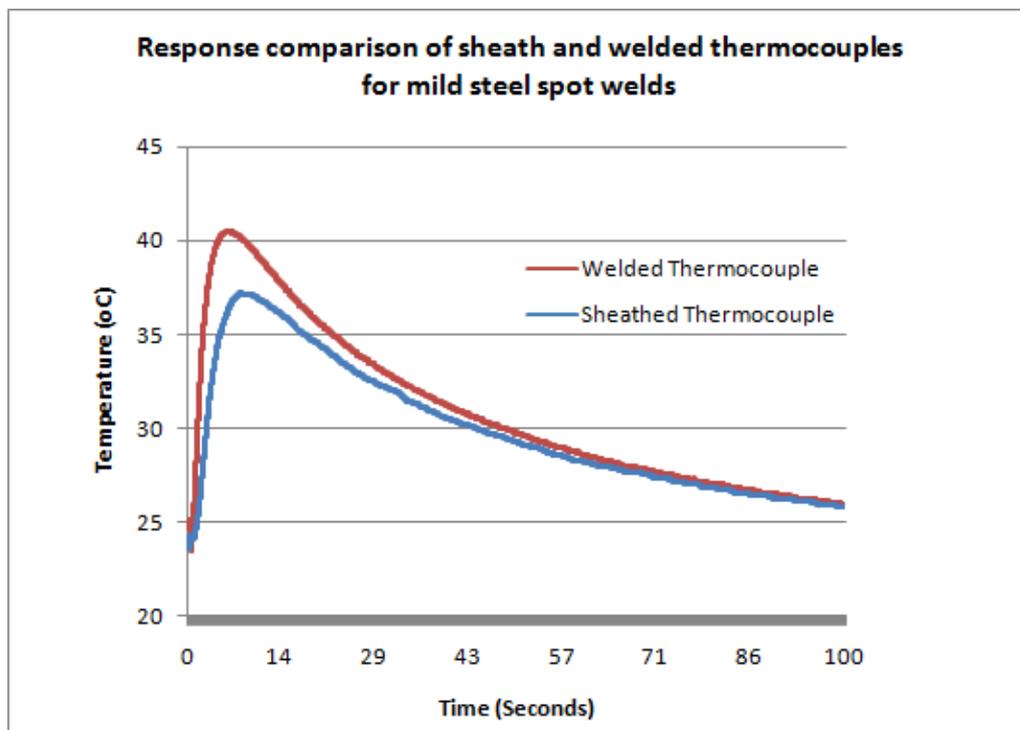
(a) Response comparison of sheathed and welded thermocouples for mild steel spot welds
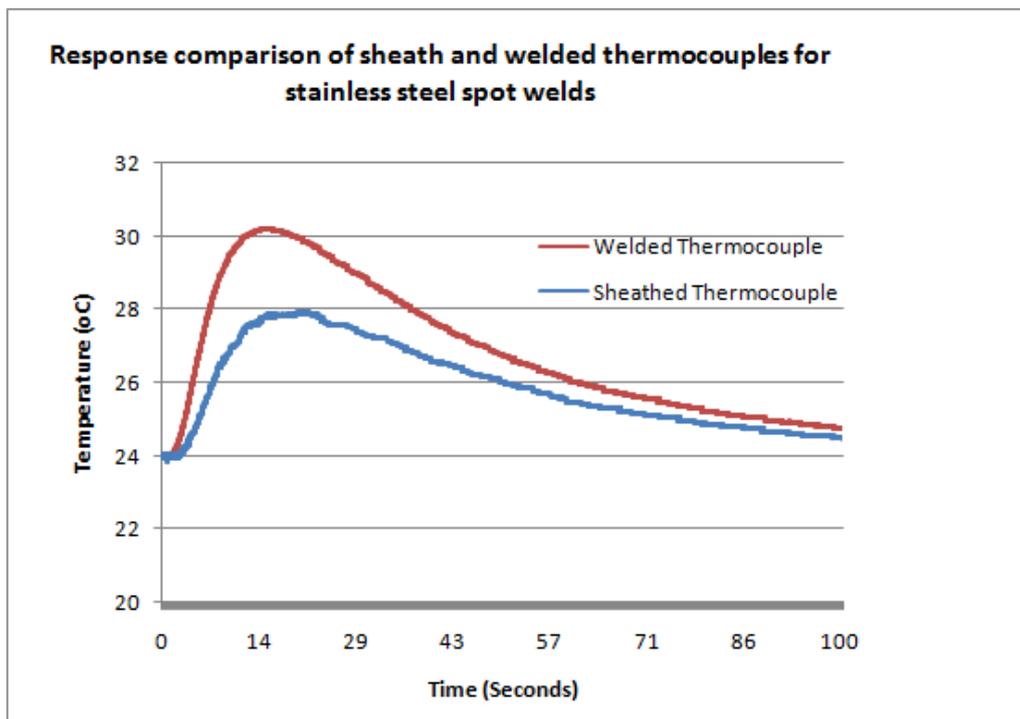
(b) Response comparison of sheathed and welded thermocouples for
stainless steel spot welds

Figure 5.4 Typical measurement results with different thermocouples method for different
material systems and locations.

5.3.2 Temperature in repeated spot welded joint

Repeated welding tests have been performed in this experimental work to assess the effects of
repeated welding. Figure 5.5 details the procedure used in which each specimen was spot
welded three times in the same location (using the same parameters). There was a waiting
period of five minutes between welds to ensure that the thermocouples read atmospheric
temperature (25°C) before executing the next weld.
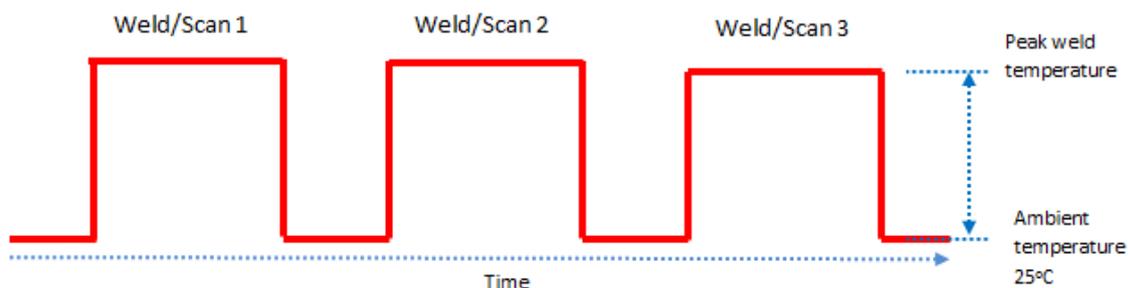
Figure 5.5 Schematic diagram of the procedure for repeated welding

The temperature data on repeated spot welding of mild steel and stainless steel were shown in Figure 5.6 and 5.7 respectively. Upon comparison of the two materials test results, the mild steel sample cools down at a more intensely rapid rate. In figure 5.6 the temperature curves for the three tests on the mild steel were almost identical. The temperature for the first weld is slightly higher. Whilst in Figure 5.7, the temperatures were clearly different between the three repeated tests for the stainless steel. The temperature becomes higher with repeated welding. This is probably associated with the different thermal properties between these two materials. The reason for the resistance change was caused by an increase in the surface area in contact between the two steel plates. After the first weld the material was deformed around the nugget. In the second and third welds the resistance was caused by the outer diameter of the nugget (HAZs) joining together.
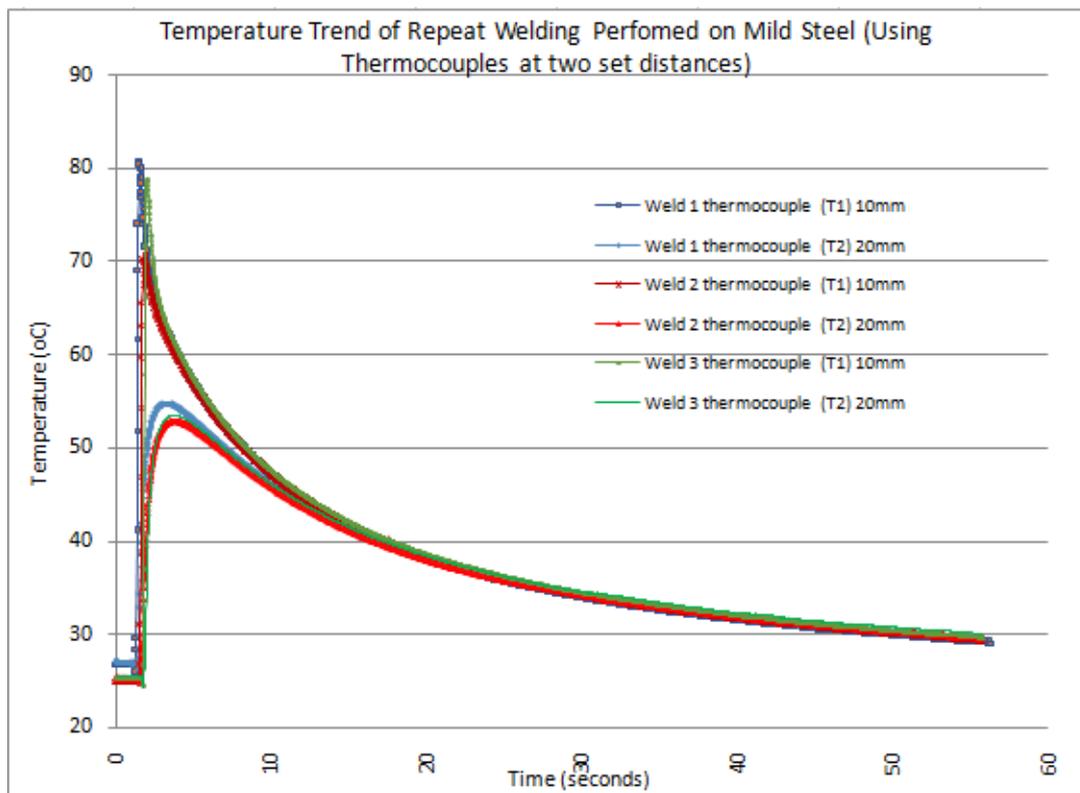
Figure 5.6 Typical temperature curves in repeated welding of mild steel
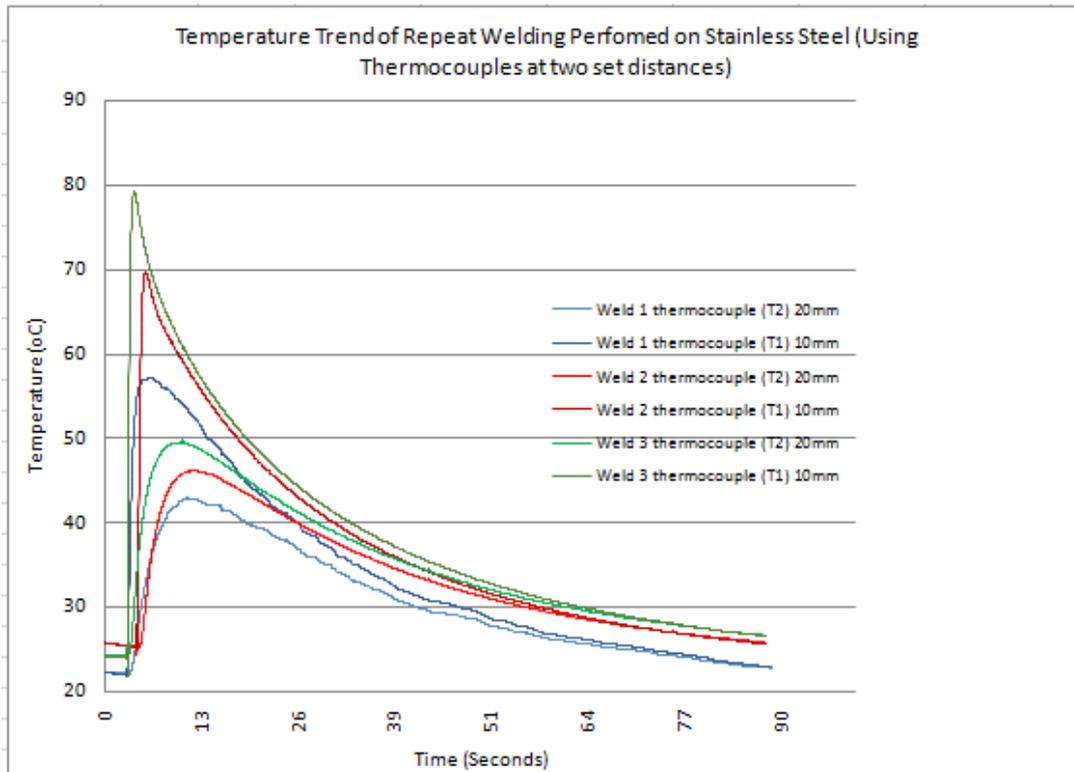
Figure 5.7 Typical temperature curves of stainless steel

5.3.3 Typical temperature curve when joining different material systems together and microstructure showing different welding zones

Figure 5.8 shows the temperature data with different materials systems and setup. Four conditions have been compared. One is welding mild steel to mild steel; one is mild steel to stainless with the mild steel on the top; the third one is stainless steel to stainless steel; the last one is stainless steel to mild steel with the stainless steel on the top. In all cases, the thermocouples were welded to the surface of the material on top. From these welding test data, it is clear that if stainless steel is the material on top the cooling rate is slower and if mild steel is on top the cooling rate is faster. The results suggest that these parameters have to be fully implemented to ensure the consistency of the results. These results showed that the remote thermocouples could produce consistent results which are sensitive to the location of the probe, material system and setup.
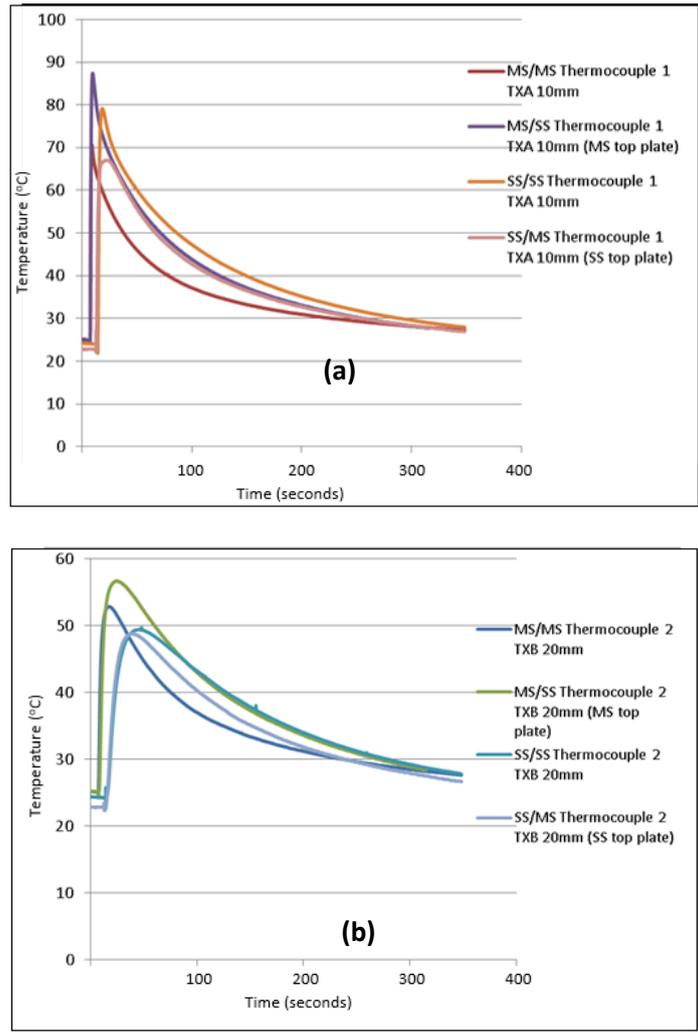
Figure 5.8 Typical temperature curve   when joining two dissimilar metals together **(a)** data for thermocouple 1 (TXA) **(b)** data for thermocouple 2 (TXB)

The welded samples were processed to reveal the welded zones within the welded joints. The process consists of cutting the sample, mounting, grinding and polishing. Figure 5.9 shows the cutting plane in which spot welded joints were sectioned. The cut was made through the centre of the nugget. The welded work-pieces are carefully cut with an abrasive saw to avoid altering or destroying the structure of the materials. However, no matter how carefully abrasive sawing or electric discharge machining is performed, a small amount of deformation occurs on the sample surface. This deformation was removed during subsequent preparation steps.

Cut weld section
mounted into sample

Section cut made to
Welded Work piece
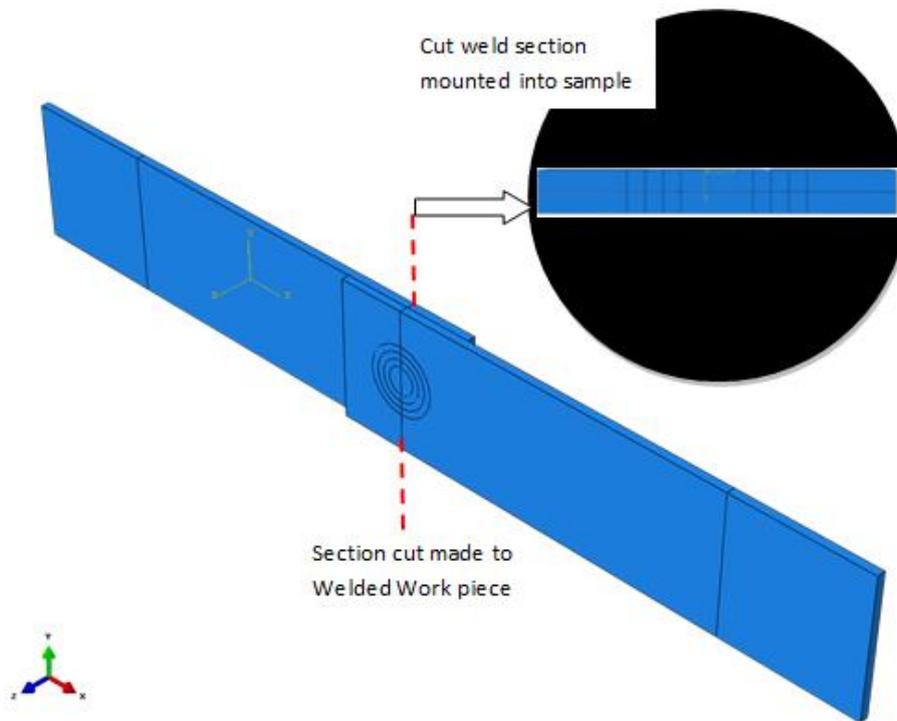
Figure 5.9 Diagram to show how the material is processed. Sectioned weld at nugget is embedded in a mounted sample

After the welded test pieces were sectioned to a convenient size, they were mounted in a thermosetting phenolic material (Bakelite), as shown in Figure 5.10. Mounting involves putting the sample in a mould and surrounding it with the bakelite powder. When the mould is heated and pressurized the setting/curing of the media occurs. The mounted sample is removed from the mould. The samples were polished to remove imperfections and scratches to analyse under a microscope. The part was then polished to remove any changes to microstructures that might have been caused by cutting the weld.

MS/DPS

SS/DPS

DPS/DPS

MS/MS

SS/SS

MS/SS

Figure 5.10 Photograph of six sectioned welds mounted into two samples

Once the weld samples had been polished they were etched in nital solution (ISO 14104) to reveal the microstructural details. Microstructural examination was performed using an optical microscope to magnify features of the welds under analysis. The features of the weld were observed as the welding process caused different microstructural zones to occur within the material. Figures 5.11, 5.12 and 5.13 show microstructure of identical metals joined together (Mild Steel to Mild Steel and Stainless Steel to Stainless Steel, respectively).

Figure 5.11 Cross-section of the MS-MS sample showing the welded zones in spot welded joints between mild steel and mild steel (MS-MS)
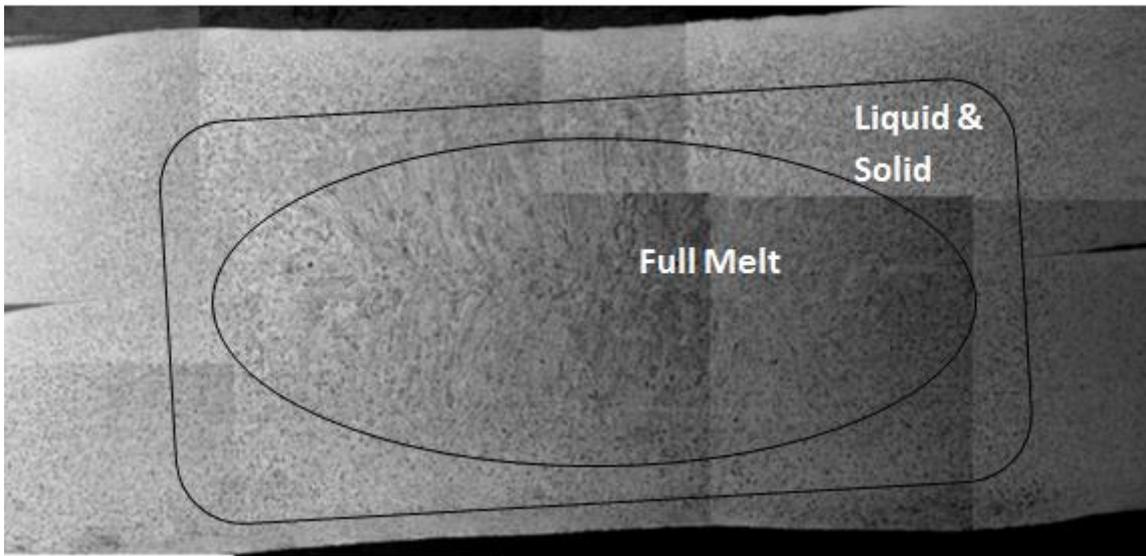

Figure 5.12 Microstructure of the cross-section for the SS-SS sample showing the welded zones in spot welded joints between stainless steel and stainless steel (SS-SS)

Figure 5.13 Microstructure of the cross-section for a DP-DP sample

The images show symmetrical patterns of microstructure defining different sections of the weld, such as, the nugget, HAZs and base material. Figure 5.11 also highlights the full melt zone at the nugget and the liquid/solid zone at the HAZ. Figure 5.14 and 5.15 show microstructures of dissimilar metals welded together (Mild Steel to Stainless Steel, Mild Steel to Dual Phase Steel and Stainless Steel to Dual Phase Steel, respectively). The images show asymmetrical patterns of microstructures defining, different atomic structure sections of the weld, such as, the nugget, HAZs and base material. The welds aren't symmetrical as dissimilar metals have been welded together. In the case of the MS-stainless steel, the stainless has extended into mild steel. In the case of MS-DP steel, the DP steel has extended into MS. The dissimilar metals have different material properties including melting point and conductivity. This has caused a tapered nugget formation.

Figure 5.14 Microstructure of the cross-section for the MS-SS sample showing the welded zones in spot welded joints between mild steel and stainless steel (MS-SS)
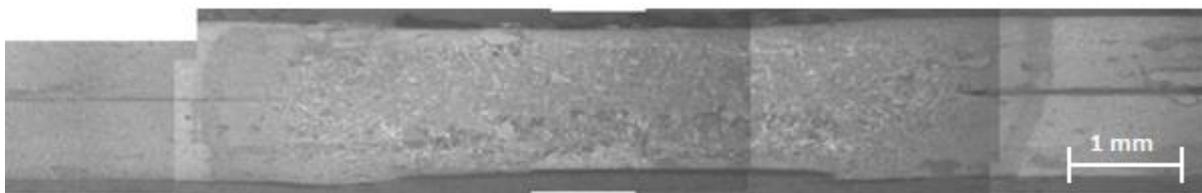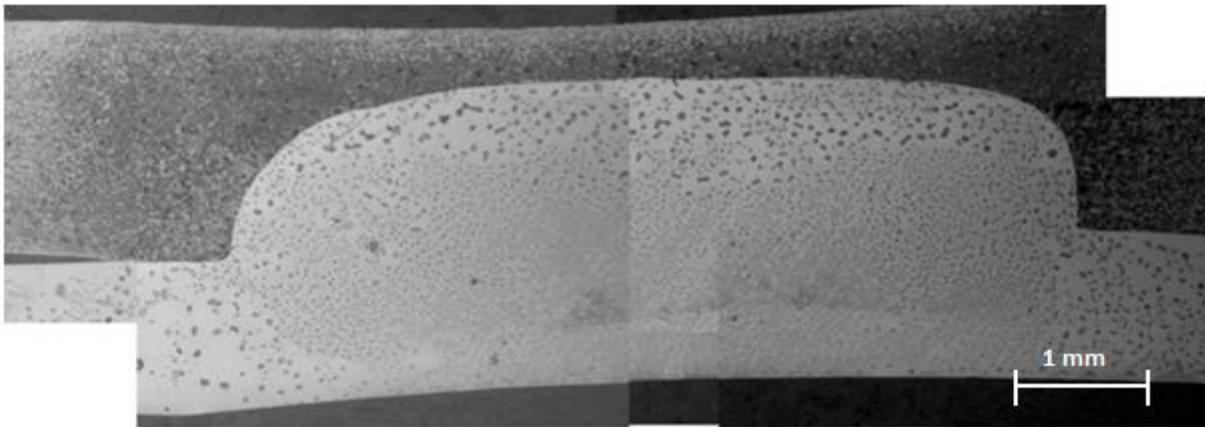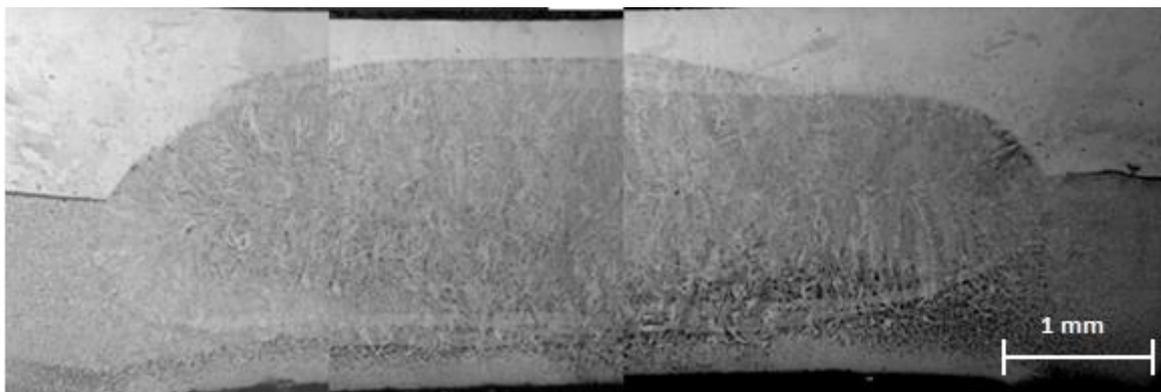

Figure 5.15 Microstructure of the cross-section for the MS-DP sample showing the welded zones in spot welded joints between mild steel and dual phase steel (MS-DP)

5.4 Mechanical-electrical-thermal modelling of the spot welding process

Figure 5.16 shows the FE model developed to simulate the electrical resistance spot welding process. The complex model used mechanical loading, electrical heating, thermal modelling. Spot welding is a process in which contacting metal surface are joined by the heat obtained from resistance to electric current flow. The resistance spot weld process is divided into sections. The first stage is the Squeeze which involves the electrodes being brought to the surface of the metal at an approach rate in cycles (or mm/sec). An initial pressure is then applied to clamp the work pieces together. During the weld heat time phase (cycles) current (kA) passes through the work pieces from the electrodes. Heat is developed mainly at the interface between two work-piece sheets causing the temperature to increase. After the current is removed, the pressure is maintained for a short period of time. The electrodes remain in place during the Quench cycle in order for the material to cool. The electrodes release the work-piece in the off cycle. To reduce the computational resource, a quarter symmetrical model is used. The thermal process could be considered to be axial symmetrical but the mechanical process (i.e. symmetric constraint is required to simulate the deformation of the material at different temperature). A range of materials properties have to be defined including density, temperature dependent elastic properties, temperature dependent plastic properties, thermal conductivity, electrical conductivity, expansion and specific heat. Other key parameters include pressure dependent surface conductance and heat conversion coefficients. The material properties are from various resources (Smithells metals reference book).
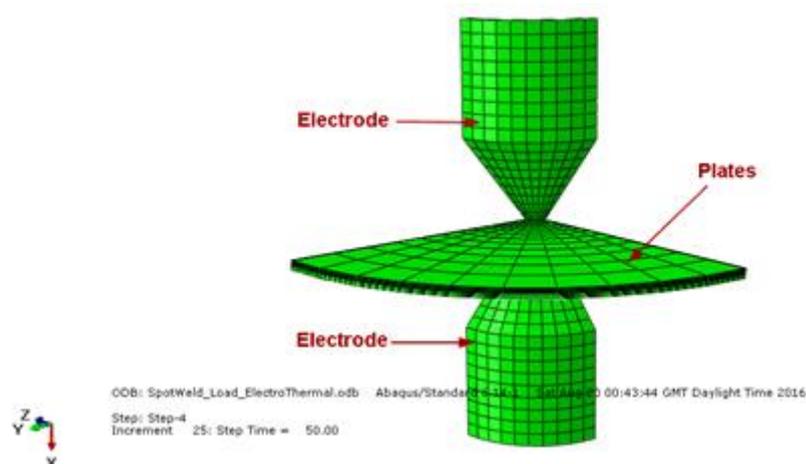
Figure 5.16 FE model of the spot welding process, with electrical, mechanical and thermal process

Figure 5.17 shows the typical temperature distribution within the spot weld joints, with a much higher temperature region in the centre as labelled. It is clearly shown that a contour plot of a spot welded model has been assembled to geometrically match the sections of nugget, HAZ and base material identified in the microstructure (b).
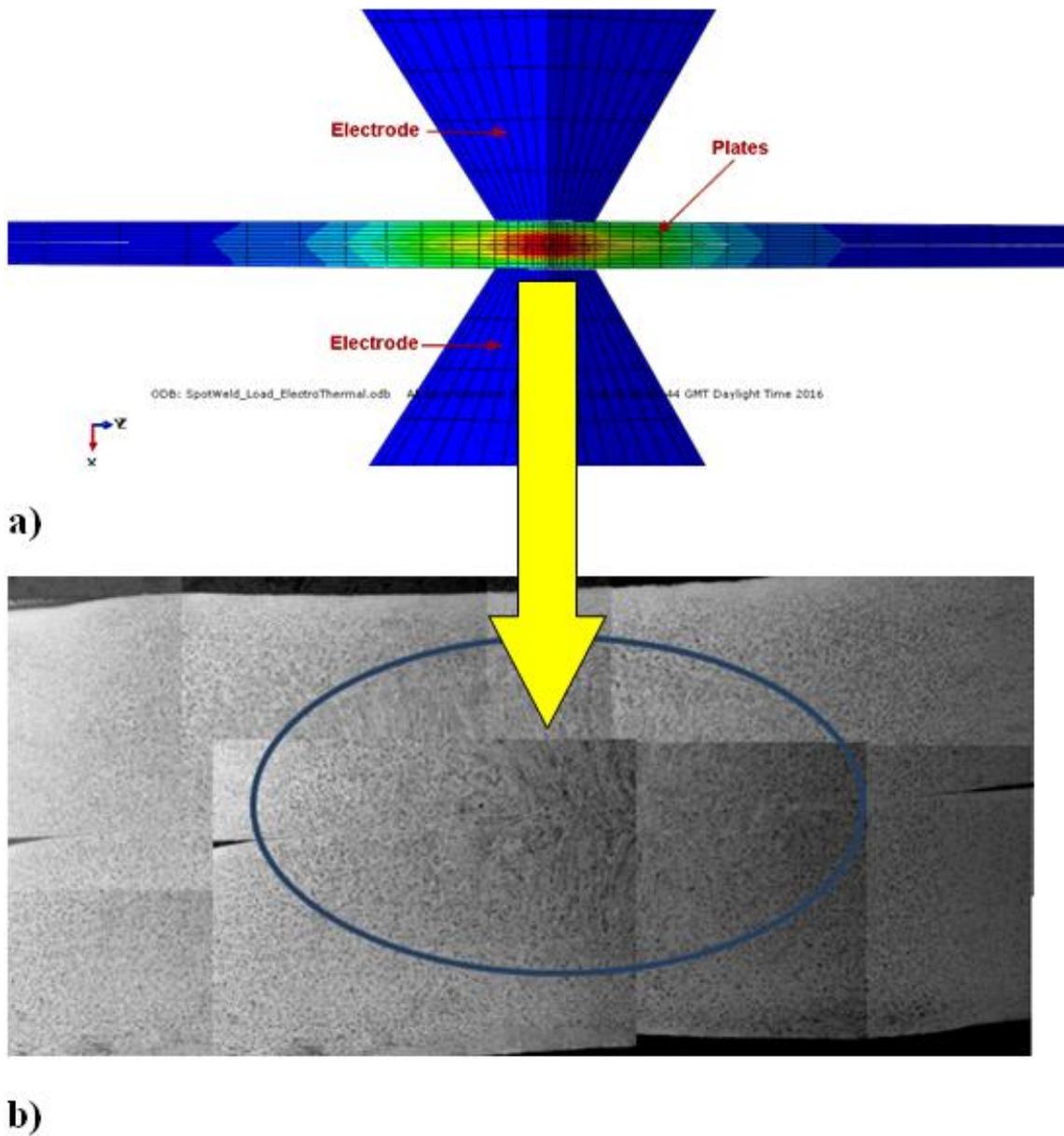
Figure 5.17 (a) Typical temperature distribution in comparison with the **(b)** microstructure

Figure 5.18 and 5.19 shows the temperature change at the HAZ region and the thermocouple position in comparison with the temperature measurement data. The data shows that heating and cooling section is in a reasonable agreement, in particular the cooling stage, the cooling rate showed a good agreement.
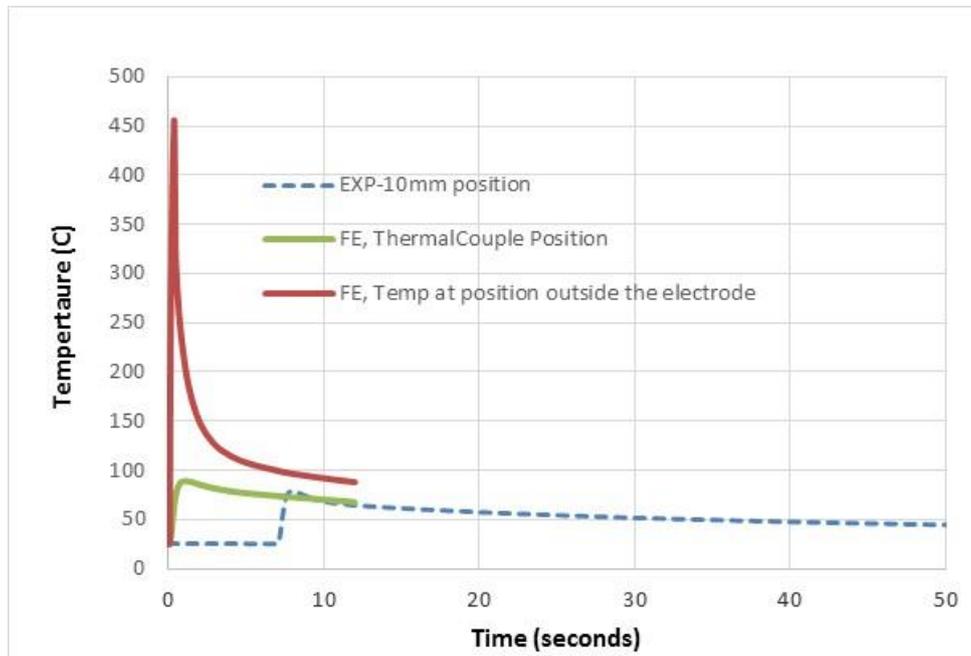
Figure 5.18 Cooling curve at the HAZ region and the thermocouple position in comparison with the temperature measurement data
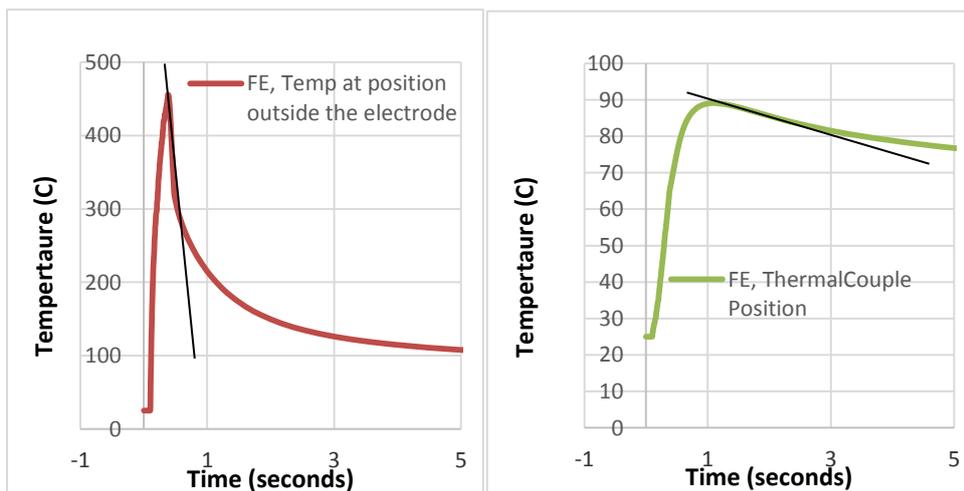
Figure 5.19 Cooling curve for the remote thermocouple and the HAZ position

5.5 Use of ANN in predict the cooling rate of HAZ from remote thermocouple temperature measurement.

The work presented in this chapter shows that the remote thermocouple can reliably measure the temperature and is sensitive to the change of material systems and positions.
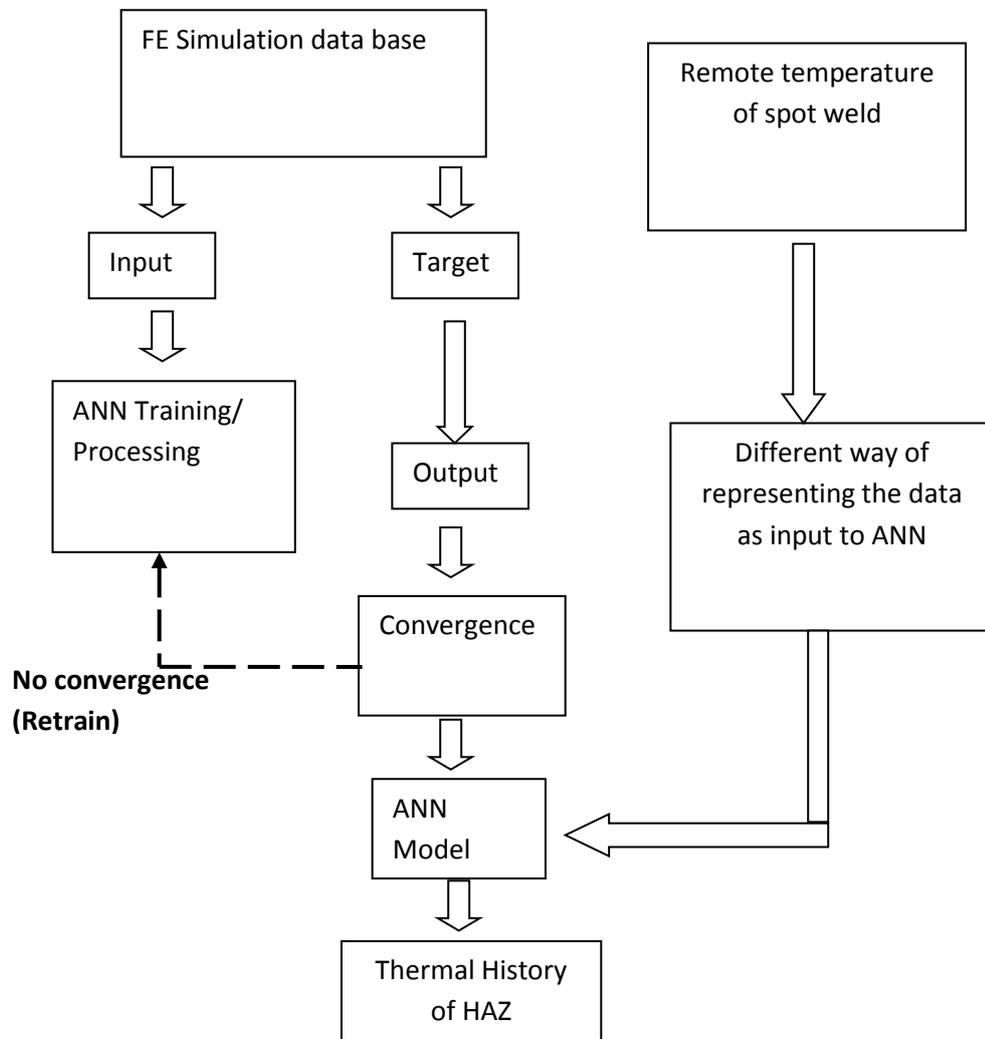
Figure 5.20 Proposed frame of inverse FE program based ANN for predicting cooling rate (thermal history) of a spot welded joint's HAZ based on remote thermocouple temperature measurement data

This section explores the use of artificial neural network based method to inversely predict the temperature and thermal history of other positions (e.g. position closer to the nugget), which are difficult to measure. Figure 5.20 illustrates the proposed inverse FE program based ANN for predicting cooling rate (thermal history), used to resemble the HAZ and thermocouples temperature response to the welding process. Highlighted is the position of a

spot welded joint HAZ in relation to the location of the two remote thermocouple temperature measurement tips (Figure 5.21).
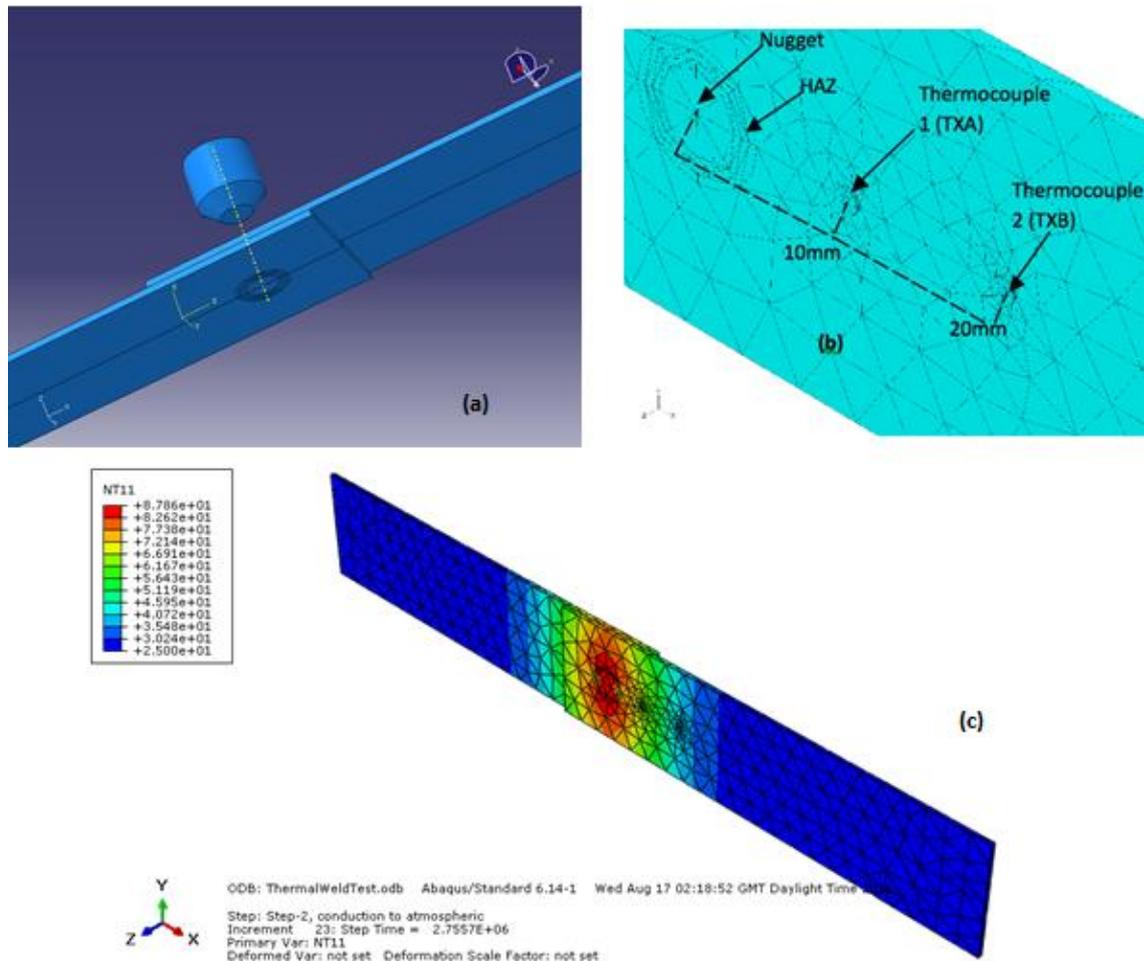
Figure 5.21 FE model of the spot welded joint (a) and thermocouple positions in relation to the centre of the nugget (b) and typical temperature distribution (c)

The framework consists of three main parts: the experimental works, the FE modelling and the ANN program. The experimental input required is in the form of temperature-time data from remotely placed thermocouples. In the FE modelling part, a numerical model mimics the geometry and boundary conditions of the spot welding tests. A series of models with different load temperatures (to be inversely predicted) over a potential range were developed with ABAQUS parametric studies. The FE simulation results were then used to simulate a thermal history database, using Matlab software. The numerical data is processed to form a simulation database as input and target data in the training and validation. The ANN program will determine the best fitting parameters (such as, number of neurons, the weighting factors, etc.) based on the training and validation data. Key factors affecting the ANN for this application including optimum training scheme, activation functions and a new early stopping

mechanism were systematically established. In the second part, the accuracy of the ANN inverse program was assessed using blind tests (i.e. numerical data with known material properties). The sensitivity of the program to potential error/noise was also analysed by introducing a control percentage error in the input data. In the next stage, the program was used to predict the thermal history resembles the position of the HAZ. The predicted cooling rates were assessed by comparing the numerical temperature curves with known results.

A range of input and target data was produced by the FE simulation model. The data sets were created using variations in spot weld load temperatures. The input temperatures ranged from $800^{\circ}C$ to $1800^{\circ}C$. Ten data sets of input and target parameters were used in this approach. Twelve simulations were performed on the spot welding FE numerical model developed. In Table 5.2 it contains the 12 nugget temperatures (load) used in the numerical model to collect data for the ANN. Each different temperature provided a thermal history cooling curve for the HAZ, Thermocouples TXA (1) and TXB (2). The temperature data gained from thermocouples TXA (1) and TXB (2) were to be used as Input parameters. The temperature data gained from the HAZ was used as Output parameters.

Table 5.2 Test numbers and corresponding melt temperatures used in the ANN

Model number	1	2	3	4	5	6	7	8	9	10	11	12
Nugget temperature ($^{\circ}C$)	800	900	1000	1100	1200	1300	1370	1400	1500	1600	1700	1800

A standardised optimum procedure was used in the ANN program. As there were three test methods to evaluate, the ANN program had to use the same operating parameters. The methods had to use eight melt temperatures for training scheme (from Table 5.2, these were temperatures 1, 2, 3, 5, 6, 9, 10, 12). The training method used was to provide the input parameters (TXA and TXB) and then give the program the expected output data as the Target parameter. The training program used epoch of 200 and a goal of 0.01. The remaining four data (from Table 5.2, temperatures 4, 7, 8, 11) were used for the blind tests to validate the program. The input parameters (TXA and TXB) were given to the program and the output/ target parameters were not entered. The program simulated the predicted outputs without knowing the target parameters.
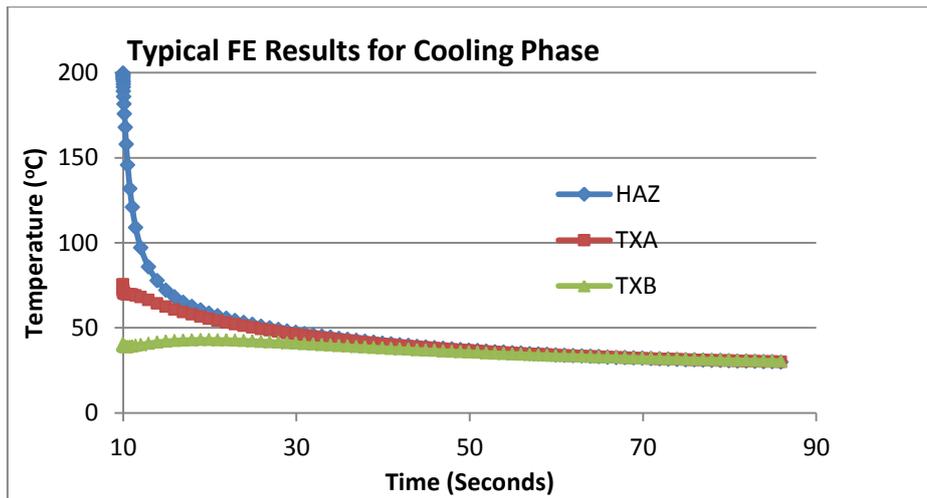
Figure 5.22 Typical numerical results data showing the temperature change and the cooling in the HAZ, thermocouple 1 and thermocouple 2

The cooling curve data sets from the FE simulations (a typical data is shown in Figure 5.22) were reduced so that the information was limited to the critical section of cooling as detailed in Figure 5.23. One important factor for ANN is the way this data is presented. Excessive or inadequate data will cause in accurate results. Three data processing approaches have been explored (i.e. point method, polynomial (non-linear) method and Slope (linear) method) as shown in Figure 5.23.
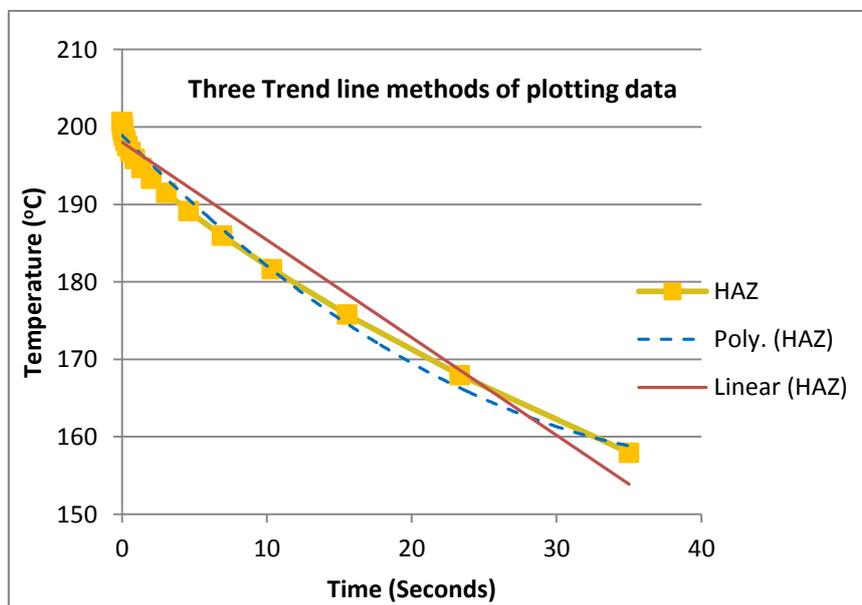
Figure 5.23 Schematic to show three proposed methods of plotting data for ANN training purposes

The first method is point based method; in the approach the cooling curve is represented by discrete temperature point data. The second method fits the data with a polynomial curves

(2nd order), then coefficients are used to represent the curve. The third approach designated as slope approach uses a simple linear relationship to describe the curve, the slope is used in ANN representing the cooling rate. All these three approaches have been proposed and implemented in the ANN program to evaluate their validity and efficiency. Details of each approach and some typical results are briefly presented in the next sections.

As shown in Figure 5.24 (a), the cooling curves of the HAZ and the temperature at the thermocouple position were broken into discrete points against fixed time point. These points were used as the input and target data. There are two sets of input parameters for this method. The first data set was the temperature of the welding process recorded by thermocouple 1 TXA. The second data set was the temperature of the welding process recorded by thermocouple 2 TXB. Each thermocouple provided over 100 (initially in the preliminary tests) sets of data (temperature measurements) per input. The temperature profile at the HAZ position from the FE simulation provided the program with the target data. The target data used in the program provided the same number of sets of data as each individual thermocouple (as the temperature profiles created were relevant to time). The data sets were reduced from over 100 values to 21 values. The 21 values were specifically selected as a representation of the critical section of the cooling curve.

As shown in Figure 5.24 (b), the Polynomial (non-linear) Trend-line based approach involves representing the cooling curve with a 2nd order polynomial trend-line. There are only two input parameters used (TXA and TXB temperatures) and one set of target data (HAZ temperature). As shown in the figure this polynomial equation provided an equation containing three values to create the trend-line curve. This meant that each set of data had been reduced from 21 (point based method) to 3. Series of polynomial equation trend-lines were created for the range of melting temperatures (800°C to 1800°C) on all of the critical cooling curves.

As shown in Figure 5.24 (c) in the third approach, the cooling was represented by a linear line in which the main coefficient is the gradient. With this method, those 21 temperature points were simplified by one linear equation. Although the linear trend line fit is not as accurate as the polynomial curve, it is still a very good fit as it intercepts all the critical temperature measurements. Correlation analysis of a range of data showed that this is a valid method with the correlation coefficient at over 99 %. This method is able to dramatically reduce the number of parameters required for the ANN program. Linear equation trend-lines

were created for the range of melting temperatures (800°C to 1800°C) on all of the critical cooling curves. The two linear equation values in the thermocouples TXA and TXB were used as the input data sets. The two linear equation values in the HAZ were used as the target data set. The eight data sets (range of temperatures 800°C to 1800°C) of input and target parameters were then used to train the ANN program.
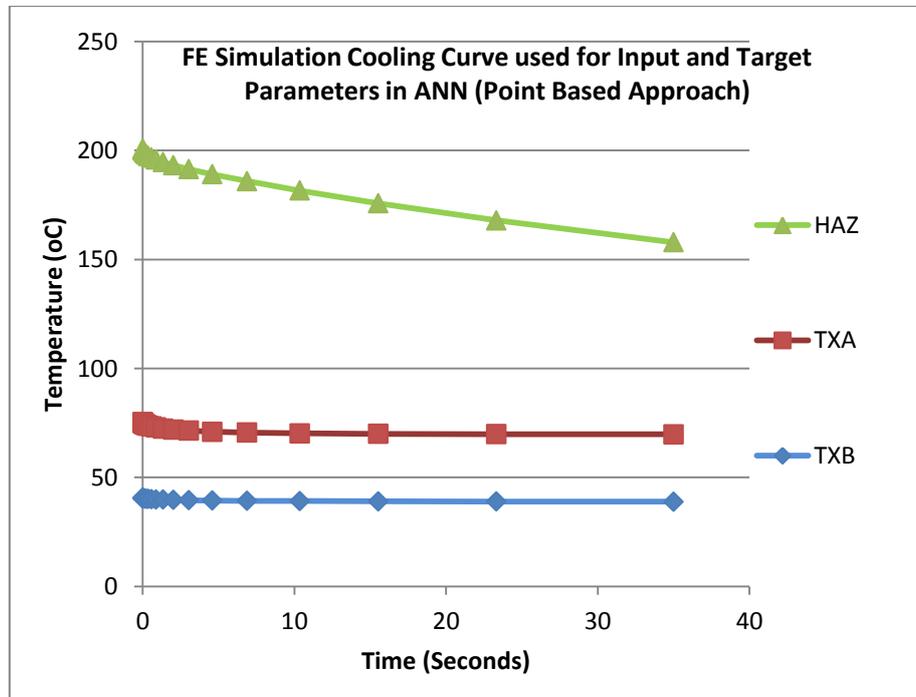
Figure 5.24 (a) Point based approach
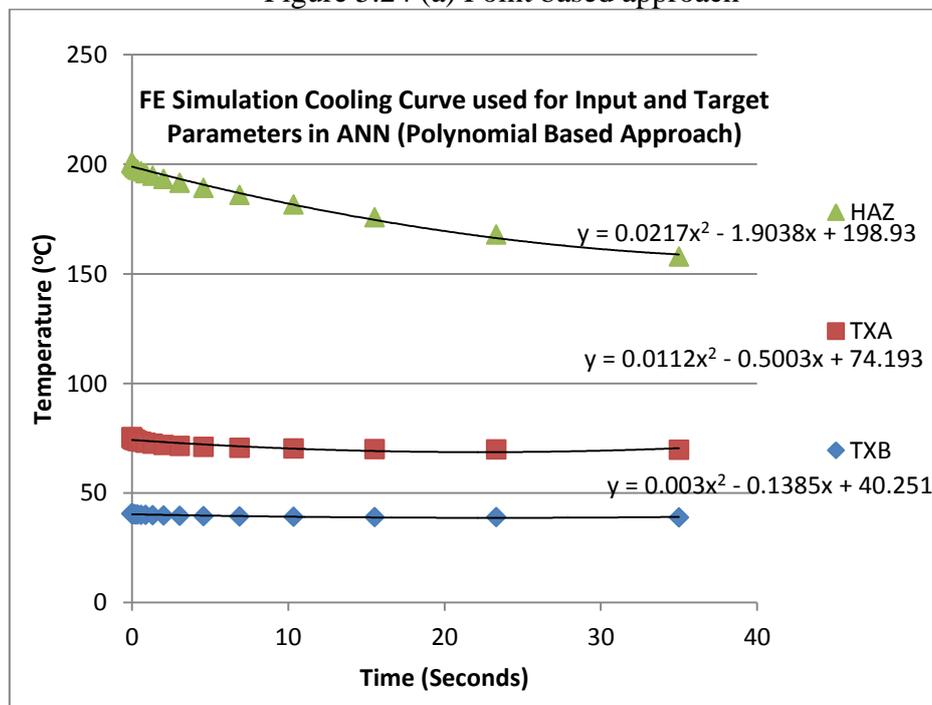
Figure 5.24 (b) Nonlinear fitting based approach

130
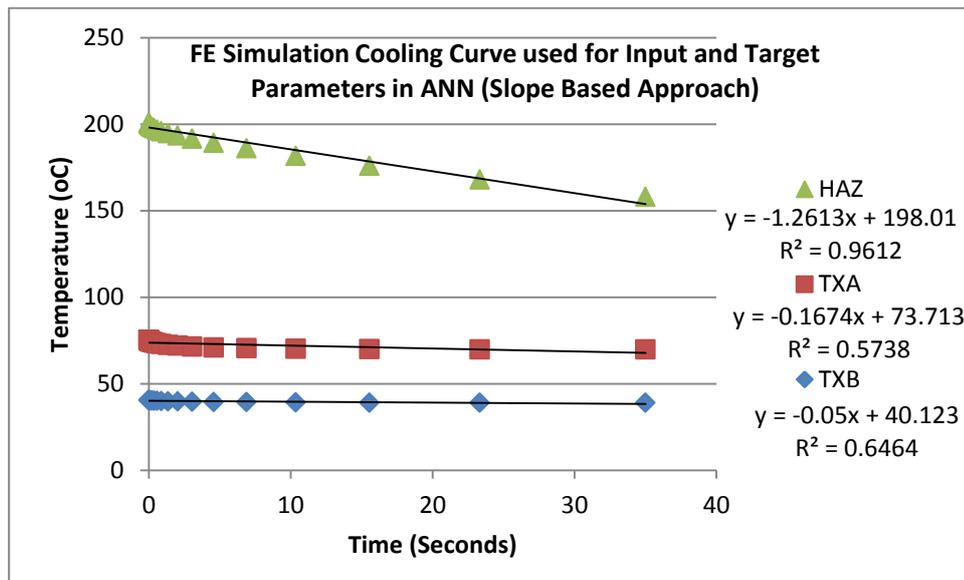
Figure 5.24 (c) Linear fitting based approach

Figure 5.24 Three different data processing methods to represent the cooling process as the input and target parameter in the ANN model. **(a)** the point method; **(b)** the Polynomial (non-linear) based method and **(c)** the Slope based method

Figure 5.25 Curve charts showing the performance of the point based method results and typical prediction with an under trained model and a fully trained model. Figure 5.25 (a) shows the training information gained.   The output data from the point based approach produced a thermal history cooling curve for the HAZ. This was compared to the Target data created by the FE simulation, as shown in Figure 5.25 (b & c). When the model is under trained, the comparison between the predicted output curve and the FE simulated curve evaluated that there was low convergence. Upon comparison of the two HAZ's the temperature curves did not match. From the training data it was established that the program required more data sets and training to improve convergence. The network was given further training (from 8 sets of data to 11 sets of data). This further training vastly improved the predicted HAZ cooling curve to converge with the simulated HAZ cooling curve, Figure 5.25 (c).
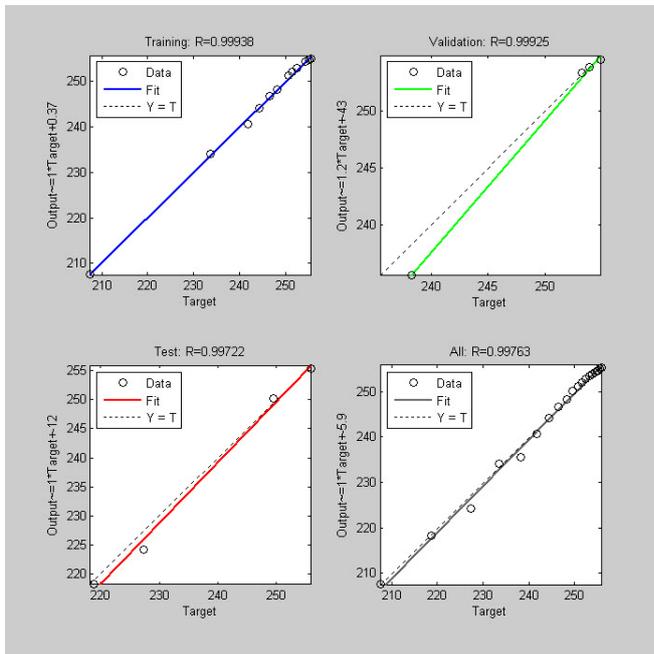
Figure 5.25 (a)

iii) Regression
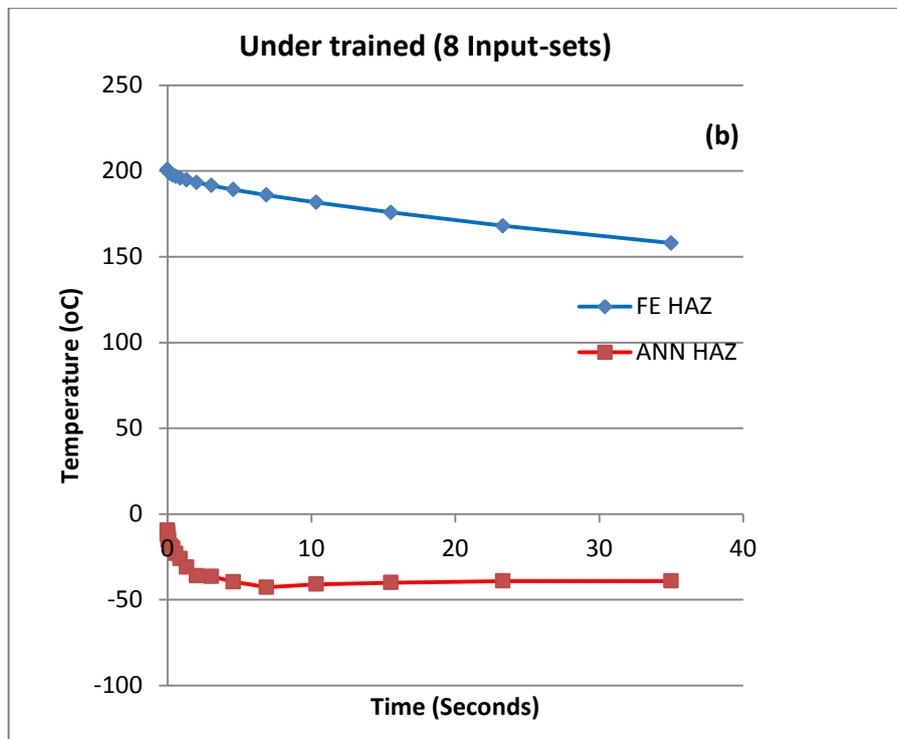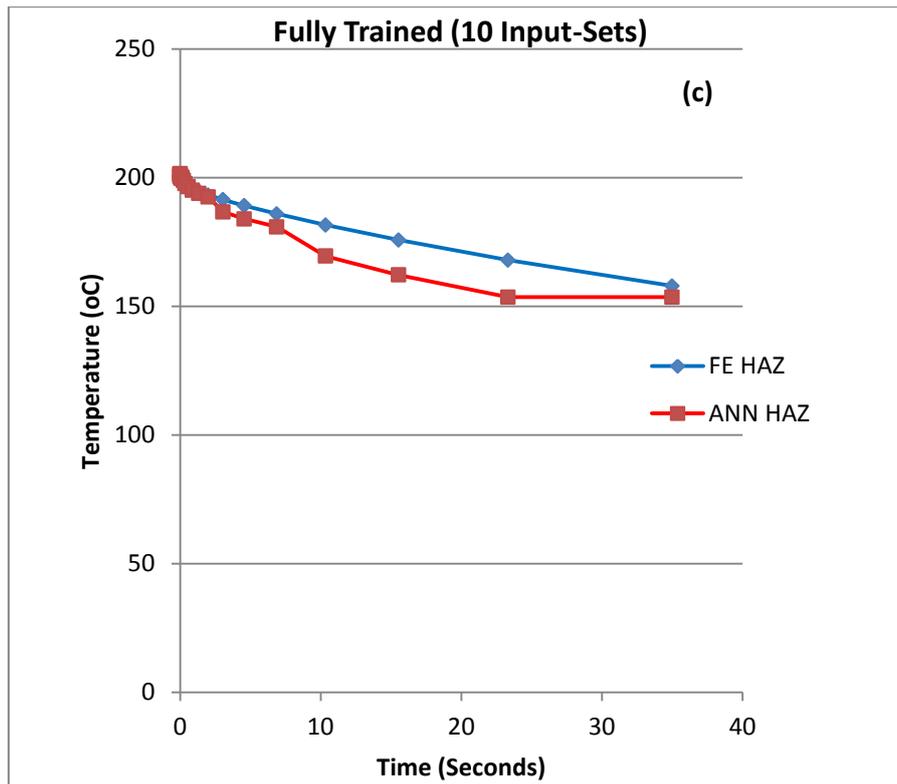
Figure 5.25 Curve charts showing the performance of the point based method results for the cooling rate in the HAZ **(a)** Typical Epoch training, validation and performance data for the point based method **(b)** Comparison between the predicted and target with 8 sets (under-trained) of training data **(c)** Comparison between the predicted and target with 10 sets (fully trained) of training data.

Figure 5.26 Curve charts showing the performance of the polynomial (non-linear) based method (a). Similar to Figure 5.25, the data for Epoch training, validation and performance data for the polynomial (non-linear) based method is presented in Figure (a). Figure (b) is a comparison between the predicted and target with 8 sets of training data (the same number of sets as in Figure 5.25 (b). Figure (c) is the Comparison between the predicted and target with 10 sets of training data.

i)   Performance

ii)   Training State

Figure 5.26 (a)

iii)   Regression

(b)

y = 0.0217x^2 - 1.9038x + 198.93

y = -0.041x^2 - 1.6936x + 239.18

Figure 5.26 Curve charts showing the performance of the polynomial (non-linear) based method **a)** Epoch training, validation and performance data for the polynomial (non-linear) based method. **(b)** Comparison between the predicted and target with 8 sets (under trained) of training data **(c)** Comparison between the predicted and target with 10 sets (fully trained) of training data

The results show that when this method is used the network can achieve the target data more efficiently than the point approach.

Figure 5.27 shows typical ANN training data and prediction results. Figure 5.27 (a) shows the training results when the Input parameter and Target parameters were entered into the network. These results show that when this method is used the network can achieve the target data more efficiently than the point approach and just as effectively as the polynomial approach. The remaining four spot weld load temperatures (data not used in the training) were then used to perform blind tests on the ANN program to validate this method. A typical result is shown in Figure 5.27(C). It is clearly shown that the output produced (i.e. the slope) was in very good agreement against the target curve than the results from the point and the nonlinear polynomial approach. The predicted HAZ temperature was very close to the target value.

i)   Performance

Figure 5.27 (a)

I)   Training State

II)   Regression

y = -1.2812x + 200.85
y = -1.2614x + 198.01
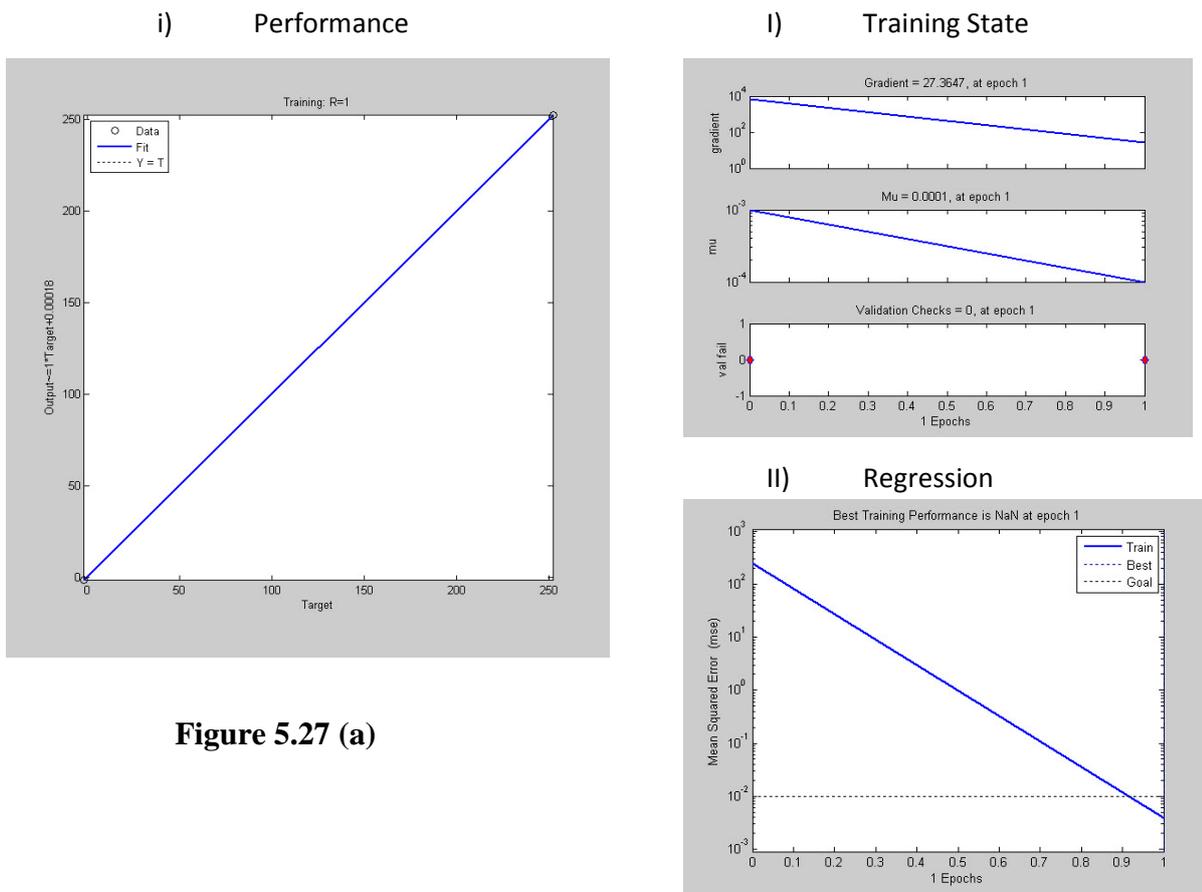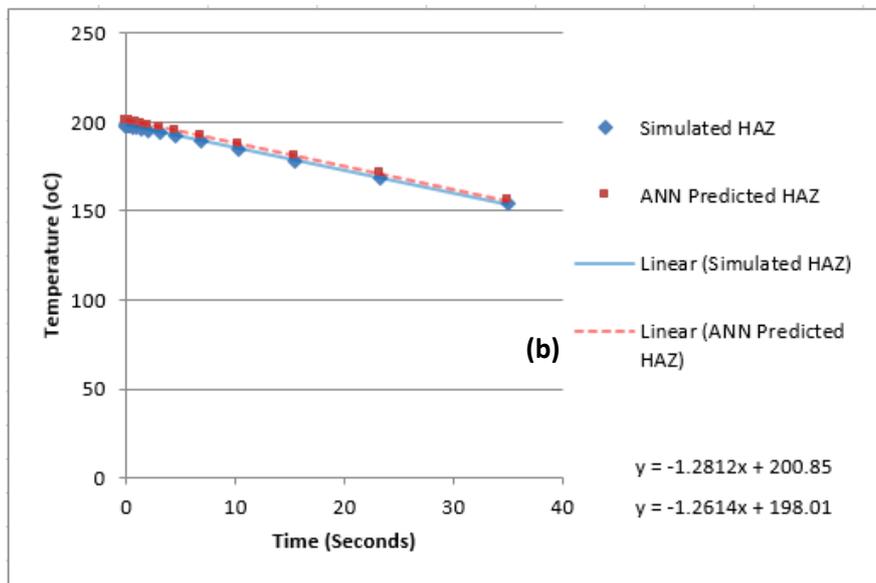
Figure 5.27 Curve charts showing the performance of the slope (linear) based method **(a)** Epoch training, validation and performance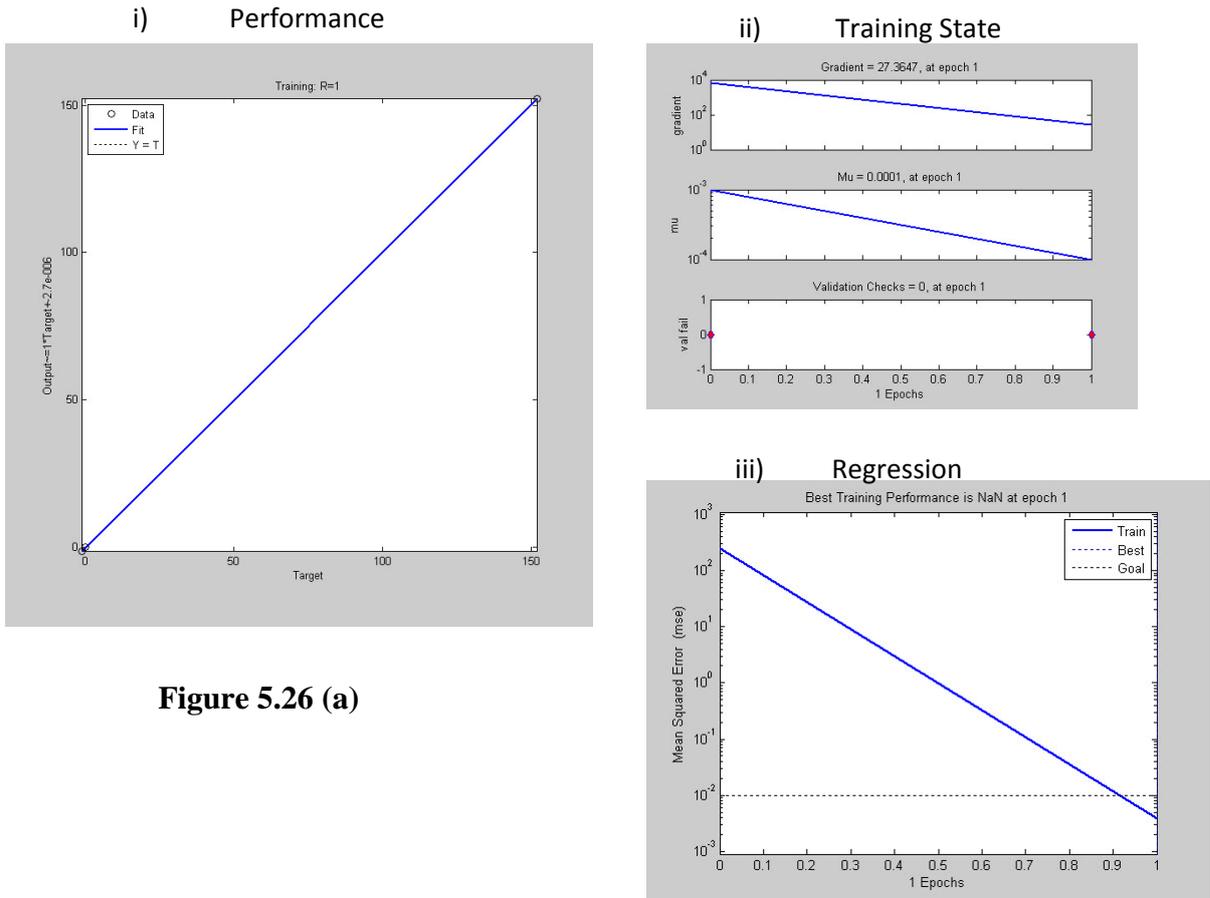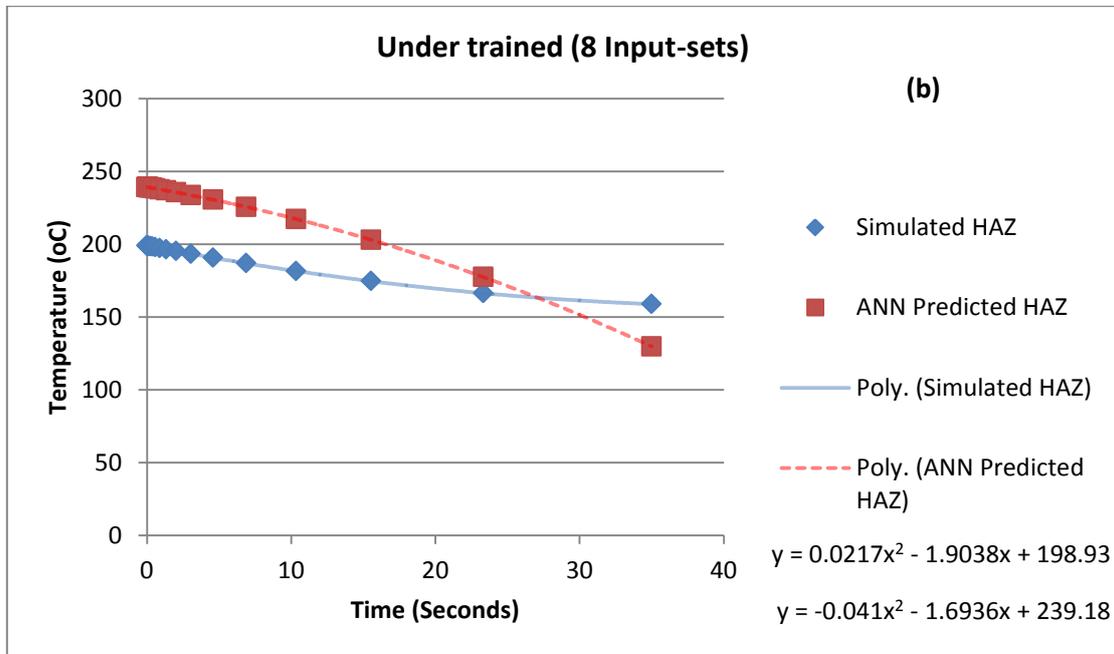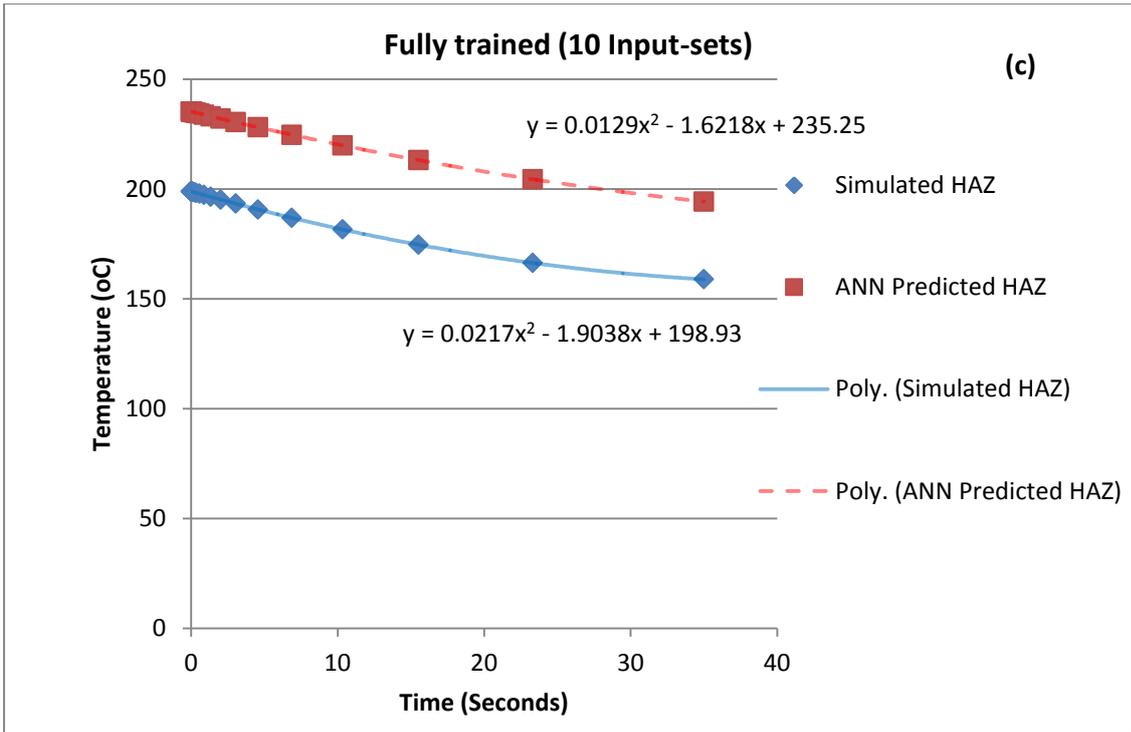 data for the slope (linear) based method. **(b)** Comparison between the predicted and target with 8 sets of training data

The FE model and the ANN based inverse program has been expanded to the study of temperature with different electrode size and sheet thickness. This was done by altering electrode sizes and thickness of the specimen in the FE model. While the remaining welding process parameters and boundary conditions were not changed, the test procedure also remained the same. The same 12 ranges of melt temperatures were used in each FE simulation model, so that the amount of data used in the ANN was identical. Figure 5.28 shows the results of tests on different electrode sizes. The electrode size was increase from 5mm to 6mm. This meant that the nugget size changed from a diameter of 4mm, 5mm to 6mm. The thermocouple positions remained the same because they were positioned at locations from the centre of the nugget (not the circumference). However, the HAZ's moved closer to the thermocouples. The material properties and dimensions also remained the same.

The 12 simulations each produced data sets for the HAZ, TXA and TXB. Figure 5.28 (a) shows a comparison of critical cooling curves for the three electrode sizes (4mm, 5mm and 6mm). The temperatures measured for the HAZ, TXA and TXB are higher when a spot weld is performed using a 6mm electrode. This is because of the greater surface area of contact on the specimen. The temperatures measured for the HAZ, TXA and TXB are lowest when a spot weld is performed using a 4mm electrode. The results showed that the temperature within the weld will change significantly with different electrode size in particularly in the HAZ. The cooling curves for the HAZ's of the three electrode sizes were analysed by introducing linear equations. The HAZ created by the 5mm produces the most rapid cooling curve. Figure 5.28 (b) shows the cooling curves created from the FE model compared with the ANN prediction for a 6mm electrode spot welded specimen. Figure 5.28 (b) shows the cooling curves created from the FE model compared with the ANN prediction for a 4mm electrode spot welded specimen. In both cases, the ANN predicted temperature drop in the HAZ showed a reasonable agreement with the target value (Figure 5.28 (a & b))
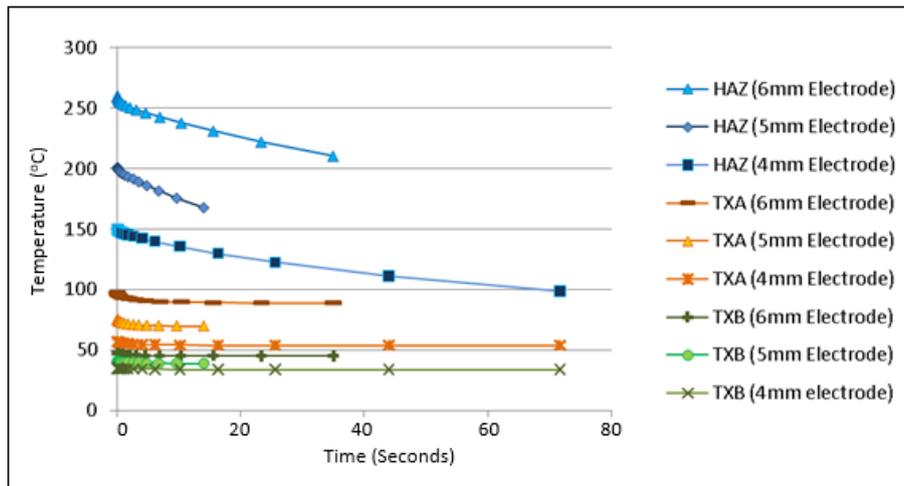
a) Typical data (taken at HAZ, TXA, TXB) with different electrode sizes
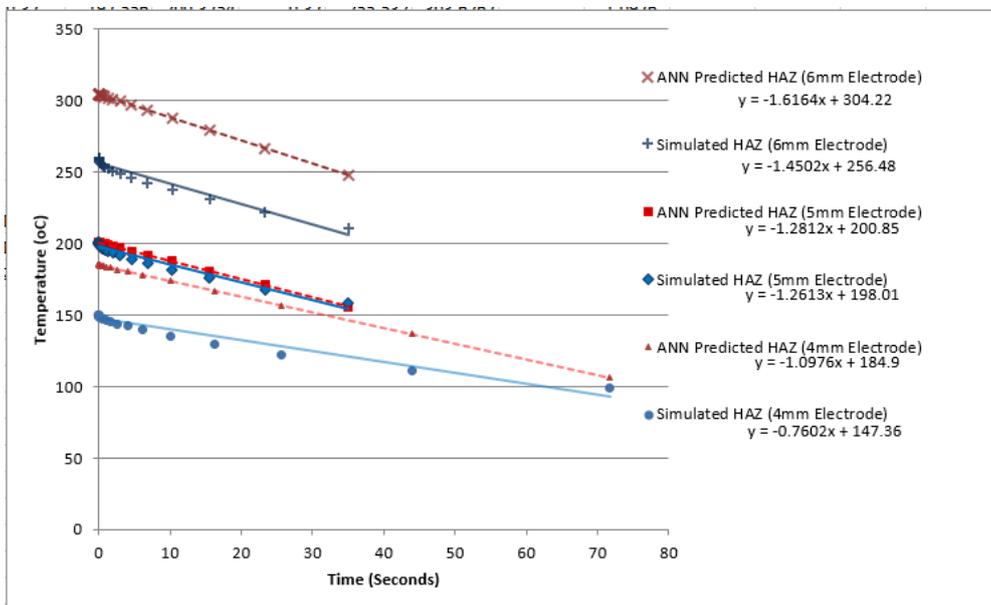
b) Comparison of FE Data and ANN predicted curve data

Figure 5.28 FE analysis study on the effects of different electrode/tip sizes (4mm, 5mm & 6mm) on the modelling and inverse modelling results. (a) temperature change in the HAZ and thermocouple positions. (b) comparison between the predicted cooling curve and the target curve.

Figure 5.29 (a) shows a comparison of critical cooling curves for the two specimen thicknesses (0.5mm and 1.0mm). The temperatures measured for the HAZ, TXA and TXB are higher when a spot weld is performed on a 0.5mm specimen. This is because the heat was transferred through less material. The temperatures measured for the HAZ, TXA and TXB are lowest when a spot weld is performed on a 1.0mm specimen. The cooling curves for the HAZ's of the two specimen thicknesses were analysed by introducing linear equations Figure

5.29 (b). The HAZ's created by both specimens produced similar cooling curves (at different temperatures). In general, the temperature change is less significant due to the thickness effect than the size of the electrode and the ANN program is able to produce a reasonable prediction. Figure 5.29 (c) shows the comparison between the ANN predicted curves and the target. In the case of thickness of 1mm, the predicted data match the target very well. But for the thickness of 0.5mm, the temperature is higher (less than 15%), but the trend is comparable. The same approach has been applied to other untrained data (data not used in the training), a similar accuracy is obtained. Given for welding process, the cooling rate is the most important factor, these result suggests that ANN approach is a viable approach.
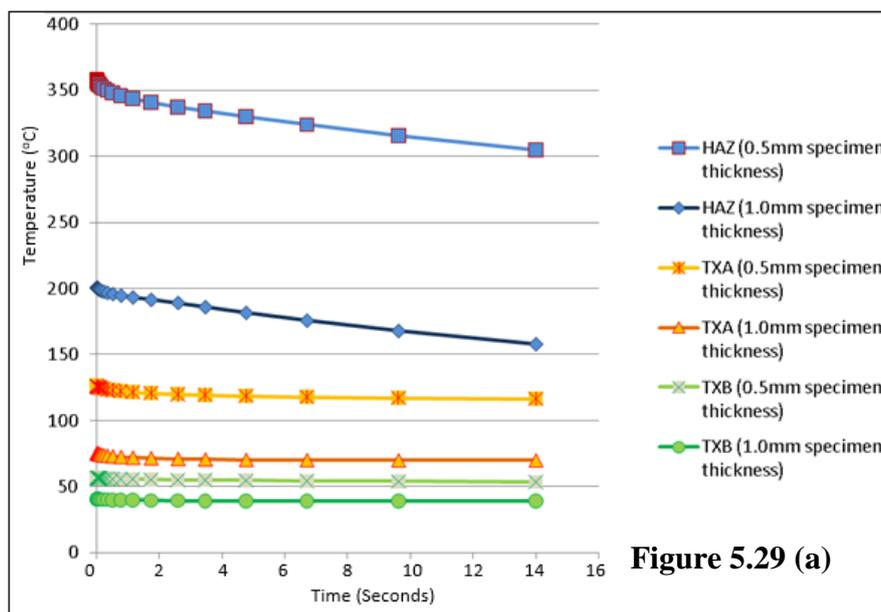
Figure 5.29 (a)
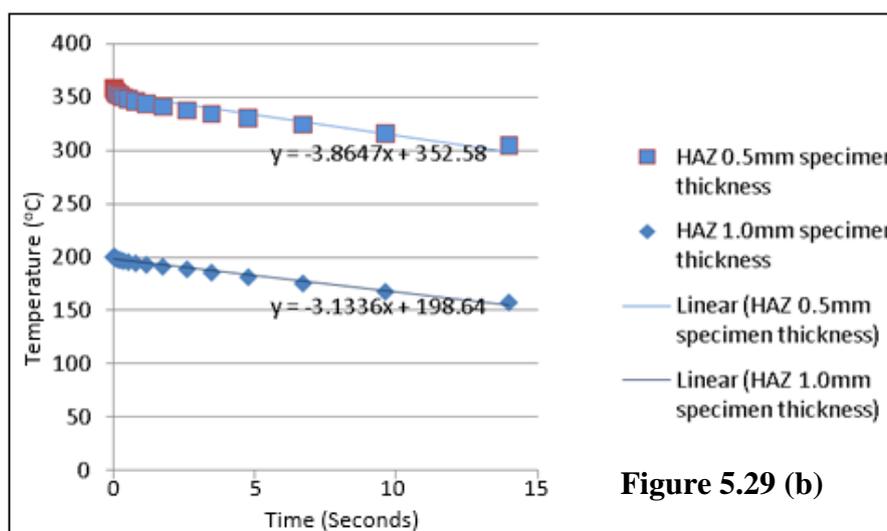
Figure 5.29 (b)
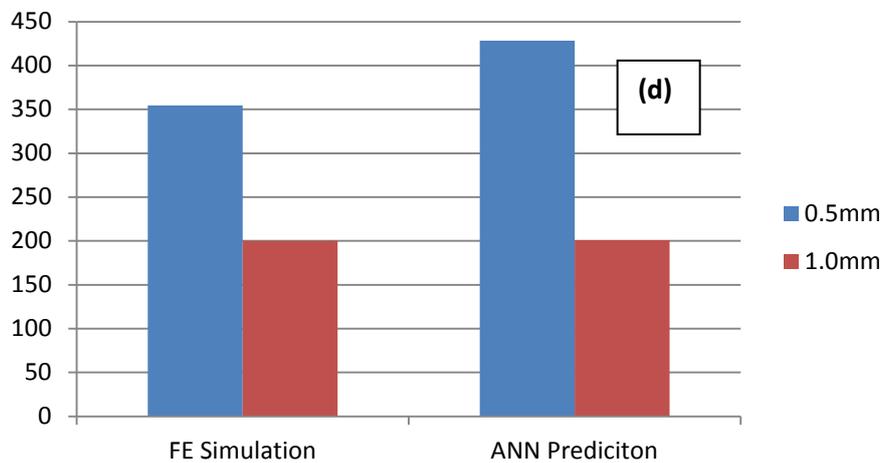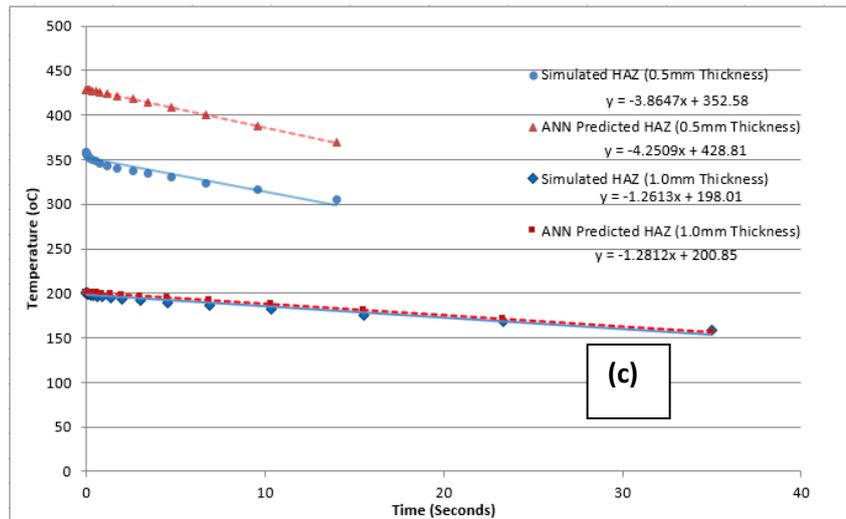
Figure 5.29 FE analysis study on the effects of different sheet thickness (0.5 and 1mm) on the modelling and inverse modelling results. (a) temperature change in the HAZ and thermocouple positions. (b) different cooling rate with different thickness (c) comparison between the predicted cooling curve and the target curve with a Bar chart (d) showing the slope to predict the cooling rate not the temperature

5.6 Discussion

5.6.1 Use of remote thermocouple method used in studying the thermal process in spot welding

The thermal process is one of the most important parts of understanding the electrical resistance spot welding process. The work in this chapter has covered serval important issues related to thermal processes for spot welding. The first part covers the remote temperature measurement in spot welding of different material systems. The second part presents FE modelling of spot welding process with a particular focus on the temperature distribution. The third part is regarding the use of artificial neural network to predict the temperature at a location resembling the location of the HAZ. These three parts are integrated and could provide important information about an electrical resistance welding process. The temperature directly influences the microstructure and properties of the spot welded joints, an effective way of temperature measurement or prediction is key to welding process improvement or quality control. The understanding of temperature in welding different material systems also helps to optimise the weldment design.

From the results presented in the first section, remote thermocouple has shown to be a consistent method to monitor the temperature change. The thermal reading varies with the position of the thermocouple. The data presented was concentrated on two positions. distance from the nugget centre of 10 and 20 mm. However, in the preliminary work, tests have been conducted on a series of positions, typical data is shown in Figure 5.30.

Shown in the figure 5.30, is the temperature for each position starts to pick up in sequence and follows a clear pattern, even though the thermocouples are just 5 mm apart. The optimum position of the thermocouple should be further enough from the nugget to avoid the interference form potential flash, spark and repulsion, but near enough to be sensitive. When using more than one thermocouple, the two positions chosen should be far apart enough to be able to pick up the difference. In other words, the difference should be large enough to minimise the effect of system or random errors.
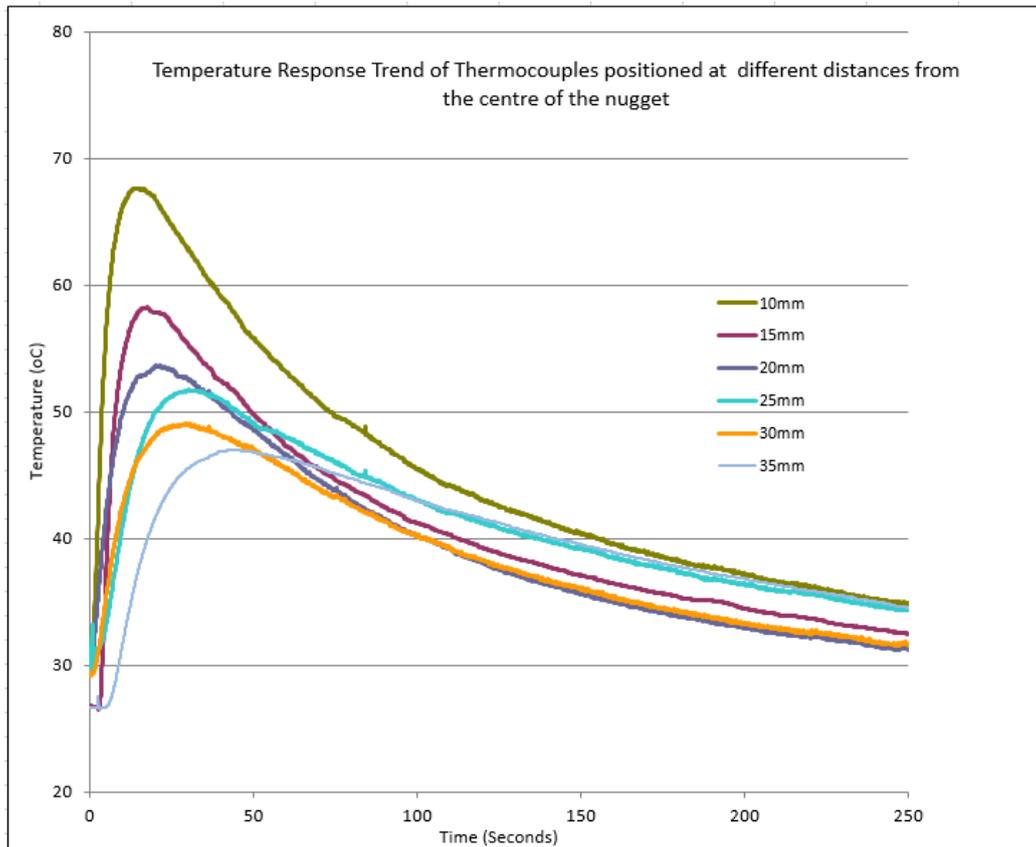
Figure 5.30 Temperature Response Trend of Thermocouples positioned at different distances from the centre of the nugget

The temperature reading and the relationship between the temperatures at different locations in certain ways also provides important information. Compared to other methods, such as, putting the thermocouple directly in the nugget or HAZ (Poorhaydari, 2005), the remote thermocouple method is more practical and potentially can be used in real engineering situations. Similar to other processes where remote the thermocouple has been used such as, machining, spot welding has a heat source with a relatively fixed position to the thermocouples. Once the material and the electrode is fixed, then the thermal process is, in general, reproducible. This is clearly shown in the test data. This made it possible to use such a method in spot welding. Choice of the thermocouple is also important, as shown in Figure 5.4, when welding mild steel and stainless steel samples, the bare-wire and the sheathed thermocouple showed a clear difference. This is a typical case that the conventional requirement on thermocouple response time is not applicable. For example, in commissioning autoclave, it is normally required that the thermocouple reaches the target temperature with 30 seconds (BE EN 285 & HTM 2010) but for an application in spot welding the thermocouple has to respond much more quickly. When using sheathed thermocouple, the

response is much slower and it is difficult to connect the thermocouple to the surface properly. A range of methods has been trialled including using magnets, thermal cement etc., none of them could provide consistent data. So a thin thermocouple will be a much better choice. However, if the thermocouple is too thin, it lacks strength and can easily be broken. The work used welded on thermocouple approach. Evident from the data, the set-up has produced reasonably good repeatability.

5.6.2 Temperature in welding different material systems

From the temperature data for different material systems it is clearly shown that the temperature varies with the material. For the single material welding, the peak temperature measured at the two thermocouple positions is similar in the first weld, but the two materials showed a different trend. There is relatively limited change temperature change in repeated tests for mild steel, but the temperature for the stainless obviously reduced in repeated tests. This is an interesting observation. Steel normally starts to soften at around 500°C, but stainless steel can maintain its strength to relatively high temperatures, the thermal conductivity is lower and stainless steel hardens more than carbon steel. The surface contact condition of the electrical resistance is similar but since stainless has lower conductivity, the reading from the remote thermocouple is relatively low.

The temperature range for welding dissimilar material is close to the temperature of welding the same work-piece. The temperature when having different steel on the top (i.e. facing the electrode), the temperature reading is different, for example as shown in Figure 5.8 the temperature varies slightly with the position of the plate (e.g. mild steel or stainless steel). When the carbon steel is used at the top, the thermocouple reading is slightly higher.

The metallurgy study of the spot welded joints of different material systems shows different welding zones. The same material welding, has similar nugget shape, the stainless steel seems to have a clear boundary between the nugget and the heat affected zone (liquid and solid mixture in welding). The welded joint of the DP steel showed a similar nugget zone. DP steel is a mixture of ferrite and martensite. During the welding process, the metal is melted and solidifies, the final structure is pearlite.

When welding dissimilar material, the shape of the nugget is different, the nugget is tapered. When welding stainless steel and the mild steel, the nugget seems to have grown from the stainless steel side to the mild steel side, with a clear boundary, very little sign of mixing.

Further work is required to conduct chemical analysis to further understand the process. Stainless steel and mild steel have a similar melting point but stainless has lower thermal conductivity and specific heat, this may cause high temperature within stainless steel, thus a high volume of melting. This observation also highlighted the potential property mismatch may exist. While the welding of MS and DP steel is different, it can be clearly seen that the two work-piece material mixed together well in the nugget. The strength of DP steel comes from martensite network, once melted, other physical properties between the mild steel and DP are similar, so different from the weld between stainless and mild steel, and there are not clear differences in the zones between mild steel and dual phase steel.

5.6.3 Use of inverse modelling for thermal problems

Inverse modelling is widely used in mechanical or thermal problems, where the variables could not be directly measured (Ren et al, 2004). For example, the work is extensively used in material properties prediction from non-destructive tests. It was also used in manufacturing and machining, etc. It is a useful method but it is not something applicable to every situation. The work is more applicable to a situation where the material system or some condition are stable. In spot welding, the thickness or the nugget size are common (unchanged), the material property is relatively stable for the same material system. So it is possible to use inverse modelling as it is not an open random system. Compare to other inverse modelling processes, ANN is a more suitable method for analysing the thermal history of spot welding. It is a complex process in spot welding within the nugget, but the relationship between the temperature outside the nugget is mainly conduction dominated, this is made is possible by using the ANN based method with a limited number of remote measurement

One of the main parts of the work was to use different approaches to represent the thermal curves. The point based method involves using a large number of data as input and output. It is straight forward without requiring the user to process the data. But in real situations, the measurements always have noise, so some form of data smoothing out processing will still be required. In addition, for longer time measurements, there will be a lot of data, therefore, requiring high computation resources. The polynomial method could represent the data with a few coefficients and fit the situation, but the system is very sensitive to training. As shown in figure 5.26, the result is not accurate when using 8 sets of data compared to 10 sets. This may cause an unstable system (i.e. the prediction shows significant change with slight variation of the input). In addition, the coefficient for a polynomial fitting could be non-unique. In other

words, the same curve data could have multiple sets of coefficients fit the curve to a similar level of accuracy (Wang, 2016), so when using a limited number of thermocouple measurements, the results may become non-unique. The use of slope is a simpler but effective method. On the surface it is not as accurate as the point based and polynomial method, but it is much more robust and more computationally efficient. In addition, in industrial prediction, it is common to use the gradient to represent the cooling rate. In the ANN work, the slope method is much more robust and requires a small set of data of training.

For an inverse program to work, the measurement is a key. One way is to use more remote thermocouples, which will give extra measurement. For spot welding this is possible, apart from using more thermocouples on the plate to generate more input, temperature measurement can also be made in other location such as, the electrode. The size and shape of the individually formed welds are limited primarily by the size and contour of the electrode faces. The electrodes are usually copper alloy based and water cooled. It was deemed important to determine the effects the electrodes have on temperature change during the welding process. To measure the thermal response of the electrodes, thermocouples were welded to both the top and bottom tips. The thermocouples were welded to the chamfered edge of the electrodes as no measuring equipment can be placed in the contact area between electrode and the work piece. The results of the tests are shown in Figure 5.31. It is clearly shown that there is a clear difference between the temperature of the top and bottom electrode. But this may require using the electrode with welded or inserted thermocouples. In preliminary work, the data is not repeatable as in the case using thermocouple on the plate. In addition, the electrode is not easy to replace without resetting the machine or stopping the process. One potential approach is to use insert thermocouple in the electrode in future works.
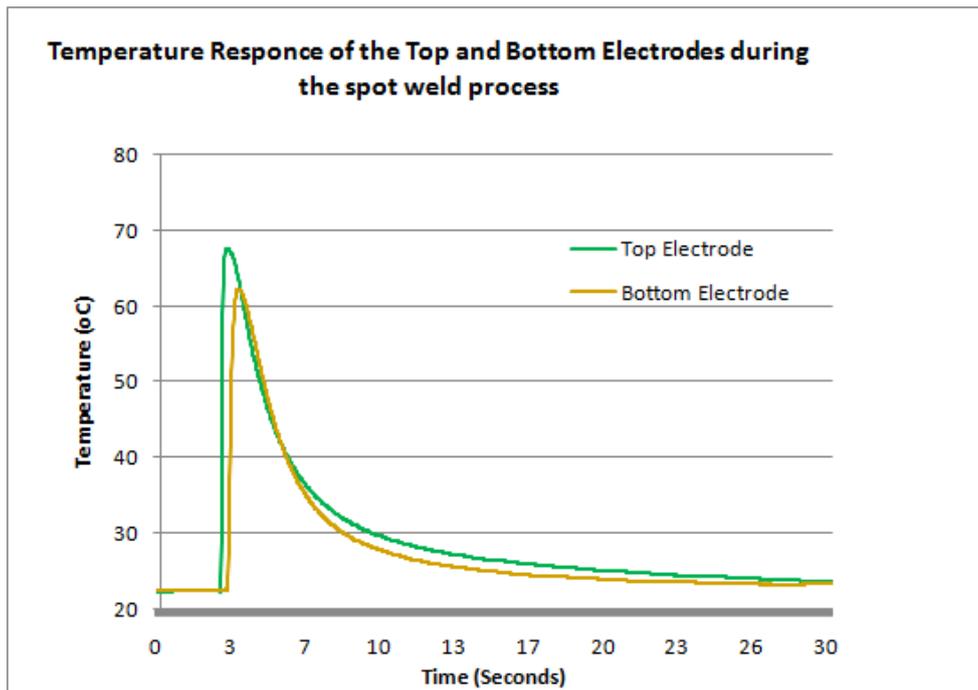
Figure 5.31 Electrode response test performed on Mild Steel sample

As shown in the work, many factors may influence the measurement. As the welding process occurs within a sub-second, then the thermocouple response becomes very important. The dynamic response of a sensor is often an important consideration in designing a measurement system. When the thermocouple (TC) is subjected to a rapid temperature change, it will take some time to respond. If the response time is slow in comparison with the rate of change of the temperature that you are measuring, then the TC will not be able to faithfully represent the dynamic response to the temperature fluctuations. Not only in spot welding, there are other situations where very quick response of thermocouple is required. The response of a thermocouple is critical for safety in the nuclear industry, TC's are associated with heating elements to measure gamma heating, Temperature measurement of fuel outlet radial distribution of the core temperature protection against nucleate boiling on fuel. TC's are also used in the pharmaceutical industry to monitor and control production of vaccines, products which are temperature critical in the case of live (cell culture) vaccines. The sterility of production and equipment has to be confirmed and thermocouples are used as a reliable instrument to validate. The efficiency of inverse modelling will be further improved with more data and accurate measurement.

146

5.8 Summary

This chapter reports the main development work and results associated with the temperature and structure of electrical resistance spot welding, including development of a testing method to remotely measure temperature in spot welding, development of FE thermal model of the spot welding process, evaluation of use of artificial neural network (ANN) based inverse modelling with remote thermocouples and discussion.

The experimental work consists of measuring the temperature during electrical spot welding process using remote thermocouples, characterisation of the welded zones for different material (mild steel, stainless steel and dual phase steels); the structure of the spot welded joint with different material systems. The effect of some key testing conditions (including using different types of thermocouples (bare-wire or sheathed) and location) were established. The results show that the temperature can be reliably measured using remote thermocouples. The welded bare-wire thermocouple shows more rapid response to the temperature change than sheathed thermocouples. The temperature measured by the remote thermocouple showed a clear difference between different materials in same material welding (MS-MS, SS-SS) and dissimilar material systems (MS-SS). The mild steel show a relatively unchanged temperature under repeated welding, while the temperature for repeated tests on stainless increases when the welding was repeated in the same position. Metallurgy observation has been conducted on several material systems and reveals that the welding zones for stainless-mild steel is different from the same material weld. Stainless forms a larger volume in the nugget and grows into the mild forming a taper shape nugget.

In numerical work, an electrical-mechanical-thermal model for spot welding is developed and temperature zone is compared with the structure observation. The FE model also provided data for developing an Artificial Neural Network (ANN) method to predict the temperature and cooling curve of HAZ from remote thermocouple measurements. The network was set up and the optimum level of training was determined. Three approaches of representing the cooling curves (i.e. point based, polynomial trend-line and linear trend-line methods), were successfully evaluated to determine prediction accuracy in the neural network; each of the methods has shown to be able to predict the temperature at the HAZ position based on the temperature history of remote thermocouples. The slope method showed a better robustness, which requires less training data. These works are important to establish an integrated approach to study the thermal, electrical and thermal process of spot welding process. Some

key issues regarding remote temperatures, including choice of thermocouples are discussed towards the end.

CHAPTER 6

Conclusions and Future Works

6.1 Conclusions

This work has focused on developing advanced modelling programs for simulating spot welded joints and using the programs to investigate the effects of the key dimensional or material parameters on the mechanical or thermal response of spot welded joints of steels and different thermocouple joints relevant to their applications. The key development and results are presented in three interlinked parts.

In the first part on "Development of Plug-in interface program for Mechanical Modelling of Electrical Resistance Spot Welded Joints", an FE model and an Abaqus plug-in of spot welded joints is developed and used to investigate the effect of nugget size and sheet thickness on the stress and deformation of spot welded joints of steel. A systematic/automatic modelling approach of spot welded joints was designed and coded using Python scripting. Several interfaces were generated to create parametric models, the approach used different features of the weld that impact the mechanical behaviours. The interfaces included; geometry, material and shear (plastic) properties, sectioning of HAZ layers, boundary, loading conditions and crack partition path. The program is able to incorporate the plastic material parameters (yield stress and work hardening coefficient) as well as fracture models. The plug-in is used in numerical modelling the elastic-plastic-fracture of spot welded joints under tensile-shear. The validated numerical models are further used to investigate effects of nugget size and thickness of the metal sheets on the strength of welded joints. The analysis on stress (Von Mises) distribution within the nugget and the HAZ zone next to the nugget and the ratio of the Von Mises stress at the inner and outer side along the loading axis suggests that the HAZ is more likely to act as the crack initiation and propagation path, which is in agreement with experimental observation.

In the second part, detailed FE models of different types of thermocouples have been developed including bare-wire thermocouple, ungrounded sheathed thermocouple and grounded thermocouple. The predicted time-temperature data showed a reasonable agreement with experimental data. Plug-in interface is developed for different types of thermocouple consisting of geometry, material and contact condition modules. For the bare-wire thermocouples, the plug-in consists of function to study influence of materials, dimension (nugget tip and wire diameter) as well as tip condition (full tip contact and partial contact). The FE model is able to predict the time period during which the measurement is prone to variation due to partial tip contact. The plug-in for ungrounded sheathed TC successfully

incorporated the function of automatic verification of the tip position, which is effective for studying the effect of key design factors on the response of the sheathed thermocouple. The results show that the temperature of tip of a sheathed thermocouple is more uniformly heated but the response time is slow due to the effect of the sheath and the insulation layers. It also shows that the position of the nugget could have significant influence on the measurement response. The plug-in for the grounded TC incorporated the key dimensions of the end of the sheath. The modelling showed that the thickness of the sheath tip could cause temperature measurement variations. The plug-ins are successfully used in systematically studying the effect of nugget size, nugget position, sheath size and the tip dimensions. It has laid a frame work for future development in more complex TC systems (including dual or multiple tip systems) and manufacturing process optimisation.

The third part reports the main development work and results associated with the temperature and structure of electrical resistance spot welding, including development of a testing method to remotely measure temperature in spot welding, development of an FE thermal model of the spot welding process, evaluation of the use of artificial neural network (ANN) based inverse modelling with remote thermocouples and discussion. The experimental work consists of measuring the temperature during the electrical spot welding process using remote thermocouples, characterisation of the welded zones for different material (mild steel, stainless steel and dual phase steels); the structure of the spot welded joint with different material systems. The effect of some key testing conditions (including using different types of thermocouples (bare-wire or sheathed) and location) were established. The results show that the temperature can be reliably measured using remote thermocouples. The welded bare-wire thermocouple shows more rapid response to the temperature change than sheathed thermocouples. The temperature measured by the remote thermocouple showed a clear difference between different materials in same material welding (MS-MS, SS-SS) and dissimilar material systems (MS-SS). The mild steel show a relatively unchanged temperature under repeated welding, while the temperature for repeated tests on stainless increases when the welding was repeated in the same position. Metallurgy observation has been conducted on several material systems and reveals that the welding zones for stainless-mild steel is different from the same material weld. Stainless forms a larger volume in the nugget and grow into the mild forming a taper shape nugget. In numerical work, an electrical-mechanical-thermal models for spot welding is developed and temperature zone is compared with the structure observation. The FE model also provided data for developing an Artificial

Neural Network (ANN) method to predict the temperature and cooling curve of HAZ from remote thermocouple measurements. The network was set up and the optimum level of training was determined. Three approaches of representing the cooling curves (i.e. point based, polynomial trend-line and linear trend-line methods), were successfully evaluated to determine prediction accuracy in the neural network. Each of the methods has shown to be able to predict the temperature at the HAZ position based on the temperature history of remote thermocouples. The slope method showed a better robustness, which require less training data. These works are important to establish an integrated approach to study the thermal, electrical and thermal process of the spot welding process. Some key issues regarding remote temperatures, including choice of thermocouples are discussed towards the end.

The contributions from this work can be summarised as follows;

The idea behind this PhD project is to incorporate all aspects of the welding process and provide an optimised approach and performance prediction using modern experimental, numerical and optimisation techniques. Following the proposed framework (Figure 1.1), the project effectively integrated different aspects of analysis of spot welded joints, contributing a holistic investigation of welds, parametrically modelling the thermal history, performance and properties. The mechanical modelling part produced a new systematic tool linking structure, meshing, and modelling of sport welded joints for different loading condition relevant to service conditions. The approach is transferable to other welding methods; The work on thermocouple is the first for this nature, which not only developed an systematic modelling method for a complex structure of sheath, insulation and element, it also produced a tool to demine the design (upper or lower limit) of thermal response which otherwise is not measureable or able to accurately quantify. The use of remote thermocouple method presented the thermal history for sport welding which is important for the structure and property prediction of spot welding. The established method is transferable to other applications and laid a solid foundation for more complex thermal measurement systems.

6.2 Recommendations for future works

This work has developed a framework for developing Abaqus plug-ins for different applications. It clearly shows that Plug-in could be a powerful research and development tool.

Apart from the spot welded joints, plug-in has been transferred to other research projects for some materials tests (e.g. indentation bending tests (Aw 2015); development of elastic materials with embedded systems (Li, 2016)). The work has laid a solid platform for future works within the following areas:

1. Use the approach to study a greater number of weld machine settings/parameters (such as, peak current) which could provide key statistical data to be used for determining the mechanical properties of welds.

2. Use the approach to accurately recreate geometrically heat affected zone layers using indentation hardness test data.

3. The methodology developed represents a viable approach which could potentially be adapted for many other welding systems (MIG, TIG, FSW, Arc).

4. The work can be used to establish more quantitative data on the influence that cooling curve thermal history has on the microstructure.

At present the functionality is limited to applying material properties to ridged sections of parts within the model. For complex material systems with varied microstructures a more refined and intricate plug-in would be required. A multifaceted Interface may also be required to model the geometry of welded dissimilar metals. The size and shape of the nugget and HAZ can be unique and unsymmetrical.

Although the material properties interface has an option to read data from a spreadsheet to populate the input fields, a standard material characterisation database could be included to automatically populate fields to input material properties. The interface could also include further features for other applications, such as, temperature dependent material properties and options for creep analysis.

Further improvement to the Post Processing Interface could be made to secure confidential information (To a cloud or secure password protected folder). The interface could also benefit from reading experimental data results and then automatically producing data comparison plots.

These additions would create a more robust plug-in to structure and analyse spot welded joints. When comprehensively tested, this structure of the plug-in graphical interfaces will be extended to include more features.

7. References:

ABAQUS Theory Manual 6.9

Akkus A., 2009. Temperature distribution study in resistance spot welding, *Journal of scientific and industrial research, vol. 68, pp.199-202*

Alenius M., et al., 2006. Exploring the Mechanical Properties of Spot Welded Dissimilar Joints for Stainless and Galvanized Steels, *Welding Journal*, 305-313

Al-Samhan A.M; Darwish S.M.H. 2002, Finite Element Modelling Of Weld-Bonded Joints

Ambroziak A,. Korzeniowski M,. 2010, Using Resistance Spot Welding for Joining Aluminium Elements in Automotive Industry, Archives of Civil and Mechanical Engineering Vol X, No 1, p5-13 p9

Aslanlar S., Ogur A., U. OzsaracU., and E. Ilhan E, 2008.Welding time effect on mechanical properties of automotive sheets in electrical resistance spot welding, Materials and design, vol 29, iss 7, p 1427-1431.

Aw J, 2015, "Inverse modelling of hyper elastic properties from indentation bending tests", PhD thesis, Liverpool John Moores University.

BAE D. H., Sohn I. S., Hong J. K., 2003, Assessing the Effects of Residual Stresses on the Fatigue Strength of Spot Welds, *Welding Journal*, 18-23

BakavosD., and Prangnell P.B., 2010. Mechanisms of joint and microstructure formation in high power ultrasonic spot welding 6111 aluminium automotive sheet. Materials Science and Engineering :A, vol.527, iss.23, pg.6320-6334.

Bayraktar E., Kaplan D., Grumbach M., 2004, Application of impact tensile testing to spot welded sheets, *Journal of Materials Processing Technology* 153–154, 80–86.

Beardsley H.E.; Zhang J"Y.M. and Kovacevic R., 1993, Infrared sensing of full penetration state in gas tungsten arc welding, Int. J. Mach. Tools Manufact. Vol 34, No. 8. P. 1079-1090

Bolzon B, Maier G, Panico M. 2004,Material model calibration by indentation, imprint mapping and inverse analysis, *International Journal of Solids and Structures 41 2957–2975*

Bonifaz E.A. 2000, Finite Element Analysis of Heat Flow in Single-Pass Arc Welds. , *Welding Journal*, 121-125

Cai X, Langtangen H P, Moe H. 2005, On the performance of the Python programming language for series and parallel scientific computations. *Scientific Programming 13, p31-56*

Capriccioli A, Frosi P. 2009, Multipurpose ANSYS FE procedure for welding processes simulation, *Fusion Engineering and Design, 4863, p8*

Cavalli M. N., Thouless, M. D. and Yang, Q. D., 2003, Cohesive-zone modeling of the deformation and fracture of spot-welded joints, *Fatigue Fract Eng Mater Struct 28, p861-874*

Chang B.H., Zhou Y., 2003. Numerical study on the effect of electrode force in small-scale resistance spot welding, *Materials processing technology*, vol 139, 1-3, pg: 635-641

Chao Y. J., 2003, Ultimate Strength and Failure Mechanism of Resistance Spot Weld Subjected to Tensile, Shear, or Combined Tensile/Shear Loads. Journal of Engineering Materials and Technology Vol. 125

Childs P.N.R., Greenwood J.R., Long C.A., 2000, Review of temperature measurement, *Review of Scientific Instruments, volume 71, number 8*

Chiozzi S, Dattoma V, Panella F. 2008, Capacitor discharge welded bars of Inconel 718 and TiAl6V4superalloys under fatigue*, Materials and Design 29 839–851*

Cho Y., Rhee S., 2003. Experimental Study of Nugget Formation in Resistance Spot Welding. *Welding Journal,* 195S–201S

Darwish S.M., 2003, Welding strengthens and balances the stresses in the spot-welded dissimilar thickness joints, *J. of Materials Processing Technology* 134, 352-362.

Dong S. J., Kelkar G. P., Zhou Y., 2002, Electrode Sticking During Micro-Resistance Welding of Thin Metal Sheets. IEEE Transactions on Electronics Packaging Manufacturing, Vol. 25, No 4

Dongqing L, Jun T, Qingguo M, Hongyuan F. 2003, Indirect measurement of material thermal and mechanical properties during welding, *J.Mater.Sci.Technol., Vol.19*

Drebushchak V.A. 2009, Universality of the emf of thermocouples, *Thermochimica Acta 496 50–53*

Dwarampudi V, Shah J, Dhillon S.S, Sebastian N.J, Kanigicharla N.S. 2010, Comparative study of the pros and cons of programming languages Java, Scala, C++, Haskell, VB.Net, AspectJ, Perl, Ruby, PHP & Scheme.

Eisazadeh H, Hamedi M, Halvaee A. 2009, New parametric study of nugget size in resistance spot welding process using finite element method, *Materials and Design 31 149–157*

Esfahani M.B, Toroghinejad M.R, Key Yeganeh A.R. 2009, Modeling the yield strength of hot strip low carbon steels by artificial neural network, *Materials and Design 30 3653–3658*

Esme U., 2009, Application of Taguchi Method for the Optimization of Resistance Spot Welding Process, The Arabian Journal for Science and Engineering, Vol 34, No 2B, p 519-528

Fan X., 2007. Simulation of distortion induced in assemblies by spot welding, *Engineering manufacture*, vol 221, 8, pg 1317-1326

Fukumoto S, Fujiwara K, Toji S, Yamamoto A. 2008, Small-scale resistance spot welding of austenitic stainless steels, *Materials Science and Engineering A 492 243–249*

Gale W. F. And Totemeier T.C., 2004. Smithells metal reference book 8th edition.

Galler M, Enzinger N, Sommitsch C. 2010, The estimation of the contact interface temperature during resistance spot welding of zinc coated steels using numerical technique, *Mat-wiss. U. Werkstofftech. 41, No11, p925-930*

Gamboni O. C., Moreto J. A., Bonazzi L. H. C., Ruchert C. O. F. T., Bose Filho W. W., 2013 Effect of Salt-water Fog on Fatigue Cark Nucleation of Al and Al-Li Alloys. *Materials Research, 17(1), p250-254*

Ge´rard A, Berry A, Masson P. 2005, Control of tonal noise from subsonic axial fan.Part 1: reconstruction of aeroacoustic sources from far-field sound pressure, *Journal of Sound and Vibration 288 (2005) 1049–1075*

Ge´rard A, Berry A, Masson P. 2005, Control of tonal noise from subsonic axial fan. Part 2: active control simulations and experiments in free field, *Journal of Sound and Vibration 288 1049–1075*

Gonçalves C.V, Scotti A, Guimarães G. 2002, Inverse technique applied in welding: A theoretical and experimental approach, *4th International Conference on Inverse Problems in Engineering.*

Gonçalves C.V, Vilarinho L.O., Scotti A, Guimarães G. 2006, Estimation of heat source and thermal efficiency in GTAW process by using inverse techniques, *Journal of Materials Processing Technology 172 42–51*

Gould J.E, Khurana S.P, Li T. 2006, Predictions of Microstructures when Welding Automotive AdvancedHigh-Strength Steels, *Welding journal 111-s*

Hasanbasoglu A., 2007. Resistance spot weldability of dissimilar materials (AISI 316L–DIN EN 10130-99 steels), Materials and Design, vol 28 , Iss 6, pg 1794–1800

Hendricks Franssen H.J., Alcolea A, Riva M, Bakr M, van der Wiel e, Stauffer F, Guadagnini A. 2009, A comparison of seven methods for the inverse modelling of groundwater flow. Application to the characterisation of well catchments, *Advances in Water Resources 32 (2009) 851–872*

Hernandez V. H. B., Panda K. S., Okita Y., Zhou N. T., 2009, A Study on Heat Affected Zone Softening in Resistance Spot Welded Dual Phase Steel by Nanoindentation, *J Mater Sci 45, 1638-1647*

HouZ., Kim I., Wang Y., Li C., and Chen C., 2007. Finite element analysis for the mechanical features of resistance spot welding process, *Journal of materials and Processing Technology*, 185, 1-3, 160-165

Joaquin A., Elliott A. N. A., Jiang C., 2007 Reducing Shrinkage Voids in Resistance Spot Welds, *Welding Journal, p24-27*

Jou M., 2003. Real time monitoring weld quality of resistance spot welding for the fabrication of sheet metal assemblies, *Materials and processing tech* (0924-0136), vol 132 iss:1-3, pg 102.

Joung C.Y., Ahn S.H., Heo S.H., Hong J.T., Kim K.H., 2013. Development of welding and instrumentation technology for nuclear fuel test rod. *Transactions of the Korean Nuclear Society Autumn Meeting Gyeongju, Korea, Oct 24-25*

KahramanN., 2007. The influence of welding parameters on the joint strength of resistance spot-welded titanium sheets, *Material and design*, vol.28.iss 2, pg 420-427.

Kauer M , Vuskovic V, Dual J, Szekely G, Bajka M. 2002, Inverse finite element characterization of soft tissues, *Medical Image Analysis 6 275–287*

Khan M. I., Kuntz M. L., Biro E., Zhou Y., 2008, Microstructure and Mechanical Properties of Resistance Spot Welded Advanced High Strength Steels. Materials Transactions, Vol. 49, No 7

Kong X., Yang Q., Li B., Rothwell G., English R., Ren X.J., 2008. Numerical study of strength of spot-welded joint of steel, *Material & Design*, 29.1554-1561

Koranne S., 2011. Handbook of open source tools, Springer

Lawrence J, Li L, 1999, Finite element analysis of temperature distribution using Abaqus for a laser-based tile grout sealing process, *Proc Instn Mech Engrs Vol 214, Part B, p 451-461*

Lek S, Gue´gan J.F. 1999, Artificial neural networks as a tool in ecological modelling, an introduction, *Ecological Modelling 12065–73*

Li B., Shan P., Lian J., Hu S., Cheng F., 2002, Finite Element Simulation of the process of Aluminum alloy resistance spot welding, *Proc. 20th CAD-FEM Users Meeting, International Congress on FEM Technology. Friedrichshafen, Germany.* 2002.

Li S.D., 2016, "Development of soft elastic materials with embedded in extensible thin sheet", PhD project (in process), Liverpool John Moores University.

Lienert T. J., Stellwag, JR. W. L., Grimmett B. B., and Warke R. W. 2003, Friction Stir Welding Studies on Mild Steel, *Welding Journal 1-s*

Lightfoot M. P., Bruce G. J., McPherson N. A., and Woods K. 2005, The Application of Artificial Neural Networks to Weld-Induced Deformation in Ship Plate, *Welding Journal 23-s*

Lin J.W-B., 2012, Why Python is the next wave in earth science computing. *American Meteorological Society, 1823-1824*

Lindgren L.E., 2005, Numerical modelling of welding, *Comput. Methods Appl. Mech. Engrg. 195 6710–6736*

Lippmann R.P. 1987, An introduction to computing with neural nets, *IEEE ASSP magazine Vol. 3, No 4, pp 4-22*

Lippold J.C., 2015, Welding metallurgy and weldability, first edition.

Luo L and Zhao M., 2011, The secondary development of ABAQUS by using Python and the application of the advanced GA. *Physics Procedia 22, 68-73*

Ma N, Murakawa H. 2010, Numerical and experimental study on nugget formation in resistance spot welding for three pieces of high strength steel sheets, *Journal of Materials Processing Technology 210 2045–2052*

Mackerle J, 1996, Finite element analysis and simulation of welding: a Bibliography, *Modelling Simul. Mater. Sci. Eng. 4 501–533*

Mart´ın O, L´opez M, Mart´ın F. 2006. Artificial neural networks for quality control by ultrasonic testing in resistance spot welding, *Journal of Materials Processing Technology 183 (2007) 226–233*

Marzocca A. L., Luppo M. I., Zalarzar M., 2013, Identification of Precoptitates in Weldments Performed in an ASTM A335 Gr P91 Steel by FCAW Process. *International Congress of Science and Technology of Metallurgy and Materials, SAM - CONAMET*

Mayra M., Gayden X. Q., 2005, Development of Requirements for Resistance Spot Welding Dual-Phase (DP600) Steels. Part 1 – The Causes of Interfacial Fracture, *Welding Journal 172-182*

Meuwissen M. H. H., Oomens C.W.J., Baaijens F.P.T., Petterson R., Janssen J.D., 1998, Determination of the elasto-plastic properties of aluminium using a mixed numerical–experimental method. *J. of Materials Processing Technology* 75, 204–211.

Moreira P.M.G.P, Fraz̃aoO, TavaresS M O, de Figueiredo M. A. V, Restivo M. T, Santos J. Land de Castro P. M. S. T. 2007, Temperature field acquisition during gas metal arc welding using thermocouples, thermography and fibre Bragg grating sensors, *Meas. Sci. Tech. 18 877–883*

Mostafa N. B., Khajavi M. N., 2006 Otimisation of Welding Parameters for Weld Penetration in FCAW. *Journal of Achievements in Materials and Manufacturing Engineering, Vol. 16*

MukhopadhyayM.,BhattacharyaS., and RayK.K, 2009. Strength assessment of spot-welded sheets of interstitial free steels, *Materials processing technology,* vol 209, iss 4:1995-2007

Neaupane K.M., Sugimoto M., 2003, An inverse boundary problem using the extended kalman filter, *ScienceAsia 29, 121-126*

Ni K., and Sankaran M., 2004. Strain-based probabilistic fatigue life prediction of spot-welded joints, *International Journal of fatigue*, vol 26, 7, 763-772.

Nodeh I, Serajzadeh S, Kokabi A.H. 2008, Simulation of welding residual stresses in resistance spot welding, FE modeling and X-ray verification, *journal of materials processing tech 2 0 5 60–69*

Pal S, Pal S.K, Samantaray A.K. 2008, Artificial neural network modeling of weld joint strength prediction of a pulsed metal inert gas welding process using arc signals,*journal of materials processing technology 202 464–474*

Poorhaydari K., Patchett B.M., Ivey D.G., 2005. Estimation of cooling rate in the welding of plates with intermediate thickness. *Welding Journal, 149-155*

Pouranvari M., Abedi A., P., Marashi P., Goodarzi M., 2008, Effect of Expulsion on Peak Load and Energy Absorption of Low Carbon Steel Resistance Spot Welds. *Science and Technology of Welding and Joining Vol. 13, No1, 39-43*

Pouranvari M., Asgari H., R., Mosavizadch S., M., Marashi P., H., Goodarzi., 2007, Effect of weld nugget size on overload failure mode of resistance spot welds, *Science and Technology of Welding and Joining. Vol 12, No3, 217-225*

Prechelt L. 2000, An empirical comparison of seven programming languages

Rahman M.M., Rosli A.B., Noor M.M., Sani M.S., and Julie J.M., 2008. An Investigation into the effects of spot diameter and sheets thickness on fatigue life of spot welded structure based on FEA, *Research Journal of Applied Science*, 3(1):10-15.

Ren X.J., Yang Q.X., James R.D., Wang L. 2004, Cutting temperatures in hard turning chromium hardfacings with PCBN tooling, *Journal of Materials Processing Technology 147 (2004) 38–44*

Ren X.J., Smith C.W., Evans K.E, Dooling P.J, Burgess A., Wiechers J.W., and Zahlan., 2006. Experimental & Numerical Investigations of the Deformation of Soft material under tangential loading, *Int. Journal of Solids and Structure*, 43.2364 – 2377

Rumelhart D.E., Hinton G.E., Williams R.J. 1986, Learning representations by back propagating errors.

Santos M.C., Machado A.R., Barrozo M. A. S., Neto L.M., Coelho E.A.A., 2013. Influence of thermoelectric junction on the electrical signals generated by the tool- workpiece thermocouple system in machining. *Measurement 46, 2540-2546*

Seberino C,. 2012, Python: faster and easier software development, *Annual Conference 2012*

Seeger F, Michel G, Blanquet M. 2008, Investigation of spot weld behavoir using detailed modelling technique, *7. LS-DYNA Anwenderforum, Bamberg, B-I-29-38*

Song Q., Zhang W., Bay N., 2005, An Experimental Study Determines the electrical Contact Resistance in Resistance Welding. *Welding Journal 73-76*

Song Z.Y, Liu C.Y., Song X.L. 2003, Mathematical model of thermocouple characteristic based on neural network, *Machine Learning and Cybernetics, 2003 International Conference on. Vol. 3. IEEE, 2003.*

Sun D.Q., Lang B., Sun D.X., Li J.B., 2007. Microstructures and mechanical properties of resistance spot welded magnesium alloy joints, Materials Science and Engineering: A, vol.460-461, pg. 494-498.

Szajek K., Kakol W., Lodygowski T., Wierszycki,. 2008. Optimization module for Abaqus/CAE based on genetic aalgorithm, Abaqus Users Conference 2008

Tan, J. C,. Westgate, S. A., Clyne, T. W., 2007. Resistance welding of thin stainless steel sandwich sheets with fibrous metallic cores: experimental and numerical studies, *Science and Technology of welding and joining*, 12, 6, 490-504

Tang H,. Hou W., Hu S. J., Zhang H., 2000. Force Characteristics of Resistance Spot Welding of Steels. *Welding Journal 175-183*

Tong W., Tao H., Jiang X., Zhang N., Marya M. P., Hector L. G., Gayden X. Q., 2005, Deformation and Fracture of Miniature Tensile Bars with Resistance-Spot-Weld Microstructures. *Metallurgical and Material Transactions Vol. 36A*

Toubal L., Karama M., Lorrain B., 2004, Stress Concentration in a Circular Hole in Composite Plate. *Composite Structures 68, 31-36*

Ure J., Chan H., Tipping D., 2012 Development and implementation of the Abaqus Subroutines and plug-in for routine structural integrity assessment using the linear matching method. *Simulia UK Regional User Meeting*

Veenstra P.C. 1969, Athermal model of the spot welding process, Thesis

Venkatraman B., Menaka M, Vasudevan M., Raj B., 2006, Thermography for Online Detection of Incomplete Penetration and Penetration Depth Estimate. *12th A-PCNDT2006- Asia-Pacific Conference on NDT*

Venkatraman B., Raj B, Menaka M, Subbaratnam R. 2007, Image processing for enhanced quality assurance of sheathed thermocouples, *Materials evaluation Vol.65, No 5, 499*

Vural M and Akkus A., 2004. On the resistance spot weldability of galvanized interstitial free steel sheets with austenitic stainless steel sheets. *Material Processing Technology* 153–6.

Vural M., Akkus A., Eryurek B., 2006. Effect of Welding nugget diameter on The fatigue Strength of the resistance spot welded joint of different steel sheets, *Journal of Material Processing Technology,* 176.127-132

Wang J., Han J., Domblesky J.P., Yang Z., Zhao Y., Zhang Q., 2016. Development of a new combined heat source model for welding based on a polynomial curve fit of the experimental fusion line. *International journal of advanced manufacturing technology* 87.5-8 (2016): 1985-1997.

Weman K., 2012 Welding Processes Handbook Second Edition, Woodhead Publishings in Materials

Williams N.T. and Parker J.D., 2004, Review of resistance spot welding of steel sheets; Part 1 Modelling and control of weld nugget formation *International Materials Reviews Vol 49, No2, 45-75*

Winkler A. and Goetz F., 2005, Automated modelling of spur gears and worm gears using ABAQUS/CAE, *ABAQUS Users' Conference.*

Xia L., 2012. Development of 3-D neutronic kinetic model and control for CANDU reactors. *Diss. The University of Western Ontario, 2012.*

Xue L., 2007. Constitutive modelling of void shearing effect in ductile fracture of porous materials. *Engineering Fracture Mechanics 75, 3343-3366*

Yang Q. D., Ren X. J., Li Y. L., Zhao Y. H. and Yao M., 2005, Effect of welding parameters on residual stress field of 20CrMnTi specimen and its numerical simulation, *Materials Science and Engineering A* 392, 240–247.

Zaw K. 2009, Development of real-time computation techniques: a novel reduced-basis method and application to inverse analysis

Zell M, Lyng J.G, Morgan D.J, Cronin D.A. 2009 Development of rapid response thermocouple probes for use in a batch ohmic heating system, *Journal of Food Engineering 93 (2009) 344–347*

Zhang W. 2003, Design and Implementation of Software for Resistance Welding Process Simulation*s, No. 2003-01-0978. SAE Technical Paper, 2003*

Zhou G., Zhao C., Song L., Tong X., 2014 Analysis on and applications of thermocouples used for airflow temperature measurements in aircraft engine compressor. *Sensors & Transducers 179.9 (2014): 234.*

Zhou X. G., Pan W,. MacKenzie D,. 2013, Identifying friction stir welding process parameters through coupled numerical and experimental analysis. *International Journal of Pressure Vessels and Piping 108-109, 2-6*